AN INVESTIGATION OF RESIDUAL STRESSES INDUCED BY FORMING PROCESSES ON THE FATIGUE RESISTANCE OF AUTOMOTIVE WHEELS

P J McGRATH

DOCTOR OF PHILOSOPHY

MAY 2001

AN INVESTIGATION OF RESIDUAL STRESSES INDUCED BY FORMING PROCESSES ON THE FATIGUE RESISTANCE OF AUTOMOTIVE WHEELS

by

PATRICK JAMES McGRATH

(Reg. No. 708648)

(HESA No. 9710731055871)

A thesis submitted to the University of Plymouth in the fulfillment for the degree

DOCTOR OF PHILOSOPHY

Department of Mechanical and Marine Engineering, Faculty of Technology

In collaboration with Port Elizabeth Technikon

MAY 2001

CONTENTS

LIST OF FIGURES

LIST OF TABLES

GLOSSARY OF TERMS

A

age hardening - hardening by ageing, usually after rapid cooling or cold working.

alignment - a mechanical or electrical adjustment of the components of an optical device so that the path of the radiating beam coincides with the optical axis or other predetermined path in the system.

alloying element - an element added to and remaining in a metal that changes structure and properties.

angle of inclination – the angle at which a component is inclined from the horizontal or vertical axis.

anisotropy – is a term used for describing the mechanical properties of sheet metal plate depending on the direction relative to a particular axis or plane.

annealing - heating to and holding at a suitable temperature followed by cooling at a suitable rate.

apex – refers to the top-most position of a bend.

as manufactured – pertains to sheet metal plate in its as manufactured form.

automotive wheel – consists of two components, both manufactured by a process known as forming. The inner component is referred to as the centre disc while the outer is referred to as the wheel rim. These components are then welded together to form an automotive wheel.

axis of rotation – refers to two independent pivotal points, symmetrically positioned about which rotation takes place.

B

bending stress - if a beam is subjected to a bending moment the fibres in the upper part are extended and these in the lower part are compressed. Tensile and

compressive stresses are thereby induced which vary from zero at the neutral axis of the beam to a maximum at the outer fibres. These stresses are called bending stresses.

bake hardening – refers to the hardening of the surface of a component subjected to a paint curing temperature.

C

carbide - a compound of carbon with one or more metallic elements.

carbo-nitrides – is the precipitation of diffused carbon and nitrogen which usually occurs at the surface of a component when subjected to elevated temperatures.

centre disc – this is the centre section of an automotive wheel which is welded to the wheel rim.

chemical polishing - a process that produces a polished surface by the action of a chemical etching solution.

coining – refers to a stamping operation inducing a compressive stress round the periphery of a punched/stamped hole.

customised strain rosette – this is a strain rosette modified and/or developed from standard strain rosettes for the purposes of residual stress measurements.

cycle count – is the number of complete cycles a fatigue specimen undergoes prior to failure.

D

depth of field - the depth in the subject over which features can be seen to be acceptably in focus in the final image produced by a microscope.

diametral axis - refers to a circular axis on a round concave/convex type component.

dislocation - a linear imperfection in a crystalline array of atoms.

E

eccentricity – displacement or off-set adjustment with reference to the centre position.

electron beam - a stream of electrons in an electron-optical system.

electron diffraction - the phenomenon, or the technique of producing diffraction patterns through the incidence of electrons upon matter.

electron microscopy - the study of materials by means of an electron microscope.

endurance limit – refers to the fatigue testing of ferrous materials which do show finite life conditions.

etchant - a chemical solution used to etch a metal to reveal structural details.

etching - subjecting the surface of a metal to preferential chemical or electrolytic attack to reveal structural details for metallographic examination.

F

fatigue – a phenomenon which results in the sudden fracture of a component after a period of cyclic loading in the elastic regime.

fatigue life – is the number of load cycles a component can withstand prior to failure.

fatigue limit – refers to the fatigue testing of non-ferrous materials which do not show finite life conditions.

fatigue performance – see fatigue life.

ferrite - generally, a solid solution of one or more elements in body-centred cubic iron. In plain carbon steels, the interstitial solid solution of carbon in α-iron.

final polishing - a polishing process in which the primary objective is to produce a final surface suitable for microscopic examination.

finite element analysis (FEA) – a mathematical computational method for solving complex engineering related problems.

flow curve – a diagrammatic representation of data with respect to two measurable parameters, each indicated on mutual perpendicular axis.

forming – refers to a manufacturing process whereby sheet metal plate is shaped by means of a stamping press.

fracture – is the loss of structural integrity through crack propagation.

fracture stress – this is the stress magnitude at fracture of a component.

full stress relief – is the maximum relieved stress obtained, usually associated with residual stress assessment conditions.

G

grain - an individual crystal in a polycrystalline metal or alloy, including twinned regions or sub-grains if present.

grain boundary - an interface separating two grains at which the orientation of the lattice changes from that of one grain to that of the other. When the orientation change is very small the boundary is sometimes referred to as a sub-boundary structure.

grain growth - an increase in the grain size of a metal usually as a result of heating at an elevated temperature.

grain size - a measure of the areas or volumes of grains in a polycrystalline metal or alloy, usually expressed as an average when the individual sizes are fairly uniform. Grain size is reported in terms of number of grains per unit area or volume, average diameter, or as a number derived from area measurements.

granular fracture - an irregular surface produced when metal fractures. This fracture is characterised by a rough, grain like appearance. It can be sub-classified into trans-granular and intergranular forms.

greatest arithmetical maximum – the greater of two or more maximum results.

grinding - removing material from a workpiece using a grinding wheel or abrasive belt.

H

hardness – is a term used for describing the resistance of a material to plastic deformation under the action of an indenter.

hardenability - the relative ability of a ferrous alloy to harden under cold working conditions.

hardening - increasing hardness by suitable treatment, usually cold working.

high speed end mill drilling – a method employed for assessment of residual stresses whose spindle speed is greater than 60.000 rpm.

homogeneous – a chemical composition and physical state of any physical small portion are the same as those of any other portion.

hot working - deformation under conditions that result in re-crystallisation.

hour-glass type specimen – usually refers to a fatigue type specimen having a waisted hour-glass shape.

I

impurities - undesirable elements or compounds in a material.

inclusion count - determination of the number, kind, size and distribution of non-metallic inclusions.

inclusions - particles of foreign material in a metallic matrix.

incremental steps – refers to the removal of material in small amounts during a drilling operation.

isotropic – having similar mechanical and micro-structural properties in all directions.

interference - the effect of a combination of wave trains of various phases and amplitudes.

intergranular - within or across crystals or grains. Same as transcrystalline and trans-granular.

L

least arithmetical maximum – the least of two or more maximum results.

linear drilling evaluation method – a drilling method whose incremental feed rate is of equal amount.

lamination - an abnormal structure resulting in a separation or weakness aligned generally parallel to the worked surface of the metal.

longitudinal axis - that direction parallel to the direction of maximum elongation in a worked material.

longitudinal direction – see longitudinal axis.

longitudinal plane - is a plane that is normal to the longitudinal axis.

M

macrograph - a graphic reproduction of a prepared surface of a specimen at a magnification not exceeding 25x.

macrostructure - the structure of metals as revealed by macroscopic examination of the etched surface of a polished specimen.

magnification - the ratio of the length of a line in the image plane to the length of a line on the imaged material.

martensite - a generic term for microstructures formed by diffusion less phase transformation in which the parent and product phases have a specific crystallographic relationship.

martensitic - a plate-like constituent having an appearance and a mechanism of formation similar to that of martensite.

maximum shear strain - a stress of this nature is said to exist on a section of a body if on opposite faces of the section equal and opposite parallel forces exist.

maximum bending strain - a cylindrical shaft is said to be subject to pure torsion when the torsion is caused by a couple, applied so that the axis of the couple coincides with the axis of the shaft. The state of stress, at any point in the cross-section of the rod, is one of pure shear, and the strain is such that one cross-section of the shaft moves relative to another.

mean stress – refers to a pre-strained loading condition.

microcrack - a crack of microscopic proportions.

micrograph - a graphic reproduction of the prepared surface of a specimen at a magnification greater than 25x.

micro structure - the structure of a prepared surface of a metal as revealed by a microscope at a magnification exceeding 25x.

N

necking – is a thinning of a material which has been subjected the strain levels beyond its tensile strength.

non-uniform plasticity – refers to a steel component subjected to strain levels beyond the tensile strength for that particular steel material, usually associated with necking.

non-uniform stress field – is where the stress along any particular plane are of unequal magnitude.

O

optical device – microscopic eyepiece having perpendicular hairline markings for the purposes of alignment and measurement.

orientation (crystal) - arrangements in space of the axes of the lattice of a crystal with respect to a chosen reference or co-ordinate system.

orientated plane – see angle of inclination.

ovality – slightly out-of-round shape having a major and minor axis.

P

parallel sided – having sides machined parallel to one another.

phase - a physically homogeneous and distinct portion of a material system.

plastic deformation - deformation that remains or will remain permanent after release of the stress that caused it.

plasticity - the capacity of a metal to deform non-elastically without rupturing.

polished surface - a surface that reflects a large proportion of the incident light in a specular manner.

polynomial drilling evaluation method – a drilling method whose incremental feed rate increases consecutively.

principal strains - the maximum and minimum direct strains in a material, subjected to complex stress are called Principal Strains. These strains act in the directions of the principal stresses.

principal stresses - at any point within a stressed material it will be found that there exist three mutually perpendicular planes on each of which the resultant stress is a normal stress (i.e. no shear stresses occur on these planes). These mutually perpendicular planes are called principal planes, and the resultant normal stresses are called Principal Stresses.

pure bending conditions – the bending of a material under unconstrained conditions

Q

quantitative – identification of relative amounts making up a sample.

quench hardening - in ferrous alloys, hardening by austenitising, then cooling at a rate so that a substantial amount of austenite transforms to martensite.

quenching crack - cracks formed as a result of thermal stresses produced by rapid cooling from a high temperature.

R

re-crystallisation - a change from one crystal structure to another, such as that occurring upon heating or cooling through a critical temperature.

relieved – allowing for freedom of movement or relaxation.

residual stress – are stresses inherent in a component prior to service loading conditions.

restrained – hold back movement in any direction.

rolling direction – refers to the direction in which the billet was rolled during sheet metal plate manufacture.

S

scanning electron microscope - an electron microscope in which the image is formed by a beam operating in synchronism with an electron probe scanning the object.

shear bands - bands in which deformation has been concentrated inhomogeneously in sheets that extend across regional groups of grains.

sheet metal forming – refer to forming.

slip - plastic deformation by the irreversible shear displacement of one part of a crystal relative to another in a definite crystallographic direction and usually on a specific crystallographic plane.

slip band - a group of parallel slip lines so closely spaced as to appear as a single line when observed under an optical microscope.

spacers – this is shim stock, plate or epoxy type solutions cast into a mould of specific sizes to raise a component or member to a specific height.

springback – is the elastic recovery after a component has undergone plastic deformation.

springback load – is the load required to return the material to its original pre-strained condition.

springback angle – is the angle between the springback position to the original pre-strained position in a pure bend plate component.

strain - strain is a measure of the deformation of a body acted upon by external forces and can be expressed as a change in dimension per unit of original dimension or in the case of shear as a change in angle between two initially perpendicular planes.

strain amplifier - the ratio of the voltage supplied to the voltage delivered by the Wheatstone Bridge as a result of the unbalance caused by a change of strain gauge resistance is equivalent to the strain and is amplified into a suitable voltage or current which can be fed into an analogue or digital indicator or graphic recorder.

strain rosettes - a combination of three strain gauges set along three axes, usually at 45° or 60°, with each other - used to determine strain at a point on a surface when the strain directions are unknown.

stress - load applied to a piece of material tends to cause deformation which is resisted by internal forces set up within the material which are referred to as stresses. The intensity of the stress is estimated as the force acting on unit area of the cross-section, namely as Newtons per square metre or Pascals.

stress amplitude – refers to a stress loading magnitude above and/or below a particular mean stress level.

stress ratio – is the ratio of minimum to maximum stress levels usually associated with fatigue testing conditions.

stress relieving - heating to a suitable temperature, holding long enough to reduce residual

stresses, then cooling slowly enough to minimise the development of new residual stresses.

stringer - a microstructural configuration of alloy constituents or foreign nonmetallic material lined up in the direction of working.

sub-surface – a location just beneath the surface of a component.

T

tempered martensite - the decomposition products that result from heating martensite below the ferrite-austenite transformation temperature.

tempering - in heat treatment, reheating hardened steel to some temperature below the eutectoid temperature to decrease hardness and/or increase toughness.

transmission electron microscope - a microscope in which the image-forming rays pass through the specimen being observed.

transverse direction – refers to the perpendicular direction in which the billet was rolled during sheet metal plate manufacture.

true fracture stress – see fracture stress.

U

uniform stress field – is where the stress along any particular plane are of equal magnitude.

uniform plasticity – refers to a condition of a component when subjected to plastic deformation between its yield and tensile strength positions.

unrestrained – free to move in any direction.

V

venting – refers to a stamping operation producing holes of specific form in a sheet metal component.

Z

zero mean stress – pertains to the fatigue testing of a component under zero pre-strain conditions.

(Note: For other definitions and nomenclature see text.)

ACKNOWLEDGEMENTS

The work presented in this thesis would never have materialised without the support from industry, academic institutions, colleagues and friends. This research work originated in the automotive wheel manufacturing industry, which was looking at improving wheel-manufacturing technology through enhancing the fatigue performance of automotive wheels.

Firstly, I would like to acknowledge the management teams of the University of Plymouth and Port Elizabeth Technikon in supporting this project and in making this joint venture an enriching experience. Special mention must be made to Professor MN James from the University of Plymouth, Dr DG Hattingh and Professor HLT Jeffery from the Port Elizabeth Technikon who were the major role players in administering this project.

The completion of this thesis would not have been possible without the support of many individuals. I would like to express my gratitude to the following people and organisations for their invaluable assistance, time and encouragement.

- Professor MN James, Chief Supervisor for his encouragement, involvement and professional guidance.
- Dr DG Hattingh, Second Supervisor for his support, involvement and professional guidance.
- Professor HLT Jeffery, Dean of the Electrical and Mechanical Faculty, for his support and encouragement.
- The staff of the Mechanical and Marine Engineering Department at the University of Plymouth for positive criticism and guidance.

- The National Research Foundation and the Port Elizabeth Technikon's Research Committee for their financial support of this project.
- The staff of the Faculty of Electrical and Mechanical Engineering at Port Elizabeth Technikon, and in particular Ms A Els-Botes, C van Huyssteen. Messrs C du Preez, R Phillips, T Tonkin, J van der Mescht, T van Niekerk and I Wedderburn.
- The industrial support received from the following companies and individuals:

  Eskom Technology Group, Mr Mark Newby, who collaborated with residual stress measurements.

  Guestro Wheels (Eastern Cape Division), Mr L Thomas for continual support and collaboration.

Finally, I would like to thank my family for their support, patience and prayers, especially my wife Sylvia and children, Sherene and Yolande, for their understanding and patience.

All honour to my Heavenly Father for giving me the insight and health to complete this work.

AUTHOR'S DECLARATION

At no time during registration for the degree of Doctor of Philosophy has the author been registered for any other university degree.

This study was financed with the aid of the National Research Foundation of South Africa, Port Elizabeth Technikon, Guestro Wheels (Eastern Cape Division) of South Africa.

A programme of advanced study was undertaken, which included attendance of courses at the University of Port Elizabeth, Physics Department; Department of Materials and Metallurgical Engineering at Port Elizabeth Technikon. Relevant scientific seminars and conferences were attended and several papers prepared for publication. Many external institutions were visited for consultation purposes where the work involving this project was shared.

Patent Application:

* Improved Strain Rosette for Residual Stress Assessment.
  South African Patent Application No. 2000/2042.
  April 2000.

Conference Publications:

- A Novel 8-Element Gauge for Residual Stress Assessment using the High Speed Centre Hole Drilling Method.
  M^{c}Grath, PJ, Hattingh, DG, James, MN & Wedderburn, IN.
  Fracture 2000 - The fifth national South African conference on fracture, Cape Town, 5 - 7 December, 2000.

* Effects of Forming Process on Fatigue Performance of Wheel Centre Discs.
  M^{c}Grath, P.J., Hattingh, D.G., James, M.N. and Els-Botes, A.
  European Conference on Fracture (ECF13), San Sebastian, Spain, September 2000.

Workshops Attended for Equipment Training Purposes:

* Measurement of residual stresses using an automatic hole drilling (milling) device.

  HBM Darmstadt, Germany, 17-20 February 1997.

* TMS Fatigue Testing Machine.

  Pretoria, South Africa, March 1999.

External Contacts:

Prof. Dr. U Beerschwinger, Fachhochschule Ingolstadt, Germany.

Prof. Dr. R König, Fachhochschule Regensburg, Germany.

Prof S Jack Hu, University of Michigan, USA.

Prof TA Callanan, University of Limerick, Ireland.

Prof M Hillary, University of Limerick, Ireland.

Dr J Robinson, University of Limerick, Ireland.

Prof B Tait, University of Cape Town, South Africa.

Dr F Scott, Technifin, Johannesburg, South Africa.

Prof. J J Neethling, University of Port Elizabeth, Port Elizabeth.

Mr L Thomas, Guestro Wheels (Eastern Cape Division), Port Elizabeth, South Africa.

Mr J Kotze, Iscor Steel Flat Products, Vanderbijlpark, South Africa.

Mr K Gehrke, HBM, Germany.

Mr T Kleckers, HBM, Germany.

Mr M Newby, TRI - Eskom, Cleveland.

Signed.....P McGraf.....

Date.....30/4/2001.....

ABSTRACT

Author: **PATRICK JAMES McGRATH**

Title: **AN INVESTIGATION OF RESIDUAL STRESSES INDUCED BY FORMING PROCESSES ON THE FATIGUE RESISTANCE OF AUTOMOTIVE WHEELS**

The nature and scope of this thesis relates to obtaining an understanding of the way in which sheet metal forming processes affect the residual stresses (plastic deformation) and the fatigue performance of wheel centre discs made of a dual phase steel.

Automotive wheels are mainly manufactured from sheet metal plate by forming processes using tools and dies. This manufacturing process is directly concerned with deforming the plate under predominantly applied tensile forces where the component acquires a stress state which is multi-axial. This stress state is both complex and difficult to assess from an analytical point of view and thus the work reported in this thesis is of an applied nature, and seeks to understand the results of this stress state on residual stresses, hardness and, hence fatigue behaviour. Components from each stage of the centre disc manufacturing process and of the assembled and painted wheel will be assessed and characterised.

The first part of the work involved a literature review of the factors influencing sheet metal forming, i.e. elongation, anisotropy, grain size, springback, residual stresses and fatigue. This review gave the researcher a background from which he could confidently approach the various investigations that were required for successful completion of this project. The residual stress analysis led to an investigation that provided a new technique for residual stress measurement using the high speed centre hole drilling method. This new measurement technique gave improved results when assessing the residual stress behaviour of textured sheet materials subjected to plastic deformation. It is felt that this technique will also

minimise the inherent scatter that is perceived by many an analyst to be a fundamental part of residual stress assessment by the hole drilling method. The concept of this measuring technique has since been patented and is subject to a South African Patent Application No. 2000/2042.

The thesis then deals with the process analysis of centre disc manufacture as well as the analysis of the fatigue properties of specimens removed from each stage of the manufacturing process and of the complete wheel. Here the complexity of the centre disc manufacturing process is discussed and assessed in terms of the process effects on microstructure, surface hardness, induced residual stresses and fatigue performance. The aim of this part of the work is to seek relationships with respect to surface hardness, induced residual stress and fatigue life in terms of the various production stage components including the centre disc of the complete wheel. The results showed that relationships do exist and that fatigue life prediction can be based on surface hardness as well as residual stress assessments for centre discs manufactured from dual phase steel plate.

The final part considers modelling the fatigue life of automotive wheels based on the mean stress models of Soderberg, Goodman and Gerber and incorporating the induced residual stresses into the equations. The Gerber model was found to give the better correlation with regard to fatigue life prediction when compared with the actual fatigue data.

In conclusion, this research has led to the development of a model showing the relation and impact of the centre disc manufacturing process on induced residual stress levels and fatigue properties of dual phase steel plate.

FOREWORD

[This foreword is referenced from a publication in 1995 by Lemmerz Werke GmbH]

After people had constructed the first wheel, they probably had little idea of how revolutionary their creation would be. The rotating wheel became the basis of many machines and appliances. Mechanisation of the wheel driving processes has offered transportation unsuspected possibilities. The duration of travelling long distances became shorter and mobility greater. This process is still on going today. The aim of this foreword is to offer a brief survey of the history of the wheel through the ages, from its origin to the nineteenth century. It shows how such a rather simple component has become the basis of our fast moving western society.

The wheel is basically a round disc, being able to turn round an axle, more or less fixed to a centre. The wheel is a fundamental part of many mechanical constructions. The rim (wheel circumference) and the central part round the axle may be linked by either a plate that may be bent or by means of spokes.

Plate (i). - First cave paintings representing a two-wheeled wagon. 2000 - 1000 years B.C.

The exact time in history when the wheel was first invented is unknown but one can imagine that it probably dates back to the stone ages. The use of wheels was first recorded between 3500 and 3000 B.C. in Mesopotamia and they were used for both the ceramic and transport industry. The first traces found in royal tombs or on works of art always referred

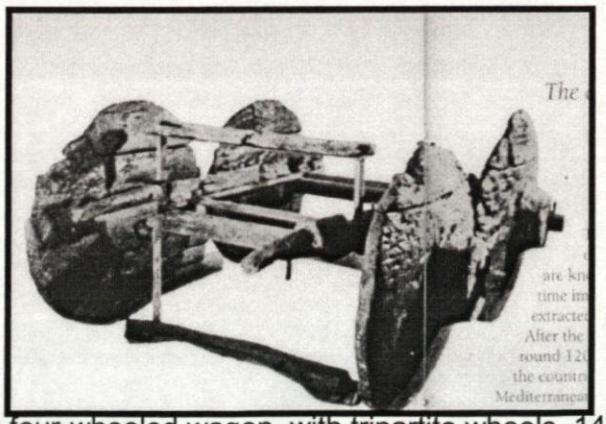

Plate (ii). - Part of a four-wheeled wagon, with tripartite wheels, 14th - 12th century B.C.

to four-wheeled carts. These carts had two special details: All the wheels were made of solid material; three wooden planks, bound together by means of cross-latches, which served as segments of a circle. A cart was rather expensive in those days and as such remained the privilege of the rich, who through their quicker transport, retained their superiority to people living in agrarian communities.

The spoked wheel was introduced round 1600 B.C. when the Egyptian Kingdom became ascendent. These spoked wheels were in themselves revolutionary as the reduction in wheel weight allowed for faster transport.

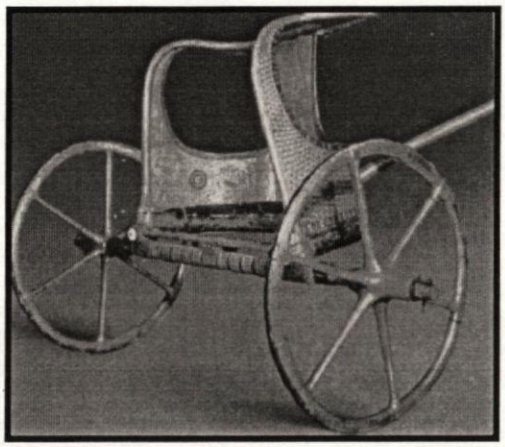

Plate (iii). - Float of Toetanchamon, an Egyptian spoked wheel, second half of 14th century B.C.

This was not possible with a solid wheel. Moreover, the spoke and hub construction proved much more stable than the plate construction of the solid wheel.

The Chalybs, a tribe under the domination of the Hettite empire, are known to be the first users of iron. Their skilled blacksmiths extracted iron from forgeable iron ore. After the fall of the Hettite empire around 1200 B.C. the Hettites spread to countries of the Near East

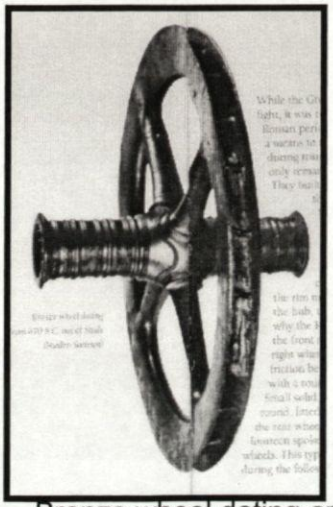

Plate (iv). - Bronze wheel dating around 870 B.C.

and Mediterranean introducing this technology to those parts of the world. The Hettites introduced the steel rimmed wooden spoked wheel which has remained in use on many a horse driven wagon today. These wheels were also used in the military context on the two-wheeled chariots. The Greeks continued using chariots for their main military attack, although cavalry replaced this during the Roman period. During the Middle Ages, animals, water and wind were the prime source of power and all these resources were exploited by use of the wheel. The wheel had a double function and was improved in two ways, on the one hand with regard to transport and on the other hand as an essential functional element of mechanical construction.

In the 19th century a new more comfortable chapter opened in the history of the wheel. This was due to a patent for pneumatic tyres. Prior to this, people had only talked about "wheels" while subsequently the word "tyre" began to gain meaning. In 1840 Charles Goodyear invented and patented the concept of vulcanisation. This led to much research for the development of pneumatic tyres, by people such as Robert William Thompson

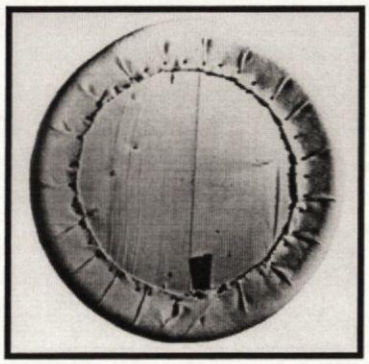

Plate (v). - Dunlop's first pneumatic tyre.

during the years 1840 - 1846. John Boyd Dunlop was another inventor of a pneumatic tyre in 1888. During this period many improvements and designs were produced in terms of wheels and tyres.

Plate (vi). - Different models of spoked wheels, left the conventional wheel and right, the flanged wheel.

Wheels were still of the spoked form and it was not until 1924 that the first stamped steel plate wheel was manufactured by Lemmerz which was fitted to the Opel Laubfrosch automobile. The first styled wheel, having perforations was manufactured in 1937.

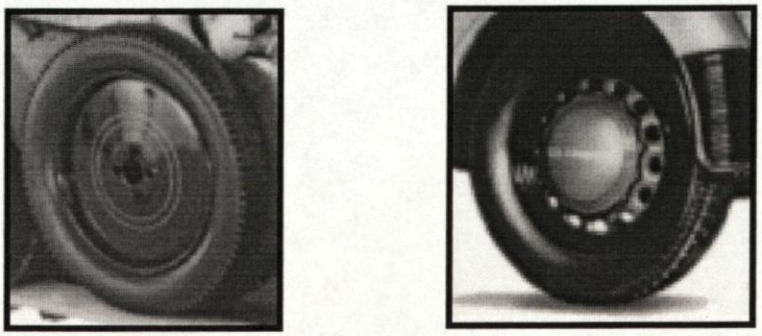

Plate (vii). - First pressed steel plate wheel, 1924 (left), and the first pressed perforated wheel, 1937 (right).

In concluding, wheels make us mobile, and have done so for thousands of years. But it is only in the last 150 years that the wheel has undergone its most far-reaching development and by the invention of the automobile that really focussed on the development of wheel technology. Manufacturers constantly set new targets for manufacture and performance, which have to be met with ever-shorter deadlines.

The future for the wheel no doubt holds many new ideas and challenges. As a result, there will always be discussions round the wheel for years to come. This thesis deals with some aspects related to the fatigue performance of the wheel centre disc.

CHAPTER 1

INTRODUCTION

Motorised private transport became a reality at the start of the 20th Century when Henry Ford produced the first motor vehicle in 1904, known as the "Model –T Ford", he also revolutionised mass production techniques and is famous for his statement: "they can have any colour they like – as long as it is black". Since then motor vehicles have become faster, lighter and more economical, while shapes and colours have also changed over the years. This progress has been the result of much research and development with respect to motorised transport and in particular passenger vehicles.

However, motor vehicles may well be considered critical safety objects, as malfunction of certain mechanical mechanisms and components could result in serious injury which is undoubtedly undesirable. Hence, vehicle components and mechanisms such as wheels, tyres, steering, power train, are considered more critical than body panels and bumpers. Designers, engineers and scientists are therefore continuously seeking ways in which to improve these components and mechanisms in terms of the overall efficiency of the motor vehicle while meeting the required safety regulations as determined by the motor federations and government legislation.

The critical safety component considered in this project is the automotive wheel, which is usually manufactured from sheet metal plate through a process known as sheet metal forming. Although many aspects of the sheet metal forming process are well understood and documented[1,2] there remain areas which still require research to more fully unlock the critical mechanism of fatigue failure in components like wheels. This does not imply that wheels fail during their service life, but rather that fatigue failure under industrial fatigue testing conditions is used as a tool in determining the wheels durability in terms of

quality/process control related to component shape, as well as to material development. One such area requiring research is the role played by residual stresses induced during the forming process and the effect they may have on the fatigue resistance of formed components.

Many researchers are using numerical modelling i.e. Finite Element Analysis (FEA)[3,4,5,6], to simulate the sheet metal forming process but factors such as residual stresses, forming compounds, anisotropy and the three dimensional stress-strain state make the problem difficult and complex to solve from a theoretical point of view. For example, forming compounds are solutions that are wiped onto the sheet plate prior to the forming operation, they reduce tool and die wear and leave the formed surface of the plate in a smooth condition[7].

Hence in this work, and in order to obtain an understanding of the materials fatigue resistance a study will be undertaken of the fatigue properties of the wheel centre disc and of how these properties change with change in component shape during the various forming stages to which the component is subjected. Residual stress analyses will also be undertaken on centre discs in an effort to further this understanding and to link residual stress behaviour with fatigue performance. This project will seek to provide an understanding of the overall forming process and more importantly, to provide knowledge on the most detrimental forming stage/s, if any, through fatigue and residual stress analysis. This information will contribute to the optimisation of automotive wheel manufacture and to design improvements, eg. a potential reduction in material thickness.

Fatigue failure inevitably occurs in areas where the induced stresses are high (usually associated with regions of plastic deformation) and of a tensile nature. Analysis of such failures in motor vehicle wheel discs forms the basis of this research programme, in which

the levels of these induced stresses will be evaluated whilst establishing the effect of the various stages of the production process on fatigue life of the centre discs. The component under consideration for this study is the centre disc of a pressed wheel, manufactured from a high strength low alloy (HSLA) Dual Phase Steel (manufacturers designation – DPS600).

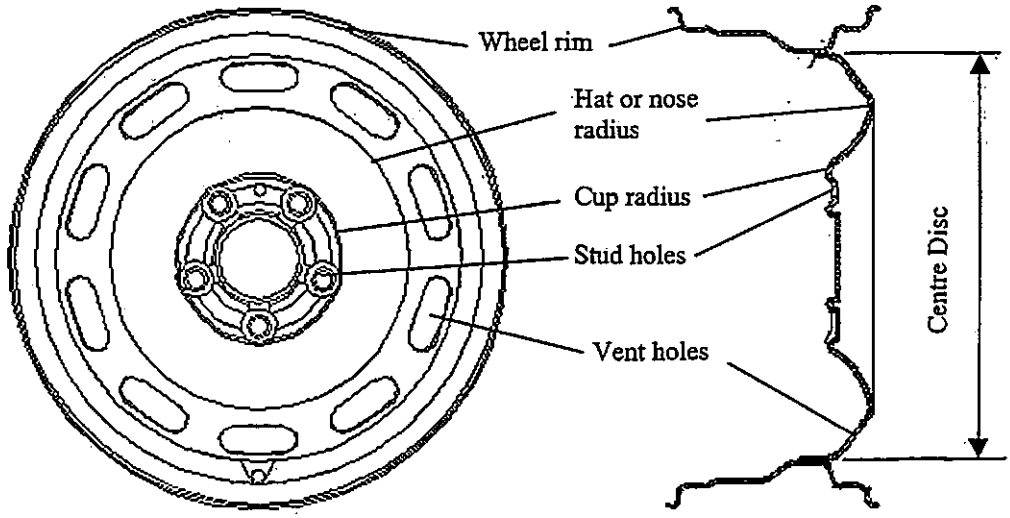

Figure 1.1. – Nomenclature of an automotive wheel.

In summary, the work described in this thesis aims to develop an understanding of the interaction between forming process parameters and the magnitude and direction of the maximum residual stresses and to incorporate this understanding into a model for fatigue life prediction.

The method of approaching the centre disc lifing problems is that of dividing the overall project into discrete, but linked, sub-problems.

Sub-problem One

To investigate the influence of forming processes on the mechanical properties of centre disc components taken from each stage of the manufacturing process. This investigation will involve surface hardness testing providing information on the work hardenability of

the material that will be related to the induced residual stresses at a later stage in this work. Micro-structural analysis will also be carried out on specimens taken from components after each stage of the manufacturing process to assess the behaviour of the materials microstructure after been subjected to forming operations.

Sub-problem Two

To investigate the residual stress fields through the various forming stages of centre disc manufacture up to, and including the centre disc of complete wheels. This will provide an understanding of the effective fatigue cycle to be applied during fatigue testing, and hence can assist in comparing the effects of each manufacturing stage (stamping, assembling and paint curing operations).

Sub-problem Three

To evaluate the fatigue performance of automotive wheels and hour-glass specimens machined from centre discs taken from each stage of the manufacturing process. The aim of these investigations is to compare, in a rational way, the rotating bending (industrial) and reversed bending (laboratory) fatigue testing results. The data obtained will also be related to hardness data in an attempt to correlate the fatigue behaviour with an indication of plastic deformation during each forming stage.

It is believed that this research has led to a better understanding of the fatigue performance of automotive wheel centre discs. This was achieved through, firstly, characterising surface hardness and residual stress data and relating them to fatigue data obtained from hour-glass specimens and, secondly, by developing an automotive wheel fatigue prediction model where the magnitudes of the induced residual stresses have been incorporated into the relevant model equation. The results obtained in this work should allow for optimising

the design and manufacturing procedure leading to the development of enhanced components.

The main aspects of the work to be investigated during this research project are illustrated schematically by Figure 1.2.

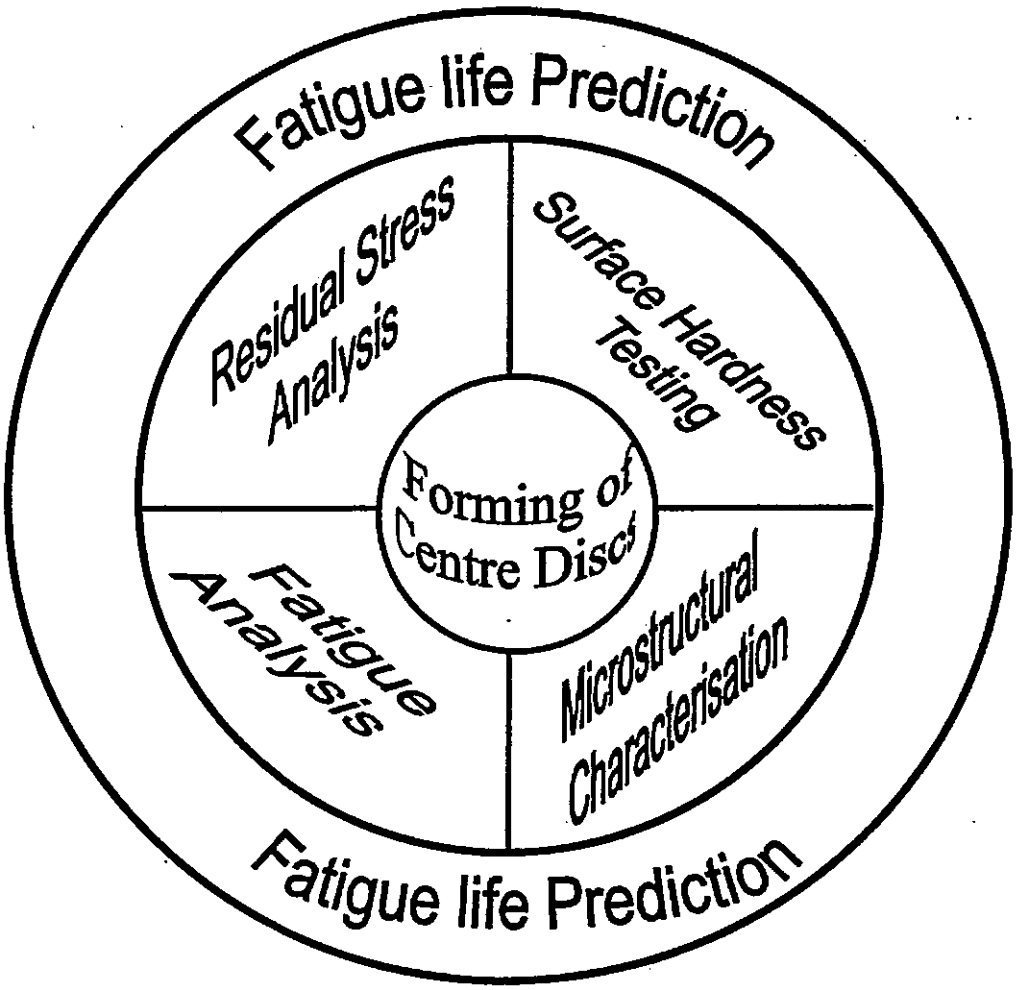

Figure 1.2. – Illustration of main research aspects.

This project has been supported by Guestro Wheels (Eastern Cape Division) who supplied all sheet materials and components used in this work. The Port Elizabeth Technikon (PET) and the then Foundation of Research and Development (FRD), now known as the National Research Foundation (NRF) provided the necessary financial support and laboratory facilities.

CHAPTER 2

FACTORS AFFECTED BY FORMING PROCESSES

Centre discs of automotive wheels are usually manufactured from sheet metal plate that are subjected to stamping operations. It is therefore relevant to consider some of the influences/effects of the stamping operations with respect to sheet metal forming. As sheet materials are generally characterised by a high ratio of surface area to thickness the uni-axial force applied to the sheet during the stamping operation is mainly tensile in nature[1,2]. This uni-axial force induces a multi-stress state condition in the component resulting in thickness changes caused by the stretching/drawing/bending of the sheet that can lead to localised necking. Stress concentrations are usually associated with areas of localised necking and are therefore considered a weakness in terms of the materials fatigue strength.

The basic mechanisms of sheet metal forming operations are **bending, stretching and drawing** in which certain factors[7,8] significantly influence the overall forming operation, the major ones being:

2.1 ELONGATION

Forming operations rarely involve simple uni-axial stretching or drawing but the observations made from simple tensile tests allow for understanding the behaviour of sheet materials. The main characteristic emanating from a tensile test is the determination of a materials work/strain hardening coefficient, n, defined as the increase in true-stress with increasing natural, or true strain and which is a measure of the materials formability. This implies that a material having a high work hardening coefficient shows a larger amount of uniform elongation thereby reducing the tendency for local necking. The strain at which this necking (instability) begins occurs at a stress level which equals the Ultimate Tensile

Strength (UTS) of that material[9]. Thus upon reaching the UTS of the material the strain hardening coefficient (n) will equal the true-strain (ε), until ε = 1 (fracture) and is given by:

$$\varepsilon = n \quad \text{.....(2.1)}$$

The elongation produced under tensile testing in obtaining the work hardening coefficient, n, is uni-axial and monotonic (gradual) loading conditions but under forming operations, the elongation produced is multi-axial and occurs under high strain rate (impact) loading conditions.

2.2 ANISOTROPY

Anisotropy is acquired during the thermo-mechanical processing history of the sheet material and is bi-axial in nature. Anisotropy is present not only in the longitudinal plane of the sheet but is also present through its thickness direction. Crystallographic anisotropy (planar anisotropy) pertains to the grain orientation (texture) and mechanical fibering (normal or plastic anisotropy) pertains to the alignment of the impurities, inclusions and voids throughout the sheet thickness[10], which also weaken the component in terms of fatigue as they act as stress raisers. Normal or plastic anisotropy in sheet materials is measured by its r-value which is also obtained from simple tensile tests, and is the ratio of width strain to thickness strain, thus:

$$r = \frac{\varepsilon_w}{\varepsilon_t} = \left[\frac{\ln \frac{w_o}{w}}{\ln \frac{t_o}{t}} \right] \quad \text{.....(2.2)}$$

Where: w_o and t_o = initial width and thickness

w and t = width and thickness taken at any point in time on a specimen during a simple tensile test.

The value of r (normal anisotropy) is not constant in all directions in the plane of the sheet, but varies with rotation from the rolling direction. The average value of normal or plastic anisotropy is termed r_{mean} and is determined by the following expression:

$$r_{mean} = \frac{1}{4}[r_{0^\circ} + r_{90^\circ} + 2r_{45^\circ}] \quad \text{.....(2.3)}$$

This r_{mean} value is used to predict the behaviour of the sheet material during deep drawing conditions. A measure of the change in anisotropy (planar anisotropy), that is, the change in r-value in the sheet plane, is Δr. Test specimen for the determination of Δr are cut from sheet material at angles of 0°, 45° and 90° with respect to the rolling direction (see Figure 2.1) of the sheet and Δr is determined using the following equation:

$$\Delta r = \frac{1}{2}[r_{0^\circ} + r_{90^\circ} - 2r_{45^\circ}] \quad \text{.....(2.4)}$$

In addition to influencing the strain/work hardening coefficient, n, the anisotropy factor r, or r_{mean}, also affects the magnitude of the limiting drawing ratio (LDR). This is determined by the ratio of blank diameter (d_o) to throat diameter of the die (d_1), see Figure 2.2, and is a measure of the materials drawability.

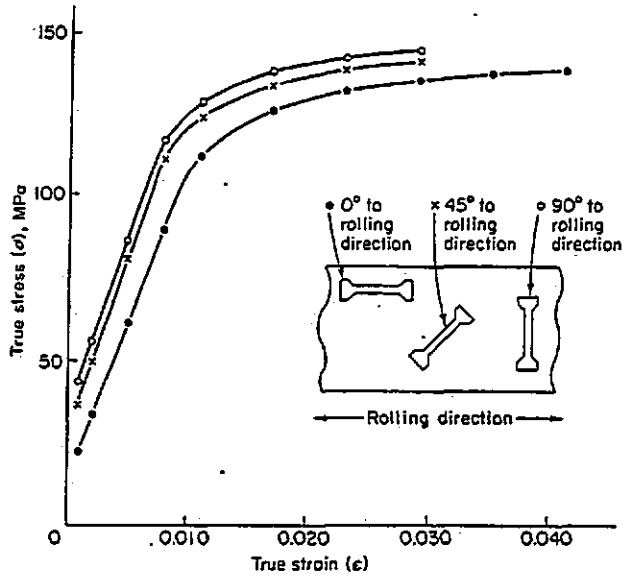

Figure 2.1[57]. – Illustration of tensile specimen locations for determining Δr.

The limiting drawing ratio is determined by the following expression:

$$LDR = \frac{d_o}{d_1} \quad \text{.....(2.5)}$$

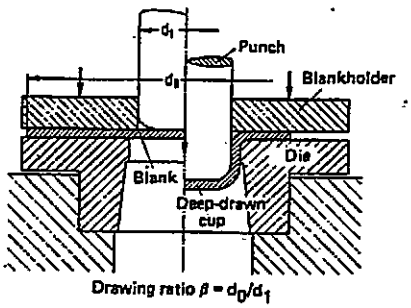

Figure 2.2[7]. – Cup-drawing test for determination of the limiting drawing ratio.

The author is of the opinion that one of the contributory factors to the multi-axial stress state and hence the induced residual stresses experienced by the component on completion of the forming operation is anisotropy. In order to clarify this contribution, the following metallurgical/mechanical aspects require consideration in terms of centre disc manufacture:

- During the manufacture of sheet metal plate, the grains become aligned/orientated in the rolling direction of the plate/sheet. Thus, during a forming operation on such a plate the basic forming mechanism encountered, in the direction of rolling, will be that of drawing-bending. This can be clarified by analysing the results from a forming limit diagram (FLD) as shown in Figure 2.3. The tension-compression condition of the measured etched circles results from the drawing-bending mechanism relative to the rolling direction. Here the induced strains will be of higher magnitude, as the grain structure is already orientated in the rolling direction.
- The forming mechanism in the transverse direction of the plate will be that of stretching-bending. Here the grains are stretched, requiring a greater force in order to deform the component to the same shape as that observed in the rolling direction.

Therefore as the angular rotation tends toward the transverse to rolling direction plane so too does the deformation of the measured etched circles change to a tension-tension condition, see Figure 2.3. Thus, the magnitude of the induced strains will be marginally lower.

- The mechanism encountered along the 45° plane will be that of drawing-stretching-bending considered as the resultant of the two previous mechanisms mentioned which also results in a tension-tension condition.

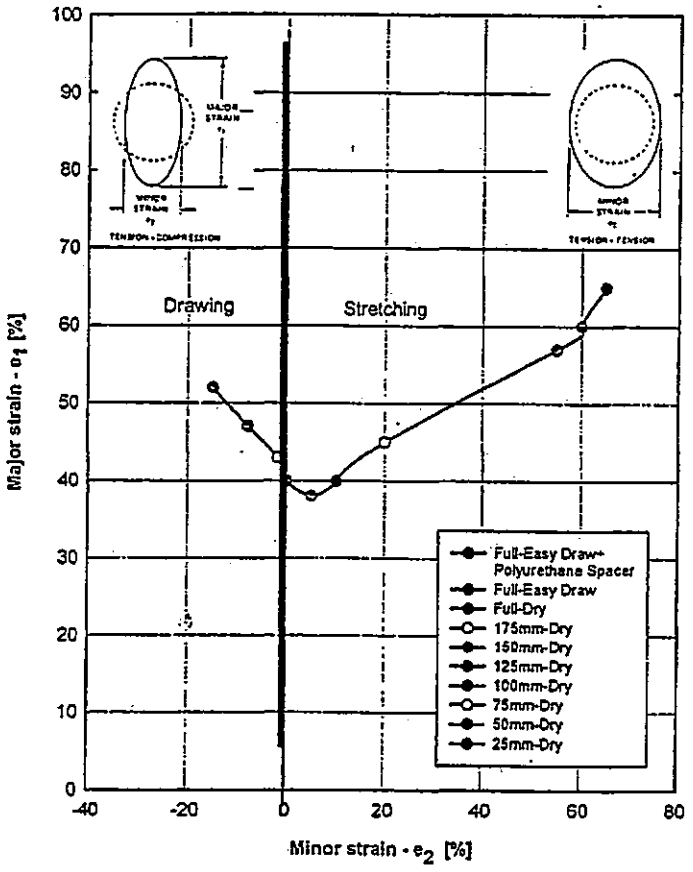

Figure 2.3[73]. – Forming limit diagram applicable to dual phase steel.

2.3 GRAIN SIZE

The grain size of sheet metal plate is important for two reasons, firstly, because of its effect on the mechanical properties of the material and secondly, because of its effects on the surface appearance/roughness of the formed component. The coarser the grain size,

the rougher the appearance of the surface, the finer the grain size the longer the yield point elongation.

An ASTM grain size of No 7 or finer (this is indicative of 7 grains x 100 magnification per square inch) is generally preferred for sheet metal forming operations and the dual phase steel used by the particular wheel manufacturer is grain size No 12 shown in Figure 2.4.

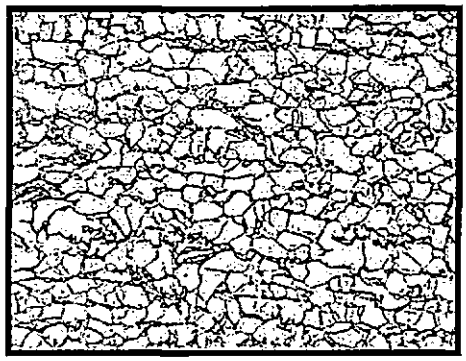

Figure 2.4. – Microstructure of DPS600 x500.

2.4 SPRINGBACK

Sheet materials are generally thin and are likely to experience springback[11], which is the amount of deformation strain recovered by elastic unloading when the component is removed from the forming press, see Figure 2.5. This is a problem encountered with all sheet materials. Davies[12] found that springback is a function of the die gap, bend radius, material thickness and the strength of the material. With constant die gap conditions springback is proportional to the yield strength of high strength low alloy steels[13,14]. Springback is an intrinsic property of sheet material (increasing with increasing yield strength) and therefore cannot be reduced or eliminated by modification of the metallurgical structure.

2.5 RESIDUAL STRESSES

Residual stresses will inevitably be induced in the sheet material due to the manufacturing process but their magnitude will depend on whether the sheet is produced by cold or hot working conditions. Residual stresses are related to yield strength of the material at the

temperature under which the plastic deformation occurs, and hence under hot working conditions will be considerably lower because of the reduction in yield strength at hot working temperatures. Design engineers of critical safety components are aware of such stresses but often they reduce the effect by using thicker gauge material. If however these stresses were to be taken into account by specifying a production route which optimises their effect, then thinner gauge material could be used which would reduce the overall weight of such components. This optimisation implies that if the residual stresses are of opposite sign to the service stresses, then part of the service load will go toward reducing their magnitude, which is generally beneficial to the likelihood of failure.

However residual stresses cannot be precisely determined as Procter and Beaney[15] report that errors of approximately 10% to 15% can be expected in measurements, using the hole drilling method, when the yield strength of the material is approached. Nickola[16] found under similar experimental conditions, to Procter and Beaney, that the error using stainless steel plate was around 20%. The experimental procedure followed by these investigators involved applying a standard 3-element strain rosette to an annealed plate specimen and upon zero balancing the bridge circuit the specimen is loaded to the proportional limit of the material and the strain values indicated by the three elements recorded. Now under the loaded (pre-stressed) condition the hole is drilled and the relaxed strains recorded. The principal stresses calculated from the relaxed strain values should then bracket the pre-stressed value.

Schajer[17] reports that residual stress magnitudes which do not exceed 80% of the original yield strength of a material contain minimal error. However, if this percentage is exceeded then, the residual stress magnitude should be taken at the 80% yield value. The present author is not sure whether this 80% of original yield value holds true for plastically

deformed sheet metal components because through work hardening a material, both yield and tensile strength increase. This is illustrated in Figure 2.5.

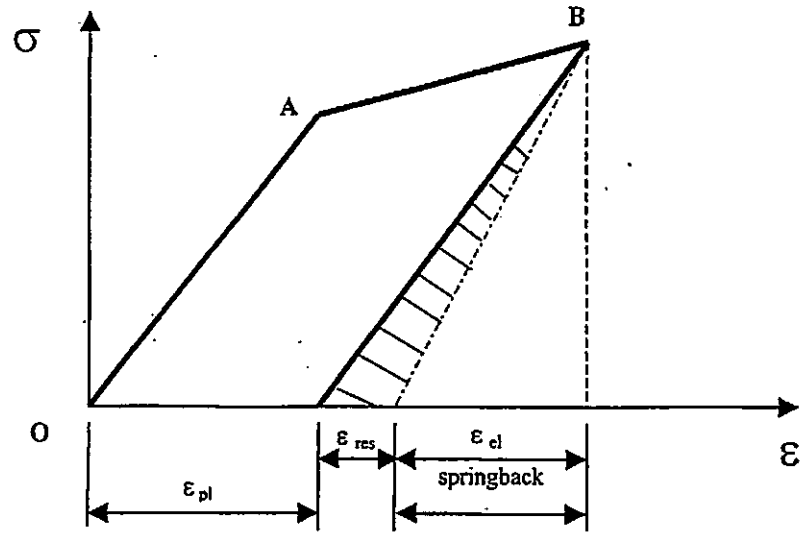

Figure 2.5 - Illustration of springback.

The hatched area in Figure 2.5 represents full relief of the residual (elastic) strain energy after springback. This residual (elastic) strain energy is representative of the residual stress that remains in the component after deformation has occurred. Under this condition, the residual stress magnitude could exceed 80% of the original yield strength (point A) of the material. This will however be evaluated when analysing the relieved residual stresses in the production stage components of the centre disc at a later stage in this project.

2.6 FATIGUE

Components formed from sheet metal are often subjected to cyclic loads during their service life and therefore the following comments on fatigue are felt important to this project. Fatigue of materials refers to the process of micro-plastic deformation, crack initiation and subsequent propagation resulting from the application of cyclic loads. Research into fatigue phenomena dates back to the nineteenth century and has long been concerned with formulating engineering approaches to design against fatigue crack initiation, propagation and failure. Fatigue of materials has emerged as a major area of

scientific and applied research which encompasses such diverse disciplines as materials science, mechanical, civil and aerospace engineering, bio-mechanics, applied physics and applied mathematics[18].

Fatigue failure investigations over the years have led to the observation that the fatigue process embraces two domains of cyclic stressing or straining that are amenable to different types of modelling. One domain of cyclic loading is that in which significant plastic strain occurs during each cycle. This domain is associated with high loads and short lives, or low numbers of cycles to produce fatigue failure, and is commonly referred to as *low-cycle* fatigue. Life prediction is generally via strain-based modelling. The other domain of cyclic loading is that for which the strain cycles are largely confined to the elastic range. This domain is associated with lower loads and long lives, or high numbers of cycles to produce failure, and is commonly referred to as *high-cycle* fatigue. Life prediction in this region uses stress-based equations.

Components formed from sheet metal are normally associated with high-cycle fatigue as the required life is usually "infinite". Low-cycle fatigue is typically associated with cycle lives from one up 10^4 cycles, and high-cycle fatigue for lives greater than 10^5 cycles. Fatigue, although a complex subject, is relatively well understood and techniques for life prediction are available to designers who are increasingly challenged by demands for components/products having higher performance, higher speeds, lighter weight, higher reliability and longer life – and all this to be achieved at reasonable cost and with shorter production times.

2.6.1 Total life or S-N approach to fatigue

The S-N approach was first used by Wöhler around 1860, to predict the fatigue performance of railway axles[19]. This approach is still widely used in design applications

where the applied stress is primarily within the elastic range of the material and the required lives (cycles to failure) are long. The two most common procedures for obtaining S-N data are the rotating-bending and reverse bending fatigue tests. In these approaches smooth test specimens are typically machined to provide a waisted (hour-glass) gauge length which is loaded in plane bend (reverse bending) and rotating bend cyclic loading conditions. S-N test data is usually presented on a graph in terms of stress amplitude, σ_a, against the number of cycles to failure, N_f, and is most useful for materials which work-harden[20].

S-N curves for ferritic steels show a fatigue limit, σ_e, (between 30 to 50% of the ultimate tensile strength for most steels), which is a stress level below which the material has an infinite life[9,20,21]. For most engineering steels the fatigue limit can be taken as the stress corresponding to $2x10^6$ cycles.

If the fatigue test is carried out with a tensile mean stress then, in order that the specimen last for the same number of cycles as a similar specimen tested under zero mean stress conditions, the stress amplitude (σ_{max}) in the latter case will have to be reduced. The fact that tensile mean stresses enhances the fatigue life or endurance limit is important and a number of investigations have been undertaken to establish the quantitative effect of tensile mean stresses[22,46].

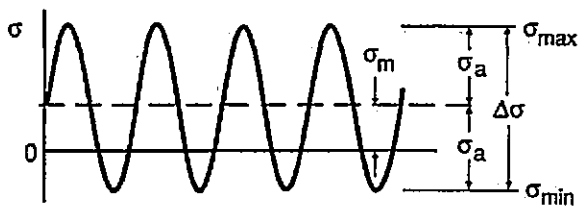

Figure 2.6[10]. – Terminology used for fluctuating tension stress cycle producing a positive (tensile) mean stress.

The following relationships and definitions are generally used when discussing mean and alternating stress;

$$Stress\ Range,\ \Delta\sigma = \sigma_{max} - \sigma_{min} \quad \text{.....(2.6)}$$

$$Stress\ Amplitude,\ \sigma_a = \frac{\sigma_{max} - \sigma_{min}}{2} \quad \text{.....(2.7)}$$

$$Mean\ Stress,\ \sigma_m = \frac{\sigma_{max} + \sigma_{min}}{2} \quad \text{.....(2.8)}$$

$$Stress\ Ratio,\ R = \frac{\sigma_{min}}{\sigma_{max}} \quad \text{.....(2.9)}$$

$$Amplitude\ Ratio,\ A = \frac{\sigma_a}{\sigma_m} \quad \text{.....(2.10)}$$

The R and A values corresponding to several common loading conditions are:

$$Fully\ reversed: \quad R = -1 \quad A = \infty \quad \text{.....(2.11)}$$

$$Zero\ to\ Maximum: \quad R = 0 \quad A = 1 \quad \text{.....(2.12)}$$

$$Zero\ to\ Minimum: \quad R = \infty \quad A = -1 \quad \text{.....(2.13)}$$

The results of fatigue tests with a non zero mean stress are usually plotted on a Haigh Diagram (alternating stress versus mean stress) with lines representing constant life drawn through the data points. Since the tests required to generate a Haigh diagram (Figure 2.7) for a particular material are expensive and time consuming, several empirical relationships have been developed to generate the line defining the infinite-life design region.

These methods (see Figure 2.8) use various curves to connect the endurance limit (S_e) on the alternating stress (σ_a) axis, to either the yield strength (S_y) or ultimate strength (S_u) or true fracture stress, σ_f, on the mean stress axis.

The following relationships according to Bannantine et. al.[20] are:

$$Gerber: \quad \frac{\sigma_a}{S_e}+\left(\frac{\sigma_m}{S_u}\right)^2=1 \qquad (Germany, \quad 1874) \qquad (2.14)$$

$$Goodman: \quad \frac{\sigma_a}{S_e}+\frac{\sigma_m}{S_u}=1 \qquad (England, \quad 1899) \qquad (2.15)$$

$$Soderberg: \quad \frac{\sigma_a}{S_e}+\frac{\sigma_m}{S_y}=1 \qquad (USA, \quad 1930) \qquad (2.16)$$

$$Morrow: \quad \frac{\sigma_a}{S_e}+\frac{\sigma_m}{\sigma_f}=1 \qquad (USA, \quad 1960) \qquad (2.17)$$

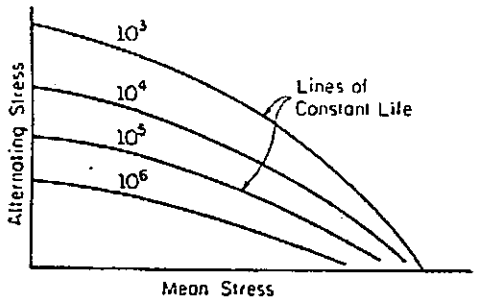

Figure 2.7[20]. - Haigh diagram

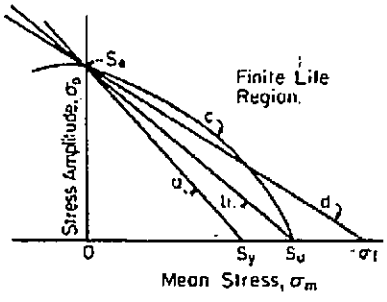

Figure 2.8[20]. – Comparison of mean stress results, a - Soderberg; b - Goodman; c – Gerber and d - Morrow.

Many authors[9,21] discussing the subject of fatigue, state that residual stress affects the fatigue performance of components and, as mentioned by Bannantine et. al.[20], the residual stress is coupled to the mean stress through arithmetic superposition of the residual static and applied cyclic stresses. This implies that the mean stress level in the applied cycle is either raised or lowered depending on the sign of the residual stress. If both mean and residual stresses are tensile in nature, then the effective mean stress level will represent the sum of the two. The same condition will apply if both mean and residual stresses are compressive in nature.

However, if the mean stress is compressive in nature and the residual stress tensile, then the mean stress level will be the difference of the two magnitudes and would either be tensile or compressive depending on the greater of the two values. Hence, if a fatigue test is supposedly carried out under zero mean stress conditions and the component has not been stress relieved (annealed), then in fact, the component is fatigued at a mean stress equal to the magnitude of the residual stress.

These mean stress models will be used when predicting the fatigue life of the automotive wheels where the assessed residual stress magnitudes will be included in these model equations. It is however not clear at this stage as to how the waisted hour-glass specimens will be fatigue tested, i.e. under mean stress or zero mean stress conditions, as the residual stresses in these specimens would have been significantly altered due to their removal from the production stage components. Clearly, a review of residual stress literature is relevant to the work in this project.

CHAPTER 3

METHODS FOR RESIDUAL STRESS ASSESSMENT IN FORMED COMPONENTS

As discussed in the last Chapter, residual stresses[23], which are often present in components, can have either damaging, or favourable effects on the fatigue strength characteristics depending on whether they act in the same sense as the service load stresses or the opposite one. The residual stress state arises from plastic deformation, micro-structural effects and differential heating and cooling rates within a component. The resultant fatigue properties reflect the complex interactions between these effects, but detailed knowledge of the residual stress state will assist in developing life prediction models, and in refining production process parameters to achieve improved component performance.

Despite the extremely large number of publications on the topic of residual stresses, the complexity of the issue means that detailed knowledge of the residual stress distribution for a particular component remains difficult and tedious to obtain. An objective of the present project is a better understanding of residual stresses in wheel centre discs, the processes that give rise to them and, their effect on service properties. This knowledge should eventually assist in the optimisation of sheet metal forming technology.

3.1 METHODS AVAILABLE FOR RESIDUAL STRESS ASSESSMENT

The following methods have been used for residual stress investigations[2]:-

- Progressive turning and boring;
- Layer removal;
- Trepanning or ring method;
- Chemical etch;
- Stresscoat brittle lacquer drilling;

- Magnetic method;
- Hardness studies;
- Ultrasonics;
- Modified layer removal;
- Photoelasticity;
- Hole drilling method;
- X-Ray diffraction;
- Neutron diffraction;

Further details of the techniques can be found in reference [2, 24].

Of these techniques, the most frequently applied are layer removal (either mechanically or chemically), hole drilling and X-ray measurement procedures. Occasionally, large scale sectioning of a component after initially coating the surface with a photo-elastic coating, a brittle lacquer or marking a grid, is useful for the semi-quantitative assessment of the type and level of residual stresses present. In each case the relaxed stresses cause deformation in the coating or grid and are therefore capable of interpretation. In the case of the brittle lacquer method the surface is coated with a proprietary brittle lacquer such as "tenslac" and after drying, is then drilled with a small hole at the point of interest. The relieved residual stresses, if of significant magnitude, will then produce a crack pattern in the lacquer that can readily be evaluated in terms of stress magnitude and type.

The layer removal, progressive turning or boring, trepanning, chemical etch, modified layer removal and hole drilling methods all rely on basically the same principle. The component is either machined, etched or drilled in stages so that the residual stresses are progressively released producing relaxations, deformations, or strains which can be measured by either mechanical methods or electrical resistance strain gauges and, after certain corrections, related to the initial residual stresses.

X-ray techniques are well established but limited to the measurement of strains at, or very near to, the surface and require very sophisticated equipment if reasonably accurate results are to be achieved. Ultrasonic and magneto-elastic methods have, until recently, not received much attention despite the promise which they show. Grain orientation and other metallurgical inhomogeneities affect the velocity and attenuation of ultrasonic waves and further development of the technique is required to effectively separate these effects from the changes due to residual stress.

The physical principles of residual stress measurement by neutron diffraction and that of X-ray diffraction are identical. The X-ray diffraction method however, is limited to sub-surface conditions (i.e. micron depths). With neutron diffraction however, the residual stresses can be measured through the thickness of a component. Both methods measure the elastic strain within the component, which is the ideal condition. The limitations with regard to these methods are that three principal strain measurements need to be taken.

The selection of an appropriate method will depend mainly upon the geometry of the component to be analysed, the number of analysis points to be taken per component and the time and cost per analysis point. These parameters will now be discussed with a view to select the most appropriate method to be used in this work.

3.2 JUSTIFICATION OF HOLE DRILLING TECHNIQUE FOR CENTRE DISCS

The profile of the centre disc, being dish shaped, limits the selection from the abovementioned methods for residual stress assessment. The main reason is that all these methods require the analysis location on the component to be set-up perpendicular to the measuring device. This limits methods such as the layer removal, X-ray and neutron

diffraction as areas around the cup radius region (see Figure 3.1) would be inaccessible for residual stress measurement by these methods. Another limitation in these methods is the size of the component, particularly when the centre disc on a complete wheel (centre disc and rim) requires analysis.

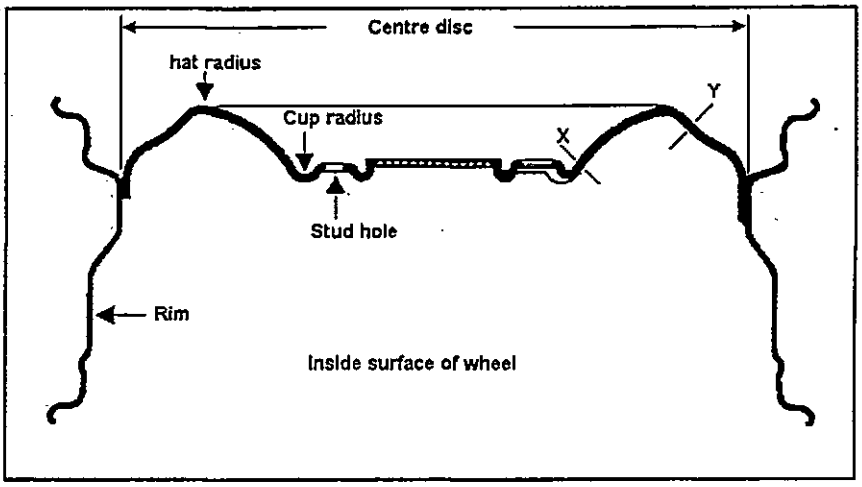

Figure 3.1. - Cross-section of complete wheel.

The area around the cup radius region is of prime importance to this project, as fracture occurs along a diametral plane just above the cup radius, see Figure 3.1, during industrial fatigue testing conditions. This fracture plane is approximately 15mm from the apex of the cup radius. Therefore, the simplest methods whose equipment would be accessible to this diametral plane are the air-abrasive system[27] (AAS) and the high-speed hole drilling[28,29,30,31] (HSHD) systems, both of which rely on strain gauge measurements. The accessible areas for these two methods is shown between 'X' and 'Y' in Figure 3.1. The position marked 'X' is 13mm from the apex of the cup radius, and is hence close to the observed fracture plane in wheel tests.

Of these two methods, the high-speed hole drilling strain gauge technique was chosen for the following reasons:

- The time to produce stress results using the AAS technique is approximately four to five hours as opposed to two hours using the HSHD system, component preparation time being similar;

- The possible number of stress results obtained using the AAS is limited to four/five when drilling to a hole depth of 2mm, whereas with the HSHD system the full stress distribution is obtained.
- A HSHD system was available in the Technikon whereas the AAS, of which there are two in South Africa, was not available in Port Elizabeth.

The HSHD was therefore used for all residual stress assessment purposes and the application of the technique will now be discussed in detail.

3.3 APPLICATION OF HIGH SPEED HOLE DRILLING TECHNIQUE

Mathar [23], reported the first results from residual stress measurements and involved drilling a hole in the surface of a component while recording the strain reaction on the surface. Since then there have been many investigations into this subject[15,17,31,32,33]. The hole drilling method is one of the least destructive of the mechanical methods, is relatively simple and economical and, as a result, has gained increasing importance. The hole drilling method [23], involves the application of a special three-element strain gauge rosette, see Figure 3.2, onto the surface of the component, centered at the measurement location. A small hole is then drilled into the component through the centre of the rosette. The production of the hole in the (stressed) material causes a relaxation of strains to occur near the hole, which can be detected and measured by the surface-mounted strain gauges. These strain measurements can then be used to calculate the original residual stresses in the component at the hole location. The development of advanced data-analysis

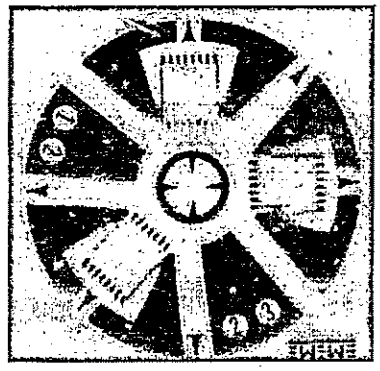

Figure 3.2. - 3-element strain rosette for residual stress assessment.

development of advanced data-analysis techniques to extract information about variation of stress with depth from the hole-drilling method has become an important aspect of assessing the integrity of a component or structure.

3.3.1 Residual stress calculation

Residual stresses are calculated using specific formulae[29]. Input is the relieved strains measured by a strain rosette that is glued to the prepared surface of a component. A hole is drilled in stages through the centre of the gauge into the component. These stages are known as incremental depths and after each incremental depth, the relieved strains are measured and recorded by a strain amplifier. The maximum and minimum relieved stresses are calculated according to ASTM E837.94a[29], where:-

$$\sigma_{max} \& \sigma_{min} = \frac{\varepsilon_3 + \varepsilon_1}{4\overline{A}} \pm \frac{\sqrt{(\varepsilon_3 - \varepsilon_1)^2 + (\varepsilon_3 + \varepsilon_1 - 2\varepsilon_2)^2}}{4\overline{B}} \quad \text{.....(3.1)}$$

Where: σ_{max} & σ_{min} - maximum and minimum principal stresses present at the hole location after drilling;

ε_1, ε_2 & ε_3 - relieved strains measured by the radially aligned strain grids;

$\overline{A}$ & $\overline{B}$ - calibration constants.

The negative square root in equation (3.1) is associated with σ_{max} because the calibration constants $\overline{A}$ and $\overline{B}$ have negative numerical values. Thus, a negative strain value will produce a positive relieved residual stress value. The following equations are used to obtain the constants $\overline{A}$ and $\overline{B}$ which include the integrating effect of a finite size strain gauge, the given material properties and the blind hole situation (a blind hole is a hole that is drilled to some depth in a material other than through the material), and is obtained by:

$$\overline{A} = -\left[\frac{1+\nu}{2E}\right]\overline{a} \quad \text{.....(3.2)} \qquad \overline{a} = \left[\frac{D_o^2}{2GW(R_2 - R_1)}\right](\theta_1 - \theta_2) \quad \text{.....(3.3)}$$

$$\overline{B} = -\left[\frac{1}{2E}\right]\overline{b} \quad \text{.....(3.4)} \qquad \overline{b} = \left[\frac{D_o^2}{2GW(R_2 - R_1)}\right] \quad \text{.....(3.5)}$$

Where: $\overline{a}$ & $\overline{b}$ - dimensionless material independent coefficients (see table 3.1);

E - Modulus of elasticity;

ν - poisson's ratio;

GW - grid width;

$(R_2 - R_1)$ - grid length;

$(\theta_1 - \theta_2)$ - measured angle corresponding to grid length;

D_o - drilled hole diameter.

Figure 3.3 shows a schematic representation of a typical residual stress and strain distribution around a hole drilled into a specimen.

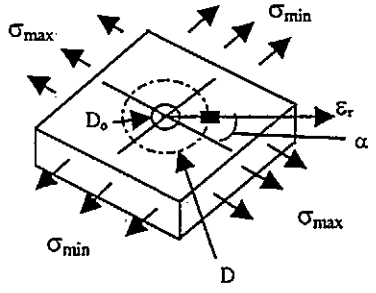

Figure 3.3. – Typical stress distribution around a drilled hole.

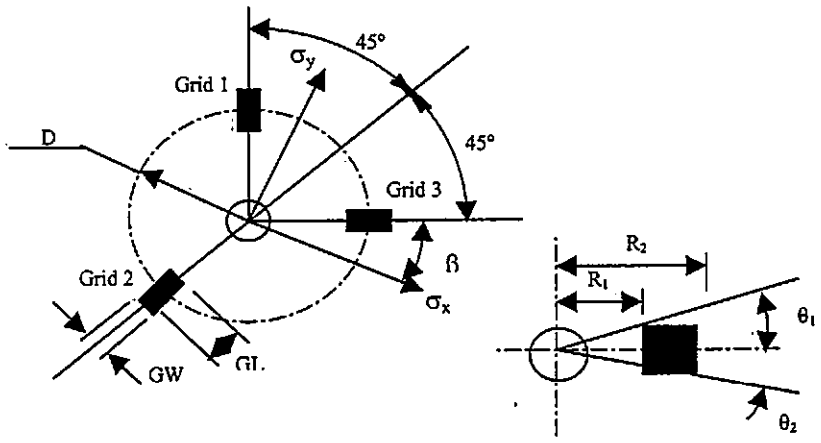

Figure 3.4. – Important parameters related to the 3-element strain rosette.

A typical three-element (clockwise) strain gauge rosette used for the hole drilling method is shown in Figure 3.4, where:-

ε_r = relieved strain measured by a radially aligned strain gauge centred at P;

α = angle measured counter-clockwise from the direction of σ_{max} to the direction of ε_r;

D = diameter of the gauge circle;

D_o = diameter of the drilled hole.

D_o/D	Through-the-thickness hole [A]		Blind hole, depth = 0.4D	
	$\bar{a}$	$\bar{b}$	$\bar{a}$	$\bar{b}$
0.30	0.089	0.278	0.111	0.288
0.31	0.089	0.295	0.118	0.305
0.32	0.101	0.312	0.126	0.322
0.33	0.108	0.329	0.134	0.340
0.34	0.114	0.347	0.142	0.358
0.35	0.121	0.364	0.150	0.376
0.36	0.128	0.382	0.158	0.394
0.37	0.135	0.400	0.166	0.412
0.38	0.143	0.418	0.174	0.430
0.39	0.150	0.436	0.182	0.448
0.40	0.158	0.454	0.190	0.466
0.41	0.166	0.472	0.199	0.484
0.42	0.174	0.490	0.208	0.503
0.43	0.183	0.508	0.217	0.521
0.44	0.191	0.526	0.226	0.540
0.45	0.200	0.544	0.236	0.558
0.46	0.209	0.562	0.246	0.576
0.47	0.218	0.579	0.255	0.594
0.48	0.228	0.596	0.265	0.612
0.49	0.237	0.613	0.275	0.630
0.50	0.247	0.629	0.285	0.648

Computed from reference [29]

Table 3.1. - Numerical Values of Coefficients for $\bar{a}$ and $\bar{b}$.

The above method is the most commonly used technique for data analysis and was developed by Rendler and Vigness[31] but should only be used for uniform stress field conditions, as it does not take any depth variation of stresses into account[30].

A typical result for relieved residual stresses, according to ASTM 837.94(a), is shown in Figure 3.5.

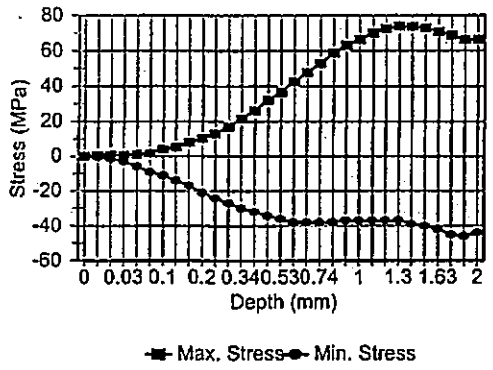

Figure 3.5. - Typical residual stress result showing full stress relief at a depth of 1.3 mm.

3.3.2 Measurement of non-uniform residual stresses

Schajer in 1987 provided information comparing various stress calculation procedures for the measurement of non-uniform residual stresses using the hole drilling method. In part I of his paper[17] the following methods were assessed:

3.3.2.1 Incremental Strain Method

This method was first introduced by Soete and Vancrombrugge[32] and further developed by Kelsey[33]. It involves measuring the strain relaxation after successive small increments in depth of the drilled hole. The stresses originally existing within each hole depth increment are then calculated by assuming that the incremental strain relaxation is wholly due to the stresses that existed within that depth increment. This assumption is however incorrect. After the first hole depth increment is drilled, subsequent strain relaxation combines the effect of the stresses contained within the new hole depth increment.

3.3.2.2 Average Stress Method

In order to overcome the theoretical shortcomings of the Incremental Strain Method, Schajer[34] introduced a new stress calculation method using the concept of equivalent uniform stress. This equivalent uniform stress is the uniform stress acting over the total hole depth that produces the same total strain relaxation as the actual non-uniform stress distribution. This method also has a significant shortcoming, in that it assumes that the equivalent uniform stress equals the average stress over the hole depth.

This would be true only if the stresses at all the depths within a given hole depth contribute equally to the strain relaxation measured at the surface. Both the Incremental Strain and the Average Stress Methods are unsatisfactory, and do not work well with non-uniform stress fields because they are calibrated using uniform stress field data.

3.3.2.3 Power Series Method

This method was introduced by Schajer[17] as an approximate, but theoretically acceptable method of calculating non-uniform stress fields from incremental strain data. Finite element calculations are used to compute a series of coefficients for the strain response equations when hole drilling into stress fields with power series variation with depth. These strain responses are then used as basic functions in a least-squares analysis of the measured strain relaxation. A limitation of this method is that it is suitable only for smoothly varying stress fields.

3.3.2.4 The Integral Method

Bijak-Zochowski[35], Niku-Lari[36], and Flaman and Manning[37] made initial developments in this area. This method is best suited to cases where the residual stress field varies abruptly and is the most general of the four methods described above. Schajer concludes in his paper, Part II[34], that the Integral method is most viable and practical procedure for computing non-uniform residual stresses from strain relaxation data measured using the incremental hole drilling method. The calibration coefficients (see Table 3.1) needed for practical applications have been evaluated using finite element calculations and are tabulated for a range of hole radii and depths.

3.3.2.5 The Schwarz-Kockelmann Method[28]

With the hole-drilling method the residual stresses in the vicinity of the hole are not completely released. In this respect, it is not permissible to determine the residual stresses from measured relaxed strains using the Hooke's Law formula, which is employed in general stress analysis. Calibrations using experimental and/or computational methods need to be carried out, taking account of the partially released character. Here the deformation reaction for a known stress state is found using the main significant parameters in the technique (mainly strain gauge and hole drilling geometrical

parameters). In the experimental calibration, the residual stresses are simulated by external loading stresses, normally in a uni-axial tensile or bending test. The effect of unknown residual stresses in the material used for the calibration sample must be eliminated by only considering the strains associated with the differences in loading (applied) stresses. With the numerical calibration, for example by using the finite element method, this problem does not occur. The basic procedure during the calibration for finding the calibration functions and their application during the determination of residual stresses on actual components is shown in Figure 3.6:

The calibration measurement or computation needs to be carried out only once and the strains in the loading direction ε_x and in the direction perpendicular to it, ε_y, are recorded at each stage of depth. From these results the calibration functions $K_x(\xi)$ and $K_y(\xi)$ are calculated as follows under consideration of the elastic constants for the material and for the uni-axial load σ:-

$$K_y(\xi) = -\left[\frac{E}{\nu\sigma}\right]\left[\frac{d\varepsilon_y(\xi)}{d\xi}\right] \quad \text{.....(3.6)}$$

$$K_x(\xi) = \left[\frac{E}{\sigma}\right]\left[\frac{d\varepsilon_x(\xi)}{d\xi}\right] \quad \text{.....(3.7)}$$

Where, E is Young's Modulus, ν is Poisson's Ratio and ξ, the hole depth z referred to the hole diameter D_o (normalised depth); $\xi = z/D_o$. The curve of this calibration function is shown in Figure 3.7 with an example of the rosette type RY61S 1.5/120 with a hole diameter of 1.83 mm. After the measurement on the component (lower part of Figure 3.6) the recorded strains are converted into the required residual stresses using the calibration functions:

$$\sigma_a(\xi) = \frac{E}{\left(K_x(\xi)\right)^2 - \nu^2\left(K_y(\xi)\right)^2}\left[K_x(\xi)\frac{d\varepsilon_a(\xi)}{d\xi} + \nu K_y(\xi)\frac{d\varepsilon_c(\xi)}{d\xi}\right] \quad \text{.....(3.8)}$$

$$\sigma_b(\xi) = \frac{E}{\left(K_x(\xi)\right)^2 - \nu^2\left(K_y(\xi)\right)^2}\left[K_x(\xi)\frac{d\varepsilon_b(\xi)}{d\xi} + \nu K_y(\xi)\left(\frac{d\varepsilon_a(\xi)}{d\xi} + \frac{d\varepsilon_c(\xi)}{d\xi} - \frac{d\varepsilon_b(\xi)}{d\xi}\right)\right] \quad \text{.....(3.9)}$$

$$\sigma_c(\xi) = \frac{E}{\left(K_x(\xi)\right)^2 - \nu^2\left(K_y(\xi)\right)^2}\left[K_x(\xi)\frac{d\varepsilon_c(\xi)}{d\xi} + \nu K_y(\xi)\frac{d\varepsilon_a(\xi)}{d\xi}\right] \quad \text{.....(3.10)}$$

With the aid of relationships from Mohr's circle the principal stresses σ_1 and σ_2 and the angle of orientation α can be found:-

$$\sigma_1 \& \sigma_2 = \frac{\sigma_a(\xi) + \sigma_c(\xi)}{2} \pm \frac{1}{\sqrt{2}}\sqrt{\left(\sigma_a(\xi) - \sigma_b(\xi)\right)^2 + \left(\sigma_c(\xi) - \sigma_b(\xi)\right)^2} \quad \text{.....(3.11)}$$

$$\alpha(\xi) = \frac{1}{2}\arctan\frac{2\sigma_b(\xi) - \sigma_a(\xi) - \sigma_c(\xi)}{\sigma_a(\xi) - \sigma_c(\xi)} \quad \text{.....(3.12)}$$

These equations may appear somewhat complicated for the evaluation of practical measurements and their manual evaluation would be very tedious and time consuming. However, with modern measurement systems and suitable software the complexity associated with the evaluation diminishes. The calibration functions form a constituent part of the evaluation software programme incorporated in the RESTAN system.

The REsidual STress ANalysis (RESTAN) System is fully automatic and its functions are software controlled. Consisting of four main components, namely, drilling device, strain amplifier, electronic control unit and computer. The drilling device houses an optical eyepiece for aligning the endmill (burr) with the drilling location of the strain rosette, it also contains a stepper motor providing the feed of the endmill during the drilling operation. The electronic unit controls the air supply to the air turbine located in the drilling head of the drilling device. The amplifier, upon instruction from the software programme, measures the strain magnitudes detected by the strain gauges. The software programme controls all the sequential steps during the drilling operation. More details of the system is given in Section 4.4, Chapter 4.

A graphical presentation of residual stress with depth distribution according to the Swartz and Kockelmann method is shown in Figure 3.8.

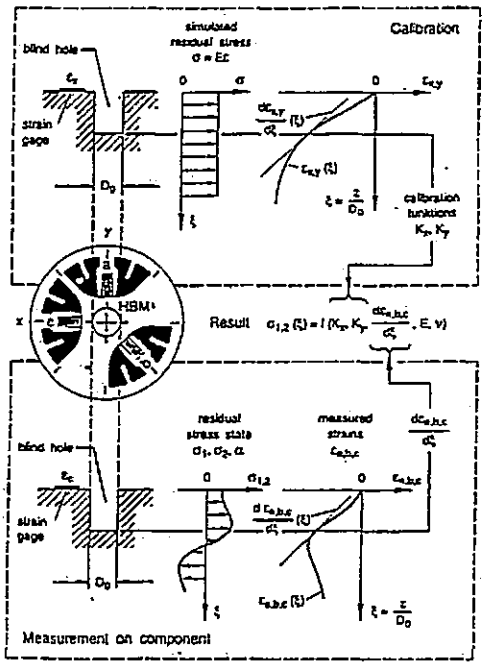

Figure 3.6[28]. - Calibration principle with simulated uni-axial loading and measurement of the strains on the component.

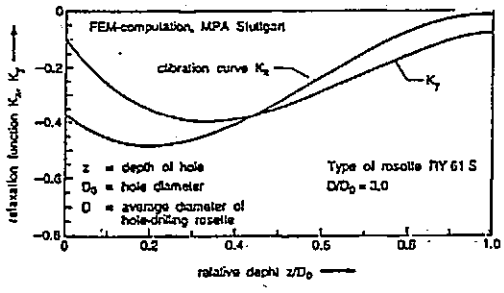

Figure 3.7[28]. - Calibration functions K_x and K_y for the HBM rosette type RY 61S 120.

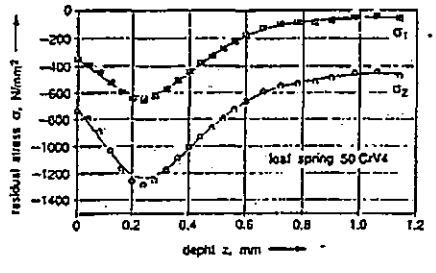

Figure 3.8[28]. - Typical residual stress result showing magnitudes with depth distribution according to Swartz and Kockelmann.

3.4 SUMMARY

The method described by Rendler and Vigness[31] forms the basis of the ASTM 837.94(a)[29] method of calculation and is mainly employed for determining the *bulk relieved residual stress* at a particular location on a component under investigation, see Figure 3.5 . Its use is also intended for uniform stress fields i.e. homogeneous and isotropic type materials. Although most materials fall outside this classification, the results of a typical analysis remain acceptable as long as the trend of the graph is smoothly varying (as indicated in Figure 3.5) and not abruptly varying. With non-uniform residual stress measurement methods the objective is to determine the actual relieved magnitude after each particular depth of cut until the final hole depth is achieved, thus portraying the actual stress distribution through the hole depth. The ASTM 837.94(a) method of calculation indicates the average relieved residual stress magnitude, which is referred to the surface of the specimen, after each particular depth of cut.

For the purposes of this research project, the ASTM 837.94(a) method will be used for all residual stress calculations.

CHAPTER 4

ASSESSMENT OF RESIDUAL STRESSES IN PURE BEND COMPONENTS

Many researchers and scientists have contributed, over the years, to the development of residual stress assessment technology since first reported by Mathar[23]. All of these workers regard residual stress analysis as a technique whose use is restricted to homogeneous and isotropic type materials[28,29]. This implies that there is no guarantee that acceptable results will be obtained in highly textured materials. Residual stress assessment by hole drilling is still widely regarded as yielding variable results which are difficult to interpret in relation to the overall stress field. This lack of certainty has a negative impact on promoting the beneficial effect of residual stresses through manipulating and controlling their magnitude and sense in the optimisation of product performance.

Residual stress assessment forms an important part of this project, in which a link will be sought between residual stress and fatigue performance of sheet metal components produced by forming operations. These sheet metal formed components are subjected to high instantaneous tensile forces which induce a multi-axial stress state in the component. This stress state is complex in nature and difficult to assess analytically, and is likely to interact with texture in the plate to obscure interpretation of hole drilling data.

A programme of work was therefore undertaken in order to obtain a feel for the influence on hole drilling residual stress measurements of texture arising from plastic deformation, and to assess the reliability and repeatability of the technique. This was done on plate specimens bent to specific angles around a fixed radius. The accuracy of experimental data for this pure bend case can be verified against first order analytical calculations.

This Chapter describes this part of the work, which led to the development of a novel eight-element strain rosette. This new customised rosette is better suited to situations that lead to ovality of drilled hole than are 3-element strain rosettes.

4.1 PREPARATION AND PRODUCTION OF BEND SPECIMENS

Four bend specimens, 250mm long were cut along the rolling direction of 4.1mm thick dual phase steel plate and machined to widths 35, 40 and 45mm. These specimens were then bent round a 20mm radius and in addition, one 40mm wide specimen was bent round a 24mm radius. The bending apparatus used was a manually operated rig consisting of a horizontal arm to which a U-bracket is attached at the pivot end, see Figure 4.1. This U-bracket houses a 75mm diameter roller that is free to rotate about its own pivotal axis during the bending operation.

The main pivot bolt passes through the U-bracket as well as a fixed bar (die) around which the plate specimens are bent. Attached to the free end of the arm is a spring balance scale which is pulled to bend the specimen allowing the pulling force to be recorded from the reading indicated by the spring balance scale. These specimens were bent progressively from 0° to 150°, at 30° intervals, with the bend angle measured by securing a protractor through the main pivot bolt.

The following parameters were recorded:

- Bend angles;
- Pulling force;
- Springback angle;
- Springback load, i.e. the load required to bend the plate from its springback position to that initial angle of bend, see Figure 4.3.

The spring balance scale [make: Salter-235 (250N)] was calibrated for use in the horizontal plane which indicated a –6% difference to the values when used in the vertical plane. This error was attributed to the internal friction forces resulting from the horizontal application.

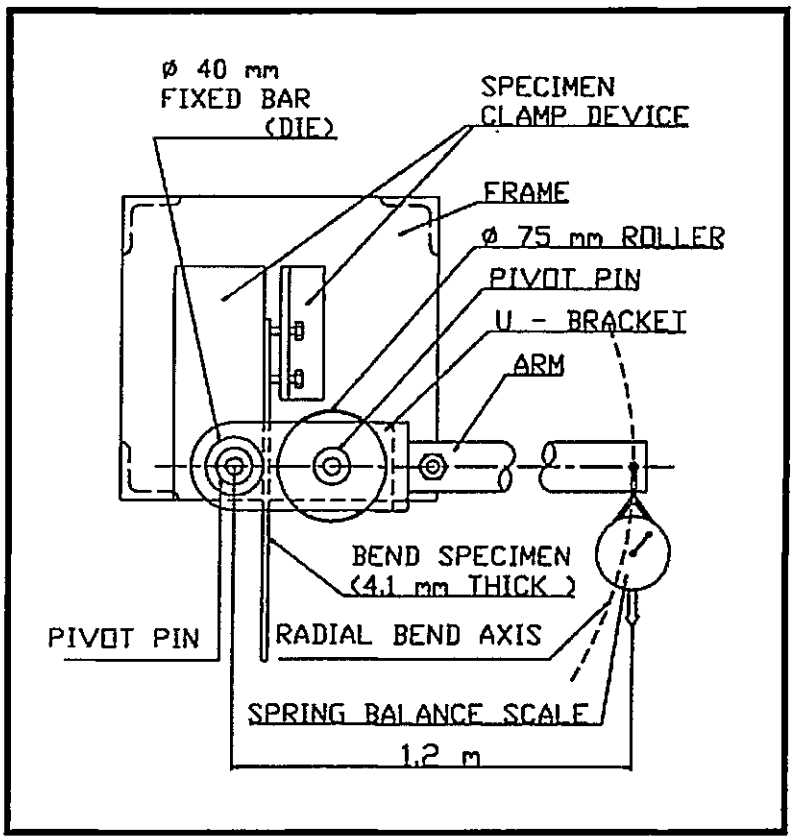

Figure 4.1. – Illustration of bending apparatus.

A typical bend specimen using the above apparatus is shown in Figure 4.2.

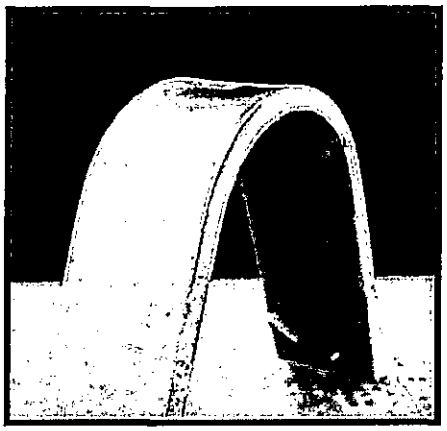

Figure 4.2. – Typical bend specimen.

The results of the bending analysis were corrected for the calibration error observed, and the corrected values are shown in Table 4.1.

	Angle (tot. incl.) (deg)	Applied Load (N)	Average Applied Load (N)	Spring-back Angle (deg)	Spring-back Load (N)	Average Spring-Back Load (N)
Specimen width 35mm	0					
	0 – 30	37.9	39.04	6	32.33	35.03
	30 – 60	37.9		8.3	36.57	
	60 – 90	38.03		11	37.63	
	90 – 120	40.55		13	34.72	
	120– 150	40.81		15	33.92	
Specimen width 40mm						
	0					
	0 – 30	44.52	44.94	5.8	42.4	42.51
	30 – 60	45.05		8.2	42.93	
	60 – 90	44.52		11.3	44.52	
	90 – 120	45.58		13.2	40.28	
	120 – 150	45.05		15.1	42.4	
Spec. width 40mm, 24mm bend radius						
	0					
	0 – 30	46.11	47.34	6.1	42.4	44.51
	30 – 60	47.7		9.5	43.99	
	60 – 90	48.26		13	47.1	
	90 – 120	47.7		15	45.05	
	120 – 150	46.91		16.5	43.99	
Specimen width 45mm						
	0					
	0 – 30	50.35	54.69	6	49.29	48.81
	30 – 60	51.4		8.5	49.82	
	60 – 90	51.4		11	50.61	
	90 – 120	60.4		13.5	45.58	
	120 – 150	59.9		15	48.76	

Table 4.1. – Results of bend testing.

The following points were observed during the bending operation:

- Because of the slow bend rate, the applied load during bend angle intervals of 30° remained constant, i.e. consider the 45mm wide specimen, where the indicated load of 50.35N remained constant from 0° through to the 30° position.
- The applied and springback load magnitudes increased with increased specimen width while springback angle and percentage elongation remained approximately constant irrespective of specimen width. This implies that springback angle and percentage elongation is a function only of the material thickness and bend radius.

- The springback load is indicative of the yield load (strength) for the subsequent bend interval. This is illustrated using values from the 40mm width – 24mm bend radius specimen where points C, F, I, L and O is indicative of this yield load (strength), in the Load – Angular Displacement graph shown in Figure 4.3.

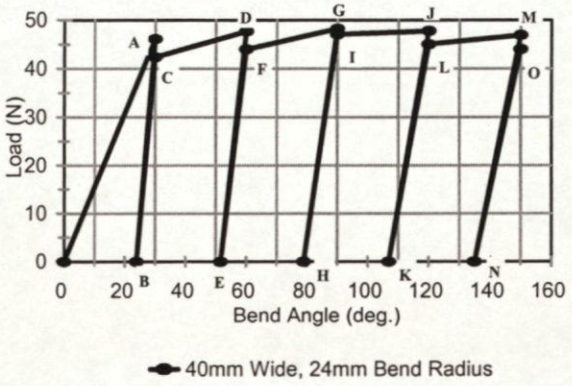

Figure 4.3. – Typical flow curve of the 40mm wide bend specimen, 24mm bend radius.

4.2 STRAIN GAUGE APPLICATION

The four bend specimens were now prepared for strain gauge application in an area around the apex of the bend. Micro Measurements strain rosettes type EA-06-062 UM-120 were used and applied such that the reference grid (grid number 1, G1 – see Figure 4.4) was aligned in the rolling direction of the steel sheet. This direction also corresponds to the bending axis of the specimens. The 3-element strain rosette was applied at the centre of the width and on the apex of the bend, see Figure 4.4.

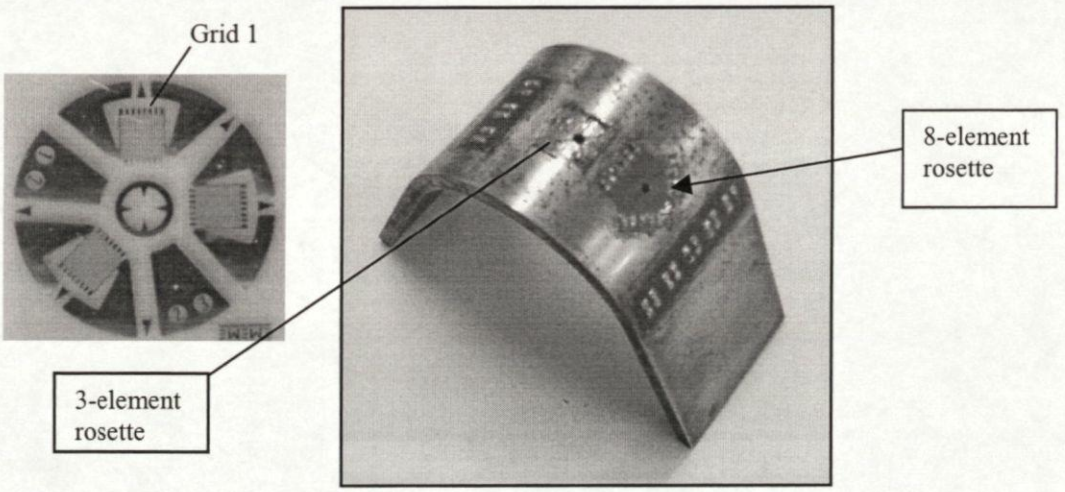

Figure 4.4. – Bend specimen indicating the positions of the three- and eight-element strain rosettes.

4.3 HOLE DRILLING PROCEDURE USING THE RESTAN SYSTEM

4.3.1 Machine description

A RESTAN high speed end mill drilling system was used, serial number 0012. The equipment or system consists of four (4) main components described as follows:-

4.3.1.1 Mechanical and optical device

The mechanical and optical device, shown in Figure 4.5, consists of a small work centre with three axes, housing the vertical-drilling head which incorporates an optical device and a high speed air turbine motor. The device is positioned on three adjustable stainless steel feet containing magnets, and ball joints on the feet allow for inclined positioning of the device. The base of the device consists of an X-Y movement platform and motion

Figure 4.5. – Frame and drilling device.

takes place via hardened steel pins and precision bearings to nullify radial clearances. Horizontal movement is actuated manually by knurled knobs and the displacement is measured by dial test indicators while fast vertical motion of the drilling head is obtained through a rack & pinion system. The drilling head houses an air turbine motor which rotates at 300 000 rpm under a pressure of 4.5 bar, and an inverted end mill is taper locked to the centre bore of the air turbine. The optical device situated in the drilling head allows

for the alignment of the end mill with the drilling location on the strain rosette as well as for hole measurement after the drilling operation. Finally, the drilling head is controlled by a stepper motor providing the vertical feed during the drilling operation.

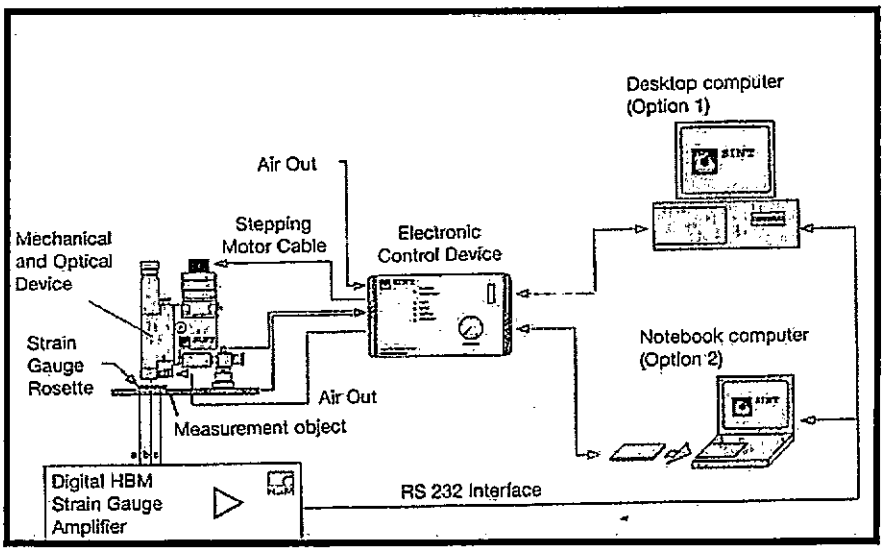

Figure 4.6. – RESTAN System layout.

The drilling of a hole can be carried out under different programmed sequences according to the software choice selected. The software allows for the drilling method to be carried out either manually (step by step) where the operator needs to instruct the software program to commence the subsequent drilling stage or automatically where the software program controls the whole operation. Stress evaluation is either by the linear method, where all the steps selected to drill a particular depth are of equal size or the polynomial method, where smaller steps are taken closer to the surface of the component which increase in size as the hole depth increases.

The controllable parameters available for selection by the analyst are:-

- the number of steps to drill a particular hole depth;
- the delay time setting;
- the feed rate of the end mill; and
- evaluation method (linear or polynomial), as the turbine speed is fixed at 300 000rpm.

4.3.1.2 MGC Amplifier

The three elements of the strain rosette are individually connected to separate channels at the rear end of the MGC amplifier as 4-wire quarter bridge circuits and record the strain readings at the end of each incremental cut after the delay time has lapsed. This amplifier has only three channels and is not unique to the residual stress assessment system, but merely acts as a slave unit within the system as a whole. It can be seen on the LHS above the computer screen in Figure 4.7.

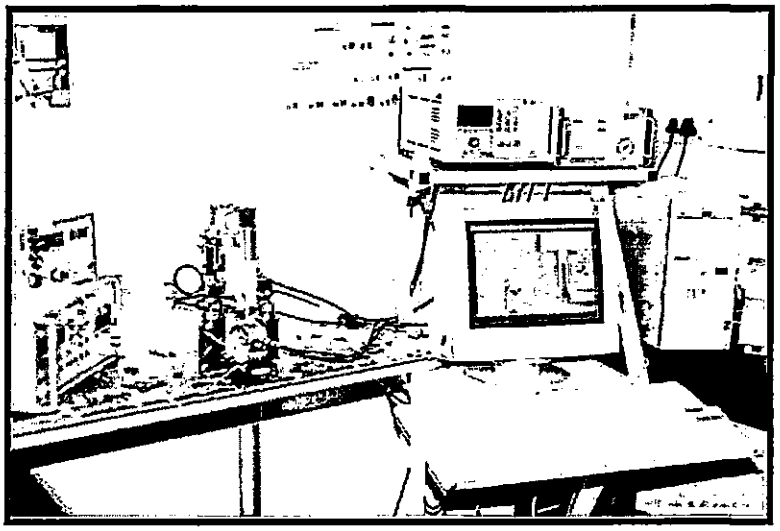

Figure 4.7. – Residual Stress Equipment.

4.3.1.3 Electronic device

Seen on the RHS of the amplifier, this unit is the heart of the system interfacing the computer signals with the solenoid valve that controls the air supply to the turbine motor, and with the stepper motor during the drilling operation.

4.3.1.4 Software programme

The programme used in this work was developed by SINT Technology of Italy in collaboration with HBM of Germany. It controls all functions of the electronic unit and amplifier, and processes all strain data, providing a spreadsheet containing all the relevant data necessary for the determination of the principal stresses.

4.3.2 Selecting the drilling parameters

For assessment of the residual stresses induced in the bend specimens, the following drilling parameters were used in the programme:

- Drilling depth: 2mm;
- Drilling method: Automatic;
- Evaluation method: Polynomial;
- Number of incremental drilling steps: 30;
- Feed rate: 0.2mm/minute;
- Delay time: 10 seconds.

These drilling parameters were chosen on the basis of a preliminary investigation undertaken to assess the optimum parameters for residual stress analysis using the RESTAN system, the recommendations are given in Appendix F.

After aligning the drilling head with the drilling location on the strain gauge, the drilling machine and specimen were secured to the worktable and the amplifier wiring was soldered to the strain gauge, upon which the drilling operation commenced.

4.4 RESIDUAL STRESS RESULTS

The results of the maximum tensile relieved residual stresses using the standard 3-element strain rosette as shown in Figure 4.8, are given in Table 4.2:

SPECIMEN	Max. Tensile Relieved Residual Stress (MPa)	Full Stress Relief Depth (mm)	Bend Radius (mm)
35mm Wide	27	1.4	20
40mm Wide	73	1.4	20
40mm Wide	27	1.4	24
45mm Wide	64	1.51	20

Table 4.2. – Maximum tensile relieved residual stress results.

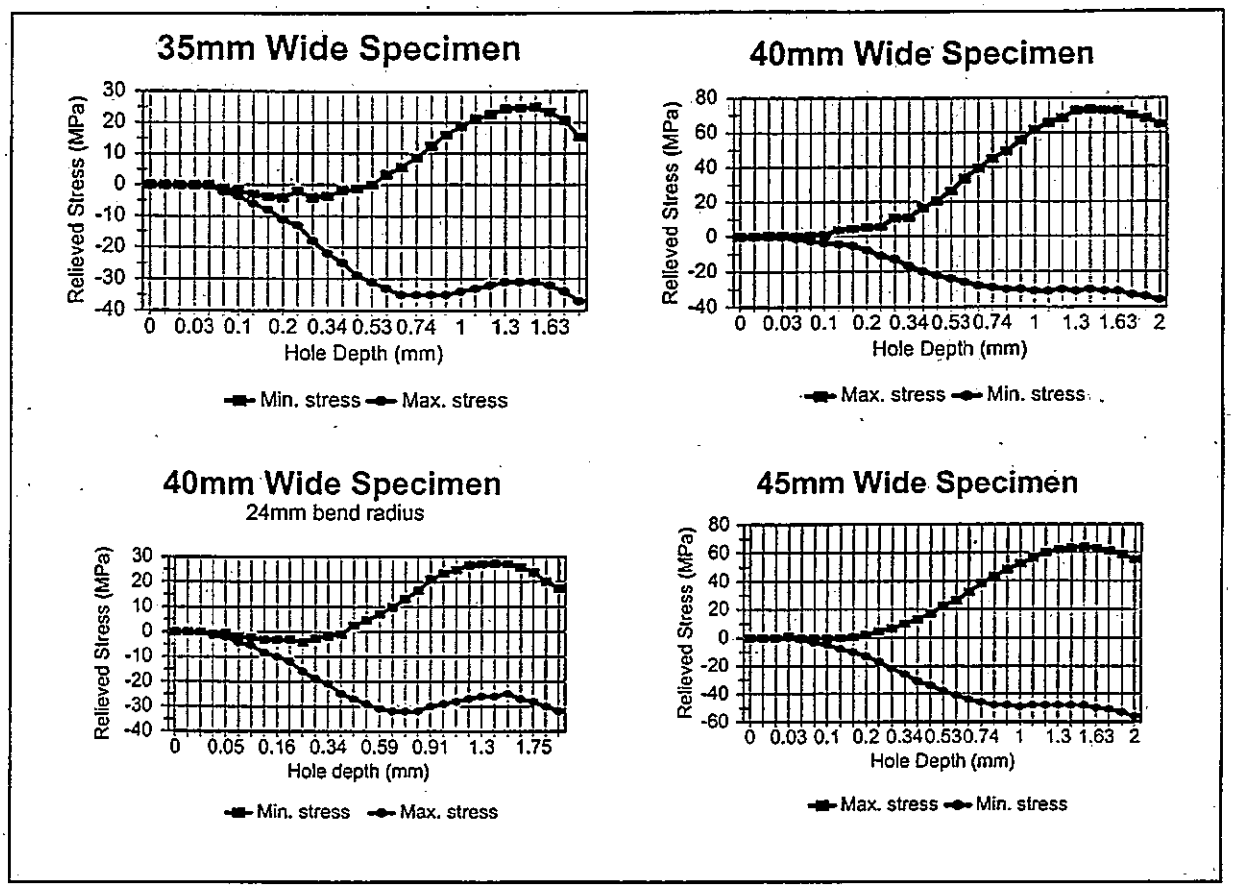

Figure 4.8. – Maximum and Minimum relieved principal stresses.

An attempt was made to analytically verify these results by use of the values given in Table 4.1 and considering simple elastic/plastic-bending theory[7]. In this approach the following points are important to the application of the theory with respect to the analysis:

- Residual stresses arise from the stored elastic (recoverable) strain energy within the plastically deformed component. When a hole is drilled into such a component, the relaxation of this energy is detected by the strain rosettes allowing for the principal relieved residual stresses to be determined.
- Residual stresses are therefore, of an elastic nature and thus elastic/plastic-bending theory should apply, under pure plastic bending conditions. Residual stresses can be approximated by considering the partially plastic bending moment (plastic flow moment) and the yield moment through each bending stage.

4.4.1 Analytical verification of residual stress results – Approach 1

The hypothesis taken in this approach is based on the assumption that had the bending operation been carried out in one uninterrupted stage (i.e. from 0° through 150°) the average applied and springback values as indicated in Table 4.1 would possibly have been revealed. Hence, for purposes of the verification method the average values related to the 45mm wide specimen are considered, thus:

The yield moment [M_y] can be calculated from the average springback load value over the 5 intervals, given in Table 4.1.

Therefore:

$$Moment\ \ at\ \ Yield,\ \ M_y = 48.81 \times 1.2 = 58.57 Nm$$

and the average value of the plastic flow moment [M_{pfm}] to continue yield over a 30° bend interval (Table 4.1) is:

$$Plastic\ \ Flow\ \ Moment,\ \ M_{pfm} = 54.69 \times 1.2 = 65.63 Nm$$

Hence the residual stresses can be considered to be derived from the residual moment [$M_{residual}$,] which is the difference between the plastic flow moment [M_{pfm}] and the moment at yield [M_y] under pure bending conditions, thus

$$M_{residual} = \left[M_{pfm} - M_y\right]$$

$$= \left[65.63 - 58.57\right]$$

$$= 7.06\ \ Nm$$

Now, the residual stress is given by the elastic bending equation, which is:

$$\sigma_{residual} = \frac{M_{residual} \times y}{I} \qquad MPa$$

where

$$y = \frac{t}{2} = \frac{4.1 \times 10^{-3}}{2} = 2.05 \times 10^{-3} \quad m$$

and

$$I = \frac{Width \times thickness^3}{12} = \frac{0.045 \times 0.0041^3}{12} = 2.584 \times 10^{-10} \quad m^4$$

thus

$$\sigma_{residual} = \frac{7.06 \times 2.05 \times 10^{-3}}{2.584 \times 10^{-10}}$$

$$\sigma_{residual} = 56.00 \qquad MPa$$

Note that the maximum relieved residual stress as assessed for the 45mm wide specimen, was 64 MPa (Table 4.2). Therefore, the percentage error between the assessed and calculated values is:

$$Percentage \quad Error = \left[1 - \frac{56.00}{64.00}\right] \times 100 = 12.5\,\%$$

Table 4.3 presents the results of this analysis for all four bend specimens using the average applied and springback load values.

Specimen	Actual Measured relieved residual stress values (MPa)	Calculated stress values (MPa)	% Error
35mm Wide	27	38.17	29.3
40mm Wide	73	23.13	68.3
40mm Wide (24mm bend radius)	27.4	26.94	1.7
45mm Wide	64	56	12.5

Table 4.3. – Verification results according to Approach 1.

50% of the results appear satisfactory as Procter and Beaney[15] report that at yield for the material error margins of 10% can be expected with respect to experimentally assessed residual stress values and 15% with respect to analytical verification methods thereof.

An alternative solution to the above approach was considered to analytically verify the experimental results obtained. This will now be discussed.

4.4.2 Alternative solution to verification of experimental results – Approach 2.

The underlying philosophy in this approach, being more specific than the previous, considers values pertaining to the particular bend interval within which the experimental measurements were taken. Here, each bend interval (of which there are 5) is considered to resemble a particular forming stage. What is also important in this approach is the assumption of approximating the induced residual stress magnitude from a previously formed and assessed component, i.e. the residual stress magnitudes taken in similar locations on components from two consecutive forming stages are subtracted, this difference then being indicative of the estimated induced magnitude with respect to the previously formed stage.

The assumption taken for this verification solution, is that the plate specimens were not annealed prior to the bending operation and therefore the residual stress magnitude of the "as manufactured" plate (assessed at 36MPa - see section 4.6.3) should be subtracted from the residual stress values assessed on the apex of the bends. This difference then being indicative of the induced residual stress, had the initial flat plate specimen been annealed. Applying this hypothesis, the solution is as follows: Firstly, the need to define the location of the apex of the bend (refer Figure 4.4) in terms of the bend interval is important, i.e. between which two bend angles does the apex reside. This was achieved by bisecting the

final bend angle of 135°, (i.e. 150° minus the springback angle of 15°), to give the apex angle. Thus,

$$Apex\ \ Angle = \frac{135^{\circ}}{2} = 67.5^{\circ}$$

From Table 4.1 it is clear that this apex angle will be constant for all four bend specimens, and falls within the 60° - 90° bend angle interval. Here, the yield moment [M_y] can be calculated from the springback load assessed at the 60° bend angle and the plastic flow moment [M_{pfm}] from the applied load at the 90° bend angle position, see Figure 4.3 (flow curve for a bend specimen). Let's again consider the values related to the 45mm wide specimen, thus:

$$Yield\ \ Moment,\ \ M_y = 49.82 \times 1.2 = 59.784Nm$$

and the

$$Plastic\ \ Flow\ \ Moment,\ \ M_{pfm} = 51.4 \times 1.2 = 61.68Nm$$

Now, the residual moment [$M_{residual}$] from which the residual stress can be calculated, is the arithmetical difference between the plastic flow moment and yield moment, under pure bending conditions, therefore:

$$M_{residual} = \left[M_{pfm} - M_y\right]$$

$$= \left[61.68 - 59.784\right]$$

$$= 1.896Nm$$

Now, the residual stress is given by the elastic bending equation, which is:

$$\sigma_{residual} = \frac{M_{residual} \times y}{I} \qquad MPa$$

where

$$y = \frac{t}{2} = \frac{4.1\times10^{-3}}{2} = 2.05\times10^{-3} \quad m$$

and

$$I = \frac{Width \times thickness^3}{12} = \frac{0.045\times0.0041^3}{12} = 2.584\times10^{-10} \quad m^4$$

thus

$$\sigma_{residual} = \frac{1.896\times2.05\times10^{-3}}{2.584\times10^{-10}}$$

$$\sigma_{residual} = 15.04 \qquad MPa$$

Now applying the above philosophy, the estimated residual stress induced will be:

$$\sigma_{residual\ (estimated)} = \sigma_{residual\ (apex)} - \sigma_{residual\ ("as\ manuf" plate)}$$

$$= 64 - 36$$

$$= 28 \quad MPa$$

and, the percentage error is given by:

$$percentage\ \ error\ \ = \left[1 - \frac{\sigma_{calculated}}{\sigma_{estimated}}\right] \times 100$$

$$= \left[1 - \frac{15.04}{28}\right] \times 100$$

$$= 46\%$$

The percentage errors for the remaining bend specimens after application of the above procedure are indicated in Table 4.4.

Specimen	$\sigma_{residual\ (apex)}$	$\sigma_{residual\ (\text{"as manuf."})}$	$\sigma_{residual\ (estimated)}$	% Error
35mm Wide	27	36	9	50
40mm Wide	73	36	37	54
40mm Wide (24mm bend radius)	29	36	7	85
45mm Wide	64	36	28	46

Table 4.4. – Results for alternate analytical solution – Approach 2.

Whilst no improvement in the above results are evident the procedure followed in this approach warrants merit as will be observed in Section 4.5, where the effect of hole ovality is investigated.

4.5 EXAMINATION OF THE DRILLED HOLES

The drilled holes in each of the four bend specimens were analysed for roundness and it was found that none were truly round (see Figure 4.9). The drilled holes in each specimen were slightly oval and, furthermore, the major axis of these ovalities did not lie in the same relative direction in each bend specimen.

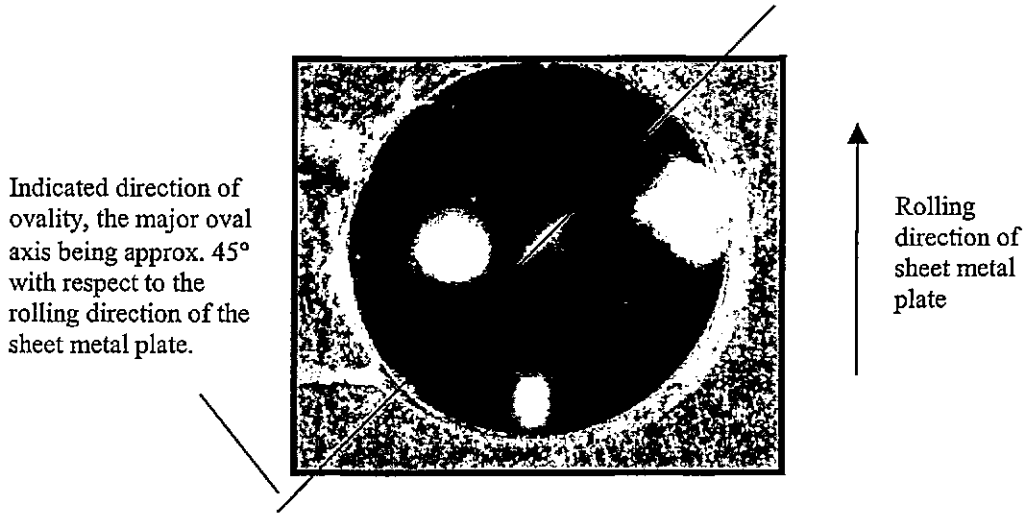

Figure 4.9. – Typical hole ovality of the 45mm wide bend specimen. The ovality is attributed to anisotropy.

This ovality indicates that plastically deformed steels are neither isotropic nor homogeneous in their residual stress assessment behaviour. Because of this ovality the individual elements of the three-element strain rosette would not necessarily be orientated

so as to detect the absolute maximum relieved strains and thus may not indicate the absolute maximum relieved principal residual stresses. This hypothesis is illustrated in Figure 4.10 where the hole ovality lies in such a direction that the maximum relieved strains will not be detected.

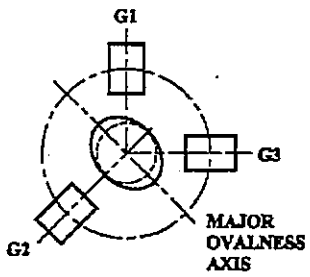

Figure 4.10. – Illustration of a clockwise 3-element rosette showing hole ovality.

It is clear from the above discussion that merely applying a 3-element strain rosette would not necessarily reveal the absolute maximum result at a particular analysis location. In order to detect the absolute maximum relieved residual stress the strain relaxation round the hole periphery should be assessed by a larger number of elements. To achieve this, strain rosettes should be placed at smaller yet equal angular displacements around the hole. This led to the development of a strain rosette that would detect the effects of hole ovality irrespective of its angular orientation with respect to the absolute maximum relieved principal strains in plastically deformed plate components.

4.6 DEVELOPMENT OF AN 8-ELEMENT STRAIN ROSETTE

In order to provide a strain rosette that will detect the uneven strain relaxations around an oval drilled hole a customised 8-element strain rosette was developed. This was achieved

The author wishes to bring to the attention of the reader that an eight-element strain rosette is obtainable through AMTEC TECHNIQUIP (South Africa) who are agents for the Japanese strain gauge manufacturers TOKYO SOKKI KENKYUJO. This strain rosette is not however freely available and in order to purchase, one must channel the application through a Prof H. Abe of the OSAKA INSTITUTE of TECHNOLOGY. The part number of this rosette is TML-FLA-05-8R and is quoted in "*Handbook of measurement of residual stresses*", Society for Experimental Mechanics, 1996. ISBN 0-88173-229-X. The SA Patent was already taken out by the time this information was brought to the attention of the author.

by using three Micro Measurement edge rosettes CEA-06-062UM-120 of the type shown in Figure 4.11.

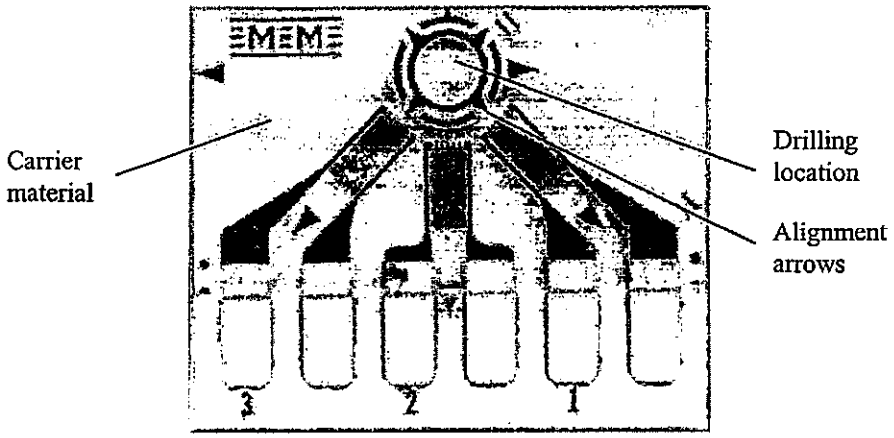

Figure 4.11. – Micro Measurement edge rosette (CEA-06-062UM-120).

The customisation procedure was as follows:

The edge rosettes were superimposed one on top of the other in succession using the alignment arrows at the drilling location as reference and removing the excess carrier material to form a butt type joint along the cutting edge. The completed customised strain rosette is shown in Figure 4.12.

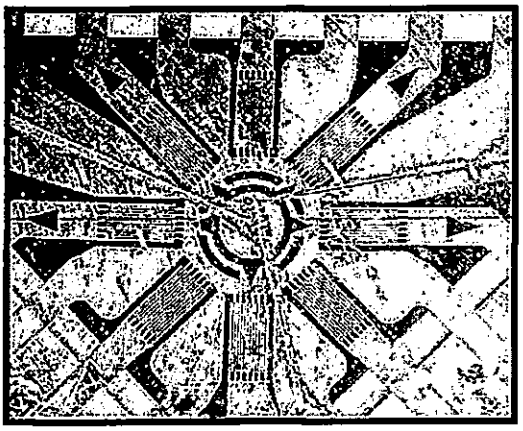

Figure 4.12. – Actual customised 8-element strain rosette after removal of the carrier material.

The eight elements are numbered in a clockwise direction starting with the uppermost as grid number 1 (G1) in Figure 4.12 and illustrated in Figure 4.13.

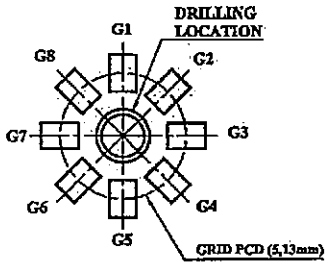

Figure 4.13. – Illustration of element numbering sequence.

By using the same residual stress calculation method as given in ASTM 837.94(a)[29] for a 3-element rosette, eight results are obtained by rotating the standard 3-element combination in sequence around the 8-element system. The standard clockwise 3-element rosette is numbered as shown in Figure 4.14.

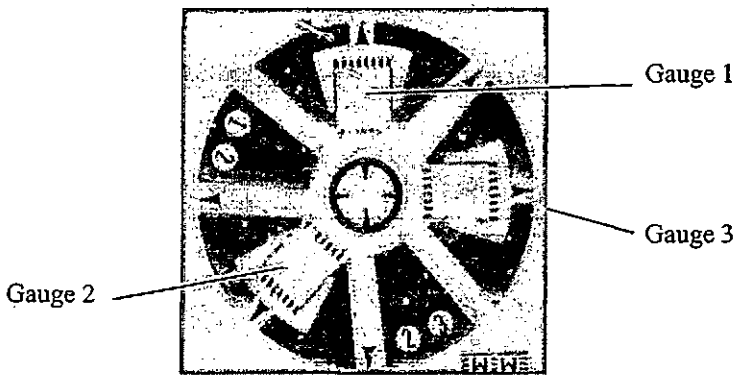

Figure 4.14. – Standard Micro-Measurement clockwise 3-element rosette, EA-06-062-UM-120.

For example, the relative positions of the individual elements shown in Figure 4.13, i.e. 1,2,3, are representative of element positions 1,6,3 in Figure 4.12. Now by rotating, in a clockwise manner, the 1,2,3 combination of a standard rosette to the adjacent (clockwise) gauge on the 8-element rosette, the combination 2,7,4 is obtained. Therefore, the eight 3-element (clockwise, CW) combinations obtained from an 8-element strain rosette are [1,6,3], [2,7,4], [3,8,5], [4,1,6], [5,2,7], [6,3,8], [7,4,1] and [8,5,2]. Thus by using the 8-element strain rosette the absolute maximum relieved residual stress magnitude will be detected and assessed irrespective of hole ovality.

4.6.1 Re-assessment of relieved residual stresses in the bend plates using the 8-element strain rosette

These customised strain rosettes were applied to the same bend specimens previously analysed, but at an angle of 45° from the apex of the bend – refer Figure 4.4.

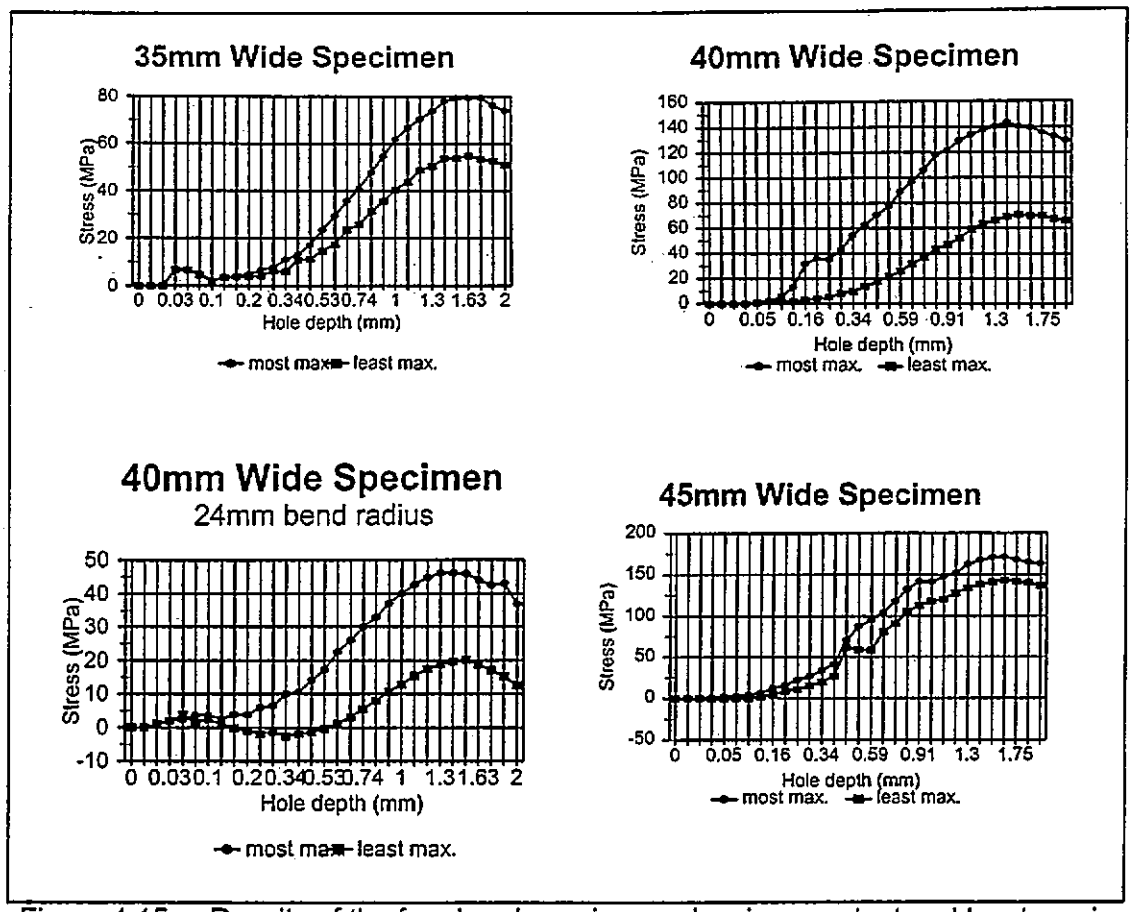

Figure 4.15. – Results of the four bend specimens showing greatest and least maximum relieved residual stress magnitudes.

Using the 8-element strain rosette the maximum and minimum relieved residual stress results relating to the 40mm wide, 24mm bend radius specimen are given in Table 4.5.

CW	Max. (MPa)	Min. (MPa)	Edge	Max. (MPa)	Min. (MPa)
1,6,3	21	-8.7	1,2,3	22.2	-9.8
2,7,4	36.5	-13	2,3,4	27.1	-2.48
3,8,5	20.2	-17	3,4,5	24.2	-21
4,1,6	41.9	-5	4,5,6	46.1	-9.2
5,2,7	36.2	-14	5,6,7	34.7	-12
6,3,8	23.9	-1	6,7,8	34.7	-12
7,4,1	37.9	-6.1	7,8,1	36.9	-5.1
8,5,2	25.2	-15	8,1,2	20.6	-11
Average Maximum relieved Residual Stress = 31 MPa					

Table 4.5. – Typical result of the 40mm wide bend specimen, 24mm bend radius, using the 8-element customised strain rosette.

As an example, consider the case of a standard three-element rosette orientated as gauge (1,6,3) in Table 4.5. Here the indicated maximum stress is 21 MPa, which is 54% less than the absolute maximum stress of 46.1 MPa indicated by edge gauge combination 4,5,6. This highlights the fact that residual stress measurements suffer from substantial variability due to small hole ovality. The results for the remaining three bend specimens are given in Table 4.6.

CW	ACW	Max. (MPa)	Min. (MPa)	Edge	Max. (MPa)	Min. (MPa)
1,6,3	3,6,1	79.5	-34	1,2,3	75.1	-30
2,7,4	4,7,2	72.28	-27	2,3,4	74.5	-30
3,8,5	5,8,3	65	-38	3,4,5	72.3	-44
4,1,6	6,1,4	68.3	-35	4,5,6	74.8	-42
5,2,7	7,2,5	61.7	-39	5,6,7	65.5	-43
6,3,8	8,3,6	62.7	-52	6,7,8	60	-49
7,4,1	1,4,7	71.6	-32	7,8,1	63.8	-24
8,5,2	2,5,8	61.7	-40	8,1,2	54.9	-33
Average Maximum relieved Residual Stress =68 MPa						

35mm Wide Specimen

CW	ACW	Max. (MPa)	Min. (MPa)	Edge	Max. (MPa)	Min. (MPa)
1,6,3	3,6,1	78.8	-43	1,2,3	76.7	-41
2,7,4	4,7,2	117	-52	2,3,4	107	-43.6
3,8,5	5,8,3	71	-57	3,4,5	94	-80
4,1,6	6,1,4	134	-32	4,5,6	143	-42
5,2,7	7,2,5	89.4	-50	5,6,7	91	-52
6,3,8	8,3,6	72.1	-56	6,7,8	84	-68
7,4,1	1,4,7	110	-50	7,8,1	92.4	-33
8,5,2	2,5,8	84.7	-56	8,1,2	70.8	-42
Average Maximum relieved Residual Stress = 95 MPa						

40mm Wide Specimen

CW	ACW	Max. (MPa)	Min. (MPa)	Edge	Max. (MPa)	Min. (MPa)
1,6,3	3,6,1	171	-8.7	1,2,3	172	-10
2,7,4	4,7,2	143	-20	2,3,4	160	-37
3,8,5	5,8,3	170	-9.4	3,4,5	167	-6.5
4,1,6	6,1,4	146	-14	4,5,6	146	-15
5,2,7	7,2,5	144	-17	5,6,7	143	-16
6,3,8	8,3,6	170	-9.4	6,7,8	153	-7.5
7,4,1	1,4,7	143	-15	7,8,1	148	-20
8,5,2	2,5,8	164	-12	8,1,2	164	-12
Average Maximum relieved Residual Stress = 157 MPa						

45mm Wide Specimen

Table 4.6. – Maximum and Minimum relieved residual stress values for the 35mm, 40mm and 45mm wide bend specimen (20mm bend radius), as assessed using the 8-element strain rosette.

4.6.1.1 Analytical verification of experimental results using the 8-element strain rosette

The aim of the verification approaches and hypothesis followed is in the first instance, to acquire reliability and repeatability with the hole drilling technique and consequently raise the confidence level of the analyst. Secondly, these approaches would indicate the best manner in which the results should be used, i.e. using the peak assessed value or the average of the peak assessed values. For the approaches that follow, the same analytical procedure is adopted as that previously used in section 4.4.1 and hence the mathematical layout of the solution is not presented but the results of the verification approaches will be tabulated instead. Consideration is given to three verification approaches and these are as follows:

- **Approach 3.**

In this approach the average calculated residual stresses taken from Table 4.3 (using the average applied loads given in Table 4.1 – approach 1) and the average maximum relieved residual stresses taken from Tables 4.5 & 4.6, are considered. The hypothesis taken in this approach is that if the magnitudes of the relieved strains correlate with hole ovality, then the concept of using the average maximum relieved residual stress values has validity. The results of this approach are shown in Table 4.7.

Specimen	Average Calculated Stress (approach 1) (MPa)	Average Maximum Relieved Residual Stress (MPa)	% Error
35mm Wide	38.17	68	44
40mm Wide	23.13	95	76
40mm Wide (24mm bend radius)	26.94	31	13
45mm Wide	56	157	64

Table 4.7. – Results of Approach 3, using 8-element concept.

Only one result from the above approach is within acceptable limits.

- **Approach 4**

This approach considers the specific bend interval within which the measurement were taken (as used in approach 2) and the absolute maximum relieved residual stress magnitude assessed using the 8-element strain rosette. Here the specific bend interval falls within the 90° – 120° bend angle and thus the yield moment was calculated from the springback load at 90° and the plastic flow moment from the applied load at 120°. The hypothesis in this approach being the same as in approach 2, i.e. that the residual stress magnitude of the "as manufactured" plate (now a maximum of 38.7 MPa – see Table 4.10) be deducted from the absolute maximum assessed residual stress magnitudes in the bend specimen, this gives the estimated induced residual stress value. Table 4.8 shows the result taken in this approach.

Specimen	Calculated Stress (using specific bend interval) (MPa)	Estimated Induced Residual Stress Magnitude (MPa)	% Error
35mm Wide	35.7	(79.5 – 38.7) = **40.8**	12.5
40mm Wide	11.6	(143 – 38.7) = **104.3**	89
40mm Wide (24mm bend radius)	6.2	(46.1 – 38.7) = 7.4	16.2
45mm Wide	93.6	(172 – 38.7) = **133.3**	30

Table 4.8. – Results of Approach 4, using 8-element concept.

In this approach 50% of the results indicated in Table 4.8 are considered satisfactory.

- **Approach 5**

The philosophy taken in this approach considers the specific bend interval within which the measurement was taken (between the 90° and 120° bend angle) and the average maximum relieved residual stresses taken from Tables 4.5 & 4.6, but considers the hypothesis of approach 2, where the residual stress magnitude of the "as manufactured" plate is subtracted from average maximum relieved residual stress magnitude to give the estimated induced average maximum relieved residual stress magnitude.

Specimen	Calculated Stress (using specific bend interval) (MPa)	Estimated Induced Average Maximum Relieved Residual Stress (MPa)	% Error
35mm Wide	35.7	(68 – 38.7) = **29.3**	18
40mm Wide	11.6	(95 – 38.7) = **56.3**	79
40mm Wide (24mm bend radius)	6.2	(38.7 – 31) = **7.7**	19
45mm Wide	93.6	(157 – 38.7) = **118.3**	20

Table 4.9. – Results of Approach 5, using the 8-element concept.

Of the three approaches followed, 4 and 5 give acceptable results. The hypothesis taken in these two approaches is assumed scientifically sound, as the residual stress value of the annealed plate would have an influence on the experimental values obtained in the bend specimens. Whilst in laboratory type investigations, such as on pure bend specimens, the applied loading and subsequent stresses can be determined, the applied loads/stresses in many industrial manufactured components are difficult to measure and hence approaches such as carried out in 3, 4 & 5 are important in terms of assessing reliability.

It follows that the method employed in approaches 4 and 5, (i.e. using the absolute peak value and the average of the absolute peak values), will be employed when residual stress values, using the 8-element rosette, are correlated to hardness and fatigue performance at a later stage in the project (see Chapter 7).

4.6.2 Re-examination of hole ovality using the 8-element strain rosette

The residual stress assessment holes drilled using the 8-element strain rosette were re-examined in terms of hole ovality. In order to show the effect of this hole ovality, a polar plot was developed (see Figure 4.16) relating the strain relaxation values from each individual strain grid to the angular orientation of the hole ovality. For the purposes of this polar plot, the results of the 35mm wide bend specimen were used. The principal direction as calculated according the ASTM 837.94(a) method are, also indicated with respect to the hole ovality.

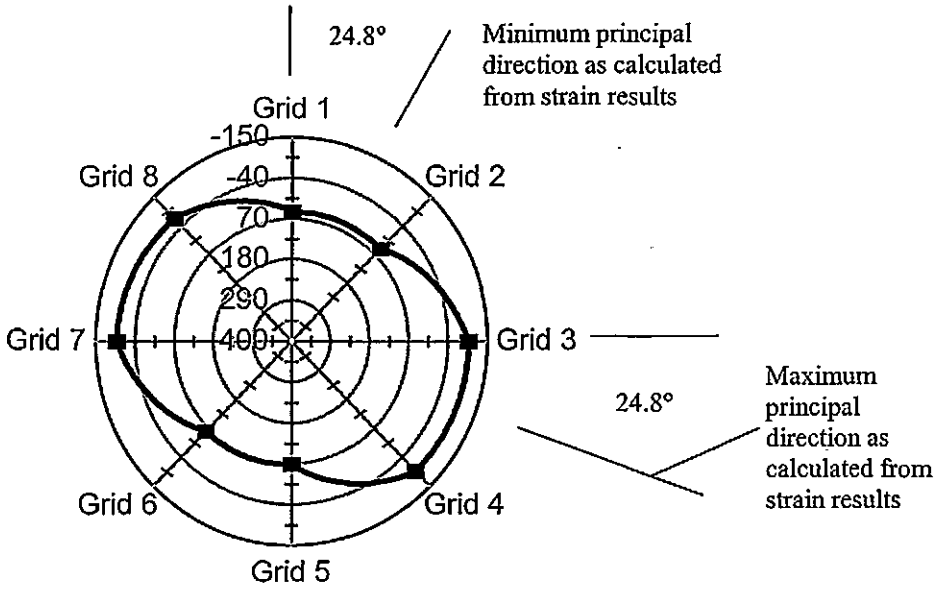

Figure 4.16. – Polar plot of individual strain values taken from the 35mm wide bend specimen showing the angular orientation of the maximum and minimum principal directions, units given in micro-strain.

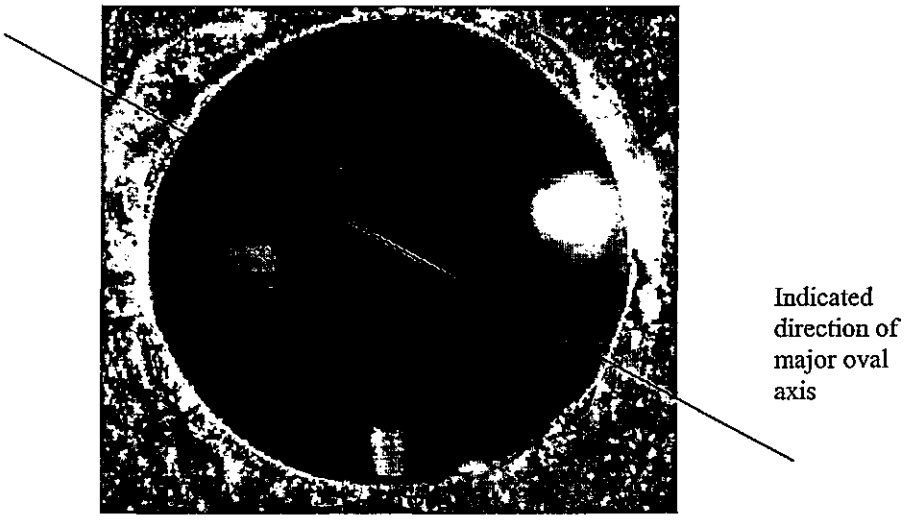

Figure 4.17. – Actual hole ovality of the 35mm wide bend specimen. The orientation of the ovality corresponds to the strain data as indicated on the polar plot in Figure 4.16.

Figure 4.16 shows the polar plot of the 8 values indicated for maximum strain. The peak value occurs in a direction rotated clockwise by 24.8° to the positive x- axis. The minimum value occurs 90° to this. Thus, the polar plot of strain closely replicates the actual hole ovality, shown in Figure 4.17. Capability of the new 8-element rosette was further assessed by determining residual stresses in an "as manufactured" plate of the DPS 600 steel.

4.7 ANALYSIS OF AN "AS MANUFACTURED" DPS PLATE

The envisaged outcome from this analysis was that the relieved strain results from all eight 3-element combinations should be of similar magnitude, based on the following assumptions:

- the plate would be defect free, i.e. would not contain micro-structural imperfections as it is manufactured to high specification levels with a small tolerance band.
- The uncoiling operation would induce a low plastic strain value, i.e. plastic deformation considered negligible.

The data obtained from the analysis of the 'as manufactured' plate showed that the 8-element concept gave repeatable results for this case of circular hole.

CW	Max. (MPa)	Min. (MPa)	Edge	Max. (MPa)	Min. (MPa)
1,6,3	36	15	1,2,3	36	15
2,7,4	37	14	2,3,4	38.7	16
3,8,5	36	15	3,4,5	36	15
4,1,6	35.2	13	4,5,6	35.2	13
5,2,7	36.6	16	5,6,7	36.3	17
6,3,8	36.6	16	6,7,8	35.6	17
7,4,1	36.3	17	7,8,1	36.3	17
8,5,2	37.6	21	8,1,2	37.6	21

Table 4.10. – Maximum and minimum relieved residual stress results as assessed from the DPS plate specimen at a hole depth of 2mm.

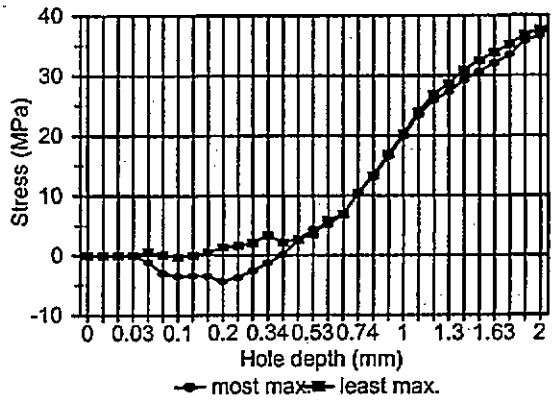

Figure 4.18. – Graphical presentation of the DPS absolute maximum and minimum relieved residual stress results.

The indicated maximum stress at a relieved depth of 2mm showed a variation of only 9% between the greatest maximum (combination 2,3,4) and the least maximum result (combination 4,1,6), see Table 4.10. However, a slightly larger difference is indicated in Figure 4.18 at around a hole depth of 0.2mm. This is attributed to the effect of the uncoiling operation which induces local strain close to the surface. Hence, as expected, any conventional 3-element rosette would have given acceptable results irrespective of reference grid orientation for the "as manufactured" DPS plate. However, when the "as manufactured" plate is subjected to secondary working conditions such as a forming operation the deformation behaviour of the material becomes non-isotropic. Under such secondary working conditions it is essential that an 8-element rosette be used to assess the absolute maximum residual stress magnitude.

4.8 SUMMARY

The results obtained using the customised 8-element strain rosette show a substantial improvement over the three-element rosette, especially when analysing components of a textured nature. The concept of the 8-element rosette has since been patented and is subject to a South African Patent Application 2000/2042. It is felt that the concept should be pursued by strain gauge manufacturers. In assessing the residual stress behaviour of centre discs in this project, customised eight-grid rosettes were used.

CHAPTER 5

PROCESS EFFECTS RELATED TO CENTRE DISC MANUFACTURE

Automotive wheels are safety critical components of automobiles and are manufactured with strict quality control throughout the production stages. Wheels must be both functionally durable and attractive. These requirements are important and must still be met when considering ways of achieving reductions in wheel weight. It must be emphasised that the fatigue resistance of rim steels used for automotive centre discs plays an important role in determining their durability. It is well known that the fatigue resistance of steel can be significantly improved by raising the strength of the steel. However, the higher the strength, the lower the formability, which is one of the most important characteristics of rim steels. Thus, optimum wheel (rim) steels must show both high strength and high formability[13].

In the mid 1970's a breakthrough was achieved in the technology of high strength low alloy (HSLA) rim steels. This breakthrough was the discovery by Rashid[38], in that a mixture of ferrite and martensite could be produced by annealing steel in the intercritical, two-phase ferrite and austenite region. This resulted in a mixed microstructure of ferrite and dispersed islands of martensite, and was designated as **Dual Phase.**

Such steels show high strength and high formability due to their good strength/ductility combinations. This has since opened the way for utilising thinner gauge rim steel for a number of formed parts in cases where component weight is of importance. The automotive industry in its quest for lighter weight vehicles and greater fuel economy have turned to this steel for the manufacture of components such as body panels and wheels, especially the centre disc of the wheel.

5.1 COMPLEXITY OF CENTRE DISC MANUFACTURE

Centre discs are produced through a manufacturing process consisting of five forming stages. The rim steel plate is received from the steel manufacturer as a coil 1.2m in width. When required for production, the rim steel plate is subjected to an uncoiling operation which is known as the *skin pass*, here the rim steel plate is subjected to its first cold working operation. The plastic deformation being kept around 0.2% strain and occurs during the flattening process of the coil. The flattened sheet is then guillotined to a strip of 400mm by 1200mm. Subsequent stages in the centre disc manufacturing process are outlined below.

5.1.1 Blanking

The plate strips are now cut to 400mm by 400mm and then subjected to the first production operation, termed blanking. The blanking operation stamps the initial square plate into a diameter of 408mm having four mutually perpendicular flats (shown in Figure 5.1), two in the rolling direction of the sheet plane and two in the transverse direction.

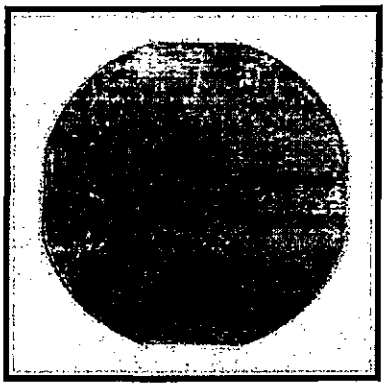

Figure 5.1. – Typical shape of the Blanking stage (cold pressed).

5.1.2 First Drawing Stage (Draw 1)

During the first drawing stage, the periphery of the blank is clamped and a bulge is formed at the inner section by a hemispherical tool. This first forming stage of the production process is considered the most crucial as sufficient material needs to be raised for stamping the inner section of the hat or nose radius region. Although this stage is

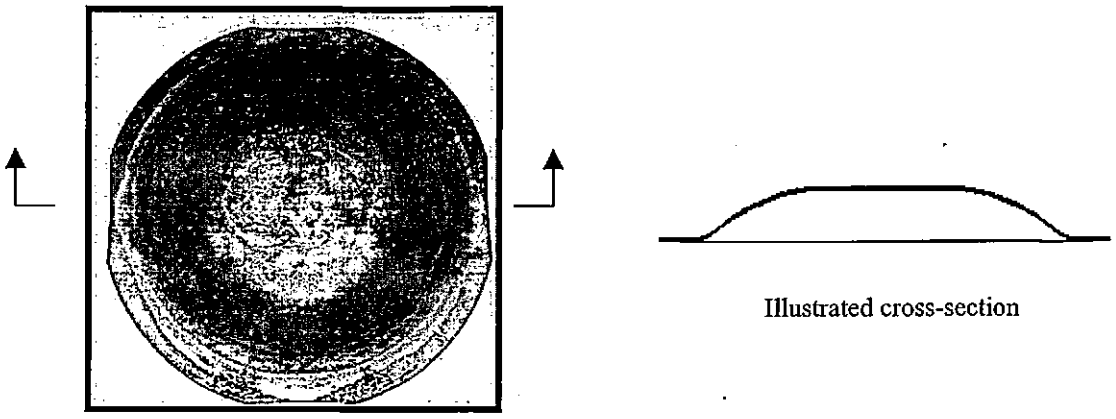

Figure 5.2. – Draw 1 stage pressing (cold formed) showing an illustration of the cross-section.

considered the most important, process parameters at the start of a production run are determined by trial and error.

5.1.3 Second Drawing Stage (Draw 2)

Here the main profile of the centre disc is formed and it is during this stage that the material experiences the most plastic deformation. Hence material is drawn over the hat radius section of the tool toward the centre section and a thinning of the cup radius occurs. This thinning is a result of localised necking and is observed only within the cup radius region. The raised stud hole locations are also formed during this stage. The geometry of this inner section is complex in nature, leaving the component in a highly stressed state around the cup radius region. Finally, a hole is punched through the centre of the disc allowing for re-distribution of the internal stresses due to material removal.

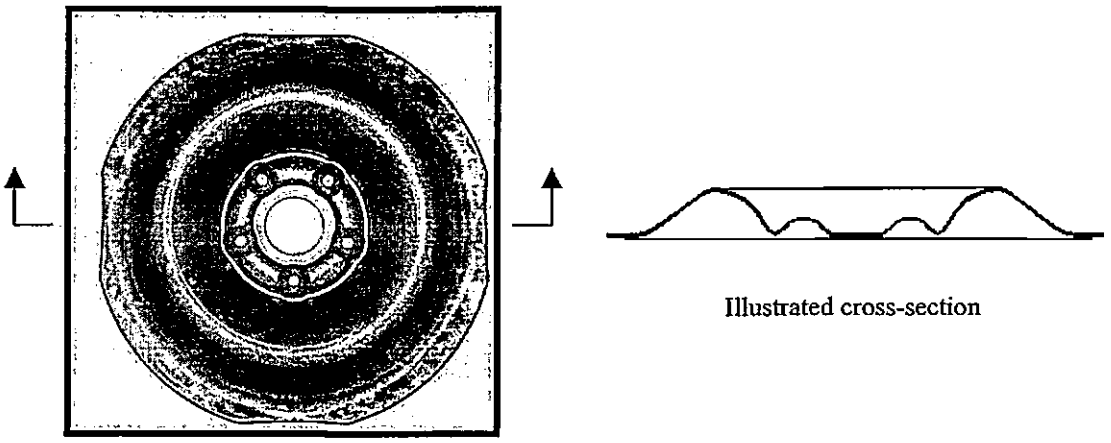

Figure 5.3. – Draw 2 stage pressing (cold formed) showing an illustration of the cross-section.

5.1.4 Third Drawing Stage (Draw 3)

The flanges of the disc are formed during this stage of the production process. Here, the flange round the periphery of the disc is formed downward while the flange of the inner hole is formed upward. During the forming of the inner flange, the section within the hat radius area actually lifts upward whereafter it is re-seated. The shape of the centre disc is now fully formed at the end of this stage.

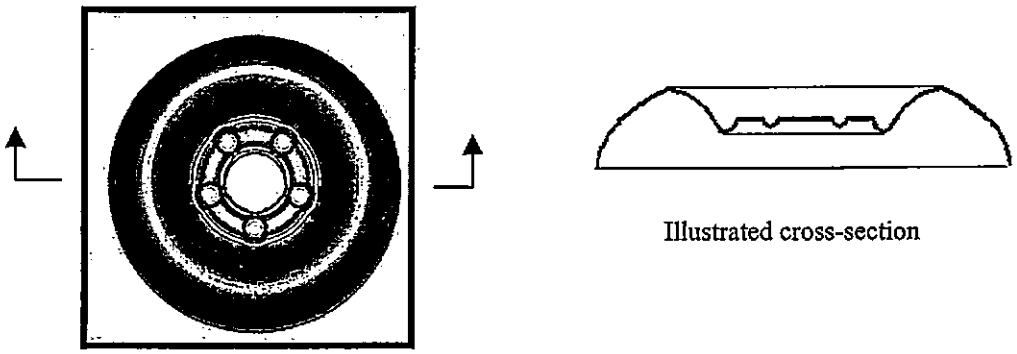

Illustrated cross-section

Figure 5.4. - Draw 3 stage pressing (cold formed) showing an illustration of the cross-section.

5.1.5 Venting stage

Prior to the venting stage, the stud holes are punched and chamfered, this is carried out on a separate punching machine. In order to produce and punch the vent holes the disc is mounted in a special jig as the surface in this area must be perpendicular to the action of the punch. The underside of the vent holes are then finally coined, this coining operation provides a slight radius around the periphery of the vent hole and induces a compressive stress around this area. This is important as crack initiation will occur from the corners of these vent holes if they are not coined. The main purpose of venting is to reduce wheel weight with a secondary purpose of making the centre disc more attractive.

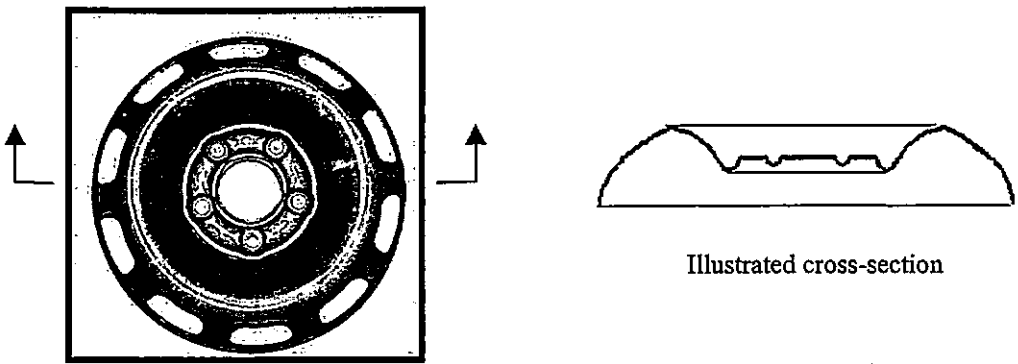

Illustrated cross-section

Figure 5.5. – Venting stage (cold formed) showing an illustration of the cross-section.

5.1.6 Assembly and Paint Curing stages

The centre disc is assembled to the wheel rim in a special fixture that allows for the correct offset adjustment between wheel rim and centre disc. The offset dimension for this particular wheel is 43mm ± 1mm which is the distance between the centre line of the rim and the mounting face of the centre disc, considering the cross section of the complete wheel (see Figure 5.6). The assembling operation takes place under a minimal interference fit and after the correct position is attained in the fixture, the centre disc is welded to the wheel rim.

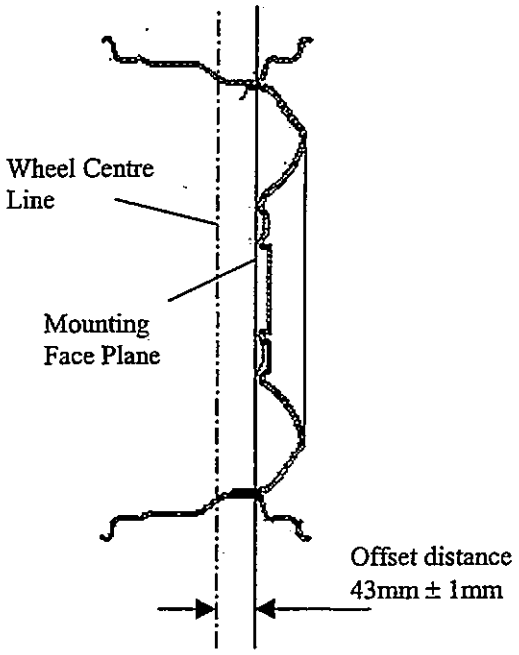

Figure 5.6. – Cross-section of wheel indicating offset distance between rim and centre disc.

The painting of the wheel is then carried out after a degreasing and cleaning process. The wheels are powder coated and subjected to a paint curing operation where the temperature is approximately 190° C. The wheels are then quality checked and prepared for shipment. In this project, because of the complex nature of the forming process, material characteristics such as surface hardness and residual stresses will be used to correlate the observed fatigue behaviour of the centre discs through the various production stages.

5.2 RELATING PROCESS EFFECTS TO MATERIAL CHARACTERISTICS

5.2.1 Residual Stress Analysis

The residual stresses induced on centre discs during successive production stages will need be determined at the same relative positions in order to facilitate comparison between the discs at each stage. Hence, from the second drawing stage through to the Final Painted Wheel (FPW) the diametral axis on which the analyses were required is the same. For the Blank and the first drawing stage, this diametral axis is non-existent so the relative assessment locations were derived by measurement approximation.

As shown in Figure 5.7 the assessment locations lay in the parallel, 45° and transverse directions to the rolling direction of the sheet plane. The residual stresses were analysed at three positions in each of the three directions which can be described as follows:

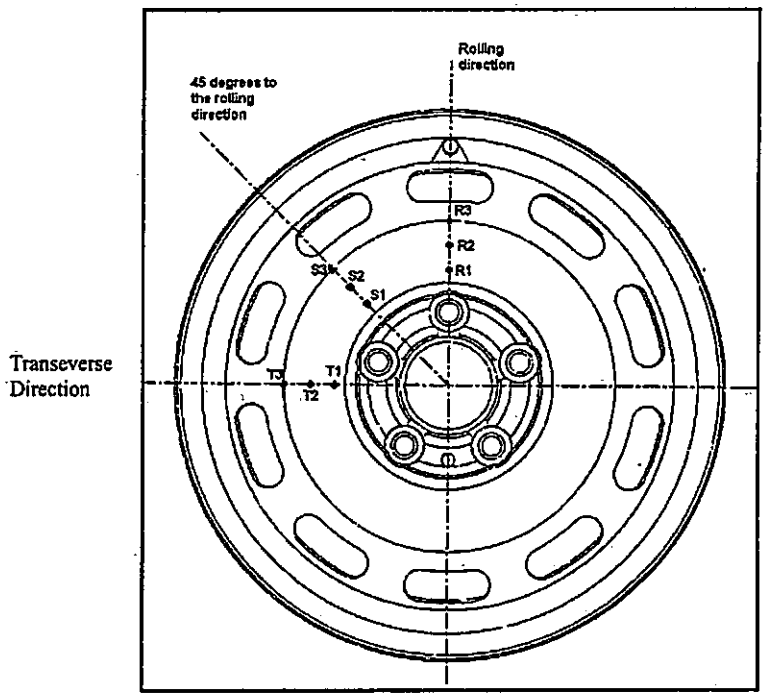

Figure 5.7. – Illustration of residual stress assessment locations.

- On the diametral axis through which fracture occurs (R1, S1, T1);
- Mid-way between the cup and hat radius (R2, S2, T2); and
- On the apex of the hat radius (R3, S3, T3).

The directions are defined as: R – rolling, S - 45° and T – transverse, and the position of the hole in each direction as: 1 – just above the cup radius, which is 13mm from the apex of the cup radius; 2 – mid-way between cup and hat radius; 3 – on the apex of the hat radius.

This Chapter deals with only the results for the diametral axis through which failure occurs in wheel testing. Full details of residual stress and hardness measurements are given in Appendix G.

5.2.1.1 Assessing the 3-grid orientation for determining the maximum relieved residual stress magnitude

The maximum relieved residual stress magnitudes could not be assessed on the diametral axis through which fracture occurs using the customised 8-element rosette because of thickness variation, position (1). Hence this rosette could not be properly seated, i.e. air-bubbles were evident under the applied rosette. Instead, a standard three-element strain rosette type EA-06-031RE-120 was used. This was not a major concern, as the direction of maximum relieved residual stress at this location could be derived from use of 8-element rosettes at positions (2) and (3).

Now, in order to assess the absolute maximum relieved residual stress using a standard three-element rosette, the following procedure was used: Firstly, residual stress assessments were undertaken in position (2) mid-way between the cup and hat radius and then on the apex of the hat radius (3) in all three directions using the 8-element customised rosette. This indicated the required orientation of the three-element combination to give the absolute maximum result at position (1). For example, in Figure 5.8, if the absolute maximum relieved residual stress was found to be 5,2,7, then the standard three-grid

rosette will be applied in that same orientation when analysing the positions on the diametral axis through which fracture occurs.

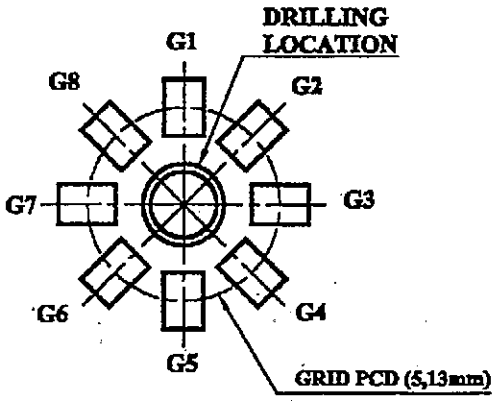

Figure 5.8. – Illustration of 8-grid rosette showing the 5,2,7 orientation.

Of 27 analysis points carried out using the customised 8-element rosette, 26% indicated that the 3,8,5 combination revealed the absolute maximum relieved residual stress magnitude. The second highest stresses observed were for the 4,1,6 combination and occurred for 22% of the analysis. The remaining maximum results were scattered among the other combinations. Based on the above assessment, the orientation of the 3,8,5 gauge combination was used in applying the standard three-element strain rosette to analyse the residual stresses in the three directions on the diametral axis under consideration.

5.2.1.2 Residual Stress Results

The residual stress results in the three directions on all production stages are indicated in Table 5.1 where the units are given in MPa.

Location	Manufacturing Stages						
	Blank	Draw 1	Draw 2	Draw 3	Venting	AUW	FPW
R1	37.8	106.3	234.1	265.8	307.4	346.8	396
S1	37.8	90.2	173.3	155.1	305.8	321.7	384.1
T1	37.8	74.1	164.1	178	300	298.3	217.2

Table 5.1. – Maximum relieved residual stress results, given in MPa, and taken on the diametral axis through which fracture occurs.

The two results shown in bold were adjusted to follow the trend as revealed by the results shown in Table 5.1. This trend shows that the maximum results are progressively increasing from the blank through to the Final Painted Wheel (FPW). Also the trend observed in the three directions is an increase in stress levels from the transverse to the rolling direction and that two values out of the 18 should show a decrease in stress value, is considered suspect. It is also possible that the 3,8,5 gauge combination was not the correct orientation for assessing the absolute maximum values for these two positions and perhaps gauge combination 4,1,6 should have been used instead, as this was the alternate combination that gave an absolute maximum result. Based on the above possibilities these two values were corrected according to the following interpolated procedure:

The average percentage difference between the second and third drawing stages for both the rolling (R1) and transverse directions (T1), were multiplied by the value of the second drawing stage in the 45° plane (S1), the corrected value then being 192.4 MPa. A similar method was used to correct the FPW value in the transverse direction (T1) where the corrected value was 381.6 MPa.

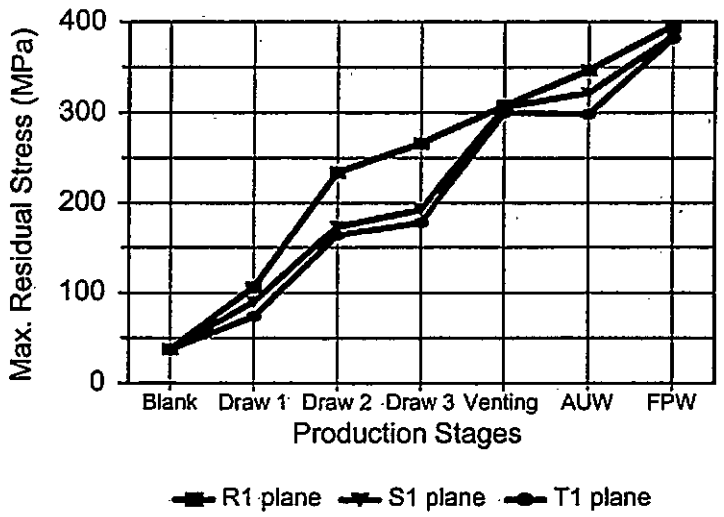

Figure 5.9. – Maximum relieved residual stresses assessed on the diametral axis just above cup radius region.

Figure 5.9 shows clearly that the values of the absolute maximum relieved residual stresses increase steadily through the first, second and third stages and are thus related to the plastic deformation occurring in the respective forming stages. There is a further increase observed between the Assembled Unpainted Wheel (AUW) and Final Painted Wheel (FPW) stages which is attributed to the bake hardening surface effect in the FPW stage. On completion of the residual stress analysis the production stage components were then machined to produce waisted hour-glass shape specimens for fatigue testing, see Figure 5.10.

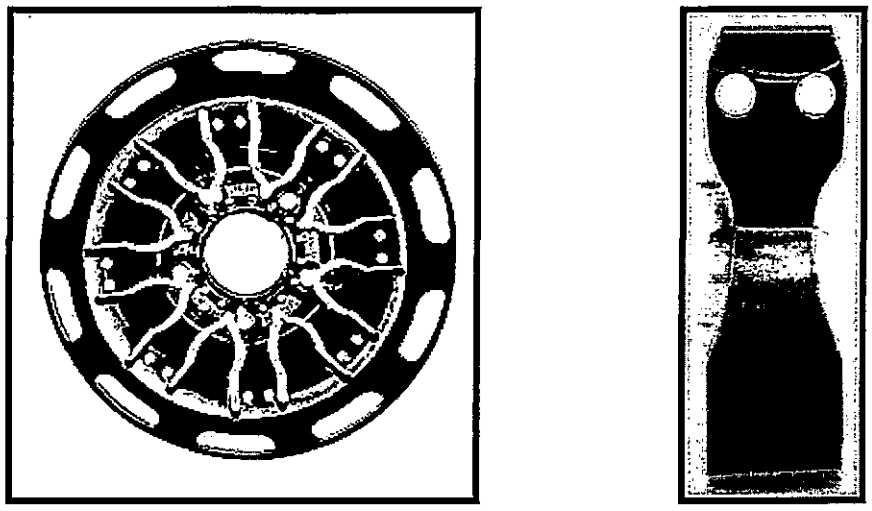

Figure 5.10. – Centre disc as machined into hour-glass shaped fatigue specimens, on the right a typical hour-glass specimen as removed from the machined disc is shown.

5.2.2 Surface Hardness Testing

Surface hardness assessment is an approximate measure of a materials tensile and yield strengths and under forming conditions gives an indication of the materials work hardening ability in terms of the degree of plastic deformation to which they have been subjected. Surface hardness refers to hardness measurements taken on the components surface in this thesis. The main aim for this testing is to estimate the materials yield strength after each stage of the production process which is required for residual stress measurement purposes where according the Schajer[17] the measurement magnitudes should not exceed 80% of the yield strength value for the particular material under analysis. Surface hardness was assessed on the hour-glass fatigue specimens as it was not

possible to take hardness measurements on the complete component due to size constraints. The anisotropic effect observed with respect to sheet materials was also taken in account through using hour-glass specimens machined from the rolling, 45° and transverse directions. The machined specimen on which the residual stress analysis was carried out was then also used for hardness testing. The measurement positions were taken on either side of the drilled hole and on the same diametral axis (see Figure 5.11). The Brinell hardness method was employed using a 2mm-diameter ball indenter and 120kg load. Assessment locations were confined to the diametral axis through which fatigue failure occurs under industrial fatigue testing conditio`ns. Further details of residual stress analysis and surface hardness testing are given in Appendix G.

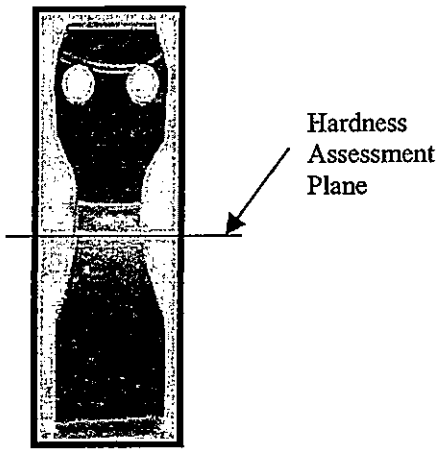

Figure 5.11. – Illustration of hardness assessment location.

5.2.2.1 Brinell Hardness Results (HB 2/120)

Brinell hardness values were measured for each production stage and is given in Table 5.2.

Location	Manufacturing Stage						
	Blank	Draw 1	Draw 2	Draw 3	Venting	Assembled Unpainted Wheel (AUW)	Final Painted Wheel (FPW)
R1	189	193	203	212	209	210	221
S1	189	194	203	216	212	211	222
T1	189	195	205	218	214	215	227
Average Hardness	189	194	204	215	212	212	223
Equiv. Tensile Strength	656	676	710	753	741	741	779

Table 5.2. – Brinell Surface hardness values taken on the diametral axis through which fracture occurs.

Hardness data are plotted in Figure 5.12, and the increase in surface hardness magnitudes during the first three drawing stages is interpreted as being due to the forming of the plate. The decrease in the surface hardness values during the Venting stage is attributed to the relaxation of the hydrostatic component of surface stress (hence making plastic flow easier) as a result of material removal. As expected assembly of the wheel has no influence on hardness. However, the hardness values increase significantly on the final

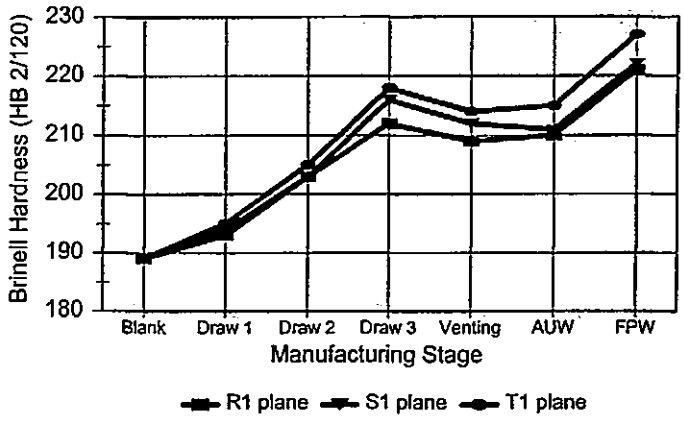

Figure 5.12. – Brinell hardness distribution considering all production stages.

painted wheel due to carbo-nitride precipitation along the grain boundaries close to the surface of the material during the bake hardening[39] at around 200°C. The tensile strengths were approximated from the Brinell hardness number according to South African Bureau of Standards specification, SABS 055-1977, and are given in Table 5.2. Tensile tests showed that the Tensile Strength (UTS) for the "as manufactured" dual phase steel plate used for the manufacture of these centre discs was 664 MPa and the Yield Strength 427 MPa which agrees well with the values for the blank – Table 5.2.

5.3 RELATING YIELD STRENGTH TO RESIDUAL STRESS

The suggestion of Schajer[17] that residual stress magnitudes should not exceed 80% of the original Yield Strength of the material if they are to be accurate will now be checked against the residual stress results from Table 5.3 (units given in MPa).

Location	Manufacturing Stages						
	Blank	Draw 1	Draw 2	Draw 3	Venting	AUW	FPW
R1	37.8	106.3	234.1	265.8	307.4	346.8	396
S1	37.8	90.2	173.3	192.4	305.8	321.7	384.1
T1	37.8	74.1	164.1	178	300	298.3	381.6
80% YS	341.6	341.6	341.6	341.6	341.6	341.6	341.6

Table 5.3. – Comparison of residual stress results to the 80% original Yield Strength value for DPS.

It is clear from Table 5.3 that values of residual stress are generally below 80% of the yield strength except for the FPW stage. The FPW data, in all three directions is above this 80% value because of the precipitation that occurred during the bake-hardening phenomenon although the exact mechanism is not clear.

5.4 SUMMARY

During the production of centre discs the initial flat plate is subjected to a number of stamping operations which work harden the material. This is evident from the surface hardness tests where the materials tensile strength has increased up to and including the third drawing stage. The decrease in hardness for the venting stage is attributed to the relaxation in surface tension according to Carlson and Sines[40]. Finally, the paint curing temperature is the prime mover for the substantial increase in surface hardness due to carbo-nitride precipitation along the grain boundaries close to the surface of the component. Interesting to note however, is that these two properties are directionally opposite in their behaviour, i.e. consider Figures 5.9 and 5.12, residual stresses are highest along the rolling direction, while hardness is highest along the transverse direction. We will now consider the analysis of the fatigue properties separately.

CHAPTER 6

ASSESSMENT OF CENTRE DISC FATIGUE PROPERTIES

Fatigue of materials refers to plastic deformation, crack initiation and subsequent propagation resulting from the application of cyclic loads. Research into fatigue phenomena dates back to the nineteenth century and has long been concerned with engineering approaches to design against fatigue crack initiation, propagation and failure. Fatigue of materials has also emerged as a major area of scientific and applied research which encompasses such diverse disciplines as materials science, mechanical, civil and aerospace engineering, bio-mechanics, applied physics and applied mathematics[18].

This project is concerned with the fatigue performance of wheels and in particular in determining how it is influenced during each stage of the production process. Attention will be paid to the effects of plastic deformation characterised by the hardness and residual stress state. Hour-glass fatigue specimens will be machined from all production stages including the painted centre disc removed from the complete wheel. The purpose of this work is to establish the most detrimental production stage/s in terms of fatigue behaviour and thereby optimise the manufacturing process through enhancing the overall fatigue performance of wheels. Factors which affect the fatigue performance of formed components include microstructure, surface conditions, stress concentrations, mean and residual stresses. These are discussed below.

6.1 FACTORS AFFECTING THE FATIGUE LIFE OF CENTRE DISCS

The purpose of fatigue testing is to gain an understanding of the effects of the various factors that influence the fatigue strength of materials and to generate data that is useful in life prediction. The main influential factors relevant to DPS and the centre discs of automotive wheels include:

6.1.1 Microstructure

The microstructure of the Dual Phase Steel plate has a grain size No. 12 according to ASTM E112-85[41]. It consists of approximately 20% dispersed islands of martensite in a predominantly ferrittic matrix, refer to Figure 2.4. The microstructure can be considered as approximately equi-axed but a tendency towards layering or banding is also evident. This is attributed to the manufacturing process of the sheet plate. Evidence of void creation is seen in the microstructure of the first drawing stage pressing. This is observed in Figure 6.1, close to the martensite grain boundaries and is a result of the stretching of the plate during this stage of the manufacturing process.

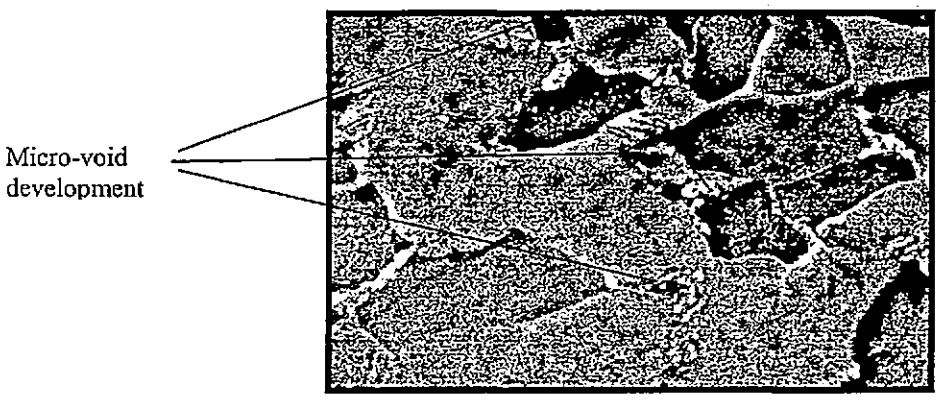

Figure 6.1. Microstructure of Draw 1 stage pressing x3865.

The microstructure of the second drawing stage pressing now shows an imperfection[42] known as stress discontinuities that are observed throughout the profile along the neutral axis. This region along the neutral axis is also referred to as the *elastic core region*[9] clearly showing a banding/layering of the microstructure in this region, and is more pronounced in the cup radius region where the bend radius is small, see Figure 6.2.

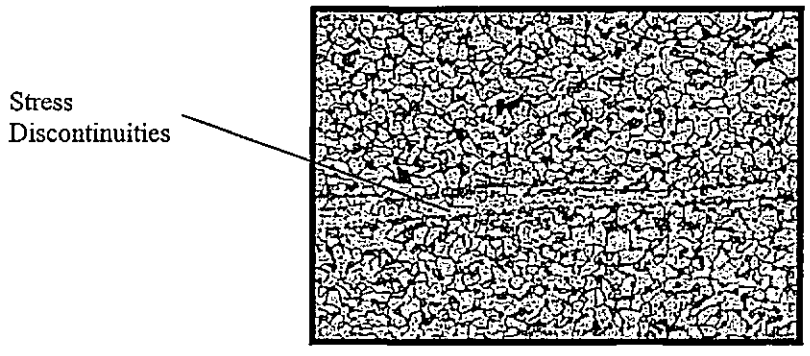

Figure 6.2. – Stress discontinuities along the neutral axis of the cup radius region x250.

These stress discontinuities are a direct result of severe plastic bending deformation resulting from the differing shearing effects on either side of the neutral axis causing a stress gradient across the thickness plane of the sheet in the formed condition. Micro-hardness tests indicate this stress gradient through the thickness plane of the cup radius, which is shown in Figure 6.3. Stress discontinuities are undesirable but unfortunately cannot be removed by either metallurgical or heat treatment processes.

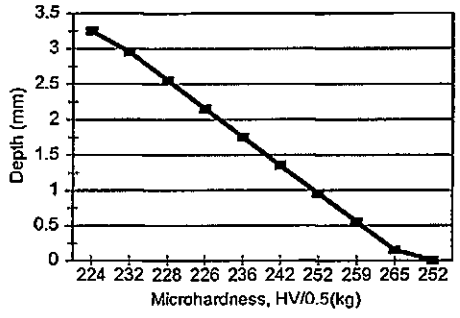

Figure 6.3. – Micro-hardness profile taken through apex of cup radius region.

The micro-voids being more pronounced in the microstructure as a result of the second drawing stage pressing, see Figure 6.4, these micro-voids act as stress raisers within the microstructure hereby weakening the component in terms of its fatigue performance. These micro-voids presumably arise as a result of the differing mechanical properties of the harder martensite and softer ferrite phases, and thus, are seen close to the martensite and ferrite grain boundaries.

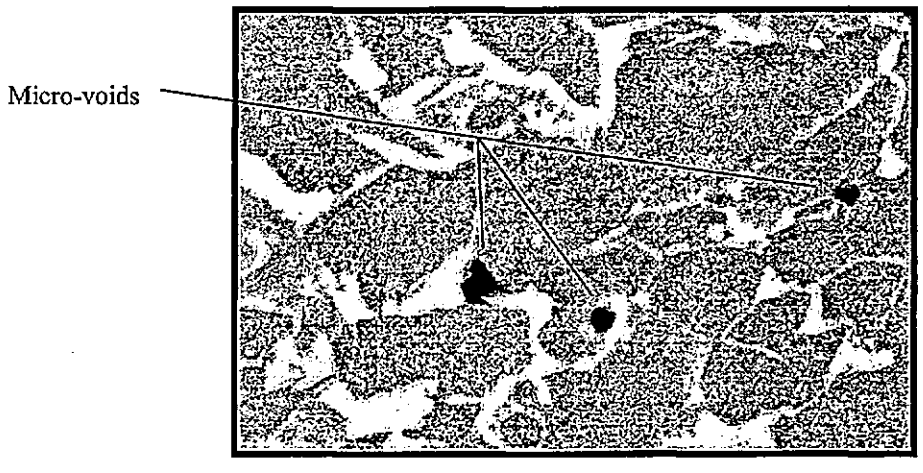

Figure 6.4. – Micro-voids close to the inside surface of the cup radius region x3865.

It should be pointed out that the forming of centre discs is mainly carried out under tensile forces that would leave the finished component in a predominantly tensile residual stress state. The complex stress state experienced by the centre disc would vary throughout the profile of the centre disc and is dependent upon the degree of cold working to which they are subjected. It is envisaged that these imperfections such as, stress discontinuities (layering), stress gradients, micro-voids all interact under cyclic loading conditions hereby reducing the fatigue life of the component although the % reduction produced by each imperfection is not clear.

6.1.2 Surface Condition

Since the development of fatigue cracking is very much a surface related phenomenon, it follows that fatigue strength is highly dependent on surface conditions such as finish, roughness, hardness and the presence of surface residual stresses. The "as-manufactured" surface finish and roughness is not considered detrimental to the fatigue failure of formed centre discs because of the fine grain structure of DPS leaves the surface within acceptable limits (see Figure 6.5).

Becker et.al.[43] conducted high cycle fatigue tests on flat plate specimens having different surface roughness (smooth, 15μm, 150μm and 500μm). They found that for a fatigue life of 2×10^7 cycles the fully reversed stress amplitude decreased by 46% from 370MPa to 200MPa in worst condition considering the smooth and 500μm specimens. The surface roughness for the production stages are shown in Figure 6.5, for specimens from the second drawing stage onward this measurement was taken in the cup radius region. Surface hardness on the other hand, varies across the profile of the centre disc and is dependent on the geometrical shape. No additional surface residual stresses (eg shot peening) are induced on completion of centre disc manufacture, which might enhance fatigue life by offsetting the applied tensile stresses that arise during cyclic loading.

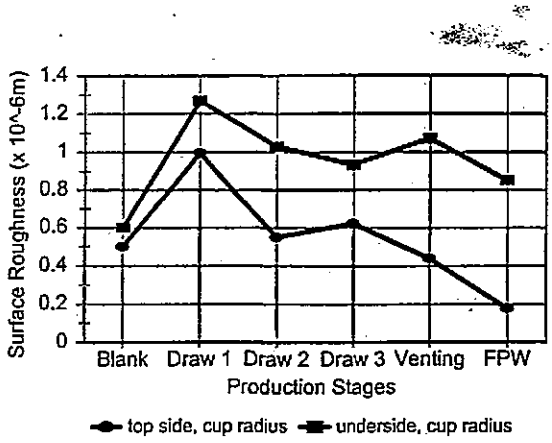

Figure 6.5. – Surface roughness results of production stage components. The FPW results include a paint finished surface.

6.1.3 Stress concentrations

Examination of a wide range of components that have failed in service from fatigue indicates that in many cases cracks initiate from a geometric detail containing a region of stress concentration generally referred to as a "notch"[19]. Notches in centre discs comprise the vent holes, stud holes, sudden changes in cross-section or tool markings left on the surface as a result of the forming operation. These are so called visible notches. Notches may also be related to metallurgical defects in the form of carbides and micro-voids. The area around the neutral axis (elastic core) which show stress discontinuities (see Figure 6.3), may also be considered as a notch because it too is a weakness in the material which produces local strain concentrations.

Under industrial fatigue testing conditions, wheels do not generally fail within the cup radius region, they are more likely to fail just above the cup radius where a sudden change in cross-section exists (see Figure 6.6), or at the corners of the vent holes. The periphery of the vent holes are thus coined (a process whereby compressive stresses are induced) to prevent fatigue failure initiating from this region.

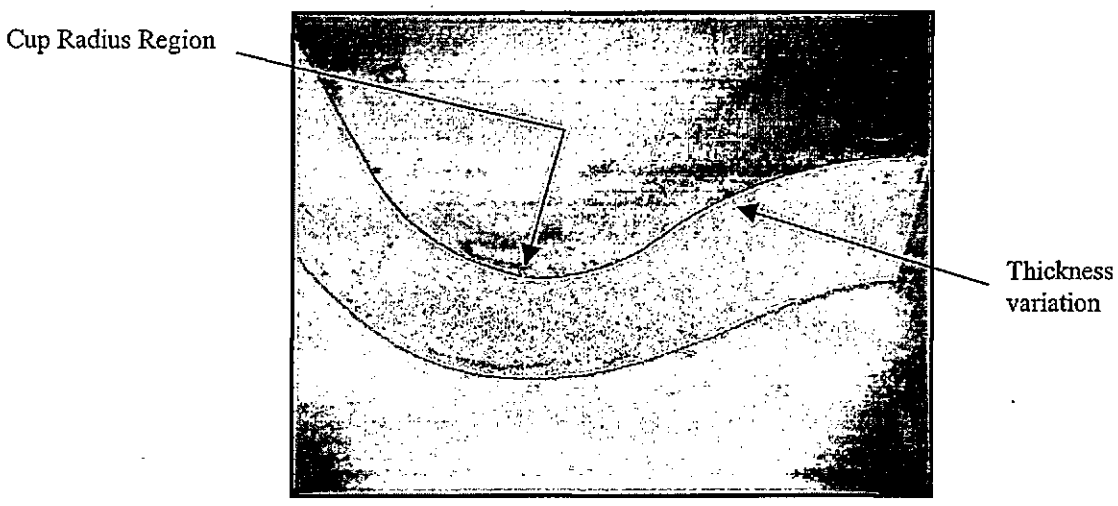

Figure 6.6. – Portion of centre discs cross-section showing thickness variation above the cup radius region.

6.1.4 Mean stress

The current industrial method for fatigue testing automotive wheels makes use of a zero mean stress condition, this is illustrated in Figure 6.7. Two strain bridge circuits attached to the lower end of the load arm sense the centrifugal effect of the rotating mass which in turn is attached to the mass force generator where the software programme converts these strain values to bending moment values. These strain bridges thus sense the same strain values through one complete revolution of the mass force generator, hereby constituting a zero mean stress fatigue test. (Further details relating to the industrial fatigue testing method is given in Section 6.2).

However, the centre disc would experience a non-zero mean stress condition on different diametral axes due to its geometrical shape and the presence of residual stresses. The intention in this project is not to change the current technology of industrial fatigue testing but rather to develop an understanding of the relationship which exists between as-manufactured residual stress magnitudes and the number of cycles to failure for this mean stress condition.

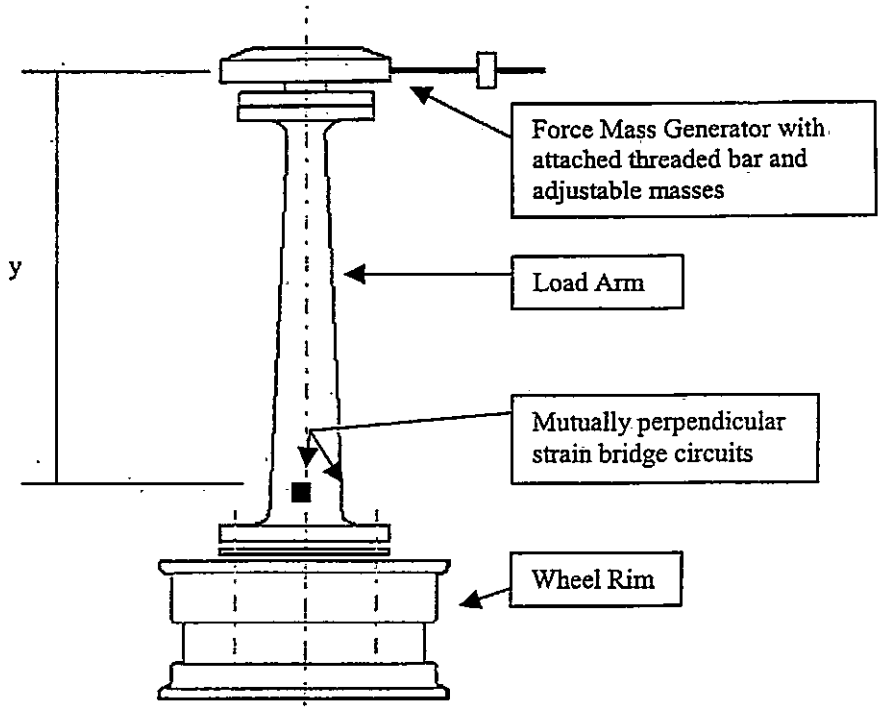

Figure 6.7. – Illustration of load sensing system applicable to the rotating bending industrial fatigue testing machine.

6.1.5 Residual stresses

It is well known that cold working processes increase the tensile strength of a material through a mechanism termed work or strain hardening[1,2,7]. The forming of sheet metal is one such manufacturing process which work hardens the material and increases its tensile strength but leaves the component in a predominantly tensile residual stress state. The residual stresses in the centre disc differ in magnitude from point to point just as the surface hardness will differ from point to point due to the local plastic deformation induced. These stresses are said to alter the mean stress level during cyclic loading[20,21] and would be detrimental to the fatigue performance if they are of a tensile nature and beneficial if compressive in nature.

We will now consider fatigue testing of both the automotive wheels and hour-glass specimens where the fatigue data will be discussed with respect to the above factors.

6.2 INDUSTRIAL FATIGUE TESTING METHOD

The most important requirement of an automotive wheel is its durability under service loads. In order to assess their durability two test methods are usually employed, these are:

1) The dynamic cornering fatigue test, which determines the fatigue strength of the wheels, mainly the centre disc under cyclic side loading corresponding to hard cornering conditions. The two types used for these tests are the rotating mass (Figure 6.8) and the cantilever (Figure 6.9) fatigue testing machines.

2) The dynamic radial fatigue test, which determines the long-term fatigue life of wheels, mainly testing the rim but also the strength of the weld between the rim and centre disc.

The dynamic cornering fatigue testing machines as mentioned in (1) above are of more relevance to this work and will now be discussed in more detail.

These tests are accelerated methods of evaluating the service life of wheels and use loads about twice as large as are actually encountered in service[44]. The recent manufacturing trend is toward complex centre disc press forming for styling purposes where the increased range of profile shapes and vent holes in centre disc manufacture become critical during these durability tests with respect to meeting the minimum fatigue specification.

The principle of operation of the two types of machines is different in that the rotating mass machine is frequency controlled whereas the cantilever machine is speed controlled. For the rotating mass machine, a load arm is bolted through the stud holes of the wheel

where the bolt torque is 90Nm. The wheel rim together with the attached load arm is mounted and clamped to the machine base. This load arm is approximately 600mm in

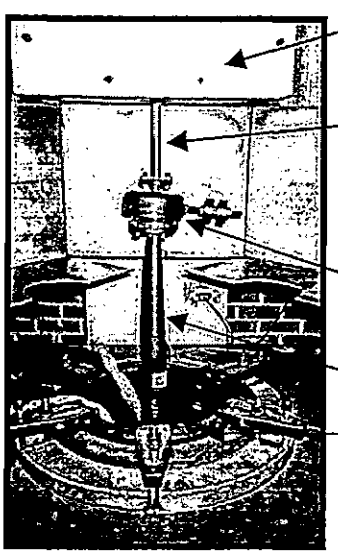

Figure 6.8. – Rotating mass testing machine.

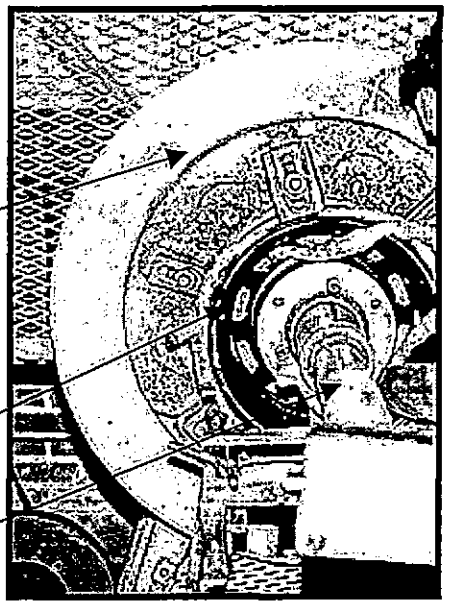

Figure 6.9. – Cantilever testing machine.

length and is tapered towards the free end to which an eccentric mass force generator is attached. This mass force generator houses a bearing that is fitted over the tapered end of the load arm, and also contains a threaded rod upon which the masses are bolted.

These masses can be adjusted along the length of the threaded rod and hence provide for the setting of the required bending moment according to the test specification. The mass force generator is connected to the motor through a drive shaft containing flexible couplings. The motor drives the mass force generator, while the centrifugal forces set up by the masses provide the rotating bending action. The bending moment is measured by two perpendicular strain gauge bridges attached to the lower end (stud hole end) of the load arm, each with its own amplifier. The outputs from these two amplifiers are added vectorially so that the resultant bending moment is obtained. If M_1 and M_2 are the bending moments acting in the two perpendicular planes, then the resultant moment[45] is given as:

$$M_{resultant} = \sqrt{M_1 + M_2} \qquad (Nm) \text{.....(6.1)}$$

The frequency of the fatigue test is set at about 63% of the natural frequency of the system, which comprises the wheel with attached load arm secured to the fatigue machine base i.e. load arm, wheel and base. After the wheel and attached load arm are secured to the machine base, a rubber mallet is struck against the load arm, and the resultant vibration is sensed by strain bridges. This data is processed by a computer programme which determines the natural frequency of the system. The test frequency (63%) is then set, which ranges between 26 and 27Hz for the dual phase wheel.

For the cantilever machine, the drum is rotated at a constant speed of 170rpm. Here a cantilever shaft is mounted to the wheel through the stud holes of the centre disc with a bolt torque of 120Nm. Aligning the shaft and wheel with the rotational axis of the drum is tedious and time consuming as this operation is carried out by a dial test indicator. Once concentricity is obtained an air cylinder is attached to the free end of the shaft which, when pressurised provides the bending moment at the wheel. For a typical fatigue test of 600 000-load cycles, the test time for these two techniques is 6.17 hours for the rotating mass machine and 58.8 hours for the cantilever machine. The rotating mass machine is hence the more efficient and is the preferred machine in industrial practice.

6.2.1 Calculating the test load for the rotating mass machine

The test specification for the wheels under investigation in this project involves the wheel surviving a specific number of cycles at 50% and 75% of the maximum wheel bending moment. The maximum bending moment ($M_{b\ max}$) is determined using the following equation[44]:

$$M_{b\ (max)} = f.F_r(\mu.r_{dyn} + e) \qquad (Nm) \text{.....(6.2)}$$

Where: $M_{b\,max}$ = 1.333 times the resultant bending moment as obtained through equation (6.1);

f = static wheel load factor = 2, for passenger vehicles;

Fr = permitted static wheel load = 5738.85N;

μ = coefficient of friction between tyre and road surface = 0.9;

r_{dyn} = dynamic tyre radius of the largest tyre permissible = 0.31m; and

e = rim offset = 0.043m.

The maximum wheel load specification for the DPS wheel is given at 585kg and the fatigue performance must exceed:

1) Short term fatigue test: 60 000 cycles at 75% of the maximum wheel load ($M_{b\,max}$ = 2750Nm.

2) Long term fatigue test: 600 000 cycles at 50% of the maximum wheel load ($M_{b\,max}$ = 1805Nm.

The endurance limit is taken at $2x10^6$ cycles corresponding to 30% of the maximum wheel load, and is equivalent to a bending moment test load of 1500Nm as is shown by the dotted line in the Wöhler diagram for the wheel, given in Figure 6.10.

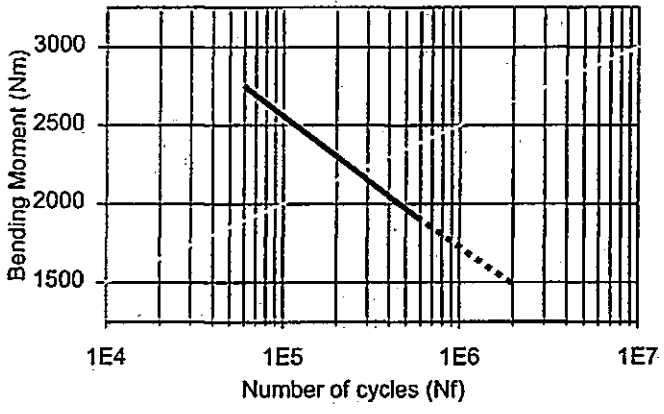

Figure 6.10. - Wöhler diagram showing the minimum fatigue test specification.

It must be noted that the test load is measured by the strain gauges attached to the lower end of the load arm and the applied load cycle has a zero mean stress test condition. The

centre disc however would experience a mean stress condition (as discussed in Section 6.1.4) other than zero, along the predominant fracture plane (slightly above the cup radius) because of:

1) the geometrical shape of the centre disc;

2) the variation in material thickness throughout the centre disc profile; and

3) the presence of residual stresses.

The importance of the first two factors was investigated so that the fatigue testing of waisted hour-glass specimens cut from the wheel centre disc could be performed with a matching applied mean stress to that assessed in the complete wheels. The investigation was carried out in the following manner. A centre disc of an automotive wheel was strain gauged in order to assess the induced principal stresses around the fracture position under normal industrial test loads, see section 6.3.1. Hence, these gauges were positioned just above the cup radius (predominant fracture plane), as well as midway between the cup and hat radius, and on the apex of the hat radius. The strain gauged wheel was then mounted on the cantilever machine and the drum was rotated by hand allowing the maximum tension and maximum compression strain magnitudes to be recorded. These were then converted to stress values.

For the purposes of this project a more complete S-N curve for this model of wheel, (other than at the two loads used in industrial testing) was acquired at a range of loads. This would indicate whether the fatigue behaviour of wheels is linearly proportional at different fatigue testing loads. Furthermore, the fatigue testing of wheels at different loads was considered fundamentally important to correlating the behaviour of the waisted hour-glass fatigue specimens machined from the centre discs. The approach would be to fatigue test

these waisted hour-glass specimens under similar loading conditions to those which the wheels experience.

6.3 FATIGUE TESTING OF AUTOMOTIVE WHEELS

Fatigue testing was carried out using the rotating mass fatigue testing method. The fatigue testing parameters for these tests were *bending moment (Nm)* vs *number of cycles to failure (N_f)*. The bending moments initially decided upon were 1500, 2125, 2750, 3375 and 4000Nm, which exceeds the current upper and lower testing limits employed by industry, and hence would provide a more complete S-N curve for this model of wheel. However, as a result of a limited number of wheels allocated to this project due to the production of this DPS plate, the actual fatigue testing loads were 1800, 2420, 3375 and 4000Nm. The number of wheels to be fatigue tested at each of the four loads were based on assumption that:

- seven wheels would be scheduled for testing at each of these loads, but if the scatter in life data at higher test loads (i.e. 3375 and 4000Nm) were observed to be within a narrow band then only four wheels would be tested at these higher loads. This assumption is based on ASTM E 739-80 (1986) which details conditions for exploratory and research related fatigue testing conditions.

The fatigue results obtained from this investigation are given in Table 6.1.

	TEST LOAD			
	1800Nm	**2420Nm**	**3375Nm**	**4000Nm**
WHEEL 1	1 808 000	400 000	186 400	70 625
WHEEL 2	>2 000 000	1 550 621	172 700	76 295
WHEEL 3	2 020 064	425 458	179 850	69 843
WHEEL 4	>2 000 000	804596	183 921	73 312
WHEEL 5	2 954 190	1 126 330	-	-
WHEEL 6	>2 000 000	1 000 000	-	-
WHEEL 7	1 079 436	628 728	-	-
Average	**1 980 242**	**847 962**	**180 718**	**72 519**

Table 6.1. – Wheel fatigue test data, run-out equals 2×10^6 cycles.

The results of the wheel fatigue tests are presented in Figure 6.11 which also includes the minimum specification required under industrial fatigue testing conditions for this wheel. The endurance limit or run-out for these wheels under test is taken at 2 x 10^6 cycles, and a value of 1500Nm is obtained by extrapolating the minimum specification line to intersect the horizontal axis at this magnitude.

The wheel results shown in Figure 6.11 indicate that a linear relationship does exists between bending moment and life, and that the slope can be characterised in terms of log-normal scales. This logarithmic fit realises a coefficient of regression and determination of 99.95% and 99.91% respectively. Also, the wheels comfortably exceed the minimum specification by approximately 20% at a fatigue life of 2 x 10^6 cycles.

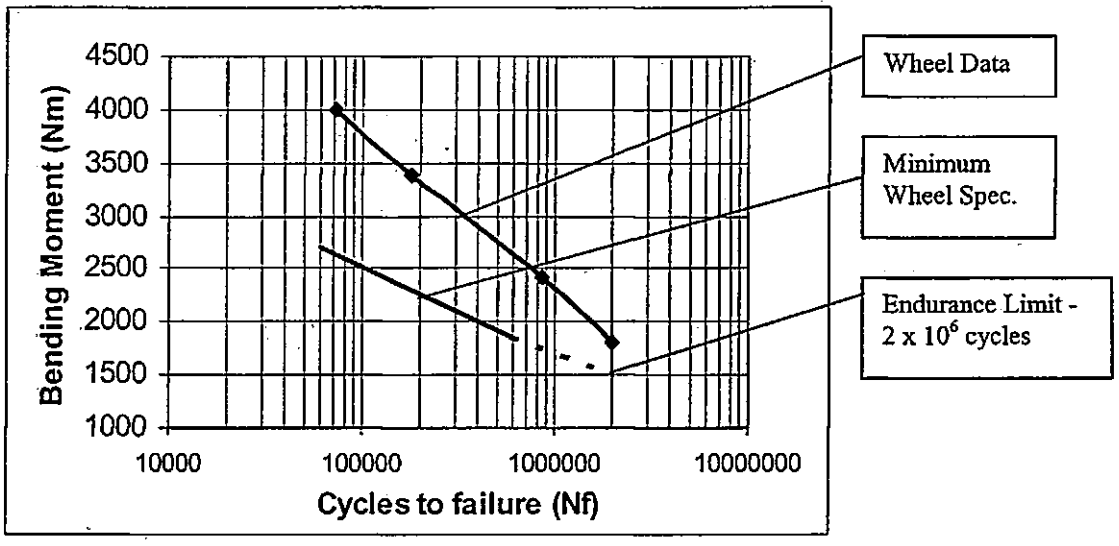

Figure 6.11. – Actual wheel fatigue results, showing the minimum required specification and predicted endurance limit (dashed line).

Thus the fatigue performance of these dual phase wheels as manufactured by Guestro Wheels, is predictable using the following expression:

$$M = -656.63 \times \ln N_f + 11344 \qquad (Nm) \ldots\ldots\ldots\ldots\ldots\ldots\ldots\ldots (6.3)$$

Where: M = Applied fatigue bending moment (Nm);
N_f = Number of cycles to failure.

This equation has some use, as considering that all forming parameters remain constant and the wheel fails prematurely, then the most likely reason for this premature failure will be micro-structurally related. Micro-structural imperfections such as inclusions and banding (segregation of alloying elements) are not visible and thus will only be reflected through premature fatigue failures. The possibility of tool markings causing premature failure is unlikely as the components are inspected between each production stage. Thus if a tool becomes blunt or damaged, this defect on the pressing will be detected by the quality inspection carried out between the forming stages.

As a first step in examining fatigue life as a function of forming stage of the centre disc manufacturing process, it was necessary to obtain an S-N curve for waisted hour-glass type specimens machined from painted centre discs (complete centre discs). This curve should correlate with the wheel testing curve if the test conditions in the hour-glass specimens (reverse bending) and the wheel (rotating bending loading) are similar. The fatigue testing of production stage hour-glass specimens would also show the stage/s most likely to be responsible for premature fatigue failure.

In fatigue testing of the hour-glass specimens the stress cycle (maximum and minimum stresses) is matched to that observed under industrial conditions. To achieve this a wheel was strain gauged and mounted to the cantilever fatigue-testing machine, as illustrated in Figure 6.9, to assess the induced principal stresses under the range of moments used, i.e. 1500 through 4000Nm.

6.3.1 Determination of induced principal stresses

For determining the induced principal stresses, a wheel was strain gauged in the parallel, 45° and transverse to the rolling direction of the sheet plane. These gauges were placed just above the cup radius, on the apex of the hat radius and at strategic positions along

these planes, where the induced stresses at these locations would probably be highest, i.e. at the corner of vent holes and between vent holes. These gauge positions are illustrated in Figure 6.12 & 6.13, the results of this analysis is given in Appendix A.

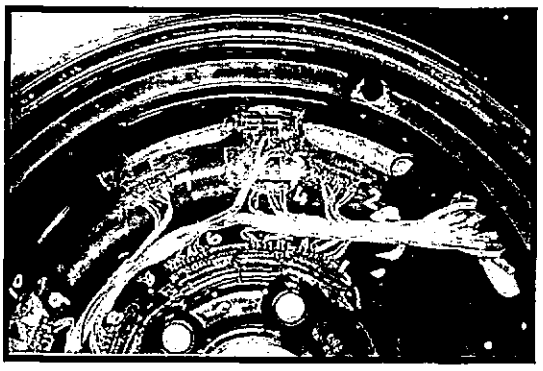

Figure 6.12. – Wheel as strain gauged.

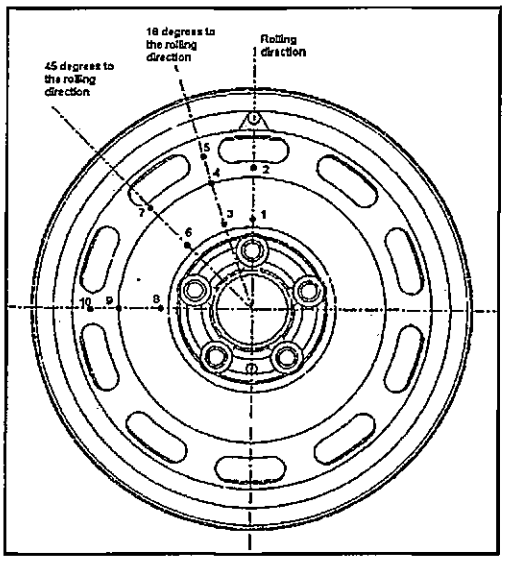

Figure 6.13. – Illustration of gauge positions.

The critical position for determining these stresses is just above the cup radius location (gauge positions 1, 6 and 8 – Figure 6.13) as failure occurs through this diametral axis.

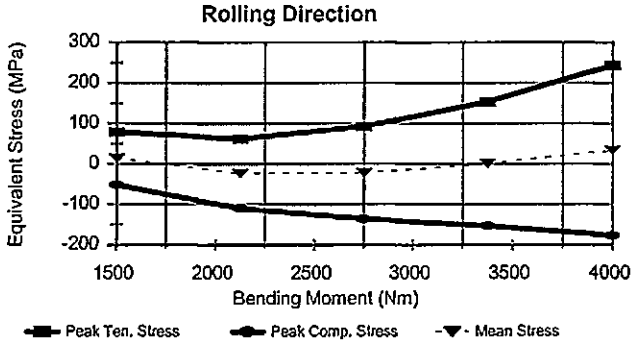

Test Load (Nm)	Equiv. Peak Tensile Stress (MPa)	Equiv. Peak Compressive Stress (MPa)	Mean Stress (MPa)
1500	79	-52	14
2125	62	-110	-24
2750	93	-136	-22
3375	154	-153	1
4000	244	-177	34

Figure 6.14. – Equivalent peak stresses as determined from gauge position 1, considering the rolling direction.

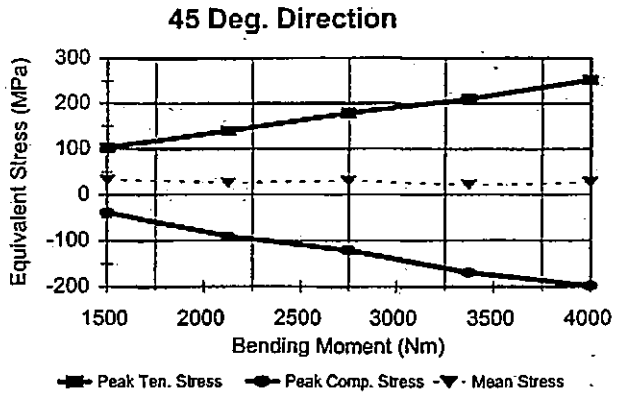

Test Load (Nm)	Equiv. Peak Tensile Stress (MPa)	Equiv. Peak Compressive Stress (MPa)	Mean Stress (MPa)
1500	103	-38	33
2125	140	-91	25
2750	179	-119	30
3375	210	-169	21
4000	252	-198	27

Figure 6.15. – Equivalent peak stresses as determined from gauge position 6, considering the 45° direction.

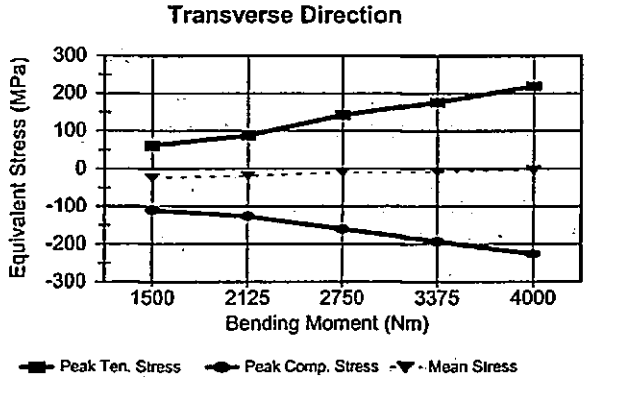

Test Load (Nm)	Equiv. Peak Tensile Stress (MPa)	Equiv. Peak Compressive Stress (MPa)	Mean Stress (MPa)
1500	62	-110	-24
2125	89	-126	-19
2750	143	-160	-9
3375	177	-193	-8
4000	219	-226	-4

Figure 6.16. – Equivalent peak stresses as determined from gauge position 8, considering the transverse direction.

The results observed for each direction show differing peak tensile and compressive stress values hence indicating that their tensile / compressive behaviour is influenced by the geometrical shape of the centre disc, especially around the cup radius region. This implies that the area just above the cup radius region (diametral axis through which fracture occurs under industrial fatigue testing conditions) is more rigid in the compressive bending mode than under a tensile bending mode. Another point to consider is the position of these strain gauges relative to the stud hole locations which will also influence the rigidity of the centre disc, i.e. the closer the gauge to the stud hole the smaller will be the assessed stress magnitude. This is clearly observed with respect to the above results. One need only consider a flat plate under similar strain gauge and loading conditions where the tensile and compressive behaviour would and should be of equal magnitude but of opposite sign.

This differing tensile/compressive behaviour indicates that the centre disc would experience a mean stress condition on this diametral axis. What is of concern however, is the fact that these mean stresses are of varying magnitude throughout the load range (1500Nm through 4000Nm) and are of different value in each direction. This is of particular importance when establishing the fatigue test procedure for the waisted hour-glass specimens where the aim is to replicate/match the industrial testing and failure criteria of the wheel.

The 45° direction however indicates the highest peak tensile and mean stress values and hence the values pertaining to this direction will be used for establishing the fatigue testing parameters for the hour-glass specimens. This is based on the assumption that the mean stress values for the other two directions are compressive in nature and thus would enhance the fatigue performance of these specimens.

Therefore, the hour-glass fatigue testing procedure for producing an S-N curve that will hopefully duplicate the industrial criteria, as observed from the above results would be:

- To use the mean stress value at the highest peak tensile stress magnitude (27 MPa), as this value of mean stress brackets the average value considering the 5 load ranges (103 MPa through 252 MPa). This assumption should not adversely affect the outcome of the fatigue performance as the percentage difference in the worst condition is 22%, i.e. first and fourth test values.
- To maintain the peak tensile stresses as observed, but alter the peak compressive stresses, accordingly. This will also not adversely affect the outcome of the fatigue performance, because, what has been lost in mean stress has been accommodated for in the tensile value by altering the compressive magnitude of the observed value.

According to the above, the fatigue testing parameters for the hour-glass specimen will be:

Test Load (Nm)	Equiv. Peak Tensile Stress MPa	Corrected Equiv. Peak Compressive Stress (MPa)	Corrected Equivalent Stress Amplitude (MPa)	Corrected Average Mean Stress (MPa)
1500	103	-49	76	27
2175	140	-86	113	
2750	179	-125	152	
3375	210	-156	183	
5000	252	-198	225	

Table 6.2. – Fatigue testing parameters for the hour-glass specimens taken from the 45° direction.

6.4 FATIGUE TESTING OF HOUR-GLASS SPECIMENS

The hour-glass specimens used for the production of the S-N curve were machined from painted centre discs (these painted centre discs were machined from complete wheels) using a CNC milling machine, see Figure 6.17. The maximum number of specimens machined from a single disc was eight of which five were smooth and three notched within the cup radius region. Figure 6.18 shows the difference between a smooth and

notched specimen. The individual specimens were removed from the machined disc by band saw.

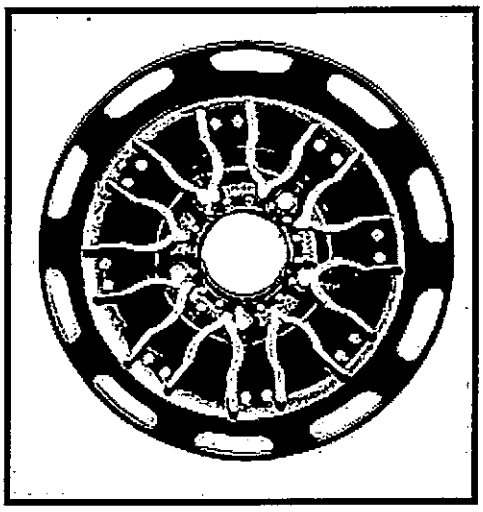

Figure 6.17. – Hour-glass specimens as machined from the centre disc.

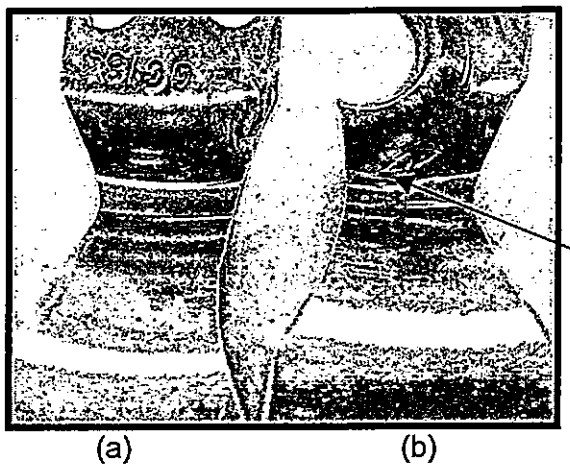

Figure 6.18.- Illustration showing the difference between smooth (a) and notched (b) specimens.

Only smooth specimens were considered for production of the S-N curve, as their fatigue performance would be more consistent because of the uniform cup radius region. Eight (smooth) specimens would be fatigue tested at each load considered. These hour-glass specimens were machined such that the diametral axis through which fracture occurs under industrial testing conditions was coincident with the axis of rotation of the laboratory fatigue testing machine. This implies that the narrowest width of the hour-glass shape, see Figure 6.18, corresponded to the fracture plane as observed on the wheel, this fracture plane also corresponds to the axis of rotation (bending axis) of the TMS fatigue

testing machine. This was done in an effort to match the fracture plane in the hour-glass specimens to that of the wheel. For this purpose a preliminary investigation was undertaken to duplicate this fracture plane observed for the wheels, but despite the various alternatives considered fracture occurred through the apex of the cup radius region for these hour-glass specimens. See Appendix E for full details of this investigation.

6.4.1 Laboratory fatigue testing set-up procedure

The fatigue testing set-up procedure for the hour-glass specimen using the values as given in Table 6.2, will be discussed and explained using Figure 6.19.

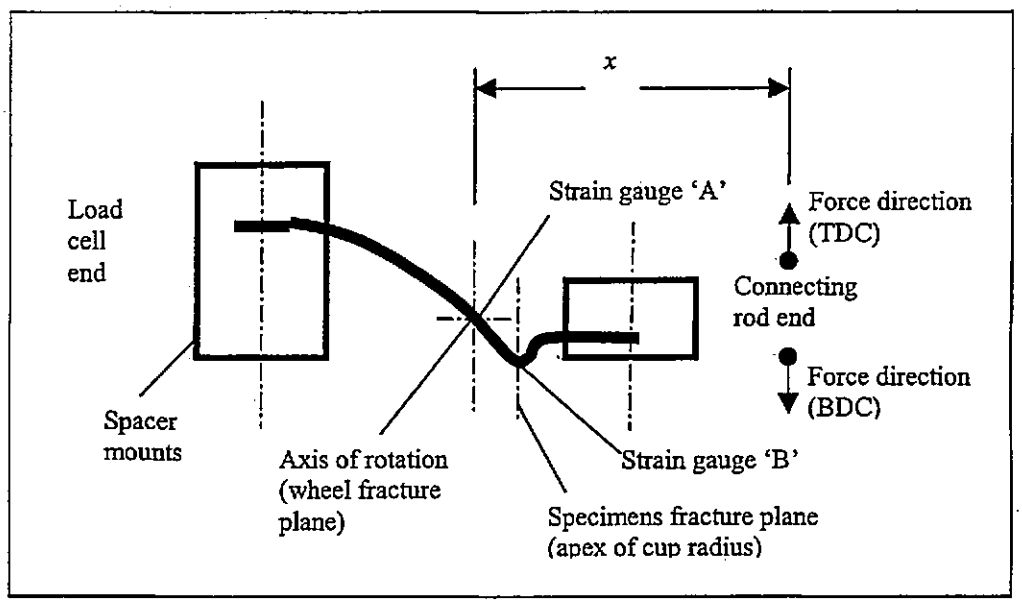

Figure 6.19.- Illustration of fatigue set-up parameters for TMS machine.

After the spacer mounts were cast, strain gauges were applied to the specimen at positions "A" (axis of rotation), this location is similar to that which was applied to the wheel, and because fracture occurred through the apex of the cup radius , strain gauge "B" was applied to the underside to assess the strain values experienced by these specimens at the plane of fracture. The initial test load considered was at the equivalent peak tensile stress of 252 MPa, and after clamping the specimen in the test jaws the strain gauges, "A" and "B", were zero-balanced, and the mean stress value of 27 MPa, tensile, (equivalent to

135μ strain) was set on strain gauge "A". The equivalent stress amplitude (Table 6.3) was now set by adjusting the eccentric situated in the flywheel of the fatigue machine to read ± 1125μ strain. The strain values observed from gauge "B" were +1261μ strain (equivalent to 252 MPa, tensile) when the connecting rod of the fatigue machine was at top dead cente (TDC) and −1699μ strain (equivalent to 340 MPa, compressive) when in the bottom dead centre (BDC) position.

Four specimens were scheduled to be fatigue tested under the above conditions and after the first specimen made 400 000 cycles the test was stopped. The remaining three specimens were nonetheless fatigue tested in which the results observed was unchanged i.e. machine was stopped after 400 000cycles.

Ind. Test Load (Nm)	Equiv. Peak Tensile Stress (MPa)	Equiv. Peak Compressive Stress (MPa)	Equiv. Mean Stress (MPa)	Equiv. Stress Amplitude (MPa)	Cycles to failure (Wheel) Nf	Cycles observed by hour-glass Specimens
4000	252	198	27	225	72 519	>400 000

Table 6.3. – Results observed considering mean stress conditions at the 252MPa test load.

It was clear from the results given in Table 6.3 that duplication of the fatigue performance was not to prevail, and that an alternative test procedure should be considered to better duplicate the fatigue performance of these specimens with respect to the wheel.

6.4.2 Alternative fatigue testing procedure

This alternative procedure is based on bending fatigue fractures[46] where the maximum tensile stress in the bending cycle is considered to govern the failure process. This is substantiated by Collins[47] in that the fatigue failure is influenced and governed by the maximum tensile stress in the applied bending cycle when a tensile mean stress is present, i.e. for a given value of maximum stress, increasing the mean stress will yield longer life. This is illustrated in Figure 6.20. The stress raiser (change in material thickness)

associated with the fracture plane in the wheel allow for the applied stresses in these areas to be highest.

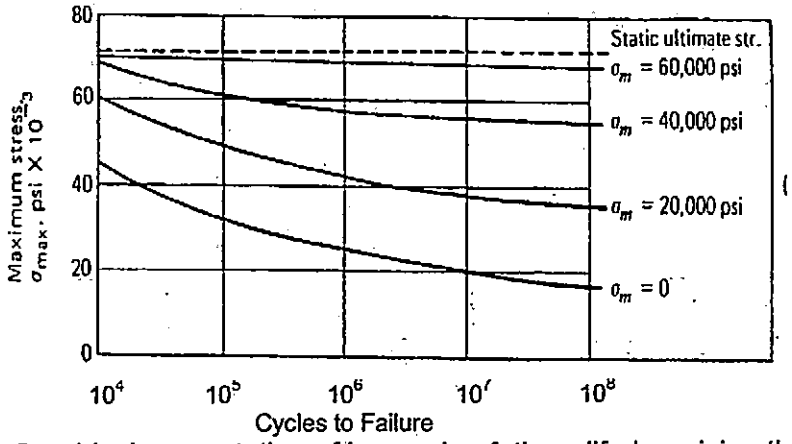

Figure 6.20[47]. – Graphical presentation of increasing fatigue life by raising the tensile mean stress value.

When observing the fatigue behaviour of the wheel this is considered true, referring to Figure 6.15 the highest peak tensile stresses occur in the 45° direction, gauge number 6 in Figure 6.13. Mean stresses[47] are considered to be associated with the crack initiation phenomenon, whereas the maximum applied stress in the cycle is associated with crack propagation and crack growth. Although a mean stress of low magnitude (σ_m / σ_{UTS} = 4%) was assessed on the diametral axis it may hence be considered negligible. Based on the above, the alternative fatigue testing procedure will consider a reversed bending, zero-mean stress condition where the equivalent maximum peak tensile values (Figure 6.15), for the five nominal stress amplitude ranges bracket the values as found in the complete wheel. Collins[47] also indicates that the most severe procedure to fatigue test components is under a zero mean stress condition.

Once again, after securing the specimen in the machine jaws, gauges "A" and "B", were zero-balanced and the stress amplitude of ± 252 MPa (equivalent 1260μ strain) was set to read on gauge "A". At this setting the values read from gauge "B" was –1540μ strain at BDC and +1420μ strain at TDC positions respectively. The result from this set-up

procedure showed that for the eight specimens tested at this load condition the fatigue failure occurred around 104 900 cycles. This indicated that under the alternative fatigue procedure the wheel results were more closely resembled. The remaining results using this alternative procedure are given in Table 6.5.

Equiv. Stress Ampl. (MPa)	Spec. 1	Spec. 2	Spec. 3	Spec. 4	Spec. 5	Spec. 6	Spec. 7	Spec. 8	Average cycles to failure, Nf
252	83800	55100	42700	120100	94800	97600	141600	203900	104950
210	293800	236500	218400	244800	197300	227900	297600	247700	245500
179	390700	336600	329200	1059600	629300	1024400	603700	608900	610500
140	$>2x10^6$	$>2x10^6$	$>2x10^6$	--	--	--	--	--	$>2x10^6$

Table 6.4. – Fatigue results of hour-glass specimens for production of S-N curve, run-out equals 2×10^6 cycles.

Comparison can now be related to the wheel data and this is shown in Figure 6.21, where the complete S-N curve giving both the wheel and minimum wheel specification values is correlated with the hour-glass data given in Table 6.4.

Equiv.Stress Amplitude (MPa)	Bending Moment (Nm)	Cycles to failure Wheels (Nf)	Cycles to failure FPW specimens (Nf)	Ratio of Wheel To FPW spec.
252	4000	72500	104900	0.69
210	3375	180700	245500	0.74
179	2750	483940*	610500	0.79
140	2125	1255861*	$>2 \times 10^6$ cycles	---
103	1500	2601415*	---	---

Table 6.5. – Hour-glass and wheel fatigue performance results, *extrapolated values using equation 6.3.

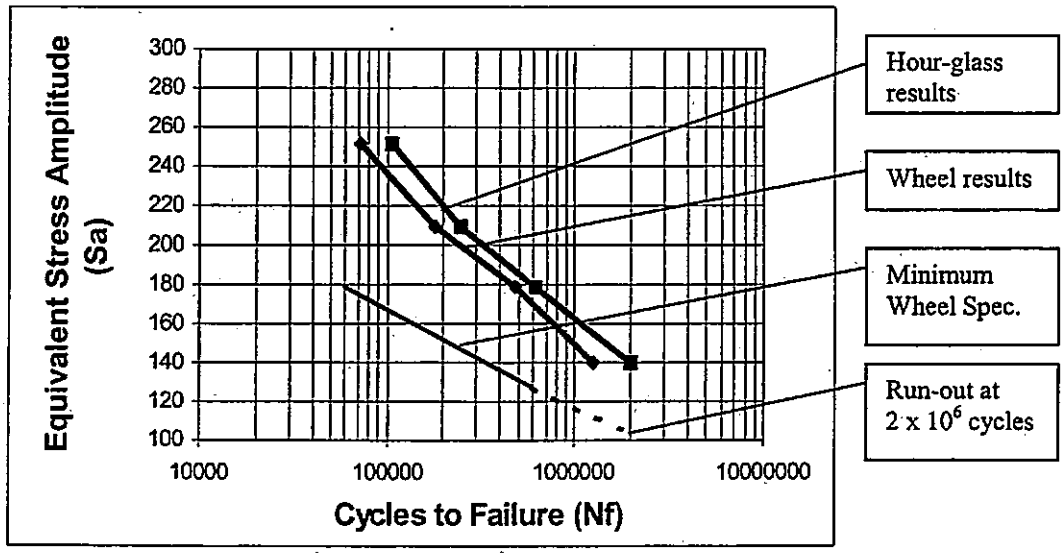

Figure 6.21. – S-N curve for hour-glass specimens showing the S-N curve of the wheel including the minimum fatigue life specification indicating run-out.

From the results indicated in Table 6.5, it is observed that the endurance limit for the specimens occur between the 179 MPa and 140 MPa stress amplitude ranges, which are 27% and 21% of the tensile strength for this DPS material, respectively. Many authors on the subject of fatigue[10,18,20,21] indicate that the endurance limit for many engineering materials fall within 30% to 60% of the UTS for that particular material. However, no indication is given by the above authors of where the endurance limit should reside for plastically deformed steel components. The endurance limit is one of the requirements for use in the fatigue life prediction model that will be employed at a later stage in this work, and hence its determination will be dealt with in Chapter 8.

From the above observations hour-glass specimens were not tested at the 103 MPa stress amplitude level. However, considering the intermediate to upper test loads (i.e. 179 - 252 MPa) the fatigue life of waisted hour-glass specimens can be predicted from the following expression:

$$S_a = -37.37 \times \ln N_f + 679.25 \qquad (MPa) \qquad (6.4)$$

Hence, a conservative relationship exists between the wheel and hour-glass specimens in the following form:

$$N_{f(wheels)} = 0.74 \times N_{f(hour-glass)} \qquad (6.5)$$

Another useful relationship is that between bending moment (M) and equivalent peak tensile stress amplitude (S_a). This was determined by the best linear fit method using values taken from Table 6.5, and is given by:

$$S_a = 0.0589 \times M + 14.88 \qquad (MPa) \qquad (6.6)$$

For fatigue testing the production stage specimens, the assessed strain values observed by strain gauge "B" on the underside of the cup radius region are important for ensuring that these specimens experience the same stress condition along its fracture location. For specimens Draw 2 through FPW this is not of concern as the equivalent stress amplitudes can be set-up at the axis of rotation because these specimens exhibit a cup radius region. But for the Blank and Draw 1 specimens this cup radius region is non-existent and hence to ensure that these two production stage specimens experience the same nominal stresses at their fracture locations (centre of waisted hour-glass shape) it is important to set the nominal stresses using the assessed values, i.e. -1540μ strain and $+1420\mu$ strain. Because run-out was observed at the equivalent (nominal) stress amplitude of 140 MPa (see Table 6.5) it was decided to fatigue test the production stage specimens at the equivalent (nominal) stress amplitude 252 MPa.

6.4.3 Fatigue testing of production stage specimens

It should be pointed out that only a limited number of production stage discs were supplied by Guestro for these analysis, allowing only four waisted hour-glass specimens from each stage to be fatigue tested at the equivalent stress amplitude of 252 MPa. This is because residual stress measurements were carried out, prior to the machining process, on the other specimens. A similar CNC machining route for these specimens was followed to that previously used. Fatigue testing commenced with the FPW specimens and ended with the "as manufactured" plate (blank) specimens.

After preparing the specimens, from each production stage for fatigue testing (casting of spacer mounts), a strain gauge was applied at their anticipated fracture planes, i.e. Draw 2 through FPW, at the underside of the cup radius region and at the centre of waisted hour-glass shape for the Blank and Draw 1 stage specimens. The fatigue data obtained from these specimens is shown in Figure 6.22.

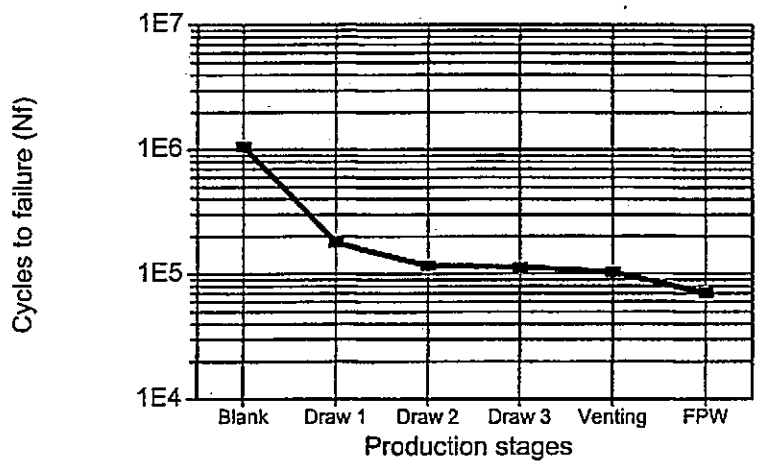

Figure 6.22. – Fatigue performance of production stage specimens.

The average number of cycles to failure for the specimens tested at each stage is given in Table 6.6, the (*) indicates results not included in the calculated average value. This is because, the centre of the specimens' thickness was not set-up through the axis of rotation for the first drawing stage component and additionally for the venting stage specimen, the failure detection device of the TMS fatigue testing machine was not activated. Figure 6.22 clearly shows that the forming processes of a wheel are detrimental to fatigue behaviour.

Prod. Stage	Spec. 1	Spec. 2	Spec. 3	Spec. 4	Ave. Number of Cycles to failure, Nf
Blank	1013900	753700	1398500	1056300	**1055600**
Draw 1	*	177200	177700	--	**177500**
Draw 2	110700	102500	126200	124600	**116000**
Draw 3	112900	113100	107500	117400	**112800**
Venting	109600	98800	99600	*	**102700**
FPW	97600	59900	52500	69900	**70000**

Table 6.6. – Fatigue results of production stage specimens.

This is odd, as one would generally expect that plastic deformation (which increases YS and UTS) would increase fatigue performance. Residual stresses, on the other hand, may act to counter this by raising the mean stress value, but one must bear in mind that the residual stresses in these hour-glass specimens have been radically reduced due to the machining process. The only other factor contributing to this fatigue behaviour is that of the micro-voids present in the substrate resulting from the forming process. Figure 6.22 is

almost a mirror image of the hardness curve in Figure 5.12, so there must be a relationship which is the inverse of the normal "hardness up – fatigue strength up" type.

Hence, the substantial decrease in cycles to failure observed for the first drawing stage specimen is attributed to the effects of plastic deformation. Here, the initial flat plate (Blank) is subjected to its first stamping operation, which takes place under a high instantaneous tensile force creating micro-voids (see Figure 6.1) at the grain boundaries between the harder martensite and softer ferrite phases. These micro-voids act as stress raisers within the microstructure weakening the component in terms of fatigue[19]. This imperfection is compounded during the second drawing stage where the component suffers further plastic deformation.

The fatigue life of the FPW specimens decreases slightly, relative to the draw 2, draw 3 and venting stages, because of the carbo-nitride precipitates that form along the grain boundaries close the components surface. This phenomenon occurs during the paint baking (curing) cycle and essentially embrittles the surface resulting in a substantial decrease in fatigue life.

6.5 FRACTOGRAPHY

The fracture surfaces of all hour-glass fatigue specimens were similar in character see Figure 6.23, i.e. ratchet markings at both top and bottom surfaces, which are more pronounced along the top surface indicating that the crack initiated from this surface. The crack growth slows as it propagates through the elastic core region in the area around the neutral axis where it grows laterally (secondary cracking) due to the stress discontinuities[42] present in this region. The neutral axis is observed to be off-set from the centre of thickness region due to the localised necking and plastic deformation which has transpired in the cup radius area. This is indicated by the stress gradient shown in Figure

6.4. As the crack grows, the overall stress level increases (σ = load/area) until the stress level at a particular crack depth equals the stress value at the underside of the cup radius and hence crack initiation commences from the bottom surface. From this point, the crack fronts then grow toward one another until catastrophic failure occurs which is observed by the 'fast fracture line' evident along the lower half in Figure 6.23.

Figure 6.23. – Typical fracture features of hour-glass specimen.

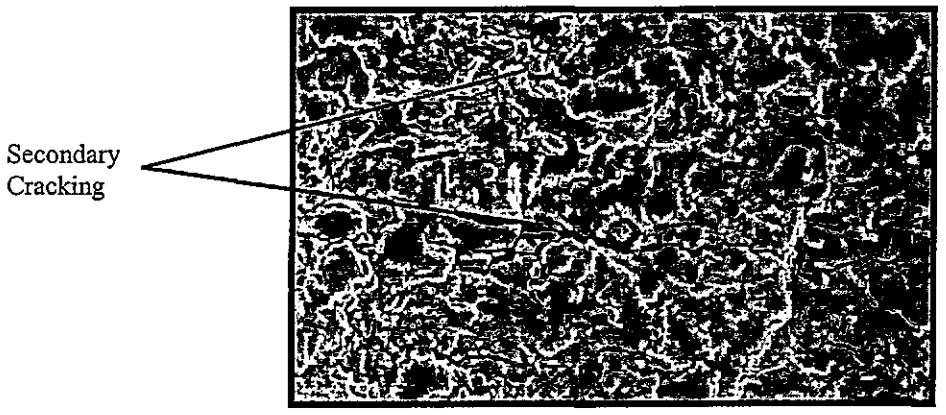

Figure 6.24. – Secondary cracking (location "A" in Figure 6.23) effects resulting from crack propagation through the elastic core (stress discontinuity) region x775.

6.6 SUMMARY

Although the centre discs of automotive wheels have been work-hardened increasing the materials UTS, the fatigue performance decreases, at constant stress amplitude, as the forming operation progresses through the production stages. This results from the fact that the forming process creates micro-voids due to the existence of bi-axial tensile stresses. A second effect is that the tensile residual stresses induced increase the level of the mean stress for the wheel, which generally decreases the sustainable stress amplitudes for a given life. These conditions are therefore considered detrimental to fatigue performance.

The fatigue testing of waisted hour-glass specimens can now be considered an effective tool for evaluating the fatigue strength of automotive wheels under similar nominal test conditions. Because industry has no means of fatigue testing full-scale production stage components, it is envisaged that the results obtained from the hour-glass specimens would be useful as a prediction tool for the effects of changes in process or alloy. Data from complete wheel and fatigue specimens indicate that the endurance limit for plastically deformed DPS plate components at a life of 2×10^6 cycles lie between 21% and 27% of the tensile strength. The fatigue results from the production stage specimens will now be considered together with the residual stress and surface hardness results in an effort to link these three material characteristics in a first order model for fatigue life prediction of the wheels.

CHAPTER 7

RELATIONSHIPS BETWEEN FATIGUE LIFE, RESIDUAL STRESS AND HARDNESS

The objective of this chapter is to establish relationships between the different material characteristics investigated, namely, surface hardness *(measurements taken on components surface, refer Section 5.2.2)*, induced residual stresses and fatigue life of components subjected to plastic deformation caused by forming operations. This will lead to a better understanding of the fatigue behaviour and contribute new knowledge in respect of life prediction for sheet metal forming processes. The relationships sought in this chapter will concentrate on the diametral axis along which fracture is observed to occur under industrial fatigue testing conditions, as this is the critical cracking location in wheels.

7.1 RESIDUAL STRESSES AND SURFACE HARDNESS

These two material properties are fundamentally important when investigating components subjected to forming operations. In the first instance, the components are work hardened, increasing the components tensile strength and subsequent yield strength and secondly, residual stresses will inevitably be induced as a result of such work hardening operations. These two material characteristics were assessed on three diametral axes and in the rolling, 45° and transverse directions, of the sheet for all production stages of centre disc manufacture.

7.1.1 Process effects on Residual Stress and Surface Hardness

PRODUCTION STAGE	RESIDUAL STRESS (MPa)				SURFACE HARDNESS (HB2/120)			
	Roll.	45 deg.	Trans.	Ave.	Roll.	45 deg.	Trans.	Ave.
Blank	37.8	37.8	37.8	**37.8**	189	189	189	**189**
Draw 1	106.3	90.2	74.1	**90.2**	193	194	195	**194**
Draw 2	234.1	173.3	164.1	**190.5**	203	203	205	**204**
Draw 3	265.8	192.4	178	**212.1**	212	216	218	**215**
Venting	307.4	305.8	300	**304.4**	209	212	214	**212**
Paint (FPW)	396	384.1	381.6	**387.2**	221	222	227	**223**

Table 7.1. – Residual stress and Surface Hardness results for the various production stages.

Considering Table 7.1, the following aspects should be noted.

- That the expressions developed in this Chapter are only applicable within the range of data presented in the respective Tables.
- The results of both surface hardness and residual stress (up to and including the third drawing stage specimens) indicate that the material behaves anisotropically under forming conditions and that the residual stress magnitudes are in the reverse order to those for surface hardness. Hence the residual stress values are generally highest in the rolling direction and lowest in the transverse direction. Hardness and residual stress results in the 45° plane tend to be close to the average of the values for the other two directions, which is perhaps not unexpected.
- The residual stress magnitudes for the Venting stage are believed to have increased due to an internal rearrangement of forces following material removal during the punching operation of the vent holes. This equilibrium seeking or re-distribution phenomenon produces stress magnitudes which are almost equal in all three directions.

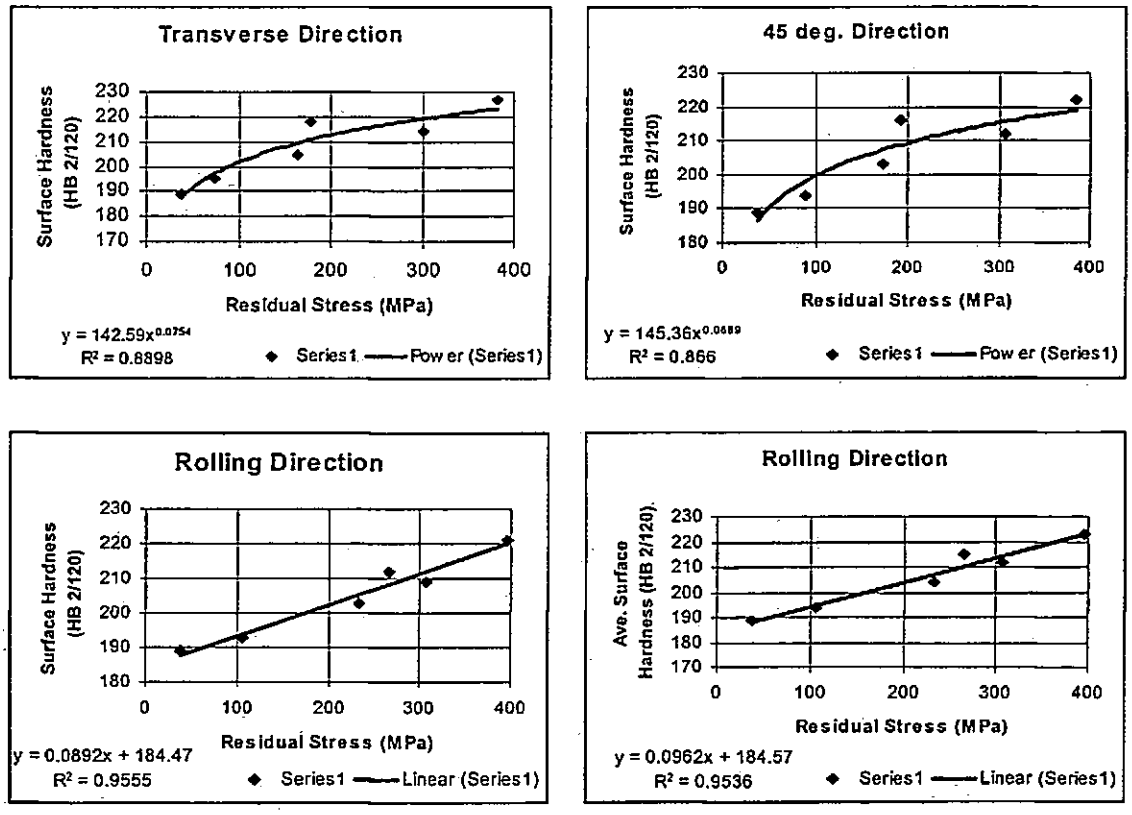

Figure 7.1. – Residual stress – surface hardness relationships.

- Only best fit relationships are presented with respect to the Figures in this Chapter.

Clearly, only the rolling direction data correlates in a linear, progressive fashion and hence these data can be used to relate hardness and residual stress across the production stages. On normal axes an expression was developed according to the following linear format:

$$y = mx + c \quad \text{.....(7.1)}$$

Now, considering the residual stress and surface hardness from the Rolling Direction in Table 7.1, the following expression was obtained:

$$HB = 0.0892 \times \sigma_{residual} + 184.47 \quad \text{.....(7.2)}$$

Where: HB = Brinell Hardness Number;
$\sigma_{residual}$ = Relieved Residual Stress.

Expression 7.2 gives a maximum error of 16% in residual stress prediction for the production stages, compared with the measured values.

An improved alternative relationship is obtained by grouping and averaging the values of both surface hardness and residual stress for the second and third drawing stages shown in Table 7.1. The hypothesis is based on:

- the assumption that the material volume is equal in the second and third drawing stage pressings;
- the clustering effect of the second and third drawing stage results, see Figure 7.1; and
- the fact that negligible plastic deformation is encountered in the cup radius region with regard to the third drawing stage as this region already exists from the second drawing stage.

Figure 7.2 shows this grouping and averaging effect and the alternate expression is given by:

$$HB = 0.0878 \times \sigma_{residual} + 184.63 \quad \text{.....(7.3)}$$

Expression 7.3 reduces the residual stress prediction error to 9.6%, a substantial decrease compared with the use of expression 7.2. **Note**, that both expressions 7.2 and 7.3 predict a surface hardness of around 184.5 at zero residual stress.

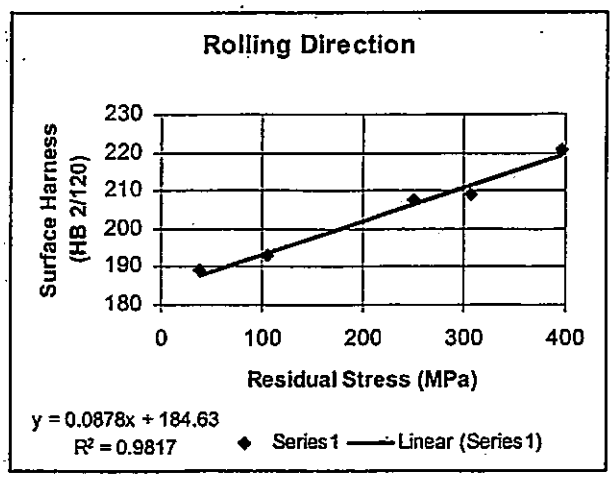

Figure 7.2. – Effect of averaging Draw 2 and Draw 3 residual stress and surface hardness values.

The relationship according to expression 7.3 allows for estimating the residual stress magnitude from surface hardness measurements for these production stages of a DPS wheel. This is important when using the mean stress fatigue models of Goodman, Soderberg, Gerber and Morrow for complete components (wheels) where the level of the mean stress is the sum of the actual or applied mean stress and the residual stress values, as was discussed in Section 2.6.1.

7.2 SURFACE HARDNESS AND FATIGUE LIFE OF PRODUCTION STAGE SPECIMENS

Surface hardness assessment is a useful technique for approximating changes in the UTS of a steel alloy. The ease with which hardness assessments are made makes it an invaluable tool in alloy characterisation. Here an attempt is made to link the fatigue

performance of centre discs to the average surface hardness for production stage specimens. The relevant data are shown in Table 7.2. This excludes the "as manufactured" plate (blank), i.e. it considers only components subjected to forming operations.

Production Stage	Cycles to failure (Nf)	Average Surface Hardness (HB2/120)
Draw 1	177500	194
Draw 2	116000	204
Draw3	112800	215
Venting	102700	212
Paint (FPW)	70000	223

Table 7.2. – Production stage fatigue performance and average surface hardness results.

The data given in Table 7.2 can be plotted to show that a linear relationship exists, which is shown in Figure 7.3.

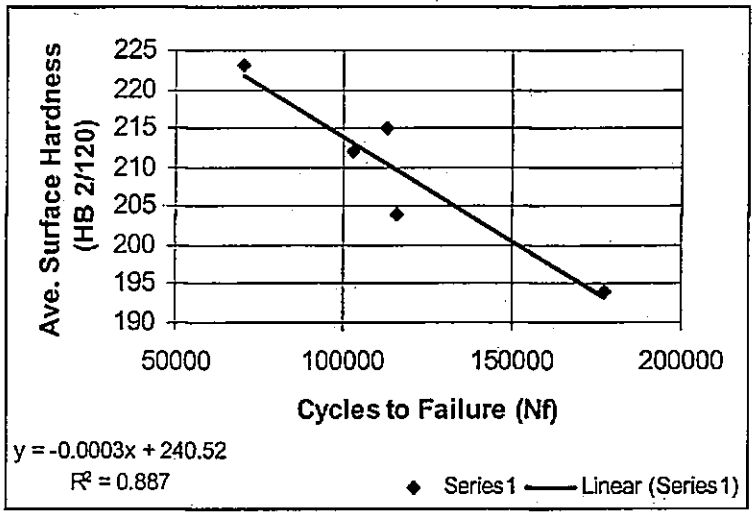

Figure 7.3. – Relation between average surface hardness and fatigue performance of production stage specimens.

The expression describing this linear relationship is given by:

$$HB = -0.3 \times 10^{-3} Nf + 240.52 \quad \text{.....(7.4)}$$

Expression 7.4 reveal errors in fatigue life of +5% with respect to the second drawing stage specimens and –24.6% with respect to the third drawing stage specimens. Thus, a fatigue life prediction with use of expression 7.4 in terms of surface hardness will have a

maximum error margin of approximately 25%. This error can be considerably reduced through grouping and averaging the number of cycles to failure and hardness for the second and third drawing stage values as was carried out according the hypothesis taken

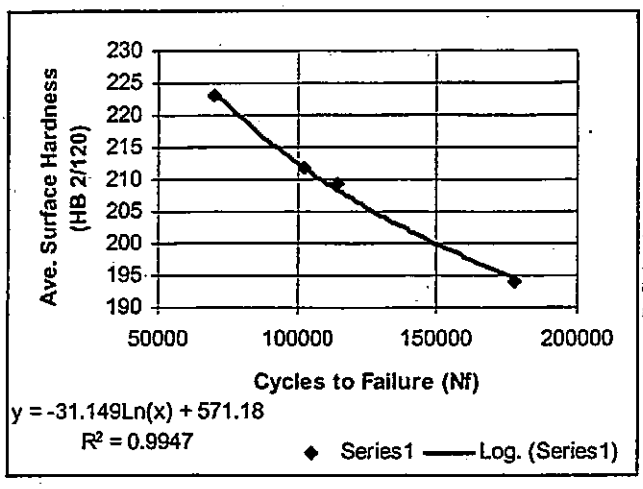

Figure 7.4. – Effect of averaging the number of cycles to failure and average surface hardness values.

in Section 7.1. The averaging effects are shown in Figure 7.4 where the expression changes from a linear to a logarithmic fit improving the coefficient of determination by 10.8%. Expression 7.5 reduces the fatigue life prediction error to -3.5%.

$$HB = -31.149 \ln Nf + 571.18 \quad \text{.....(7.5)}$$

7.3 RESIDUAL STRESS AND FATIGUE LIFE OF PRODUCTION STAGE SPECIMENS

This section concentrates on finding a relationship between the 'as assessed' residual stress values and the fatigue performance of production stage components, so that a fatigue life prediction can be made in terms of residual stress. Table 7.3 indicates the values considered in seeking this relationship.

Production Stage	Residual Stress (Mpa)			Cycles to failure (Nf)
	Roll.	45 deg	Trans	
Draw 1	106.3	90.2	74.1	177500
Draw 2	234.1	173.3	164.1	116000
Draw 3	265.8	192.4	178	112800
Venting	307.4	305.8	300	102700
Paint	396	384.1	381.6	70000

Table 7.3. – Residual stress and fatigue performance values.

Residual stress/fatigue data for the rolling direction are plotted in Figure 7.5 and indicates that the following logarithmic expression may be useful:

$$\sigma_{Residual} = -316.37 \ln Nf + 3936.7 \qquad (MPa) \ldots\ldots\ldots\ldots\ldots\ldots (7.6)$$

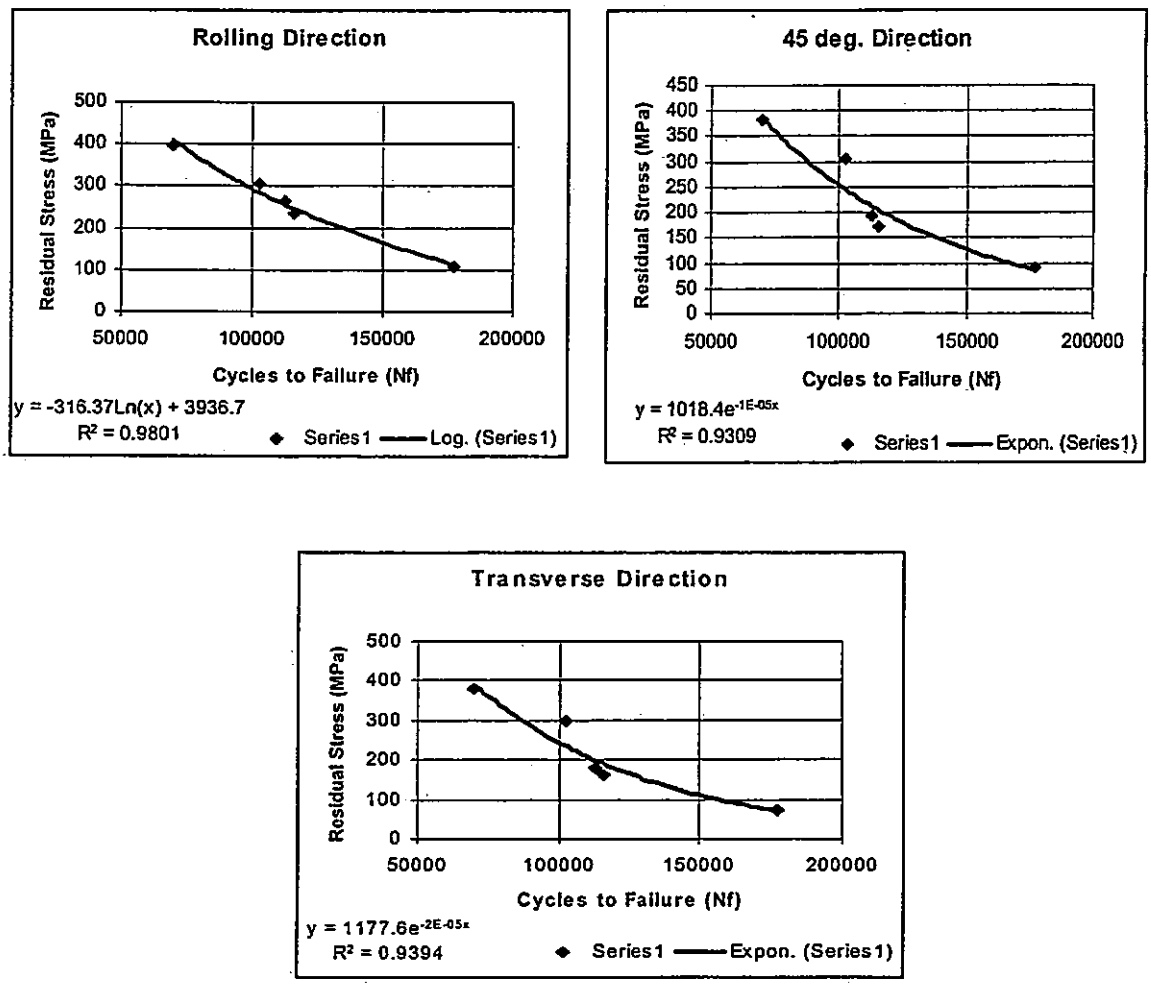

Figure 7.5. – Relations between residual stress and fatigue performance of production stage specimens.

The above expression (7.6) gives predicted values for fatigue life from residual stress data within 4.3% of the observed values. On the other hand, residual stress prediction from fatigue life reveals a 5.5% error, in the worst case.

The positive outcome of the expressions 7.3 and 7.6 in which the residual stress values are related to hardness and fatigue life respectively validates the necessity for such an 8-grid strain rosette. Although a 3-element strain rosette was used for assessing the residual stress magnitudes on the critical diametral axis under consideration, the alignment of this 3-element grid was in actual fact determined by use of the 8-element rosette from assessments made on the other two diametral axes.

7.4 COMPARISON BETWEEN PREDICTIVE CAPABILITY OF FATIGUE LIFE, RESIDUAL STRESS AND HARDNESS

A comparison will now be made between the ability of hardness and residual stress to predict the fatigue life of production stage specimens. Table 7.4 gives the relevant data while Figure 7.6 plots it.

Production Stage	Average Suface Hardness (HB 2/120)	Residual Stress (MPa)	Fatigue Life (Nf) x1000 cycles
Blank	189	37.8	1000
Draw 1	194	106.3	177.5
Draw 2	204	234.1	116
Draw 3	215	265.8	112.8
Venting	212	307.4	102.7
Paint (FPW)	223	396	70

Table 7.4. – Material characteristic values used for showing the combined effects

The following conclusions can be drawn from the graph shown in Figure 7.6 with respect to the mechanical properties and fatigue life for the various production stage components. The trends indicated in the data are attributed to the results of cold working operations experienced by the components up to and including the third drawing stage of the

production process, where the surface hardness and residual stress values increase with a decrease in fatigue life.

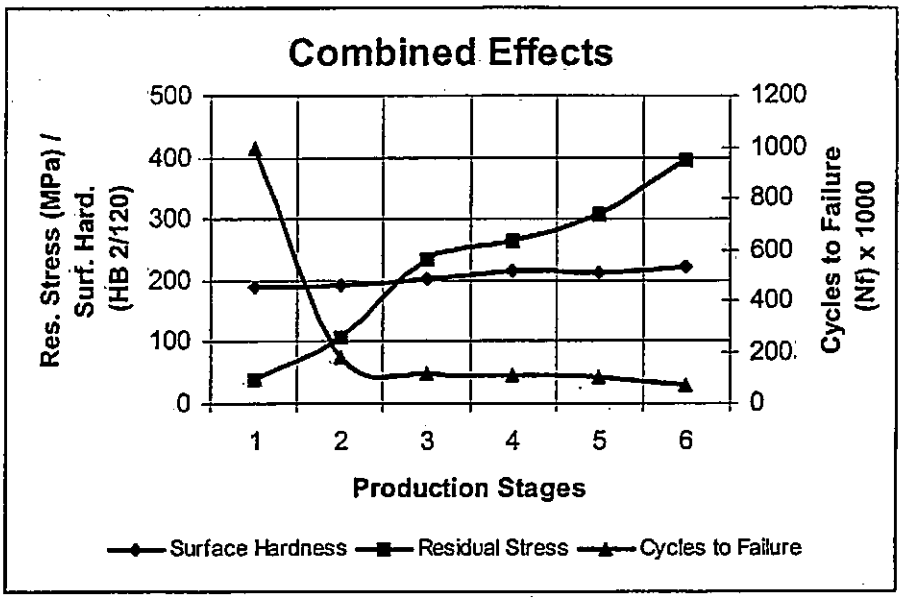

Figure 7.6. – Combined effects of the material characteristics.

During these three draw stages, first through third, the sheet material is progressively work hardened and subjected to increasing bi-axial plastic deformation under tensile conditions which induces micro-void formation (see Figure 5.9). The decrease in fatigue life is therefore attributed to:

- The micro-voids acting as stress raisers and increasing the fatigue notch sensitivity of the alloy.

During the Venting stage, the surface hardness decreases, as too does the fatigue life while the residual stress increases substantially. Here, no further plastic deformation is experienced by the component along the fracture plane and hence a similar surface hardness result is obtained to that of the third drawing stage. However, because of the punching of the vent holes the residual stresses increase, as a result of the redistribution of the forces in the component. The paint curing temperature is around 200°C and the observed increase in residual stress and surface hardness is related to a bake-hardening phenomenon where carbo-nitrides precipitate along the grain boundaries embrittling the

surface of the component. The fatigue notch sensitivity also increases as a result of the surface embrittlement and hence a substantial decrease in the fatigue life is observed.

7.5 SUMMARY

Clearly, the hardness and rolling direction residual stress values can be linearly related on semi-log plots, to the fatigue life of the production stages. It must be noted that the expressions developed from the data obtained are approximate, as many factors can influence the fatigue life. Such factors include micro-structural imperfections, like stress discontinuities, micro-voids, banding, inclusions etc., tool markings and surface finish.

The fact that surface hardness can be related to the fatigue performance is industrially useful because the procedure is quick, easy to undertake and is inexpensive. While a relationship can be said to exist in all three directions regarding residual stress values with surface hardness and fatigue, the rolling direction however gives the best linear fit although the reason for this is not all that clear. Consideration will now be given to predicting the fatigue performance of the complete wheels.

CHAPTER 8

AUTOMOTIVE WHEEL FATIGUE LIFE PREDICTION MODEL

Historically, the stress analysis used for design assumed "ideal" materials, i.e. with isotropic, homogeneous and continuous properties. We now know that this is untrue and that defects will always be present in the material and its fabrication however good the design. As design cannot provide defect-free components or materials, appropriate defect tolerance should be the aim of the designer or manufacturer. Hence, the concept of fail-safe components has been introduced for safety-critical components. Wheels, however, are not fail-safe items and fatigue life prediction techniques need to be improved in the manufacturers quest to provide lighter weight, durable and attractive wheels.

The author is of the opinion that, for vehicle wheels, the residual stress magnitude plays the predominant role in determining mean stress value, and hence in the sustainable stress amplitude for a given life (see Sections 2.6.1). This is because the applied mean stress and residual stress add algebraically to produce a higher level of mean stress. This implies that if the mean stress magnitude is small and tensile in nature and the residual stress magnitude is larger and also tensile in nature, then instead of fatigue testing about a low mean stress level the actual magnitude of the mean stress level would now shift to a higher level by the inclusion of the greater residual stress magnitude. This summing of the actual measured mean stress and the residual stress values will be termed the "effective mean stress" in this thesis.

This chapter considers the results of investigations carried out on the automotive wheel, where the relationships developed would hopefully correlate to the fatigue data of the hour-glass specimens. The model used in this work relates to the standard mean stress relationship given by Gerber[20,21] but includes the effects of residual stress. This choice of model is based

on Suresh[21] who indicates that the Söderberg relationship gives rather conservative life estimates for most engineering alloys, while the model by Goodman matches experimental observations quite closely for brittle alloys and for ductile materials the Gerber model is more widely used for life prediction. DPS falls in this latter category and hence it will be shown from the assessed wheel data that residual stress plays a major role with respect to the fatigue performance of automotive wheels. Here the life prediction method as described by Juvinall and Marshek[10] will be used in conjunction with the Gerber relationship in an endeavour to develop a life prediction model for automotive wheels and hence to compare these predictive values to the actual wheel fatigue results. This will now be discussed in more detail.

8.1 Life prediction method according to Juvinall and Marshek[10]

This procedure can be used for a variety of engineering steels, in this method a point at 1000 cycles [S_{1000}] is established on the vertical axis [S_n], and then a straight line from this point is drawn to an estimated fatigue limit [S_e] at a specified number of cycles (usually $1x10^6$ cycles). This straight line is indicated as the Juvinall and Marshek prediction line in Figure 8.1. Using the applicable mean stress relationship, the completely reversed stress amplitude [S_n] is determined (see section 8.2.1). The number of cycles at S_e for life prediction of the wheels will be taken at $2x10^6$ cycles, as this number corresponds with the minimum specification for this model wheel[44].

The point at 1000 cycles [S_{1000}] is estimated by taking advantage of the observation that the completely reversed fatigue strength at this life is only a little below the ultimate tensile strength, and hence for most steels this point is taken at 90% of the materials UTS. Also, the many factors that strongly affect the fatigue limit, such as size and surface finish, have little or no effect at this life (i.e. 1000 cycles). Many authors[20,21] indicate that the estimated fatigue limit [S_e] for steel lies between 30% to 60% of the UTS, the value used for this prediction model will hence be determined from the wheel data assessed in Chapter 6,

considering the observations made and discussed in section 6.4.2, where it was indicated that the endurance limit for sheet metal formed components lie between 21% and 27% of the UTS. The model parameters are illustrated in Figure 8.1.

Life prediction is then carried out by plotting the fully reversed stress amplitude values [S_n], calculated from the relationship of Gerber against the Juvinall and Marsheks' life prediction line and then to read off the estimated or predicted life on the horizontal axis, N_f, shown in Figure 8.1.

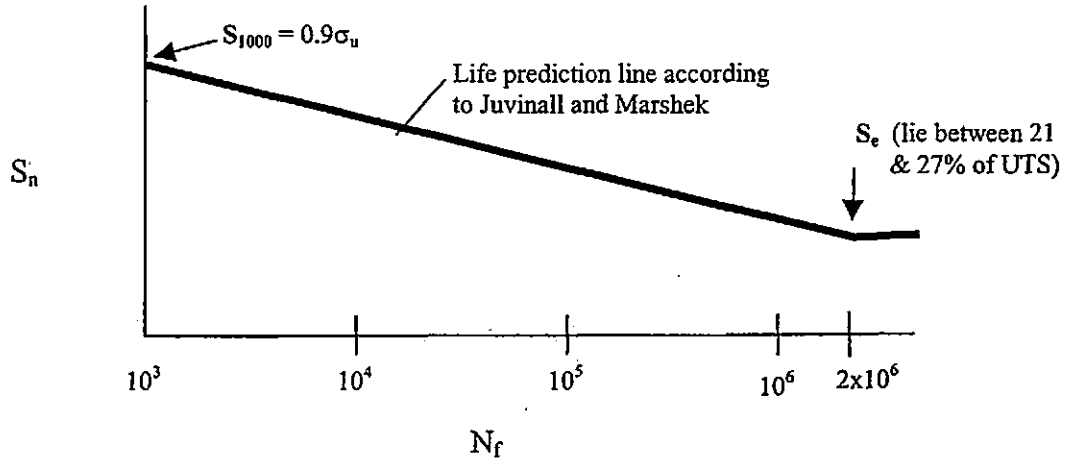

Figure 8.1. – Fatigue life prediction parameters according to Juvinall and Marshek[10].

8.2 Requirements for Mean Stress Modelling

The model requirements for calculating the fully reversed stress amplitude values [S_n] according to Gerber include:

- The 'effective' mean stress, σ_m;
- The equivalent stress amplitude, σ_a;
- The Tensile Strength, S_u;
- The Yield Strength, S_y;

8.2.1 Determining the Mean Stress modeling requirements

The mechanical properties of this DPS600 material are:

Tensile Strength, S_u = 664 MPa

Yield Strength, S_y = 427 MPa

The other requirements as listed in 8.2 above were determined by using the values found in the investigations undertaken, as follows:

$$"Effective" \ Mean \ Stress, \ \sigma_m = \left[\frac{\sigma_{max} + \sigma_{min}}{2}\right] + \sigma_{residual}$$

For the calculation procedure that follows, values pertaining to the 4000Nm test load and 45° direction will be used, see section 6.3.1. Hence, the values for σ_{max} and σ_{min} are taken from Table 6.2, and $\sigma_{residual}$ is taken from Table 5.4, thus the "effective mean stress" is given by:

$$"Effective" \ Mean \ Stress, \ \sigma_m = \left[\frac{252 + (-198)}{2}\right] + 384$$

$$\sigma_m = 411 \ MPa$$

and, the equivalent stress amplitude, σ_a, by:

$$\sigma_a = \left[\frac{\sigma_{max} - \sigma_{min}}{2}\right]$$

$$\sigma_a = \left[\frac{252 - (-198)}{2}\right]$$

$$\sigma_a = 225 \ MPa$$

S_{1000} is determined at 90% of the Tensile Strength[10], which is:

$$S_{1000} = 0.9 \times 664 = 598 \ MPa$$

The Endurance Limit, S_e, will now be determined from the wheel data given in Table 6.3 and indicated in Figure 6.13, as follows:

As previously mentioned in Section 6.4.2, the endurance limit should lie between 21% and 27% of the UTS for the material, as observed from the hour-glass fatigue data (Table 6.3) which was carried out under zero mean stress conditions. Hence, the equivalent peak stress (103 MPa) indicated at the predicted 2 x 10^6 cycle limit (run-out) for the minimum wheel specification need be considered in terms of its zero-mean stress (fully reversed) value in order to correlate and establish the endurance limit. This zero-mean stress (fully reversed) value determined from the Gerber equation considers the effective mean stress value as obtained above. Hence, at the minimum specification for the wheel, the fully reversed value is given by:

$$S_n = \frac{\sigma_a}{1 - \left[\left(\frac{\sigma_m}{S_u}\right)^2\right]}$$

$$S_n = \frac{103}{1 - \left[\left(\frac{413}{664}\right)^2\right]}$$

$$S_n = 168 \ MPa$$

This value of 168 MPa is the fully reversed stress magnitude corresponding to run-out at 2 x 10^6 cycles. The endurance limit can now be determined and is hence the ratio of the fully reversed stress magnitude, to the UTS for the material, and is given by:

$$Endurance Limit, \ S_e = \left[\frac{168}{664}\right] \times 100$$

$$S_e = 25.3\%$$

This percentage value of UTS corresponds well to the average percentage values as discussed in section 6.4.2, i.e. between 21% and 27% of UTS, the average being 24%. The endurance limit for use in the Juvinall and Marshek prediction model will hence be taken at 25% of the UTS which is 166 MPa.

From these calculated values for S_e (166 MPa, taken at 2 x 10^6 cycles) and S_{1000} (598 MPa, taken at 1000 cycles) life prediction, according to the life prediction line of Juvinall and Marshek (see Figure 8.1), can hence be determined by the following linear relationship:

$$S_n = -56.84 \times \ln N_f + 991 \qquad (MPa) \qquad \text{.....(8.1)}$$

8.2.2 Determination of the fully reversed alternating stress values

The values indicated in Table 8.1 will be used in the Gerber equation for determining the fully reversed stress amplitude which, include the equivalent stress amplitude and the effective mean stress values taken from Table 6.2. This will be referred to as prediction 1.

Fatigue Test Load (Nm)	Equivalent Stress Amplitude, σ_a (MPa)	Effective Mean Stress, σ_m (MPa)
4000	225	384+27=411
3375	189	384+20+404
2420	132	384+26=410
1800	93	384+29=413

Table 8.1. – Stress amplitude and "effective mean stress" (residual stress plus the applied mean stress, prediction 1) values as calculated, the latter two stress amplitude and applied mean stress values are interpolated using equation 6.5.

Now the fully reversed alternating stress values (S_n) are calculated as follows: **Gerber:-**

$$S_n = \frac{\sigma_a}{1 - \left[\left(\frac{\sigma_m}{S_u}\right)^2\right]}$$

$$S_n = \frac{225}{1 - \left[\left(\frac{411}{664}\right)^2\right]}$$

$$s_n = 365 \ MPa$$

The fully reversed stress magnitude of 365 MPa fits well within the S_{1000} value of 598 MPa, this is important as the S_n value must fall below the S_{1000} value for the fatigue life prediction model to be effective, see Figure 8.1. Because this S_n value calculated from the Gerber equation falls within the required value of 598 MPa, the calculated S_n values relating to the remaining three fatigue test amplitudes are given in Table 8.2.

Fatigue Test Loads (Nm)	Fully Reversed Alternating stress values, S_n (MPa)
4000	365
3375	300
2420	213
1800	152

Table 8.2. – Fully reversed alternating stress values as calculated for the fatigue test amplitudes.

The S_n values as indicated in Table 8.2 are used in the fatigue life prediction model where they are compared to the actual industrial fatigue test results, given in Table 6.1.

8.3 FATIGUE LIFE PREDICTION MODEL

Fatigue life prediction is obtained using the fully reversed amplitude values given in Table 8.2 for substitution in expression 8.1. The predicted lives for the four test loads are given in Table 8.3 and shown in Figure 8.2.

Fatigue Test Load (Nm)	Actual Wheel Fatigue Life (N_f)	Predicted Wheel Fatigue Life (prediction 1) (N_f)
4000	72519	60680
3375	180718	190409
2420	847962	879883
1800	1980242	2573383

Table 8.3. – Fatigue life prediction according to Gerber vs actual fatigue life (prediction 1). Note that 2×10^6 cycles is considered run-out.

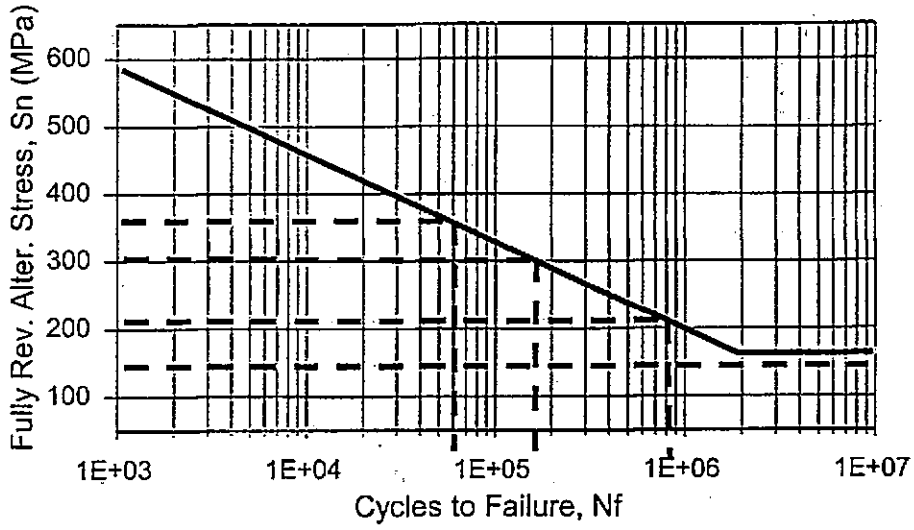

Figure 8.2. – Fatigue life prediction model according to Gerber.

The results indicated in Table 8.3 give an under estimated life prediction at the 4000 Nm test load of 16%, while at the 3375 Nm and 2420 Nm an over estimate of 5% and 4% is predicted respectively. The fatigue lives at 1800Nm are considered run-out. A point to note is that fatigue testing of automotive wheels is seldomly carried out above the 3375 Nm test load value.

The Haigh diagram shown in Figure 8.3 is produced using prediction 1 test data.

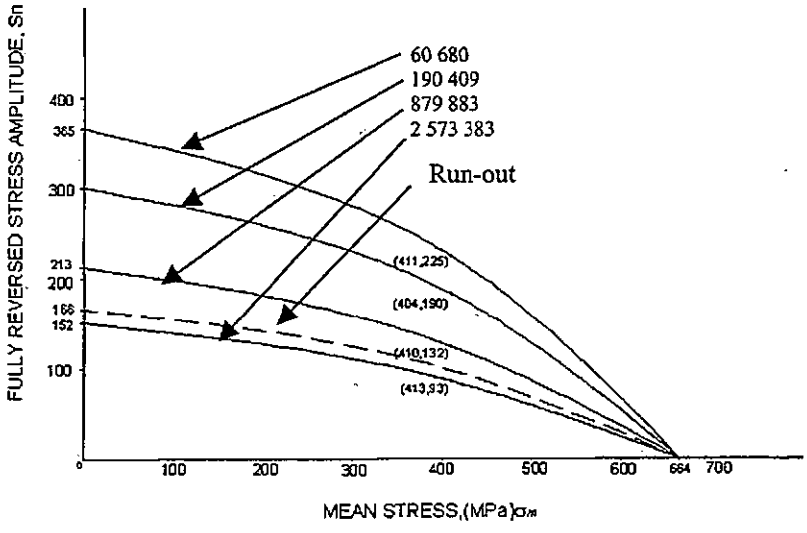

Figure 8.3. – Haigh diagram according to Prediction 1.

To show the effect of altering the "effective" mean stress value the procedure followed in prediction 1, will be adapted to exclude the applied mean stress values. This approach will be referred to as prediction 2. This implies that only the relieved residual stress values will be considered as the "effective" mean stress in the Gerber equation for determination of the fully reversed stress amplitudes for the four test loads. The required values for this approach are given in Table 8.4.

Fatigue Test Load (Nm)	Equivalent Stress Amplitude, σ_a (MPa)	Effective Mean Stress, σ_m (MPa)
4000	252	384
3375	210	384
2420	159	384
1800	119	384

Table 8.4. – Stress amplitude and "effective mean stress" (residual stress) values, the equivalent stress amplitudes for the latter two test values are interpolated, using equation 6.5.

Now, using the values indicated in Table 8.4 the fully reversed stress amplitudes given in Table 8.5, were determined as follows:

$$S_n = \frac{\sigma_a}{1 - \left[\left(\frac{\sigma_m}{S_u}\right)^2\right]}$$

$$S_n = \frac{225}{1 - \left[\left(\frac{411}{664}\right)^2\right]}$$

$$S_n = 379 \ MPa$$

Fatigue Test Loads (Nm)	Fully Reversed Alternating stress values, S_n (MPa)
4000	379
3375	316
2420	237
1800	176

Table 8.5. – Fully reversed alternating stress values as calculated for the fatigue test loads.

Life prediction is given by substituting the fully reversed alternating stress values from Table 8.5 into expression 8.1. This is shown in Table 8.6 together with the actual wheel data.

Fatigue Test Load (Nm)	Actual Wheel Fatigue Life (N_f)	Predicted Wheel Fatigue Life (prediction 2) (N_f)
4000	72519	47433
3375	180718	143694
2420	847962	576832
1800	1980242	1687053

Table 8.6. – Fatigue life prediction according to Gerber, comparing actual fatigue data. Note that 2×10^6 cycles is considered run-out.

Prediction method 2 leads to underestimates of fatigue life. Even though the applied mean stress is only 7% of the "effective" mean stress for the 4000Nm test load (prediction 1), the life is under estimated by as much as 35%. Hence, for a small reduction in "effective" mean stress, a substantial decrease in fatigue life is observed. This emphasises the significance of the residual stress assessment technique in that if the absolute maximum relieved residual stress magnitude is not assessed then the same outcome as above would occur, i.e. under estimation of fatigue life. Therefore, when considering fatigue life prediction models for complete components such as wheels, it is important that both applied mean stress and absolute maximum relieved residual stress be assessed and incorporated in the relevant model equation for predicting the life to within acceptable limits.

The above predictions (1 & 2) considered the maximum relieved residual stress value (384MPa) assessed in the 45° direction. This value is above the 80% yield strength (YS) value for the material in terms of Schajers[17] observation, refer to section 5.3. Hence, in terms of this observation the 80% YS value as given in Table 5.4, i.e. 341 MPa, will now be used to predict the fatigue life of wheels where the "effective" mean stress will also include the applied mean stress values - prediction method 3. The fully reversed alternating stress

values calculated using the Gerber equation together with the "effective" mean stress values are given in Table 8.7.

Fatigue Test Loads (Nm)	Effective Mean Stress (MPa)	Fully Reversed Alternating Stress values, S_n (MPa)
4000	341 + 27 = 368	325
3375	341 + 20 = 361	268
2420	341 + 26 = 367	190
1800	341 + 29 = 370	135

Table 8.7. – Revised S_n values considering the residual stresses taken at 80% of yield strength, prediction method 3.

Now using expression 8.1 the following predicted cycles to failure is estimated and given in Table 8.8.

Fatigue Test Load (Nm)	Actual Wheel Fatigue Life (N_f)	Predicted Wheel Fatigue Life (N_f)
4000	72519	122651
3375	180718	334341
2420	847962	1318742
1800	1980242	3470527

Table 8.8. – Life prediction method 3, using residual stress values taken at 80% of yield strength, see Table 5.3. Note that 2 x 10^6 cycles is considered run-out.

Life prediction by considering the residual stress value at 80% of YS is somewhat over conservative. This indicates that a 12.5% difference in relieved residual stress between the actual assessed magnitude and the 80% value as suggested by Schajer, resulted in an over estimate in fatigue life of 85% when related to the 3375 Nm test load. The maximum relieved residual stress magnitude assessed in the 45° direction is 90% of the yield strength. One can now appreciate the importance of assessing the absolute maximum residual stress magnitude when it comes to fatigue life prediction of sheet metal formed components.

In concluding this section the predicted wheel fatigue data (prediction 1) and the hour-glass fatigue data will be plotted against the actual wheel fatigue data (Figure 8.4 and Table 8.9). The upper control limit (UCL) established from the wheel fatigue data is also plotted on the graph, this will give some indication of where the predicted and hour-glass data (H-G Spec.) lie in relation to the wheel data and its respective UCL. This is shown in Figure 8.4.

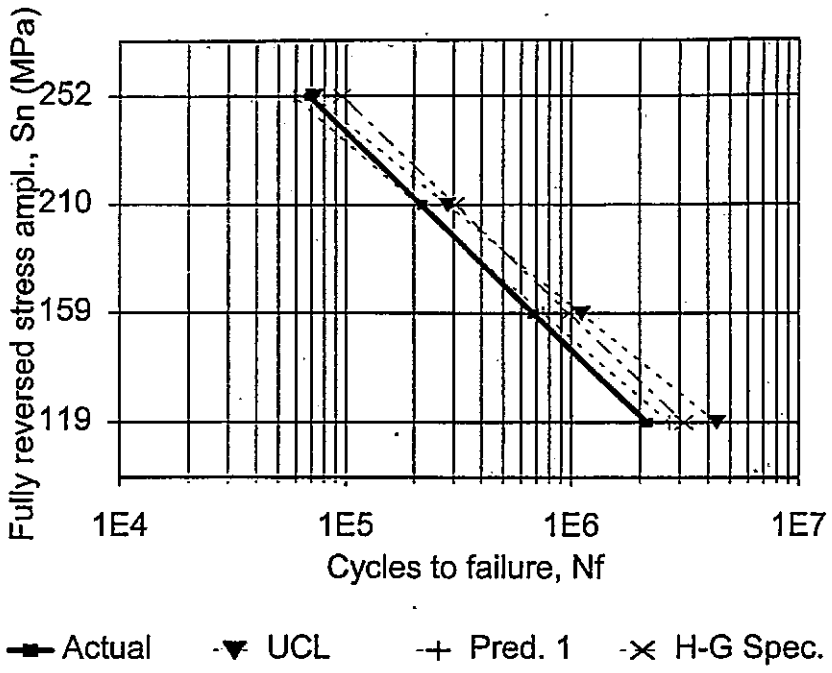

Figure 8.4. – Comparison of life predictions with respect to the upper control limit of the wheel.

Fatigue Test Load (Nm)	Actual Wheel Fatigue Life (N_f)	Predicted Wheel Fatigue Life (prediction 1) (N_f)	Hour-glass Fatigue data (N_f)
4000	72519	60680	104900
3375	180718	190409	245500
2420	847962	879883	1169603
1800	1980242	2573383	$>3x10^6$ cycles

Table 8.9. – Fatigue data related to the wheel, hour-glass and prediction 1. Note that 2×10^6 cycles is considered run-out.

It can be concluded from Figure 8.4 that both prediction techniques, i.e. the fully reversed alternating stresses as per Gerber's relationship and the equivalent peak tensile stress amplitudes (refer section 6.3.1) as per hour-glass fatigue testing method, are valid in terms of correlating their respective predicted lives to that of the actual wheel fatigue data. This is further substantiated by the relationship which exists (see Figure 8.5) between the fully reversed alternating stress amplitudes which account for applied mean and assessed residual stresses and the equivalent peak tensile stress amplitudes which do not account for the applied mean or residual stresses.

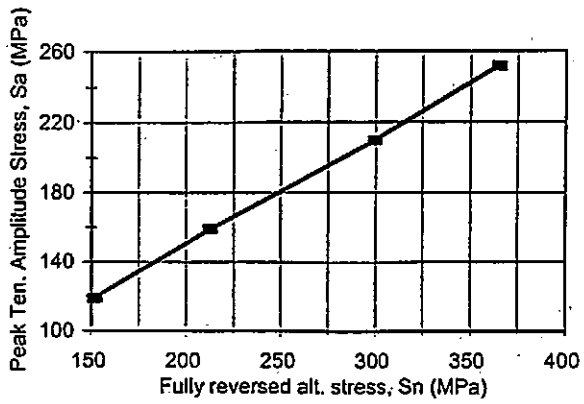

Figure 8.5. – Relationship between fully reversed and peak tensile stress amplitudes.

The expression relating the S_n values to the equivalent peak tensile stress amplitudes, S_a, is given by:

$$S_n = 1.615 \times S_a - 41.4 \ \ (MPa) \quad \text{.....(8.2)}$$

This expression is felt useful in that assessment of the equivalent peak tensile stress measured on the fracture location of the centre disc of a wheel, the fully reversed alternating stress amplitude (which accounts for the applied mean stress and the absolute residual stress) can be determined. Hence, the absolute residual stress magnitude can now also be estimated through Gerber's relationship after assessment of the peak tensile (σ_{max}) and peak compressive stress (σ_{min}) values measured on the fracture location of the centre disc of the wheel. This is obtained by equating expression 8.2 to the Gerber equation, as follows:

$$1.615 \times S_a - 41.4 = \frac{\sigma_a}{1 - \left[\left(\frac{\sigma_{m(effectice)}}{S_u}\right)^2\right]} \quad \text{.....(8.3)}$$

Where

$$\sigma_{m(effective)} = \sigma_{residual} + \sigma_{m(applied)}$$

and

$$\sigma_a = S_a - \sigma_{m(applied)}$$

also

$$\sigma_{m(applied)} = \frac{\sigma_{max} + \sigma_{min}}{2}$$

Substitution of the above expressions into equation 8.3 will realise an estimated value for the absolute maximum residual stress inherent in the material at the fracture location.

Another useful expression emanating from this S_n / S_a relationship is one that relates the fatigue life of the wheel to the equivalent peak tensile stress at the fracture location. This is achieved by equating expression 8.1 to expression 8.2, such that:

$$1.615 \times S_a - 41.4 = -56.84 \times \ln N_f + 991$$

which then simplifies to,

$$S_a = -35.2 \times \ln N_f + 639.26 \quad (MPa) \ldots\ldots\ldots\ldots\ldots\ldots\ldots\ldots\ldots\ldots (8.4)$$

Hence from assessing the equivalent peak tensile stress on the fracture location of the wheel the number of cycles to failure can be predicted by expression 8.4 which accounts for the applied mean and absolute maximum residual stresses. This may be considered as a modified alternate solution to predicting the fatigue life of wheels. Although the Juvinal/Marshek and the Gerber relationship may seem time consuming, a software programme can be written to simplify their solution to life prediction of wheels.

Now predicting the wheel fatigue life by use of expression 8.4, the equivalent peak tensile stress amplitudes, S_a, as assessed in section 6.3.1 is considered.

For the equivalent peak tensile stress amplitude of 252 MPa (4000 Nm test load), we get:

$$252 = -35.2 \times \ln N_{f(wheel)} + 639.26$$

$$N_{f(wheel)} = 59976 \ \ cycles$$

Table 8.10 shows the prediction data using expression 8.4.

Test Load (Nm)	Equiv. Peak Ten. Stress Ampl., S_a (MPa)	Estimated Wheel Life (N_f)	Actual Wheel Life (N_f)
4000	252	59976	72519
3375	210	197775	180718
2420	159	842181	847962
1800	119	2623746	1980242

Table 8.10. – Predicting Wheel Life from the equivalent peak tensile stresses assessed on the wheel fracture location. Note that 2×10^6 cycles is considered run-out.

The results shown in Table 8.10 compares favourably with the actual wheel fatigue data as well as with the approach taken in Prediction 1.

Thus, in order to bridge the gap between small hour-glass specimens and data from real wheels, the relationship developed in section 6.4.2, i.e. expression 6.5, is useful. To show its usefulness, let us consider the following scenario taking actual hour-glass fatigue data:

Using expression 6.5, the estimated wheel fatigue life at the equivalent peak tensile stress amplitude, S_a, of 252 MPa (4000 Nm test load), will be:

$$N_{f(wheel)} = 0.74 \times N_{f(hour-glass)}$$

Therefore,

$$N_{f(wheel)} = 0.74 \times 104900$$

$$N_{f(wheel)} = 77626 \ \ cycles$$

Test Load (Nm)	Equiv. Peak Ten. Stress Ampl., S_a (MPa)	Hour-Glass Fatigue Data (N_f)	Multiplication Factor	Estimated Wheel Life (N_f)	Actual Wheel Life (N_f)
4000	252	104900	0.74	77626	72519
3375	210	245500	0.74	181670	180718
2420	159*	1111916**	0.74	822818	847962
1800	119*	$> 3 \times 10^6$	0.74	$> 3 \times 10^6$	1980242

Table 8.11. – Wheel fatigue life predicted from hour-glass fatigue data. Note that 2×10^6 cycles is considered run-out.
(* & ** interpolated values using equation 6.6 and 6.4 respectively)

The results shown in Table 8.11 indicate that hour-glass laboratory specimens can be an effective means of predicting the fatigue performance of wheels when the equivalent peak tensile stress is used in reverse bend testing conditions.

8.4 DISCUSSION

- The Juvinal and Marshek model together with Gerber's relationship give good correlation to actual wheel fatigue test data as life estimates within 20% can be expected considering the approach taken in prediction 1.
- The fact that residual stress values increase the mean stress level is important and must be taken into consideration when establishing life prediction relationships for complete components (see approach taken in life predictions methods 2 & 3 for percentage errors)
- It is interesting to note that plastic deformation can be said to decrease the endurance limit of ductile steels. In the first instance, the endurance limit was established at 25% of the UTS for the DPS centre discs as calculated from the minimum wheel specification line that was extrapolated to intersect at the 2×10^6 cycles - see section 6.3. Secondly, the hour-glass fatigue results also gave indication that this limit would fall between 21% and 27% of the UTS - see section 6.4.2.
- Life estimates where residual stress values are taken at the 80% original yield strength value according to Schajer, proved rather over conservative with respect to the higher test loads of 3375Nm and 4000Nm - see Table 8.8. These estimates are also greater in value

compared to the hour-glass data for the same test loads, comparing the results of Table 8.8 with that of the hour-glass results in Table 8.9.

- The estimated fatigue lives for the approach followed in prediction 1 (see Table 8.3) and the hour-glass specimen (see column - "estimated wheel life" in Table 8.11) are considered acceptable when related to the actual wheel fatigue data (Table 8.11). This implies that when components subjected to cyclic loading experience a low mean stress value that this condition may be considered negligible when replicating their fatigue behaviour using waisted hour-glass specimens.
- Hence, it can be concluded from the results indicated in Tables 8.6 & 8.8, that by reducing the residual stress magnitude in formed centre discs, the fatigue life will be enhanced.

8.5 SUMMARY

Good correlation exists between the actual wheel fatigue data and Gerber's model for fatigue life prediction when considering the effect of the relieved residual stresses, with or without taking the applied mean stress values into account. It follows that for plastically deformed sheet metal components the maximum relieved residual stresses lies around the 90% original yield strength value and that the endurance limit can be taken at 25% of UTS value. Of the approaches taken in this chapter, i.e. prediction 1 & 2 and the 80% of yield strength (Schajer), it is clear that the maximum relieved residual stresses play a major role in the fatigue performance of sheet metal formed components and that reduction of their magnitude is important in order to enhance the fatigue lives of such components. An additional significant outcome achieved in this work is the improved results obtained by use of the 8-element strain rosette.

CONCLUSION

The study of the mechanical properties of alloy steels under sheet metal forming operations is complex and difficult to model analytically[7]. Hence the process parameters in sheet metal forming are still, to a large extent, determined by trial and error. As a result, there is no present means of assessing or predicting the product's fatigue performance other than by testing the final product itself. The main aim of this work was to provide knowledge linking the induced residual stresses and forming deformation to the fatigue performance of centre discs. This part of the work described in Chapter 6 bridges the wheel fatigue performance data to that of the hour-glass specimens in which a relationship was found to exist between the rotating bending and reverse bending test methods. The testing procedure followed with respect to the hour-glass specimens, i.e. zero-mean stress conditions, is considered valid although the failure planes were observed to be different to that observed in the wheel. The attempt to relate the material properties of surface hardness and residual stress, to each other as well as the fatigue performance of hour-glass specimens machined from the FPW may also be considered successfully accomplished.

This work in characterising the material properties of surface hardness and residual stress for production stage specimens as described in Chapter 7 indicates that relationships do exist between these parameters and their effect on fatigue performance of such components. Consequently, this particular manufacturer can now predict the fatigue performance of the finished wheel by applying these relationships to production stage components. Although hardness would provide the easier and less expensive method of life prediction, jigging of the component will need investigation because of its size and also to make the critical diametral plane accessible to the indenter of the hardness equipment. Residual stress analysis on the other hand will have a two-fold outcome, firstly it will be useful for life prediction and secondly it will indicate its relation to the UTS of the material. The latter point is important, as reduction of the residual stress magnitude would provide for longer life and if its

magnitude can be controlled through changes in tooling then the use of thinner gauge sheet material can be investigated.

The work reported in Chapter 8, which attempted to link residual stress to fatigue performance was found to yield useful relationships. Their summation to the applied mean stress value in providing the "effective mean stress" proved paramount in terms of life prediction using the Gerber equation and Juvinal and Marsheks' life prediction model. Also of interest is that the results of the prediction methods used (hour-glass and prediction 1) correlates well with the actual wheel fatigue data.

This linking of residual stress to fatigue performance and the relationships found in Chapter 7 would not have been accomplished without the development of the customised 8-element strain rosette as investigated in Chapter 4. The concept of this strain rosette has since been patented and subject to a South African Patent Application No. 2000/2042 and is currently being marketed. This rosette offers far-reaching advantages in that residual stress assessment, now being less subject to scatter resulting from hole ovality potentially allows for incorporation of residual stress data into product design systems. This will facilitate manufacturing lighter weight products using thinner gauge material while retaining the fatigue performance and safety standards of their thicker counterparts.

Future Research

The following research programmes are intended for candidates studying toward their Magister Technologiae qualification. These fundamental research projects are related to sheet material subjected to forming operations in an endeavour to further understand their behaviour under such processes. The hypothesis of these research projects include:

1. **An investigation into the material characteristics of plate specimens subjected to uni-axial instantaneous tensile plastic deformation.**

   Aim: By subjecting DPS plate specimens to different percentage plastic deformation under instantaneous (impact) loading conditions in order to assess their fatigue performance and residual stress behaviour with respect to the volume fraction of micro-voids. The results would indicate the degree of fatigue deterioration per increase in plastic deformation under impact conditions relative to the volume fraction of micro-voids. This is felt important in that if the same deformation can be imparted to the component through each production stage then it is envisaged that the fatigue life of such components can also be enhanced. Hence by modification of the tooling can this be achieved.

2. **An investigation into the fatigue behaviour of automotive wheels through re-distributing the residual stress magnitude on fracture locations.**

   Aim: This work will involve investigating the relieved residual stress magnitudes for different automotive wheel models at their fracture locations. Then to subject subsequent model wheels through a re-stamping operation, i.e. subjecting a compressive force to the fracture location. After the re-stamping operation the wheels will be re-assessed for their residual stress behaviour. If reduction in residual stress magnitude is observed then the wheels will be fatigue tested after such re-stamping operation to assess any improvement

in fatigue performance. This implies that if improvement is observed then an additional re-stamping operation will need to be incorporated within the production route, then implementation thereof will rest with the particular manufacturer.

3. **An investigation into material characteristic relationships for steel plate specimens subjected to different forming operations.**

   Aim: The intention of this investigation will be to develop an understanding of the residual stress, microstructural, hardness and fatigue behaviour in sheet metal plate subjected to different forming operations, such as, pure bend (where the applied loading is of a gradual nature), stretch bend (where the ends of the plate specimen are clamped and then subjected to a bending operation, the applied loading condition will be instantaneous (impact)) and lastly, a pure stamping operation (free ends i.e. ends not clamped) where the specimen will be subjected to an impact loading condition. These investigations which are fundamental in nature will provide for an understanding of the materials behaviour when subjected to different forming conditions and that at least two different bend radii will be considered. The characterisation of the mechanical properties under the above loading conditions will lead to a better understanding of the materials behaviour with respect to their fatigue performance.

REFERENCES

1. Kalpakjian, S. – *"Manufacturing Processes for Engineering Materials"*, Second Edition, Addison-Wesley, 1991.
2. Hearn, E. – *"Mechanics of Materials"*, Second Edition, Pergamon Press, 1985, ISBN 0 080 30529 6.
3. Kok, S. and Stander, N. – *"Optimisation of a Sheet Metal Forming Process using Successive Multipoint Approximations"*, Technical Paper, Pretoria University, pp. 1 – 23, undated.
4. Antúnez, H.J. and Kleiber, M. - *"Sensitivity of forming processes to shape parameters"*, Computer methods in applied mechanics and engineering, 1996.
5. Kleiber, M. et. al. - *"Parameter sensitivity of elastoplastic response"*, Engineering computations, 1995.
6. Ohata, T. et. al. - *"Development of optimum process design system by numerical simulation"*, Journal of materials processing technology, 1996.
7. Lange, K. – *"Handbook of Metal Forming"*, Second Edition, McGraw-Hill Book Company Ltd, 1985, ISBN 0 07 036285 8.
8. Sachs, G. – *"Principles and Methods of Sheet-Metal Fabrication"*, Second Edition, Reinhold Publishing Company, pp. 95 – 115, 1966.
9. Johnson, W. and Mellor, P. – *"Engineering Plasticity"*, Von Nostrand Reinhold Company Ltd., 1973, ISBN 0 442 30234 7.
10. Dowling, N.E. - *"Mechanical behavior of Materials"*, Second Edition, Prentice Hall, 1998. ISBN 013 905720 2.
11. Bassett, M.B. and Johnson, W. – *"The Bending of Plate using a Three-Roll Pyramid type Plate Bending Machine"*, Journal of Strain, 1, (5), 1966, pp. 398 – 414.
12. Davies, R.G. – *"Forminmg Problems Encountered in Application of High Strength Steels to Automotive Components"*, Technical Report, No. 8306-021, 1980, pp. 467 – 473.
13. Mizui, M., Sekine, T. and Soneda, S. – *"Application of High Strength Steel Sheets for Automotive Wheels"*, Society of Automotive Engineers, No. 850540, 1985, pp. 1 – 13.
14. Mizui, M. and Takahashi, M. – *"High Strength Steels for Automotive Wheels"*, Mechanical Working Steel Process (MWSP) conference, 29, 1992, pp. 57 – 64.
15. Beaney, E.M. and Procter, E. – *"A critical evaluation of the centre hole technique for the measurement of residual stresses"*, Strain Journal, 1974, pp. 7 – 15.
16. Nickola, W.E. – *"Post-Yield Effects on Center Hole Residual Stress Measurements"*, Experimental Mechanics, 1984, pp. 126 – 136.

17. Schajer, G.S. – *"Measurement of Non-uniform Residual Stresses Using the Hole-Drilling Method. Part I – Stress Calculation Procedures"*, Journal of Engineering Materials and Technology, 1, (110), 1988, pp. 335 – 343.
18. Miller, K.J. - *"Materials science perspective of metal fatigue resistance"*, Journal of Materials Science and Technology, 9, 1993, pp. 453 – 462.
19. Metals Handbook, Ninth Edition, *"Failure Analysis and Prevention"*, 11, updated 1986, pp. 102 – 144.
20. Bannantine, J. *et al.*, - *"Fundamentals of Metal Fatigue Analysis"*, Prentice-Hall Inc., 1990, ISBN 0 13 340191 X.
21. Suresh, S. – *"Fatigue of Materials"*, Cambridge University Press, 1991, ISBN 0 521 43763 6.
22. Francois, D. – *The Influence of Microstructure on Fatigue"*, Conference: Localised Damage II, Fatigue and Fracture Mechanics, 1992, pp. 173 – 180.
23. Mathar, J. – *"Determination of Initial Stresses by Measuring the Deformations Around Drilled Holes"*, Translated for American Society of Mechanical Engineers, 56, (4), 1934, pp. 249 – 254.
24. Hetényi, M. (ed.) - *"Handbook of Experimental Stress Analysis"*, John Wiley & Sons, Inc., New York, 1950.
25. Beaney, E.M. - *"Instruction Manual for CEGB Air Abrasive System for Measuring Residual Stresses"*, 1986.
26. Wnuk, S.P. - *"Residual Stress Measurements in the Field Using Airabrasive Hole Drilling Method"*, Technical Committee for Strain Gauges, Spring Meeting of SESA, Dearborn, Michigan, June 1981.
27. Segal, A.M. and Tait, R.B. – *"Residual Stress Evaluation using the Air Abrasive Hole Drilling Technique"*, R & D Journal, 12, (2), 1996, pp. 54 – 67.
28. Schwarz, T. and Kockelmann, H. – *"The hole drilling method – the best technique for the experimental determination of residual stresses in many fields of application"*, Translated article from MTB, 29, (2), 1993, pp. 33 – 38.
29. Standard Test Method for Determining Residual Stresses by the Hole-Drilling Strain-Gauge Method, ASTM Designation E 837 – 94 (a), pp. 661 – 667.
30. Flaman, M.T. and Boag, J.M. – *"Comparison of Residual-stress Variation with Depth-analysis Techniques for the Hole-drilling Method"*, Experimental Mechanics, 30, 1990, pp. 352 – 355.
31. Rendler, N.J. and Vigness, I. - *"Hole Drilling strain Gage Method of Measuring Residual stresses"*, Experimental Mechanics, 1966.

32. Soete, W. and Vancrombrugge, R. - *"An Industrial Method for the Determination of Residual Stresses"*, Proceedings of the Society of Experimental Stress Analysis, 1950.

33. Kelsey, R.A. - *"Measuring Non-uniform Residual Stresses by the Hole Drilling Method"*, Proceedings of the Society of Experimental Stress Analysis, 1956.

34. Schajer, G.S. - *"Measurement of Non-uniform Residual Stresses Using the Hole-Drilling Method. Part II – Practical Application of the Integral Method"*, Journal of Engineering Mechanical Engineers, 110, (2), 1988, pp. 344 – 349.

35. Bijak-Zochowski, M.A. - *"Semi-Destructive Method of Measuring Residual Stresses"*, VDI-Berichte, 1978.

36. Niku-Lari, A., Lu, J. and Flavenot, J.F. - *"Measurement of Residual Stress Distribution by the Incremental Hole Drilling Method"*, Experimental Mechanics, 1985.

37. Flaman, M.T. and Manning, B.H. - *"Determination of Residual Stress Variation with Depth by the Hole Drilling Method"*, Experimental Mechanics, 1985.

38. Gerbase, A. & Embury, B. - *"Structure of Properties of Dual Phase Steel", 1979.*

39. Piplani, R.K. and Raghavan, V. – *"Microstructure and its Correlation with Properties in Dual Phase Steel"*, Steel India, 4, (1), 1981, pp. 1 – 22.

40. Sines, G. and Carlson, R. – *"Hardness Measurements for Determination of Residual Stresses"*, ASTM Bulletin, (180), 1952, pp. 35 – 37.

41. Annual Book of ASTM Standards, *"Metals Test Methods and Analytical Procedures"*, Section 3, 3.01, 1988.

42. Metals Handbook, Ninth Edition, *"Forming and Forging"*, 14, updated 1988.

43. Becker, K. and Rukwied, A., *et al.*, - *"The Effect of Surface Degradation on Fatigue and Fracture behaviour"*, Materials and Design, 14, (3), 1993, pp. 175 – 182.

44. Technote, *"Regulation for the testing of Special Wheels for motorcars, motorbikes and Trailers"*, TueV, 1995, pp.1 - 24.

45. MTM Technote, *"Rotating Mass Industrial Fatigue Testing Machine"*, undated.

46. Avner, S. – *"Intoduction to Physical Metallurgy"*, Second Edition, McGraw-Hill Book Company, 1974, ISBN 0 07 002499 5.

47. Collins, J. – *"Failure of Materials in Mechanical Design"*, Second Edition, John Wiley & Sons, 1993, ISBN 0 471 55891 5.

Complimentary Literature

FATIGUE & FRACTURE

48. Oehlers,D.J., Ghosh, A. and Wahab, M., - *"Residual Stress approach to Fatigue Design and Analysis"*, Journal of Structural Engineering, 121, pp. 1271 – 1279, 1995.

49. Parker, A.P., - *"Stress Intensity Factors, Crack Profiles, and Fatigue Crack Growth Rates in Residual Stress Fields"*, Residual Stress effects in Fatigue, ASTM STP 776, American Society for Testing Materials, 1982, pp. 13 – 31.
50. Gustavsson, A. and Melander A., - *"Fatigue Design of Pressed Steel Sheet"*, Conference: Fatigue Design, 1, 1995, pp. 159 – 170.
51. Wei, D.C., - *"Rim section fatigue results of various HSLA steel wheels"*, ASME International Conference on Advances in Life Prediction Methods, 1983, pp. 285 – 291.
52. Rice, R.C., Leis, B.N. and Tuttle, M.E., - *"An Examination of the Influence of Residual Stresses on the Fatigue and Fracture of Railroad Rail"*, Residual Stress Effects in Fatigue, ASTM STP 776, American Society for Testing and Materials, 1982, pp. 132 – 157.
53. Nishitani, H. and Kawagoishi, N., - *"Fatigue Crack Growth Laws in Small and Large Cracks and their Physical Background"*, JSME International Journal, Series 1, 35, (1), 1992.
54. Miller, K.J. – *"Metal Fatigue – Past, Present and Future"*, Mechanical Testing Methods, Translated from Zavodskaya Laboratoriya, 60, (3), 1994, pp. 31 – 44.
55. Gerard, D.A. and Koss, D.A. – *Porosity and Crack Initiation during Low Cycle Fatigue"*, Materials Science and Engineering, A129, 1990, pp. 77 – 85.
56. Solin, J. *et al.*, - *"Fatigue Design"*, International Symposium on Fatigue Design, 1993, ISBN 0 85298 884 2.
57. Felbeck, D. and Atkins, A. – *"Strength and Fracture of Engineering Solids"*, Second Edition, Prentice-Hall Inc., 1996, ISBN 013 856113 3.
58. Parker, A.P. – *"The Mechanics of Fracture and Fatigue"*, E. & F. N. Spon Ltd, 1981, ISBN 0 419 11460 2.
59. Ross, B. – *"Investigating Mechanical Failures"*, Chapman and Hall, 1995, ISBN 0 412 54920 4.
60. Metals Handbook, Ninth Edition, *"Failure Analysis and Prevention"*, 11, updated 1986, pp. 102 – 144.
61. Instruction Manual, - *"TMS Fatigue Machine"*, 1, 1999.

RESIDUAL STRESS ASSESSMENT

62. Schajer, G.S. and Altus, E. – *"Stress Calculation Error Analysis for Incremental Hole-Drilling Residual Stress Measurements"*, Transactions of the ASME, 118, 1996, pp. 120 – 126.

63. Weng, C.C., Lin, Y.C. and Chou, C.P. – *"A study on the induced drilling stresses in the centre hole method of residual stress measurement"*, Strain Journal, 28, 1992, pp. 45 – 51.

64. Measurements Group Tech Note, TN-503-3, Measurements Group Inc, 1988, pp. 1 – 19.

65. Bush, A.J. and Kromer, F.J. – *"Simplification of the Hole-Drilling Method of Residual Stress Measurement"*, ISA Transactions, 12, (3), 1973, pp. 249 – 259.

66. Flaman, M.T. – *"Brief Investigation of Induced Drilling Stresses in the Center-hole Method of Residual-stress measurement"*, Experimental Mechanics, 1982, pp. 26 – 30.

67. Sandifer, J.P. and Bowie, G.E. – *"Residual Stress by Blind-Hole Method with Off-center Hole"*, Experimental Mechanics, 18, (8), 1978, pp. 173 – 179.

68. Winegar, J.E. - *"X-ray Measurement of Residual Stress in Metals at Chalk River Laboratories"*, Atomic Energy of Canada Limited Report, AECL-6961, 1980.

69. Ruud, C.O., DiMascio, P.S. and Yavelak, J.J. – *"Comparison of Three Residual-Stress Measurement Methods on a Mild Steel Bar"*, Experimental Mechanics, 1985, pp. 338 – 343.

70. Zhonghua, L. and Haicheng, G. – *"Bauschinger Effect and Residual Phase Stresses in Two Ductile-Phase Steels: Part I. The Influence of Phase Stresses on the Bauschinger Effect"*, Metallurgical Transactions, 21A, 1990, pp. 717 – 724.

71. Zhonghua, L. and Haicheng, G. – *"Bauschinger Effect and Residual Phase Stresses in Two Ductile-Phase Steels: Part II. The Effect of Microstructureand Mechanical Properties of the Constituent Phases on Bauschinger Effect and Residual Phase Stresses"*, Metallurgical Transactions, 21A, 1990, pp. 725 – 732.

72. Metals Handbook, Ninth Edition, *"Mechanical Testing"*, 8, updated 1985.

FORMING

73. Withfield, J.J. – *"Forming Limit Diagrams (FLD) for Wheel Pressing Steels"*, Technical Report, No. FLC001P, Iscor Ltd, 1996.

CHARACTERISTICS OF HIGH STRENGTH STEELS

74. Golovanenko, A. and Fonshtein, N.M. – *"New group of ferritic-martensitic steels with high formability"*, Steel in the USSR, 7, 1980, pp. 615 – 620.

75. Park, S.H., Ro, K.S. and Kwon, O. – *"Microstructure and Mechanical Properties of Hot Rolled High Strength Formable Steels for Automotive Wheels"*, International

Symposium on Low Carbon Steels for the 90's, The Minerals, Metals & Materials Society, 1993, pp. 355 – 365.

76. Kawagoishi, N., Nishitani, H. and Toyohiro, T. – *"Effect of Microstructure on the Characteristics of Small Fatigue Crack Growth in Dual Phase Steel"*, JSME International Journal, Series A, 36, 1993, pp. 126 – 133.
77. Kunishige, K., Yamauchi, N., Taka, T. and Nagao, N. – *"Softening in Weld Heat Affected Zone of Dual Phase Steel Sheet for Automotive Wheel Rim"*, SAE Technical papers, No. 830632, 1983, pp. 1 – 5.
78. Ahn, J. and Thomas, G. – *"Design of High-Strength dual-phase steel"*, Wire Journal International, 1987, pp. 70 – 79.
79. Maid, O. – *"Production of hot-rolled strip from Dual-Phase Steel by applying coiling Temperatures below the Martensitic Start Temperature"*, Iscor translation Service 85-11-437, Thyssen Technische Berichte, Heft 1/85, 1985, pp. 28 – 33.
80. Okita, T., Mitsuji, H., Inoue, I., Nakano, F. and Hashimoto, Y. – *"Production and Quality of Hot Rolled Dual Phase Steel"*, Nippon Kokan Technical Report, (43), 1985, pp. 25 – 32.
81. Pascoe, K. – *"An Introduction to the Properties of Engineering Materials"*, Third Edition, Von Nostrand Reinhold Company Ltd, 1978, ISBN 0 442 302320 0.
82. Horrocks, D. and Johnson, W. – *"On Anti-clastic Curvature with Special Reference to Plastic Bending: A Literature Survey and some Experimental Investigations"*, International Journal of Mechanical Science, 9, 1967, pp. 835 – 861.
83. Kokubo, S. – *"On the Change in Hardness of a Plate Caused by Bending"*, Science Reports of the Tohoku University, 21, 1932, pp. 256 – 267.
84. Metals Handbook, Ninth Edition, 12, *"Fractography"*, updated 1987,

STRAIN GAUGE APPLICATION

85. Hoffmann, K. – *"An Introduction to Measurements using Strain Gages"*, Hottinger Baldwin Messtechnik GmbH, 1989.
86. Hoffmann, K. – *"Applying the Wheatstone Bridge Circuit"*, Hottinger Baldwin Messtechnik, GmbH, version number vd72001e.
87. Hoffmann, K. – *"Measuring Elementary Load Cases with Strain Gauges"*, Hottinger Baldwin Messtechnik, GmbH, version number vd73002e.
88. Hoffmann, K. – *"The Strain Gauge a Universal Tool of the Experimental Stress Analysis"*, Hottinger Baldwin Messtechnik, GmbH, version number vd73004e.

89. Hoffmann, K. – *"Practical Hints for the Application of Strain Gauges"*, Hottinger Baldwin Messtechnik, GmbH, version number vd84005e.

GENERAL

90. Davis, H.E., Troxell, G.E. and Wiskocil, C.T. – *"The Testing and Inspection of Engineering Materials"*, Third Edition, McGraw-Hill Book Company Inc, 1941.

91. Dictionary of Science and Technology, Larousse, Kingfisher Chambers Inc., 1995, ISBN 0 752300 105.

92. Hattingh, D.G. - *"Fatigue Properties of Spring Steel"*, Doctoral Thesis, University of Plymouth, 1998.

APPENDIX - A

APPENDIX - A

Maximum Tensile Stresses

Bend. Mom.	UPM40-GNo	Gauge No.	E	Poiss. R	k	Grid (a)	Grid (b)	Grid (c)	Max. Strain	Min. Strain	Max. Stress	Min. Stress	Ave. Strain	Angle Pos.
1500Nm	0,1,2 (1)	1	2.00E+11	0.3	1.91	2.70E-04	2.42E-04	2.21E-04	0.00027025	0.00022075	73950355.2	60003451	0.000342	-77.498071
1500Nm	3,4,5 (1)	3	2.00E+11	0.3	1.91	3.09E-04	2.78E-04	1.94E-04	0.00031481	0.00018819	81597560.7	54471656	0.000333	-59.337557
1500Nm	**6,7,8 (1)**	**6**	**2.00E+11**	**0.3**	**1.91**	**4.16E-04**	**3.44E-04**	**1.52E-04**	**0.000429**	**0.000139**	**103450019**	**58835695.3**	**0.000324**	**-29.919806**
1500Nm	0,1,2 (2)	8	2.00E+11	0.3	1.91	2.20E-04	2.00E-04	9.20E-05	0.00023367	7.833E-05	56520036.5	18898108.9	0.000176	-35.699891
1500Nm	3,4,5 (2)	2	2.00E+11	0.3	1.91	1.04E-04	1.03E-04	8.40E-05	0.00010745	8.055E-05	28926931.2	28017559.4	0.000221	-76.607189
1500Nm	6,7,8 (2)	4	2.00E+11	0.3	2	4.14E-04	3.04E-04	1.20E-04	0.00041858	0.00011542	99606477.3	57773191.5	0.0004555	-22.19395
1500Nm	0,1,2 (3)	5	2.00E+11	0.3	2	2.31E-04	4.60E-05	7.00E-05	0.00028241	1.859E-05	63293993	-10107908	9.3E-05	-23.505263
1500Nm	3,4,5 (3)	7	2.00E+11	0.3	2	1.87E-04	1.61E-04	2.30E-05	0.0002043	5.702E-06	45276543.5	8222053.03	0.0001035	-7.97573
1500Nm	6,7,8 (3)	10	2.00E+11	0.3	2	4.00E-04	1.22E-04	5.30E-05	0.00042904	2.396E-05	95874304.1	-23369020	0.000114	-8.6928478
2125Nm	0,1,2 (1)	1	2.00E+11	0.3	1.91	2.21E-04	1.30E-04	1.11E-04	0.00023173	0.00010027	57541542.8	18898108.9	0.000176	-45.258148
2125Nm	3,4,5 (1)	3	2.00E+11	0.3	1.91	2.85E-04	2.38E-04	1.02E-04	0.00029525	9.175E-05	70939135.2	28017559.4	0.000221	-29.125942
2125Nm	**6,7,8 (1)**	**6**	**2.00E+11**	**0.3**	**1.91**	**5.63E-04**	**4.29E-04**	**2.41E-04**	**0.00056525**	**0.00023875**	**139972262**	**57773191.5**	**0.0004555**	**-36.80208**
2125Nm	0,1,2 (2)	8	2.00E+11	0.3	1.91	3.35E-04	3.21E-04	1.70E-04	0.00035973	0.00014527	88639943.1	52128727.3	0.0003305	-45.846564
2125Nm	3,4,5 (2)	2	2.00E+11	0.3	1.91	1.40E-04	1.32E-04	1.12E-04	0.00014123	0.00011077	38343314.8	31689256.7	0.000178	-75.963339
2125Nm	6,7,8 (2)	4	2.00E+11	0.3	2	5.64E-04	4.32E-04	1.67E-04	0.00057484	0.00015616	136635190	40058832	0.000383	-22.799689
2125Nm	0,1,2 (3)	5	2.00E+11	0.3	2	3.56E-04	1.10E-04	9.40E-05	0.00039932	5.068E-05	91103530.5	-9953443.3	0.000149	-19.743805
2125Nm	3,4,5 (3)	7	2.00E+11	0.3	2	2.82E-04	2.50E-04	4.90E-05	0.00030942	2.158E-05	69427003.5	17129295.7	0.000174	-11.864302
2125Nm	6,7,8 (3)	10	2.00E+11	0.3	2	5.50E-04	1.62E-04	1.04E-04	0.00060441	4.959E-05	136106393	-26308796	0.000185	-13.13818
2750Nm	0,1,2 (1)	1	2.00E+11	0.3	1.91	3.27E-04	2.36E-04	2.11E-04	0.00033573	0.00020227	87123420.2	47818358.5	0.000329	-61.197703
2750Nm	3,4,5 (1)	3	2.00E+11	0.3	1.91	3.52E-04	3.14E-04	1.43E-04	0.00037136	0.00012364	89770415.8	42176762.2	0.0003	-34.369572
2750Nm	**6,7,8 (1)**	**6**	**2.00E+11**	**0.3**	**1.91**	**7.27E-04**	**5.36E-04**	**2.84E-04**	**0.00072909**	**0.00028191**	**178827037**	**64662373.3**	**0.000552**	**-32.649252**
2750Nm	0,1,2 (2)	8	2.00E+11	0.3	1.91	5.23E-04	5.16E-04	3.58E-04	0.00055233	0.00032867	143062137	106891363	0.000616	-65.250204
2750Nm	3,4,5 (2)	2	2.00E+11	0.3	1.91	1.80E-04	1.59E-04	1.40E-04	0.00018002	0.00013998	48795052.5	37799629.5	0.0002195	-74.054007
2750Nm	6,7,8 (2)	4	2.00E+11	0.3	2	6.04E-04	5.43E-04	1.91E-04	0.00065011	0.00014489	152434715	59441247.5	0.0004625	-24.796358
2750Nm	0,1,2 (3)	5	2.00E+11	0.3	2	5.83E-04	1.98E-04	1.58E-04	0.0006442	9.68E-05	147965063	-11526477	0.000257	-20.40277
2750Nm	3,4,5 (3)	7	2.00E+11	0.3	2	4.87E-04	4.01E-04	1.07E-04	0.0005136	8.04E-05	118180376	30187441.4	0.0003075	-15.709378
2750Nm	6,7,8 (3)	10	2.00E+11	0.3	2	8.02E-04	2.52E-04	2.05E-04	0.00089383	0.00011317	203907319	-23019097	0.000331	-18.966902
3375Nm	0,1,2 (1)	1	2.00E+11	0.3	1.91	5.03E-04	4.34E-04	3.45E-04	0.00050363	0.00034437	133393687	92530044.5	0.000562	-65.389967
3375Nm	3,4,5 (1)	3	2.00E+11	0.3	1.91	4.82E-04	4.30E-04	2.51E-04	0.0004983	0.0002347	124991944	71527392.8	0.000466	-47.366122
3375Nm	**6,7,8 (1)**	**6**	**2.00E+11**	**0.3**	**1.91**	**8.78E-04**	**5.40E-04**	**2.52E-04**	**0.000879**	**0.000251**	**209735774**	**35750442.8**	**0.000522**	**-21.917582**
3375Nm	0,1,2 (2)	8	2.00E+11	0.3	1.91	6.50E-04	6.42E-04	4.14E-04	0.00069332	0.00037068	176818394	125168981	0.000735	-60.305859
3375Nm	3,4,5 (2)	2	2.00E+11	0.3	1.91	2.21E-04	1.76E-04	1.69E-04	0.0002272	0.0001628	60668514.1	41804772	0.000257	-72.896622
3375Nm	6,7,8 (2)	4	2.00E+11	0.3	2	7.14E-04	6.88E-04	2.27E-04	0.00079699	0.00014401	184658457	77660221.5	0.000571	-24.959957
3375Nm	0,1,2 (3)	5	2.00E+11	0.3	2	7.14E-04	2.40E-04	1.99E-04	0.00079292	0.00012008	182185514	-13427982	0.000319	-21.138584
3375Nm	3,4,5 (3)	7	2.00E+11	0.3	2	5.82E-04	4.92E-04	1.42E-04	0.00061754	0.00010646	142742209	41714676.2	0.000388	-17.865443
3375Nm	6,7,8 (3)	10	2.00E+11	0.3	2	9.65E-04	3.00E-04	2.63E-04	0.00108495	0.00014305	247882924	-24763785	0.000413	-20.556491
4000Nm	0,1,2 (1)	1	2.00E+11	0.3	1.91	7.93E-04	6.80E-04	5.23E-04	0.00079478	0.00052122	209043207	140016378	0.000863	-62.688009
4000Nm	3,4,5 (1)	3	2.00E+11	0.3	1.91	6.18E-04	5.81E-04	4.39E-04	0.00063226	0.00042474	166963346	125830005	0.0007295	-67.812629
4000Nm	**6,7,8 (1)**	**6**	**2.00E+11**	**0.3**	**1.91**	**9.96E-04**	**7.48E-04**	**4.99E-04**	**0.000996**	**0.000499**	**251802275**	**117719009**	**0.000873**	**-45.100782**
4000Nm	0,1,2 (2)	8	2.00E+11	0.3	1.91	8.05E-04	7.88E-04	5.46E-04	0.00084704	0.00050396	219391006	189010787	0.001199	-64.614139
4000Nm	3,4,5 (2)	2	2.00E+11	0.3	1.91	2.58E-04	2.05E-04	1.98E-04	0.0002658	0.0001902	70958567.3	59571446.9	0.0003605	-73.140869
4000Nm	6,7,8 (2)	4	2.00E+11	0.3	2	8.74E-04	8.20E-04							

4000Nm	0,1,2 (3)	5	2.00E+11	0.3	2	8.31E-04	3.31E-04	2.76E-04	0.00090919	0.00019781	212863774	105328218	0.0009965	-26.448797
4000Nm	3,4,5 (3)	7	2.00E+11	0.3	2	6.35E-04	5.54E-04	2.08E-04	0.00067277	0.00017023	159086072	110070045	0.000912	-25.949706
4000Nm	6,7,8 (3)	10	2.00E+11	0.3	2	8.72E-04	2.75E-04	2.15E-04	0.00096777	0.00011923	220557925	92087541.1	0.0010095	-18.137091

APPENDIX - A

Maximum Compressive Stresses

Bend. Mom.	UPM40-GNo	Gauge No.	E	Poiss. R	k	Grid (a)	Grid (b)	Grid (c)	Max. Strain	Min. Strain	Max. Stress	Min. Stress	Ave. Strain	Angle Pos.
1500Nm	0,1,2 (1)	1	2.00E+11	0.3	1.91	-1.74E-04	-5.80E-06	-8.00E-06	2.795E-05	-0.0002099	-7700687.1	-27679678	-1.09E-05	-2.7498243
1500Nm	3,4,5 (1)	3	2.00E+11	0.3	1.91	-7.20E-05	-6.80E-05	-2.70E-05	-2.037E-05	-7.863E-05	-9661468.9	-18486085	-6.1E-05	-30.966453
1500Nm	**6,7,8 (1)**	**6**	**2.00E+11**	**0.3**	**1.91**	**-1.43E-04**	**-1.41E-04**	**-6.40E-05**	**-4.903E-05**	**-0.000158**	**-21192108**	**-37882535**	**-0.0001345**	**-39.01666**
1500Nm	0,1,2 (2)	8	2.00E+11	0.3	1.91	-3.75E-04	-3.15E-04	-2.50E-04	-0.00025	-0.000375	-79662640	-95797879	-0.0004075	-63.437871
1500Nm	3,4,5 (2)	2	2.00E+11	0.3	1.91	-9.10E-05	-6.90E-05	-6.60E-05	-6.28E-05	-9.42E-05	-20013138	-22908456	-0.0001005	-69.254258
1500Nm	6,7,8 (2)	4	2.00E+11	0.3	2	-3.18E-04	-2.43E-04	-8.60E-05	-7.897E-05	-0.000325	-38786206	-73524299	-0.0002075	-20.347684
1500Nm	0,1,2 (3)	5	2.00E+11	0.3	2	-3.88E-04	-1.59E-04	-1.48E-04	-0.0001059	-0.0004301	-51630789	-79943987	-0.0002275	-31.657845
1500Nm	3,4,5 (3)	7	2.00E+11	0.3	2	-3.42E-04	-2.46E-04	-1.31E-04	-0.0001306	-0.0003424	-51274988	-79075010	-0.000254	-31.840408
1500Nm	6,7,8 (3)	10	2.00E+11	0.3	2	-2.93E-04	-1.00E-04	-8.80E-05	-5.376E-05	-0.0003272	-33392395	-57486440	-0.000138	-23.227814
2125Nm	0,1,2 (1)	1	2.00E+11	0.3	1.91	-3.71E-04	-2.03E-04	-1.22E-04	-0.0001146	-0.0003784	-50139244	-79105038	-0.0002235	-26.104616
2125Nm	3,4,5 (1)	3	2.00E+11	0.3	1.91	-2.82E-04	-2.59E-04	-2.13E-04	-0.0002111	-0.0002839	-65119487	-75340812	-0.0003425	-72.051881
2125Nm	**6,7,8 (1)**	**6**	**2.00E+11**	**0.3**	**1.91**	**-3.67E-04**	**-2.90E-04**	**-2.13E-04**	**-0.000213**	**-0.000367**	**-71010989**	**-90587557**	**-0.000358**	**-54.137083**
2125Nm	0,1,2 (2)	8	2.00E+11	0.3	1.91	-4.91E-04	-4.18E-04	-3.38E-04	-0.0003379	-0.0004911	-106647029	-126441656	-0.000547	-65.648871
2125Nm	3,4,5 (2)	2	2.00E+11	0.3	1.91	-1.31E-04	-1.16E-04	-9.70E-05	-9.688E-05	-0.0001311	-29938007	-34471243	-0.000155	-70.68428
2125Nm	6,7,8 (2)	4	2.00E+11	0.3	2	-4.41E-04	-2.26E-04	-1.05E-04	-9.855E-05	-0.0004475	-51161451	-90680285	-0.000218	-17.354599
2125Nm	0,1,2 (3)	5	2.00E+11	0.3	2	-5.05E-04	-1.97E-04	-1.91E-04	-0.0001302	-0.0005658	-65916232	-103276951	-0.0002895	-31.306681
2125Nm	3,4,5 (3)	7	2.00E+11	0.3	2	-4.42E-04	-3.05E-04	-1.42E-04	-0.0001414	-0.0004426	-60265144	-99734811	-0.0002945	-25.337617
2125Nm	6,7,8 (3)	10	2.00E+11	0.3	2	-4.68E-04	-1.78E-04	-1.57E-04	-0.0001069	-0.0005181	-57655267	-94116126	-0.000246	-26.780587
2750Nm	0,1,2 (1)	1	2.00E+11	0.3	1.91	-4.55E-04	-1.92E-04	-7.40E-05	-6.067E-05	-0.0004683	-44213031	-88363178	-0.00017	-10.987545
2750Nm	3,4,5 (1)	3	2.00E+11	0.3	1.91	-4.23E-04	-4.03E-04	-3.96E-04	-0.0003945	-0.0004245	-114694873	-117798120	-0.0005975	-86.099608
2750Nm	**6,7,8 (1)**	**6**	**2.00E+11**	**0.3**	**1.91**	**-4.70E-04**	**-4.09E-04**	**-2.72E-04**	**-0.000265**	**-0.000477**	**-89685778**	**-119824307**	**-0.0004765**	**-53.95449**
2750Nm	0,1,2 (2)	8	2.00E+11	0.3	1.91	-6.22E-04	-5.33E-04	-4.24E-04	-0.0004235	-0.0006225	-134120299	-160329796	-0.0006905	-64.972867
2750Nm	3,4,5 (2)	2	2.00E+11	0.3	1.91	-1.72E-04	-1.58E-04	-1.29E-04	-0.0001277	-0.0001733	-39496832	-45919470	-0.000208	-71.565876
2750Nm	6,7,8 (2)	4	2.00E+11	0.3	2	-5.85E-04	-3.69E-04	-1.42E-04	-0.0001419	-0.0005851	-69769716	-126615440	-0.0003265	-17.780774
2750Nm	0,1,2 (3)	5	2.00E+11	0.3	2	-5.20E-04	-2.35E-04	-1.86E-04	-0.0001485	-0.0005575	-69398332	-107907195	-0.0003035	-29.110645
2750Nm	3,4,5 (3)	7	2.00E+11	0.3	2	-4.45E-04	-3.14E-04	-1.47E-04	-0.0001459	-0.0004461	-61481689	-101269339	-0.000304	-26.26503
2750Nm	6,7,8 (3)	10	2.00E+11	0.3	2	-5.24E-04	-1.69E-04	-1.54E-04	-8.775E-05	-0.0005902	-58203775	-101924023	-0.0002385	-22.588786
3375Nm	0,1,2 (1)	1	2.00E+11	0.3	1.91	-5.23E-04	-2.22E-04	-1.08E-04	-8.791E-05	-0.0005431	-55128574	-102913520	-0.000219	-14.582908
3375Nm	3,4,5 (1)	3	2.00E+11	0.3	1.91	-4.92E-04	-4.20E-04	-2.96E-04	-0.0002926	-0.0004954	-96972916	-125000827	-0.000506	-56.495058
3375Nm	**6,7,8 (1)**	**6**	**2.00E+11**	**0.3**	**1.91**	**-6.51E-04**	**-5.83E-04**	**-4.10E-04**	**-0.0003991**	**-0.0006619**	**-131349875**	**-169098123**	**-0.0007015**	**-59.560355**
3375Nm	0,1,2 (2)	8	2.00E+11	0.3	1.91	-7.37E-04	-6.11E-04	-6.03E-04	-0.0005807	-0.0007593	-177693978	-193438037	-0.0009085	-77.4725
3375Nm	3,4,5 (2)	2	2.00E+11	0.3	1.91	-2.14E-04	-2.04E-04	-1.60E-04	-0.0001551	-0.0002189	-48519939	-57974304	-0.000262	-71.351598
3375Nm	6,7,8 (2)	4	2.00E+11	0.3	2	-6.92E-04	-4.79E-04	-1.84E-04	-0.0001807	-0.0006953	-85560122	-154638597	-0.0004235	-19.924098
3375Nm	0,1,2 (3)	5	2.00E+11	0.3	2	-6.36E-04	-2.76E-04	-2.31E-04	-0.000177	-0.00069	-84389532	-131376447	-0.000369	-29.695523
3375Nm	3,4,5 (3)	7	2.00E+11	0.3	2	-5.46E-04	-3.78E-04	-1.78E-04	-0.0001773	-0.0005467	-75014057	-123436102	-0.000367	-25.822602
3375Nm	6,7,8 (3)	10	2.00E+11	0.3	2	-6.49E-04	-2.13E-04	-1.78E-04	-0.0001042	-0.0007228	-70559731	-125678301	-0.0002845	-20.691366
4000Nm	0,1,2 (1)	1	2.00E+11	0.3	1.91	-6.05E-04	-2.99E-04	-1.84E-04	-0.0001633	-0.0006257	-77152688	-125618415	-0.0003335	-23.607619
4000Nm	3,4,5 (1)	3	2.00E+11	0.3	1.91	-5.91E-04	-5.36E-04	-3.12E-04	-0.0002884	-0.0006146	-103908216	-152078178	-0.00058	-48.208181
4000Nm	**6,7,8 (1)**	**6**	**2.00E+11**	**0.3**	**1.91**	**-7.82E-04**	**-6.33E-04**	**-5.40E-04**	**-0.0005368**	**-0.0007852**	**-169749847**	**-198487425**	**-0.0008565**	**-65.865189**
4000Nm	0,1,2 (2)	8	2.00E+11	0.3	1.91	-8.63E-04	-7.31E-04	-6.93E-04	-0.0006809	-0.0008751	-207342825	-226842521	-0.0010585	-76.218879
4000Nm	3,4,5 (2)	2	2.00E+11	0.3	1.91	-2.53E-04	-2.47E-04	-1.89E-04	-0.0001798	-0.0002622	-56799618	-69278525	-0.0003125	-71.294069
4000Nm	6,7,8 (2)	4	2.00E+11	0.3	2	[illegible]	[illegible]	[illegible]	[illegible]	[illegible]	[illegible]	[illegible]	[illegible]	[illegible]

4000Nm	0,1,2 (3)	5	2.00E+11	0.3	2	-7.67E-04	-2.81E-04	-2.02E-04	-0.0001363	-0.0008327	-84864806	-150074223	-0.0003425	-19.662679
4000Nm	3,4,5 (3)	7	2.00E+11	0.3	2	-6.87E-04	-4.73E-04	-1.59E-04	-0.0001543	-0.0006917	-79519738	-152262996	-0.0003955	-16.772563
4000Nm	6,7,8 (3)	10	2.00E+11	0.3	2	-1.00E-03	-3.24E-04	-2.67E-04	-0.0001538	-0.0011132	-107199934	-192901839	-0.000429	-19.996673

APPENDIX - B

DUAL PHASE STEEL

1 Introduction[B1, B2, B3]

It is well known that the strength of steel depends on its carbon content and that although increasing the carbon content leads to an increase in strength it is also associated with a decrease in the formability and weldability of the steel[B1]. This being of paramount importance to the sheet metal forming fraternity, where high strength steels with good formability is required.

Initial developments in this regard were discovered by metallurgists and researchers where it was found that by increasing the alloying elements, such as manganese and nickel in a low carbon steel, the strength and toughness can be improved but the formability remained unchanged[B3]. Further developments were achieved through the addition of alloying elements like chromium and molybdenum as well as subsequent heat treatments such as quenching and tempering, thereby further improving the strength of the steel. Steels developed in this manner were classified as high strength low alloy (HSLA) steels.

Microalloyed steels, which are a class of high strength low alloy steels, were developed during 1960 to 1975, where refinement of the ferrite grain size along with precipitation hardening was achieved by microalloying additives, such as vanadium, titanium and niobium[B3]. This grain refinement results in an increase in both the strength and toughness and can be produced directly from controlled hot rolling without the need for subsequent heat treatments; therefore a more economical production process can be achieved.

Despite these developments, low carbon low strength steels were still predominantly used, as the formability of these microalloyed steels could not meet the requirements of the automobile industry.

In the mid 1970s, a breakthrough was achieved in the technology of high strength low alloy (HSLA) steels[B1], this being prompted by the automotive industry in its quest to produce lighter weight vehicle components and to improve fuel efficiency by the increasing use of higher strength, thinner gauge sheet steels.

The breakthrough came with the discovery that formable low carbon steels can be strengthened markedly by introducing dispersed islands of the hard martensite microconstituent in place of the softer pearlite constituent normally found in the microstructure. The introduction of the martensite islands, however, does not reduce the excellent formability of the alloys, and thus a new family of alloys exhibiting both high strength and formability was generated. This family of alloys was called the dual phase steels, which refers to the microstructure which consists of islands of martensite in a matrix of the much softer ferrite, the ferrite making up 80 – 85% of the microstructure[B3]. This new family of steels disproved the traditional concept that high strength and high formability were incompatible properties.

This excellent strength-ductility combination has opened the possibilities of utilizing thinner gauge, higher strength alloys in a number of highly formed parts such as pressed automobile components[B1].

1.1 Manufacture of Dual Phase Steel

In normal steel heat treatment processes, steels are generally heated to a temperature where the structure is completely austenitic. If ,however, steel is heated to a temperature in the two phase austenitic plus ferrite region, intercritical region, between the upper (A_3) and lower (A_1) critical temperature lines as shown in the iron-iron carbon constitutional diagram in Figure 1.1, and held at that temperature; carbon will diffuse out of the ferrite and into the austenite where it is more soluble. If the steel contains a significant alloy content, then this

factor coupled with the enriched carbon content will cause the austenite to transform into a product called martensite, which is extremely strong. Ordinarily steel of this type, which is given a conventional heat treatment, would transform to ferrite and pearlite but the dual phase version of the material has a structure of ferrite and martensite. Such steels are characterised by lower yield strengths but have higher rates of work hardening. Therefore they develop high tensile strengths and high n values (stretch forming).

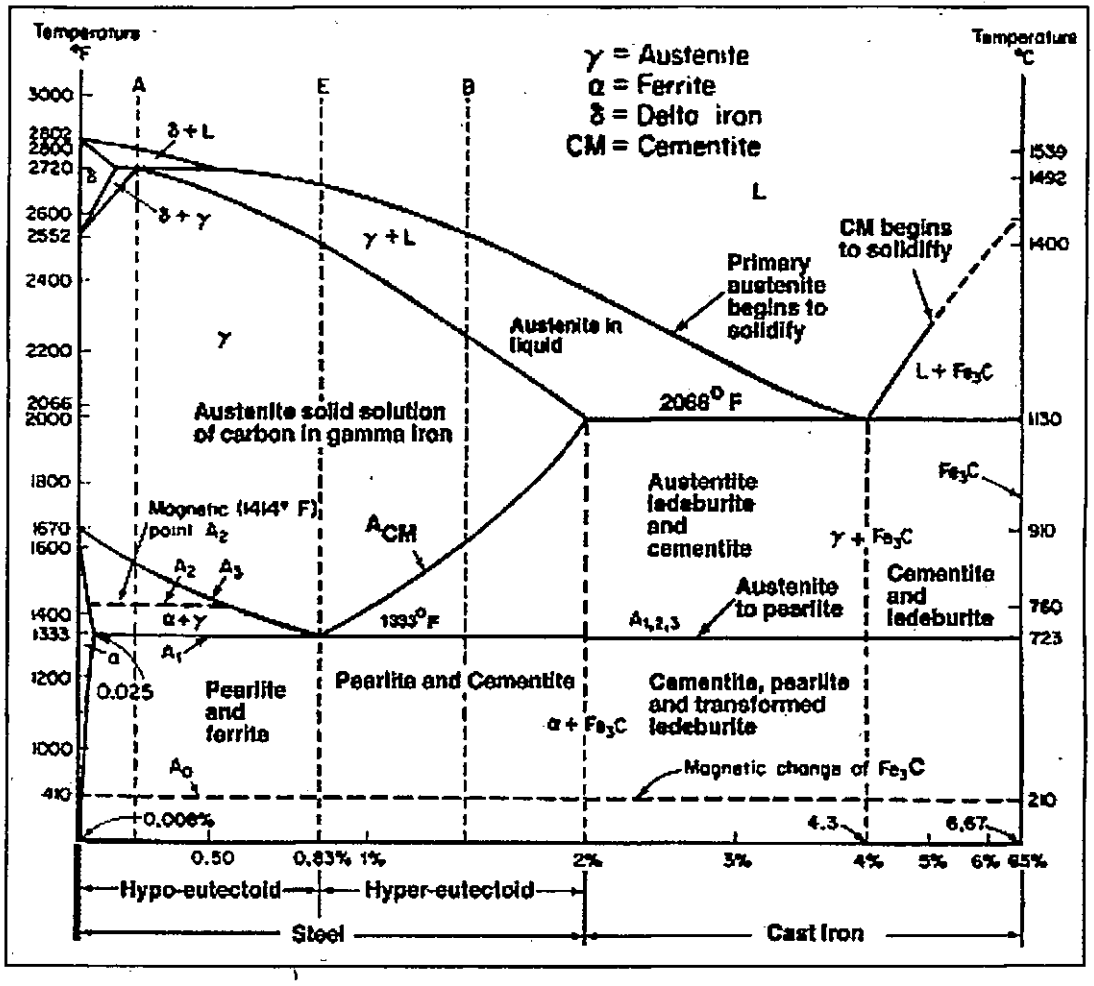

Figure 1.1 Iron-iron carbide constitutional diagram showing equilibrium phase transformation temperatures. [Horizontal axis shows percentage carbon content.]

Hot rolled dual phase steel is classified according to its manufacturing method. Firstly it can be manufactured as a heat treated Si-Mn steel, by continuous or batch annealing, after conventional hot rolling. The second manufacturing method is by use of steel which has a high content of Si, Cr and Mo produced only by conventional hot rolling. The third method

is by use of a simple Si-Mn steel produced by thermomechanical hot rolling utilizing controlled cooling and an extra low temperature coiling method[B1]. The latter method for the manufacture of dual phase steel is employed by ISCOR SA

1.1.1 Hot Rolling Process with Coiling Temperatures below the Martensite Start Temperature

The thermo-mechanical process of producing dual phase steel coil is represented in Figure 1.2. The sheet finally hot rolled in austenite (γ) region above the upper critical line (A_3) adopts rapid cooling, having undergone a two-step regulated rapid cooling process on the runout table. A sufficiently long air cooling stage is required after leaving the finishing train so that the minimum quantity of 80% ferrite required for good formability can be achieved, since during the air cooling process at intermediate temperature region of 750 to 830°C, ferrite (α) of about 80% in volume fraction finely precipitates. The remaining austenite is transformed to martensite (α') during rapid cooling at a temperature approximately 200°C, in which the dual phase ($\alpha + \alpha'$) microstructure is finally formed[B1].

By coiling the hot strip below the martensite start temperature, approximately 200°C; it is possible to save on alloying elements. The cooling cycle and the quantity of alloying elements, mainly silicon and manganese, determine the percentage austenite existing at the coiling temperature while the increased manganese content of approximately 1.5% brings about a delayed ferrite formation[B1].

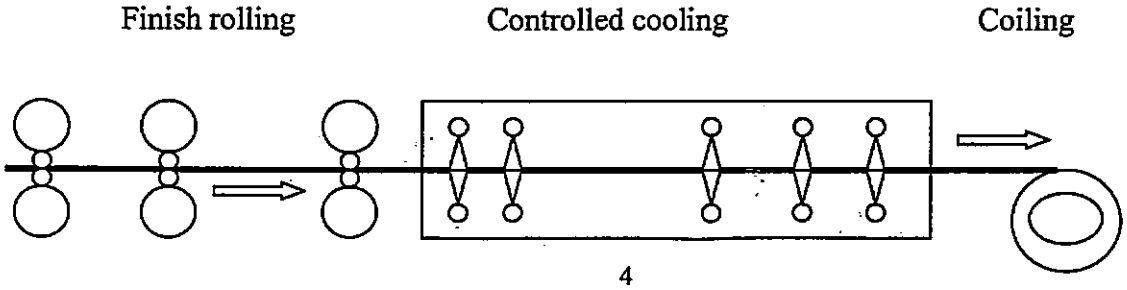

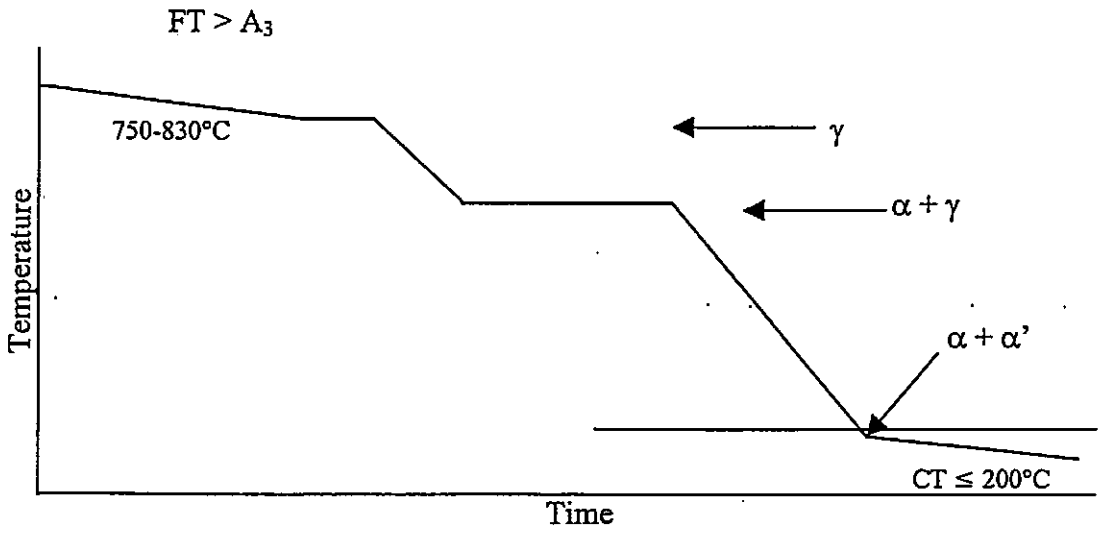

Figure 1.2 Cooling pattern in manufacturing process of as hot rolled dual phase steel. [Where: FT is the finish rolling temperature, CT is the coiling temperature.]

2 Chemical Composition

The chemical composition of the dual phase steel for the purpose of this research, as manufactured by ISCOR SA, is as shown in the Table 2.1 below[B2]:

DESIGNATION	C%	Mn%	P%	S%	Si%	Al%	Cr%	Ni%	Ti%	Mo%	Cu%
Dual Phase Steel (DPS)	min 0.05 max 0.12	min 0.5 max 1.3	min 0.01 max 0.09	min 0 max 0.006	min 0 max 0.65	min 0.02 max 0.06	min 0 max 0.9	min 0 max 0.25	min 0 max 0.015	min 0 max 0.05	min 0 max 0.35

Table 2.1 Typical chemical composition of dual phase steel

2.1 The Role of Individual Alloying Elements

The following is a summary of the effect of individual alloying elements in achieving the required microstructure in dual phase steels[B3].

2.1.1 Carbon

The overall carbon content required in dual phase steel is 0.12% or lower, being in the range 0.06 – 0.09%. If the carbon content is too high the martensite phase will become brittle.

2.1.2 Manganese

Manganese lowers the critical temperature and tends to produce a finer grain size in the transformation products. In solution, it moderately increases the strength of the ferrite without adversely affecting the ductility. It is effective in increasing the hardenability of austenite. The concentration varying between 1.0 – 1.5%. Higher concentrations tend to accentuate banding in the steel.

2.1.3 Silicon

Silicon produces a cleaner ferrite and enhances its ductility. It contributes in an important way to solid solution strengthening of ferrite. The concentration can be as high as 0.65%.

2.1.4 Molybdenum

Molybdenum effectively increases the hardenability of austenite, also minimizing the possibility of pearlite formation during cooling. Concentrations can be as high as 1.5%.

2.1.5 Vanadium

Vanadium refines the ferrite grain size but, in solution, can contribute to the hardenability of the austenite. About 0.03% vanadium in solution can make the steel non-aging.

2.1.6 Chromium

Chromium increases the hardenability of austenite. It also increases the connectivity of martensite and retards the formation of bainite.

2.2 Microstructure

As previously stated dual phase steels have a microstructure which consists of 80 – 85% of ferrite in which islands of a second phase, martensite, are dispersed. Though this second phase is assumed to be mainly martensite, bainite and/or retained austenite may also be present and in some cases, the overall percentage of retained austenite may be as high as 8%, which is 30 – 40% of the second phase. If microalloying elements are present in the steel, undissolved alloy carbonitride precipitates may be present in the microstructure.

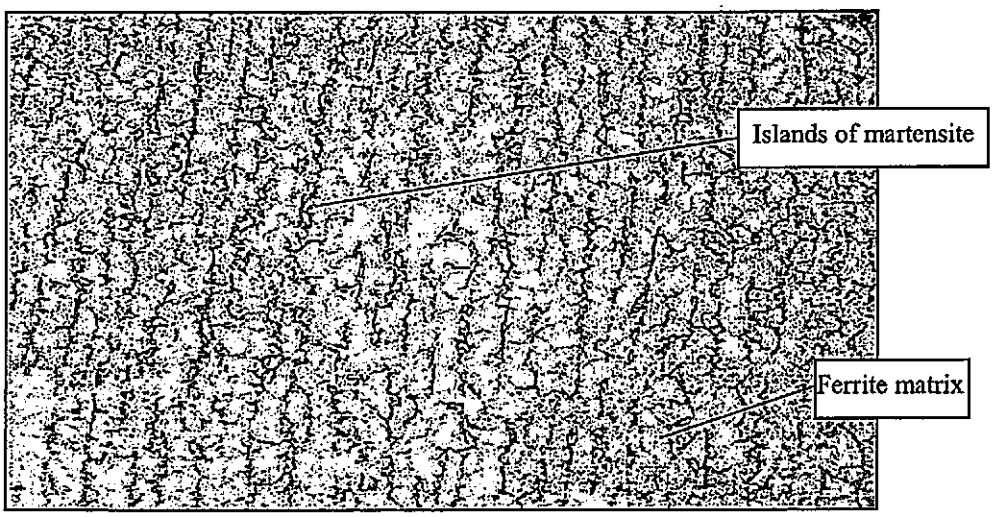

Figure 2.3 Microstructure of dual phase steel showing dispersed islands of martensite in a ferrite matrix. [100x magnification.]

2.2.1 The Ferrite Matrix

The features of the ferrite matrix that affect the mechanical properties of the dual phase steel are the morphology of the ferrite, the ferrite grain size, the presence of precipitates in the matrix and the interstitial and substitutional solutes dissolved in it[B3].

The ferrite grains should preferably be equiaxed (polygonal) in shape and as fine grained as possible since this gives improved and uniform mechanical properties. The yield strength of ferrite is a function of its grain size and follows the Hall-Petch relationship[B3], which states that a finer grain size results in an increased yield strength. Acicular ferrite on the other hand, which forms at lower transformation temperatures, impairs the ductility though the yield strength usually increases.

The presence of carbide or carbonitride precipitates, especially in a finely distributed form, is not considered desirable in the ferrite matrix since it lowers the ductility. The composition and heat treatment of dual phase steel should be controlled in such a way that fine carbide precipitates be kept to a minimum, particularly at the grain boundaries, thereby producing superior ductility[B3]. These precipitates cannot however be totally eliminated.

Considering the substructure of ferrite a high density of dislocations are revealed near the interface of the second phase particles, believed to be caused by the martensitic transformation, this leads to an increase in hardness and strength[B3].

2.2.1.1 Morphology of Martensite

The mechanical properties of the martensite phase depend on its morphology and substructure. The plate martensite obtained at higher carbon levels in the austenite tends to be brittle, while the lath martensite forming at lower carbon contents has a high strength but is not brittle. A lath morphology is therefore desired in dual phase steels[B3]. The strength of martensite is also a function of its carbon content, with increased carbon content the martensite becomes stronger, until a stage is reached when the martensite morphology changes from parallel laths to non-parallel internally twinned plates, these being brittle in nature.

2.2.1.2 Retained Austenite

Retained austenite has been identified in three different forms in dual phase steels in amounts varying between 1 to 8%. In one form it can occur as thin layers interspersed between the laths of martensite. This amount is usually less than 1% and requires selected area diffraction in an electron microscope for indentification. Retained austenite can also occur as a part of the second phase (martensite), in a more coarse form and can be identified by X-ray methods, this comprising the majority of retained austenite. Lastly it can form fine isolated island like particles of retained austenite at the grain corners or within the ferrite grains. It is believed that retained austenite contributes significantly towards the high work hardening rate of dual phase steels.

2.2.1.3 Distribution of the Second Phase

The nature and distribution of the two phases in the microstructure is determined by the

nucleation conditions for the formation of the various phases during heating or cooling. The distribution of the second phase has an influence on the mechanical properties of the steel, with the ductility of the steel being the most influenced by the second phase distribution. This second phase distribution however tends to have little influence on the strength of the steel.

Nucleation has the following effect on the nature and distribution of the two phases: If nucleation occurs predominantly at the grain corners a dispersion like structure is obtained. If however nucleation occurs predominantly at the grain boundaries a network structure is obtained and finally if nucleation occurs equally rapidly on grain boundaries and on sub-boundaries within grains in an initially cold worked matrix a fine dispersion is achieved.
It has been found that even dispersion of the martensite, that is where the martensite grains are isolated, leads to better ductility then when long chain like-islands of martensite occur along the ferrite grain boundaries[B3].

2.2.2 Microstructure and Mechanical Properties

The ductility of dual phase steel arises from the ductility of the ferrite matrix and in this regard interstitially dissolved elements such as carbon and nitrogen, which drastically decrease the ductility of ferrite, should be kept to a minimum.

The tensile strength of dual phase steel is as a result of the martensitic phase. The strength of the martensite being a function of its carbon content. When the carbon content is increased this results in a corresponding increase in the strength of the martensite, until a percentage level is reached where the martensite morphology changes from parallel laths to non-parallel internally-twinned plates which are brittle. A percentage carbon content in the range of 0.3 to 0.4% results in a maximum strength without brittleness. The tensile strength of dual phase steel increases as the microstructure becomes finer and the volume fraction of the martensite

second phase increases due to higher contents of carbon resulting in higher hardenability. Although conversely, the product of the tensile strength and elongation, which gives an index indicating the strength-ductility balance, attains a peak as the martensite volume fraction lies between the range 10 to 20%. The yield ratio also shows a minimum at the same fraction of second phase. Thus the chemical composition and hot rolling process of dual phase steel are controlled so as to achieve about a 15% martensitic second phase by volume fraction[B1].

2.2.3 General Characteristics

Dual phase steels have low ratios of yield strength/tensile strength (~0.5 – 0.6). The initial work hardening rate is high, the yield strength increasing typically from 350 to 550 MPa within the first 3% strain. This means that a high strength is obtained in the final formed part even in portions that experience relatively small strains. The total elongation of 30% is high compared with 18 – 20% for a nominal microalloyed steel with the same tensile strength. Further, there is no definite yield point elongation, i.e., no discontinuous yielding, in dual phase steels[B3].

2.2.3.1 Press Formability

The superior stretch formability in the dual phase steel results from its high uniform elongation. With regard to so-called complex press forming, where both deep drawing and stretch forming cooperate simultaneously, thus dual phase steels are considered to be superior to other types of HSLA steels[B1].

2.2.3.2 Bake Hardenability

Another characteristic of dual phase steel is its bake hardenability, which is a phenomena that remarkably increases the yield strength of stamped steel components after baking at a temperature of about 170°C; a process which is carried out to cure painted components. This comes about as a result of the amount of interstitial elements such as C or N in solution

diminishing through the rapid cooling from high rolling temperatures to very low coiling temperatures[B1]. Bake hardening is effective in strengthening stamped products[B1].

2.2.3.3 Susceptibility to Brittle Fracture after Press Forming

The susceptibility to deep drawing-induced brittleness in dual phase steel appears to be generally high due to its high silicon content in terms of its basic chemistry and resultant high transition temperature when compared with the conventional HSLA steels. Dual phase steels with less than 0.7% Si have enough resistance to brittle fracture even after deep drawing operations[B1].

2.2.4 Variation of Properties Throughout Coil

Variations in tensile strength as well as percentage elongation, in both the length and width of the coil, can be found where the manufacturing process is not controlled correctly. This brings about an inhomogeneous microstructure causing variations in the material properties.

By employing a constant speed rolling technique instead of normal zooming rolling the homogeneity of the coil quality can be improved. The controlled cooling on the runout table is kept stable by using this technique, producing a coil having less variation in mechanical properties along its length and width, through the improvement of microstructural homogeneity. Furthermore, constant rolling temperature in the finish rolling stage is achieved by controlling the cooling between each finish-rolling stand[B1].

APPENDIX - B

References

B1. Tomoyoshi. O et.al. Production and Quality of Hot Rolled Dual Phase Steel, Nippon Kokan Technical Report, No. 43, 1985, p 25 - 32.

B2. Maid, O, Production of Hot-Rolled Strip From Dual Phase Steel by Applying Coiling Temperatures Below the Martensite Start Temperature, Thyssen Technische Berichte, Heft 1/85, Iscor Translation Services 85-11-437, p 28 – 33.

B3. Piplani, R.K, Raghavan, V. Microstructure and its Correlation with Properties in Dual Phase Steels, Steel India, Vol. 4 No.1, April 1981.

APPENDIX - C

1. MATERIAL CHARACTERISTICS RELATED TO DUAL PHASE STEEL (DPS600).

On approval of this research project only certain mechanical properties related to dual phase steel as manufactured by Iscor of South Africa were obtainable from Guestro Wheels (Eastern Cape) the company sponsoring the components for this project, which were, Yield Strength, Ultimate Strength and % Elongation.

Wanting to know the magnitudes of these properties was not the only concern but the question, "how does this material react under heat treatment conditions and how does heat treatment affect the mechanical properties? as dual phase steel plate (DPS600) was also new to this particular wheel manufacturer. All sheet metal plate exhibit a phenomena called anisotropy, i.e. having different mechanical properties in different planes with respect to the rolling direction during manufacture, and being considered superior to the conventional HSLA steels then these properties should not vary greatly in magnitude with respect to these planes.

To clarify these concerns hardness tests, residual stress analysis, impact energy tests, and microstructural analysis were undertaken considering the parallel, 45° and transverse planes all with respect to the rolling direction of the sheet metal plate. These preliminary investigations would provide a basis in order to more fully understand the materials behaviour when components such as the centre disc or complete wheels are heat treated for analysis purposes at a later stage of the project.

1.1 PLATE SPECIMENS

Seven samples were cut from dual phase steel plate each of size 80mm x 80mm and of 4,1mm thickness, the centre discs are also manufactured from the same thickness plate.

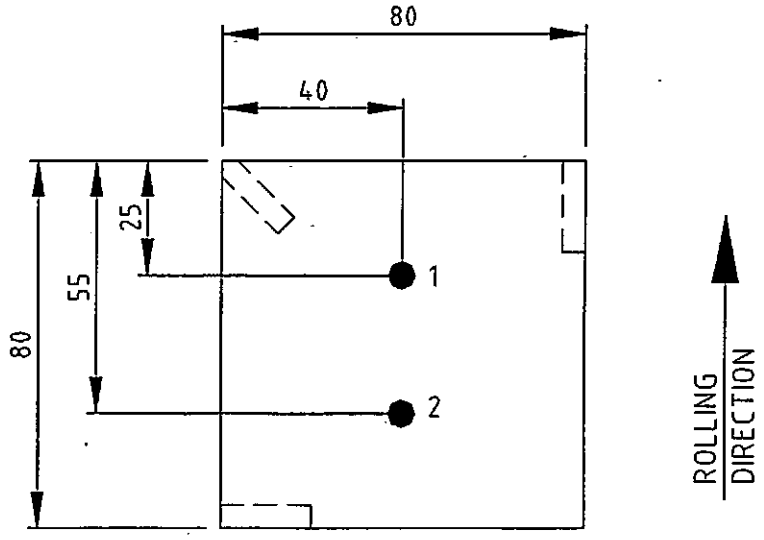

Figure 1.

Figure 1 shows the positions where:-

- the specimens were removed for the hardness and microstructural analysis, three adjacent corners;
- the residual stress measurement locations indicated as ① and ②.

Six of the specimens were heat treated from 200°C through 700°C at 100°C intervals for a period of 2 hours at each temperature level and allowed to cool down in the furnace itself. The plates were marked according to the temperature gradient to which they were subjected upon which the residual stress analysis was carried out and finally the microspecimens were then removed from the adjacent corners.

1.2 RESIDUAL STRESS ANALYSIS

Two residual stress measurements were taken from each plate as indicated in figure 1 above, making sure that the distance between drilling locations were according to ASTM 837.94(a) requirements i.e. 5D (five times the grid diameter of the gauge – 5 x 5.13mm). Both measurements revealed similar results on all seven specimens.

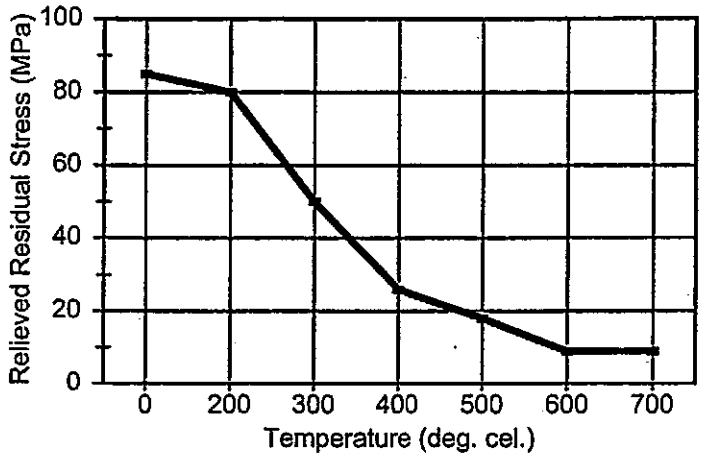

Figure 2. – Residual stress results of heat treated plate specimens.

DISCUSSION

- The measurement pertaining to the "as manufactured" specimen was assumed at 85 MPa, this assumption is in accordance with ASTM 837.94(a) standards when the stress graph does not flatten off (full stress relief)[C1] which is 0.4 x hole depth, D_o.
- The trend of the graph in figure 2, whereby the stress magnitudes decreases with increase in temperature were to be expected. A steep drop in magnitude is evident over the 200°C to 400°C range, this is interesting as temper embrittlement occurs over this same temperature range. Also interesting to note is the fact that after cooling from 700°C residual stress still exists although a minimum.

- The high stress magnitude for the "as manufactured" plate specimen is related to the uncoiling operation of the sheet material which is carried out under cold working conditions and the fact that these plate specimens were taken from the end of the coil section.

1.3 HARDNESS ANALYSIS

Micro-specimens removed from the corners as indicated in Figure 1 were of approximate size 15mm x 5mm and mounted such that the cross-sectional plane was uppermost and visible, upon which they were marked, ground, polished and etched using 2% nital solution

Vicker's hardness (HV10) tests were carried out across the centre of the cross-sectional plane (see Figure 3) where an average of five (5) readings were taken per specimen. The results taken from the 45° plane were coincidental to that of the transverse plane and is as indicated in the legend of Figure 4.

Figure 3. – Micro-specimen

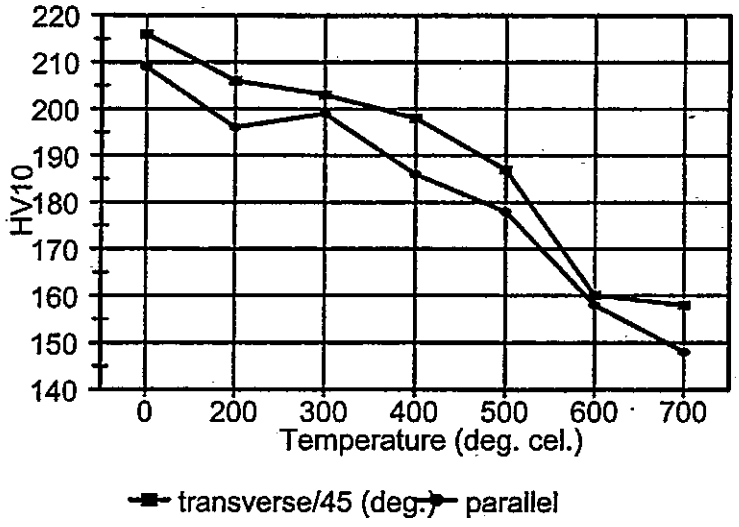

Figure 4. – Hardness test results

DISCUSSION

- The trend was also envisaged but expecting the transverse direction to be the hardest of the three directions, it was surprising that the 45° plane was equal in magnitude to that of the transverse plane, although the hardness values vary marginally with respect to the parallel plane.

1.4 IMPACT ENERGY ANALYSIS

A further seven (7) specimen were removed from dual phase steel plate of size 120mm x 120mm x 4,1mm thick of which six (6) were subjected to the same heat treatment process i.e. 200°C thru' 700°C at 100°C intervals and furnace cooled. These specimen were then marked and cut as shown in Figure 6 after completion of the heat treatment process.

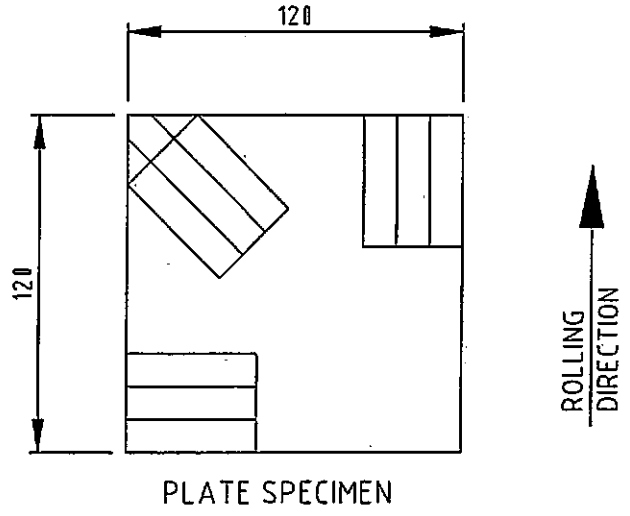

Figure 6. – Illustration showing planes from which specimens were removed.

The test specimen, three from each direction (with respect to the rolling direction) were ground and machined in accordance with BS131 specification for providing the V-notch Charpy type specimen, see Figure 7.

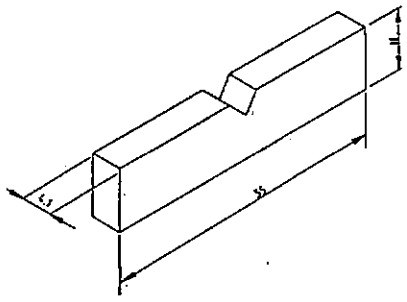

Figure 7. – Impact Charpy type specimen.

The results obtained from the Impact Charpy Test are shown in Figure 8 below.

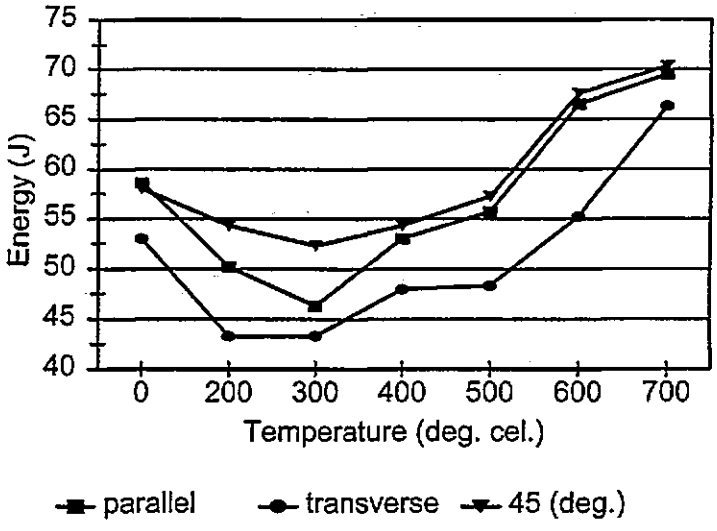

Figure 8. – Impact Charpy Test Results.

DISCUSSION

- All specimen exhibit temper embrittlement, which is clearly evident between 0°C and 400°C, this phenomenon is not unique to dual phase steel but occurs in all metals.

- Although the magnitudes differ marginally between the three planes, what is clear is that the harder the material the less ductile its behaviour when comparing the impact to hardness results considering the transverse plane

CONCLUSION

- The hardness and impact analysis carried out indicate that the transverse plane, in terms of anisotropy, is the slightly weaker of the three planes analysed and will thus be considered for all future investigations regarding this project. Although where applicable, reference will be made with respect to the remaining two planes i.e. parallel and 45° planes.

1.5 MICROSTRUCTURAL ANALYSIS

Only three (3) specimens were considered for the microstructural analysis which were:-

1.5.1 DP9 – "As manuf." – Transverse plane;

1.5.2 DP8 – H/T to 700°C – Transverse plane; and

1.5.3 DP8 – H/T to 700°C - 45° Plane.

These specimens were re-ground, polished and etched using 2% nital solution upon completion of the HV10 analysis. The specimens are designated in the following manner: DP – Dual Phase; Number pertains to type of heat treatment (if any) to which the specimen were subjected as well as the plane from which the specimen were removed.

1.5.1 DP9 – "AS MANUF." – TRANSVERSE PLANE

The grain size was analysed as No. 7 which according to ASTM standards is the minimum grain size recommended for sheet metal forming processes. The micrograph of the "as manuf." specimen shown in Figure 9 consisting of four (4) parts indicates very clearly the surface that was subjected to the adjustable rollers during the manufacturing process

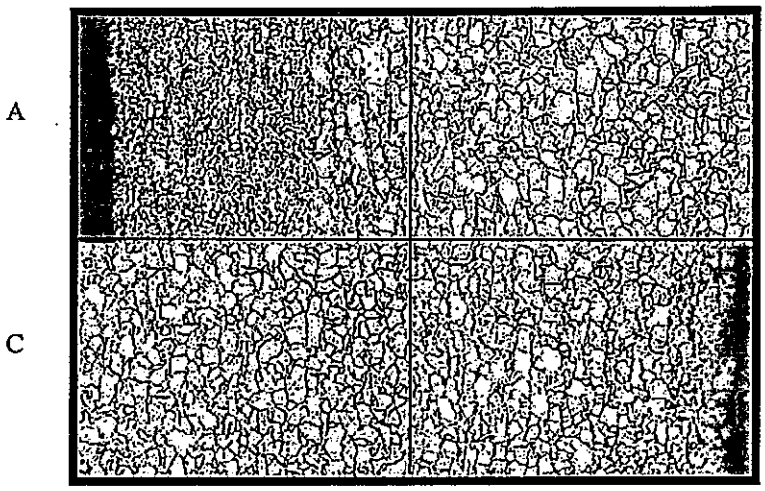

Figure 9. – Microstructure of "as manuf." DPS plate x 500 mag. Micrograph sequence is, A - top surface; B - above N/A; C - below N/A; D - bottom surface.

(top left). The bottom right is that which is in contact with the bottom (fixed) rollers, while the other two parts (top right and bottom left) indicate the microstructure within the cross-section. Spheroidised precipitates on both ferrite and martensite (darker regions) grain boundaries are evident. They are more pronounced however along the martensite grain boundaries.

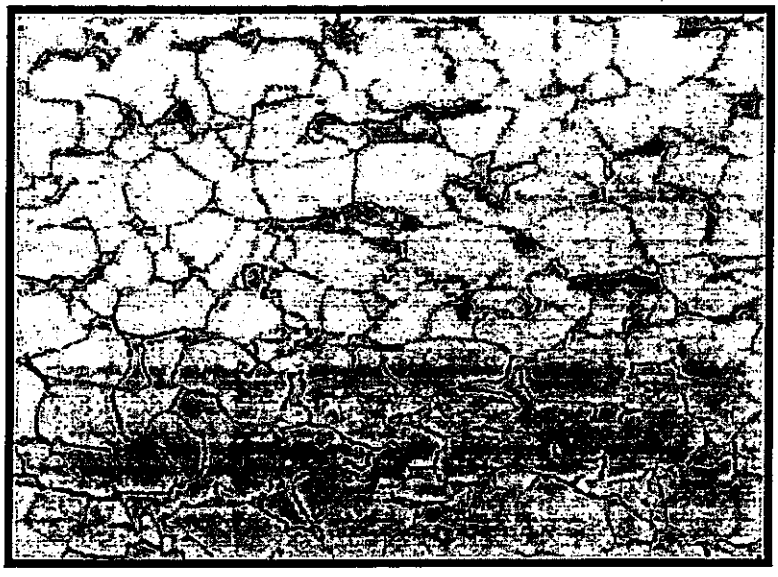

Figure 10. – Microstructure of "as manuf." DPS plate x 1000 mag. showing spheroidised iron carbide precipitates.

These precipitates are iron-carbides as the coiling temperature of this dual phase steel is above 200°C[C2] and are of a feathered nature. The martensite on the other hand, is precipitate free at ambient temperature while at a coiling temperature of 100°C cementite precipitates are seen along the grain boundaries (also evident in Figure 10) and at coiling temperatures above 200°C tempering effects are indicative.

1.5.2 DP8 – H/T to 700°C – TRANSVERSE PLANE

This specimen although heat treated to 700°C which is below the sub-critical temperature of 723°C, shows the effects of grain growth and recrystallisation as is indicated in Figure 11, according to Avner[C3] the grain growth and recrystallisation process which is evident in Figure 11, and may occur at lower temperatures and depends upon the amount of cold working carried out prior to the heat treatment process as well as the soaking time at a particular temperature. The specimen heat treated at 700°C were subjected to an uncoiling operation thus providing the prime mover for recrystallisation to take place together with a soaking time of 2 hours at this particular temperature, would thus be proof of what is seen in Figure 11.

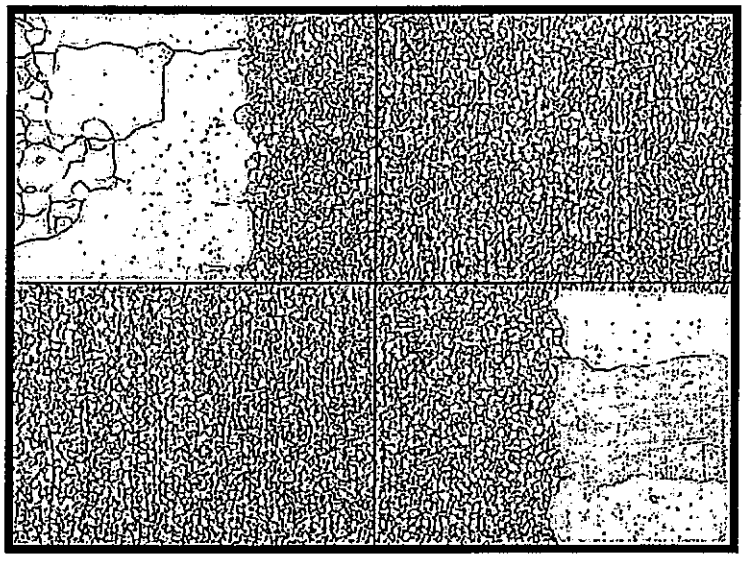

Figure 11. – Microstructure of DP8 transverse plane x 200 mag. H/T to 700°C. Micrograph sequence is, A - top surface; B - above N/A; C - below N/A; D - bottom surface.

The above micrograph, also in four parts, indicates that recrystallisation has taken place within the grain growth section (top right) and is the top surface of the plate. The bottom surface (bottom right) indicating grain growth only while the remainder (top right and bottom left) is indicative of the microstructure from within the cross-section.

Cementite carbides are pronounced along and within the martensite grains at this heat treatment temperature as is evident in Figures 12 and 13 below.

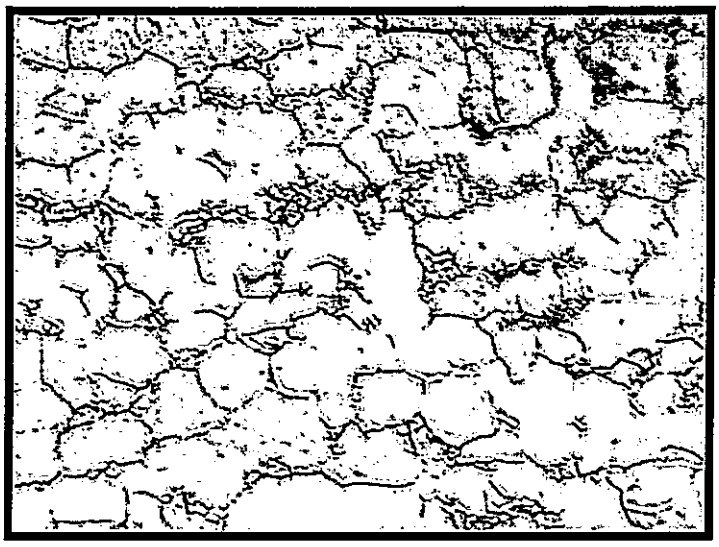

Figure 12. – Microstructure of DP8 transverse plane x 1000 mag.

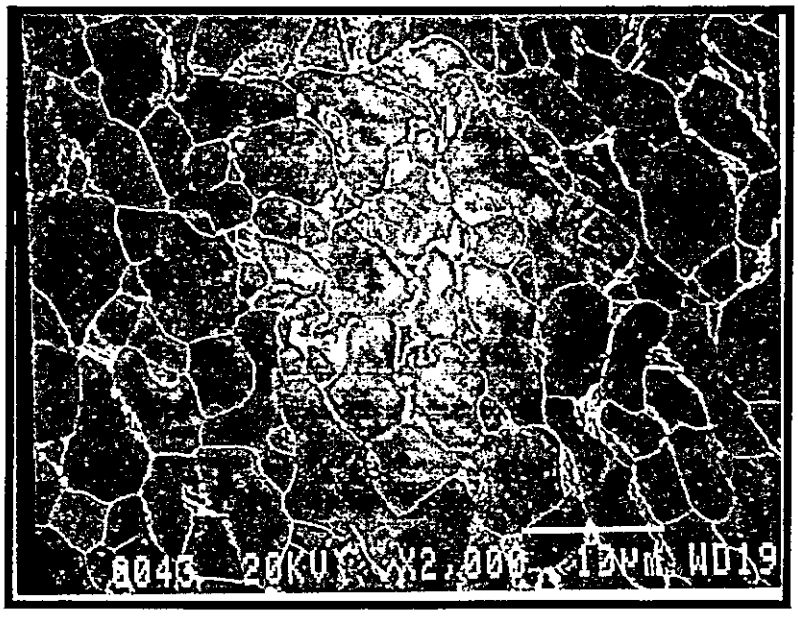

Figure 13. – Microstructure of DP8 transverse plane x SEM 2000 mag.

1.5.3 DP8 – H/T to 700°C – 45° PLANE

The microstructure for the above specimen are similar to that as analysed to the transverse plane, see Figures 14 and 15 below.

Figure 14. – Microstructure of DP8 - 45° plane x 200 mag. Micrograph sequence is, A - top surface; B - above N/A; C - below N/A; D - bottom surface.

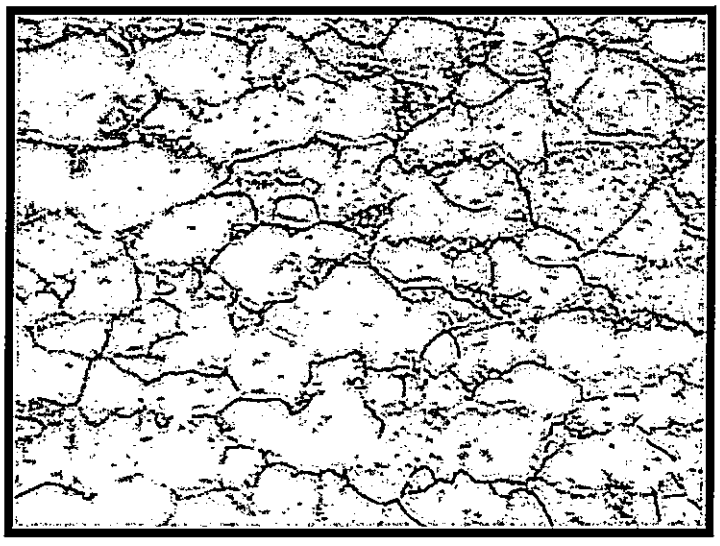

Figure 15. – Microstructure of DP8 - 45° plane x 1000 mag.

Recrystallisation texture is evident in Figures 12 and 15 where the ferrite grains tend to lie on different levels.

References

C1. ASTM E 837 – 94a, Standard Test Method for Determining Residual Stresses by the Hole Drilling Strain Gauge Method, Annual Book of ASTM Standards, Vol. 03.01, October 1994.

C2. Niku-Lari, A., Lu, J. and Flavenot, J.F. - *"Measurement of Residual Stress Distribution by the Incremental Hole Drilling Method"*, Experimental Mechanics, 1985.

C3. Avner, S.H., Introduction to Physical Metallurgy, 2nd edition, McGraw-Hill, 1974.

APPENDIX - D

1. ASSESSMENT OF TMS FATIGUE TESTING SYSTEM

1.1 Machine Description

The system consists of four essential components and is described as follows:-

- Motor Controller;
- Fatigue machine;
- Strain amplifier; and
- Computer.

1.1.1 Motor Controller

This panel houses the pre-settable cycle counter and the motor controlling device which allows for setting the motor speed from 2Hz to 50Hz. One of the failure detection devices is also connected to this panel which is explained in Section D 1.3.

1.1.2 Fatigue Machine

The frame of the machine consists of a 20mm thick box section of size 700mm long by 350mm wide by 350mm high and houses a 2000kg load cell to which one of the control arms are attached. The motor and plumber blocks (2 off) are attached to a vertical baseplate allowing for mean stress adjustment (pre-stressing), the motor shaft passes through these plumber blocks to which an eccentric flywheel is attached allowing for the setting of the test load. A connecting rod is connected to the eccentric flywheel and to the other control arm of the fatigue machine. These control arms are in turn pivoted by bearings whose axis of rotation is 6.5mm from the mounting base to which the fatigue specimens are attached, see Plate 1.

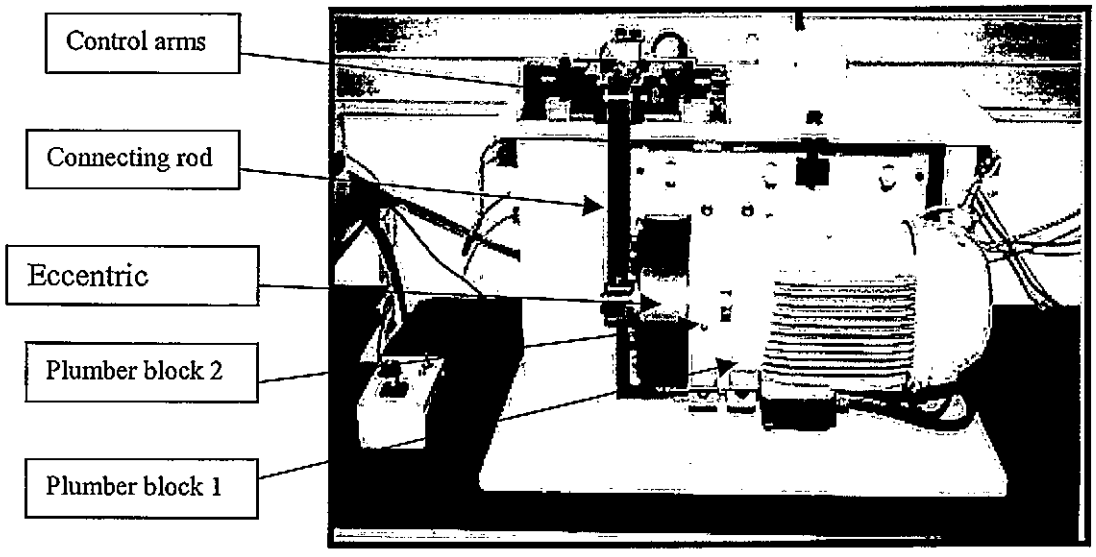

Plate 1. – Fatigue machine showing various parts.

1.1.3 Strain Amplifier

This strain amplifier has two channels, one controlling the applied load at the load cell and the other controls the applied load at the specimen. The amplifier is a Micro Measurement unit

1.1.4 Computer

The software programme controlling the fatigue testing procedure is called ESAM. The data acquisition from the amplifier, load cell and specimen, is transmitted to the software programme for later data processing. During a test the display screen shows the induced loads from the load cell and specimen in terms of milli-volts vs time.

1.2 Specimen Preparation

Once the specimen has been machined one surface is cleaned and prepared for strain gauge application, the strain gauge is located such that the centre of the grid is aligned with the centre of the throat (narrowest section of the hour-glass shape). Applying a protective covering for the strain gauge two coats of non-conductive paint is sprayed over the surface.

A narrow strip of conductive silver lacquer (silver dac) is painted round the periphery of the hour-glass shape, starting and ending on solder tabs which is applied onto the non-conductive paint, see Plate 2.

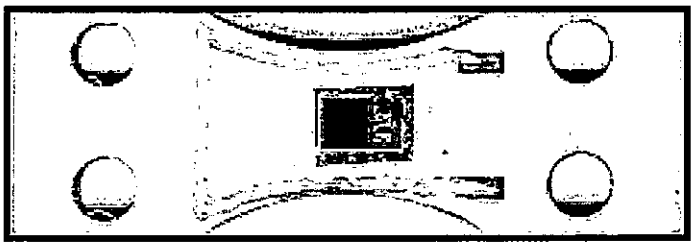

Plate 2. – Specimen prepared for fatigue testing.

1.3 Operation of fatigue machine

The specimen having been mounted to the two independent control arms by means of cap screws assuring that the centre axis of the specimen is coincidental with that of the rotational axis of the control arms, this is achieved through the use of spacers.

The two electrical leads from the motor control panel are connected to the solder tabs on which the silver dac has been painted and the strain gauge connected to the amplifier. On zero balancing the strain gauge the test load (in micro-strain) is set by means of the eccentric mechanism on the eccentric flywheel and the test can now commence.

1.4 Investigation into temperature/strain hardening effects

Fatigue testing of mild steel plate specimen was carried out in order to develop a working knowledge of the machines operating parameters. These specimen were machined from flat bar of cross-sectional dimensions 50mm by 5.2mm and were ground to a final thickness of 5mm. After preparing the specimen according to Section D 1.2 and having set the test load (strain amplitude) to 1900 micro-strain the cycle counter being set to 10 000 cycles in accordance to Section D 1.3 above, the test was started setting the motor speed at 33Hz.

On completion of the 10 000 cycles the following was observed:-

- The temperature of plumber block 2, the eccentric flywheel and the bottom end of the connecting rod had increased substantially from a cold start;
- Rotating the eccentric flywheel by hand, it was noted that the strain magnitude had also increased from the initial setting of 1900 micro-strain by an amount of 500 micro-strain. Although this increase was expected as the applied load was above yield for the material, it was not known whether the temperature had any effect.

This aspect was discussed with the particular manufacturer who knew that the temperature of these parts increased but was unsure as to the effects it would have on the fatigue results. These concerns led to this investigation and was carried out as follows:-

Two K-type thermocouples were each connected to plumber block 2 (see Plate 1) and the bottom end of the connecting rod respectively, as shown in Plate 3.

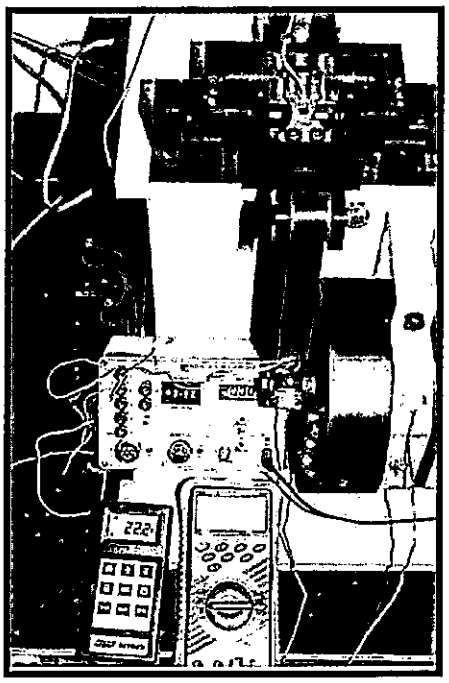

Plate 3. – Investigating temperature effects.

A strain gauge was applied to the connecting rod to establish a change in length due to the increase in temperature. The initial specimen was removed and replaced by another and the

system connected and set as previously mentioned except for the number of cycles which was pre-set to 5 000. The following measurements were recorded:-

- Amplitude strain;
- Connecting rod strain;
- Connecting rod temperature;
- Plumber block temperature; and
- Number of cycles.

It must be noted that once the 5 000 cycles is reached the motor takes 20 cycles to come to rest, thus the readings were taken after every 5 020 cycles. This test was carried through to failure which occurred at 105 420 cycles.

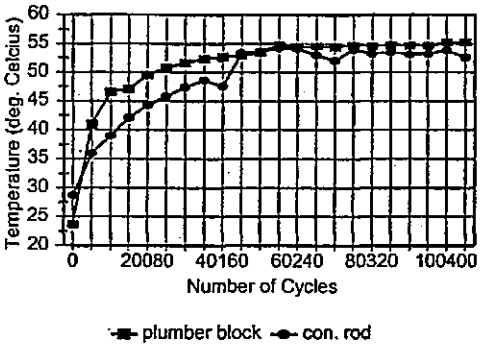

Figure 1. – Connecting rod operating temperature.

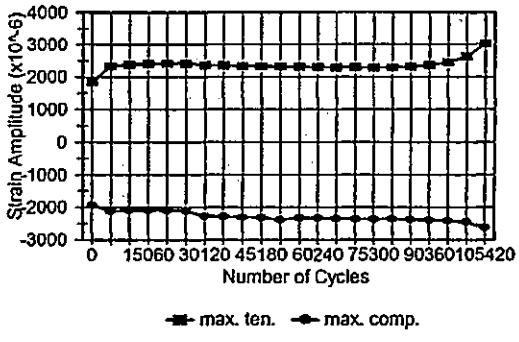

Figure 2. – Strain magnitudes as assessed. on the hour-glass specimen during fatigue test.

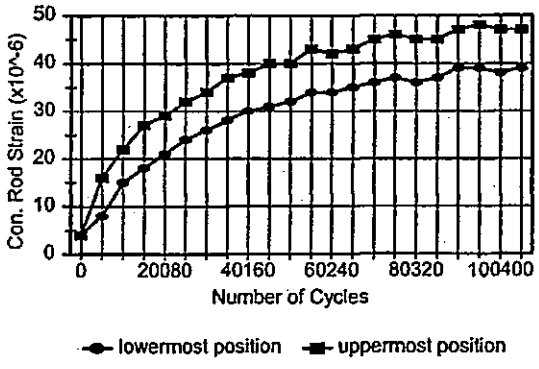

Figure 3 – Result showing difference in connecting rod strains.

The operating temperature of these parts stabilizes around 55°C which occurs after 55 000 cycles (see Figure 1), it was expected that the rise in temperature of the connecting rod would lag the plumber block initially as the heat transfer is time dependent, see Figure 1. The increase in strain magnitude indicated in Figure 2 which takes place over the first 5020 cycles is due to strain hardening where after it too stabilizes prior to fracture. This being an indication that temperature plays little or no part in the fatigue results obtained. This point is substantiated in Figure 3 where the difference in strain magnitude remains constant at ± 8 micro-strain from approximately 40 000 cycles. The upward trend of the graph is temperature related as strain gauges are sensitive to temperature but the difference will have an effect on the fatigue result and in this case can be considered negligible. The reason for this is that if temperature played a role in the fatigue result then the tensile and compressive magnitudes as shown in Figure 2 would be of increasing nature.

In order to prove this point, a third specimen was inserted and connected in the same manner as before applying the same test settings but the counter set to 60 000 cycles. The test commenced from a cold start and upon reaching 60 000 cycles the machine was stopped keeping the amplifiers on. The strain readings for the specimen was noted at +2295 and –2345 micro-strain on stopping the machine and 16 hours later the readings were +2285 and –2335 micro-strain. Again indicating that temperature has no effect on the fatigue test result as the difference in strain magnitude indicated by this last exercise is similar to that indicated in Figure 3.

APPENDIX - E

1 ASSESSING THE CHANGES IN FATIGUE PROPERTIES OF DUAL PHASE STEEL PLATE SUBJECTED TO FORMING OPERATIONS

The following investigations will be undertaken to ascertain the fatigue behaviour of Dual Phase Steel Plate subjected to forming operations, these include:-

- Establishing fatigue testing parameters for waisted hour-glass specimen machined from centre discs (investigation completed);
- Fatigue testing of "as manufactured" DPS plate;
- Fatigue testing components from stage 1 of the forming process;
- Fatigue testing components from stage 2 of the forming process;
- Fatigue testing components from stage 3 of the forming process; and
- Fatigue testing components from the final stage of the forming process.

1.1. Establishing fatigue testing parameters for waisted hour-glass specimen

The predominant fracture plane under industrial fatigue testing conditions occur slightly above the cup radius, it was decided to retain this plane as having the narrowest section (width) for all hour-glass machined specimens. For this investigation two specimen shapes were to be machined, one having a waisted hour-glass shape and the other a parallel sided shape, both machined to ASTM E468-82 standards.

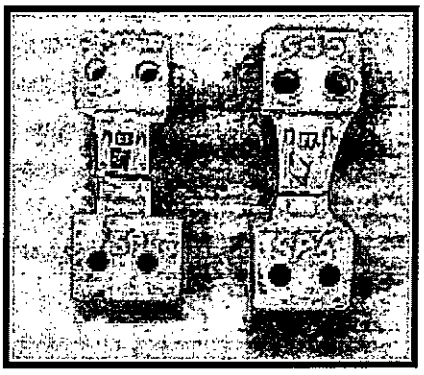

Figure 1.1 – Top view of parallel sided and wasted hour-glass shaped specimen.

A CNC milling machine was employed for the machining operation of which only the sides of the specimens were machined in order to maintain rigidity of the centre disc during the machining process. The mounting holes of the specimens also required machining as this operation would have been difficult to accomplish using a drill press, as the holes had to be produced through an inclined surface. The specimens were finally obtained by angle grinding the ends.

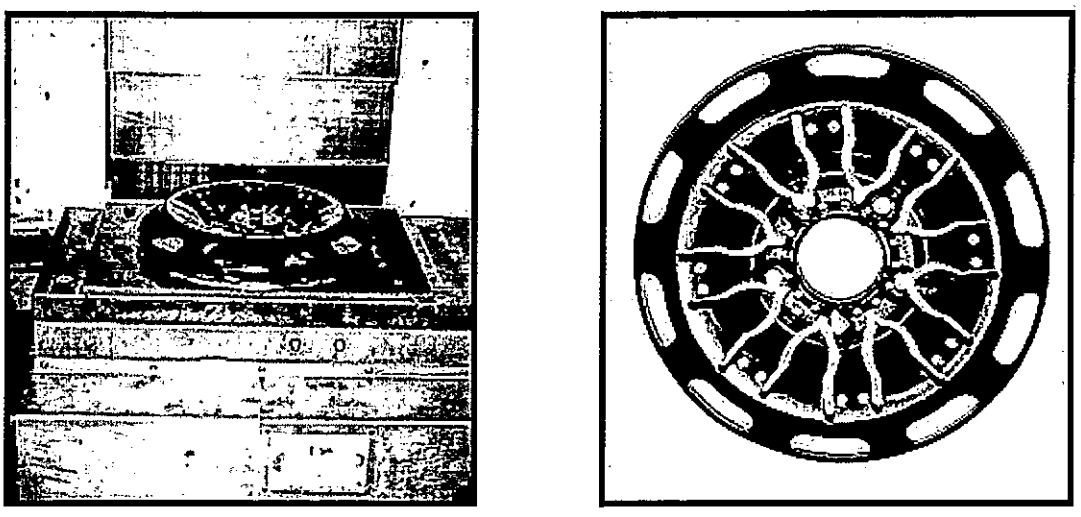

Figure 1.2 – Centre disc mounted to machine bed for CNC machining (left) and machined centre disc (right).

Initial investigations to establish the most effective method of fatigue testing these peculiar shaped specimens were undertaken, these included:-

- The angle of inclination of the specimen between the mounting points these being horizontal and high heel orientated;
- Which end of the specimen should be mounted to the connecting rod side of the fatigue machine; and
- Should the underside of the cup radius be clamped (see Figure 1.3) so as to simulate the effects of bolting down the arm to the centre disc which is required when either industrial type fatigue testing machine is used.

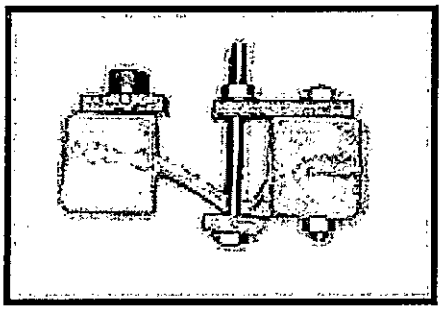

Figure 1.3 – Horizontal orientated specimen showing clamp mechanism.

- The type of compound required for producing spacer mounts that would conform to the geometrical shape of the specimen being somewhat complex, but rigid enough to withstand the necessary forces under fatigue testing conditions.

1.1.1 Spacer mounts

The first objective was to find a suitable compound for producing spacer mounts, this was achieved by using LECOSET 7007 which is a cold curing resin used for metallographic

applications. Other compounds used for this purpose were an epoxy resin E18A and E18B purchased from Exaton Composities but was found unsuitable as basic compression and impact tests were carried out on castings produced from these compounds revealing that the cold curing resin was the best suited for this application.

1.1.2 Moulds

Moulds had to be manufactured according to the angle of inclination of the specimen in order to cast the resin. These were manufactured from mild steel sections as shown in Figure 1.4.

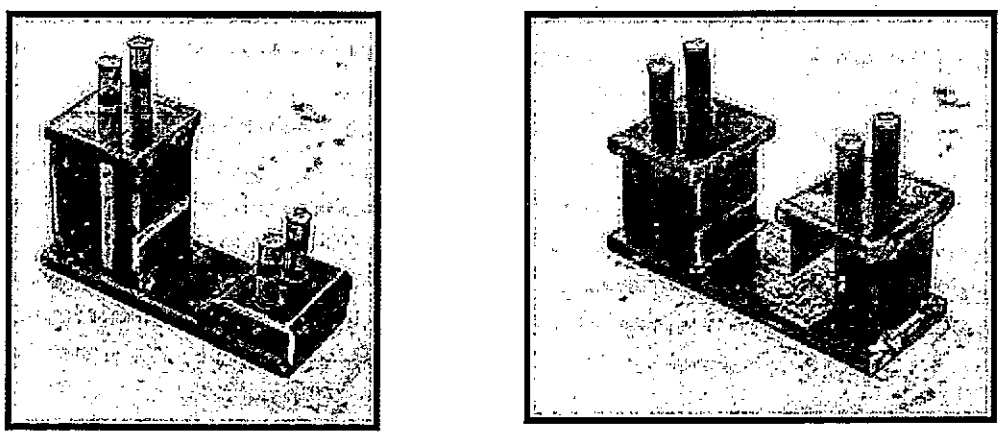

Figure 1.4 – Moulds for producing the spacer mounts according to angle of inclination. High heel (left) and horizontal (right).

The moulds were manufactured such that the predominant fracture plane as observed under industrial conditions coincided with that of the rotational axis of the fatigue machine.

1.1.3 Fatigue analysis

Five hour-glass and five parallel sided specimen were machined and prepared for fatigue testing, these specimen would be tested in pairs under similar testing and mounting conditions. After casting the spacer mounts the specimens were finally prepared as set out in Section E 1.3.3.2.

The results of this investigation are indicated in Table 1.

Discussion

- The fracture plane was found to be the same for all specimens tested, i.e. through the apex of the cup radius indicating that specimen shape has no significant impact on fatigue performance.
- The angle of inclination also had no effect in relation to the fracture plane or fatigue performance.
- Specimen SP1 is not included in Table 1 due to inconsistent testing parameters.
- Except for specimens SP4 and SP4a all were mounted such that the cup radius end was secured to the connecting rod side of the fatigue machine.
- Specimens SP2, SP2a, SP5 and SP5a were clamped as shown in Figure 1.3, this had no effect on the fracture plane although it was envisaged that it would shift toward the predominant fracture plane. A significant decrease in fatigue life was observed.
- Specimens SP3, SP3a, SP5 and SP5a were horizontally orientated.
- The cup radius shows necking effects and thus the maximum stresses would undoubtedly occur in this region as the cross-sectional area is smaller than at the narrowest section (throat) of the hour-glass shaped specimen.

2.1 RECOMMENDED FATIGUE TESTING PARAMETERS

- Waisted hour-glass shaped specimens is preferred in view of subsequent residual stress assessment.
- The horizontal orientation mounting method will be used to ensure equal volume of resin used for spacer mounts at either end of the specimen.
- The test frequency will be maintained at 33Hz, this is 3Hz above the natural frequency of the combined structure i.e. specimen and machine.

- The following stress amplitudes will be considered in light of this investigation:-

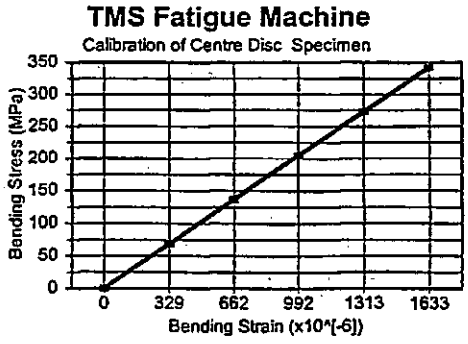

Figure 1.5 – Calibration curve.

252MPa $\propto$ 1260μ strain

210MPa $\propto$ 1050μ strain

179MPa $\propto$ 895μ strain

140MPa $\propto$ 700μ strain

103MPa $\propto$ 515μ strain

It is hoped to fatigue test eight specimens at the above stress amplitudes as per calibration curve and under zero mean stress conditions for the purposes of obtaining the S-N curve.

APPENDIX - E

HOUR-GLASS SPECIMEN						PARALLEL FACED SPECIMEN					
Spec. No.	Test Freq. (Hz)	Test Date	Applied Strain ($x10^{-6}$)	Cycles To Fail.	Comments	Spec. No.	Test Freq. (Hz)	Test Date	Applied Strain ($x10^{-6}$)	Cycles To Fail.	Comments
SP2	33	2/6/99	±1850	18 500	Failure, fractured occurred between apex of cup radius and predominant fracture plane of wheel. Spec. pre-strained to -646μ strain by clamping cup radius.	SP2a	33	2/5/99	±1640	20 900	Failure, fracture plane same as for specimen SP2. Specimen pre-strained to -680μ strain by applying clamp to cup radius.
SP3	33	4/6/99	±1890	16 300	Failure. Horizontal orientated.	SP3a	33	4/6/99	±1970	11 000	Failure. Horizontal Orientated.
SP4	33	5/6/99	±1900	23 400	Failure, hat radius side of specimen was mounted to connecting rod end of fatigue machine.	SP4a	33	5/6/99	±1860	16500	Failure, hat radius side of specimen was mounted to the connecting rod end of fatigue machine. Fractured through apex of cup radius.
SP5	33	8/6/99	±1800	7 300	Failure, Specimen pre-strained to –1010μ strain by applying clamp to cup radius. Horizontal orientated.	SP5a	33	7/6/99	±1870	6 600	Failure, Specimen pre-strained to –1000μ strain by applying clamp to cup radius. Horizontal orientated.

NOTE:-

a) Unless otherwise stated the fracture plane of the above tested specimens occurred through the apex of the cup radius, this location is ± 5mm from the axis of rotation, the axis of rotation coincides with the notched plane where most wheel fractures occur.

b) By clamping the underside of the cup radius, which simulates the effect of the bolt torque prior to the fatigue testing of wheels under industrial conditions, actually shifts the fracture plane closer to the predominant fracture plane as experienced by industry.

c) Unless otherwise stated all specimens were mounted having the cup radius side affixed to the connecting rod end of the fatigue machine.

Table 1. – Results of preliminary fatigue analyses.

APPENDIX - F

Systems for Measuring Residual Stress and Hardness Testing

1 Introduction

The measurement of residual stresses for purposes of this research will be undertaken by means of the Hole-drilling method, with all residual stress analyses being made using an automatic hole-drilling system, RESTAN, supplied by SINT, Italy.

The RESTAN system makes use of a high speed air turbine, running at approximately 300 000 rpm, which allows for the drilling of a hole by means of an inverted endmill. This has been shown to be a process which induces negligible stresses during drilling.[F1, F2]. Further advantages of the RESTAN system are that a number of operations for which the operator was previously responsible have been simplified, automated and computerized, thereby providing more accurate and complete control of testing. The principle advantages are:

- an increased accuracy in the centering of the drilling axis to the centre of the strain rosette,
- automatic identification of the dimension of the hole at the start of each depth increment and measurement of the depth of the hole after each increment,
- accurate control of the depth increments for drilling as well as the measurement of relaxed strain after each increment,
- measurement of the final diameter of the hole and any eccentricity, if any.

These advantages allow for numerous strain readings to be made with great precision, throughout the depth of the hole.

Herein follows a detailed description of the RESTAN system as well as the operating procedure.

1.1 Description of RESTAN System

The system consists of the drilling unit, electronic control unit, PC-PLM-16 I/O card for system interface with a desktop computer, a desktop computer minimum 486 MHz operating with Windows 95/NT/3.1/3.1J or DOS, and strain gauge amplifier (The digital strain gauge amplifier HBM-MGC is used in the research system). Shown in Figure 1.1 is a diagram of the various sub-systems making up the test configuration.

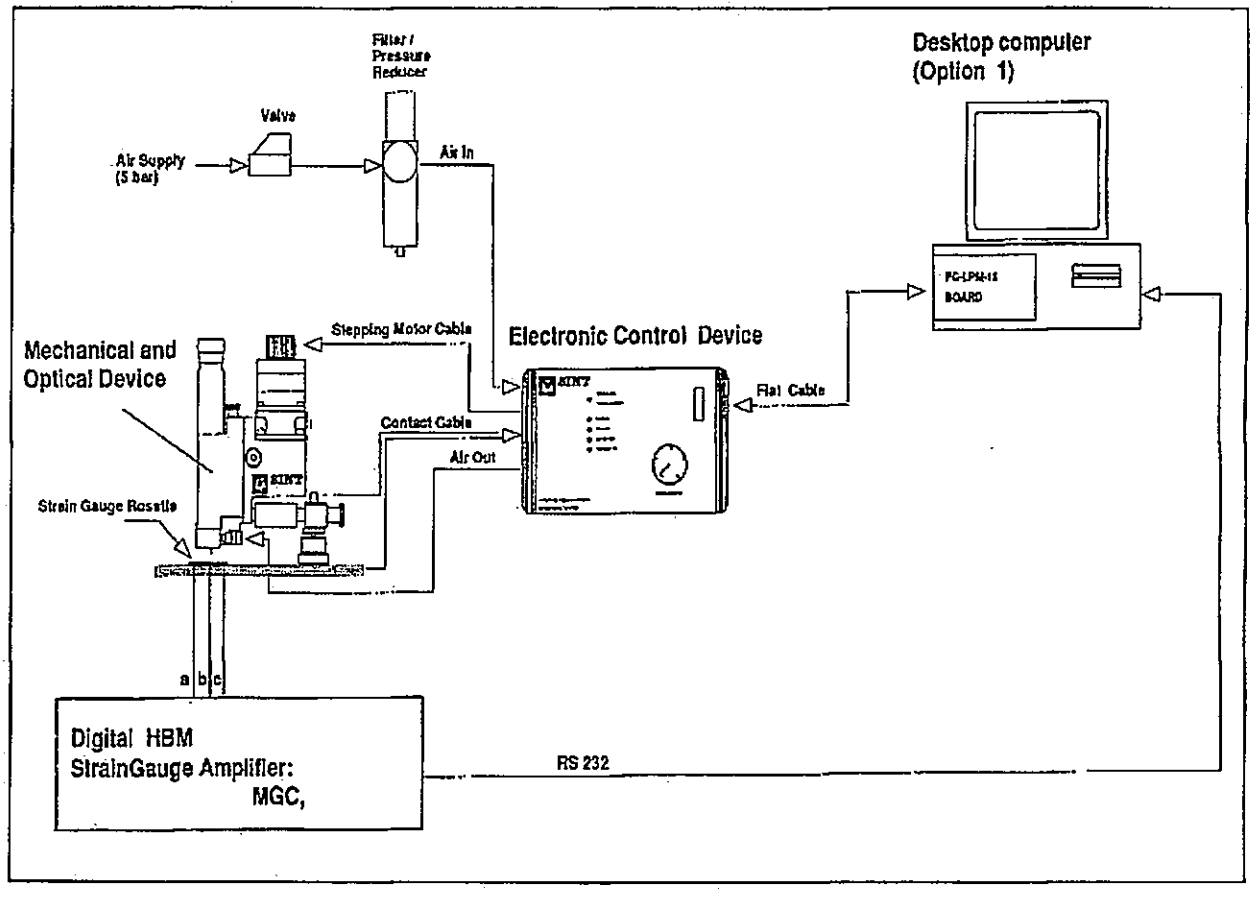

Figure 1.1. - Schematic of RESTAN system instrumentation layout

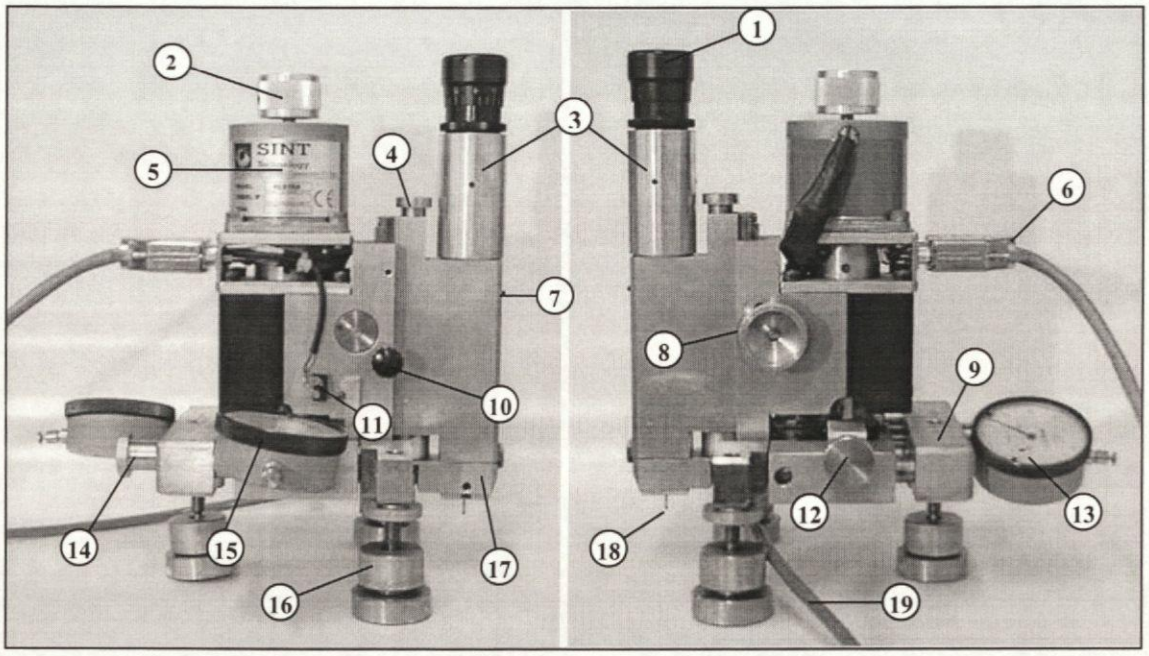

Figure 1.3. - Sides views of RESTAN drilling unit

1. Eyepiece
2. Knob for slow manual feed
3. Optical centering device (OCD)
4. Drill-head revolver release hand
5. Stepper motor
6. Electrical supply and control from electronic control device
7. Microscope locking screw
8. Knob for vertical fast feed
9. Base
10. Grip screw for locking vertical motion
11. Microswitch for limiting height
12. Knob for horizontal motion (x –axis)
13. Dial gauge (y – axis)
14. Knob for horizontal motion (y – axis)
15. Dial gauge (x – axis)
16. Support foot
17. Revolvable drill-head
18. Inverted endmill
19. Air supply hose (4.5 bar)

The drill-head and OCD are attached to the drilling unit by means of a dovetail rack and pinion mechanism, which is moved vertically by means of the fast vertical control knob for height adjustment, or the stepper motor during positioning and incremental drilling. Drilling must be undertaken perpendicularly to the surface of the workpiece. This is achieved by

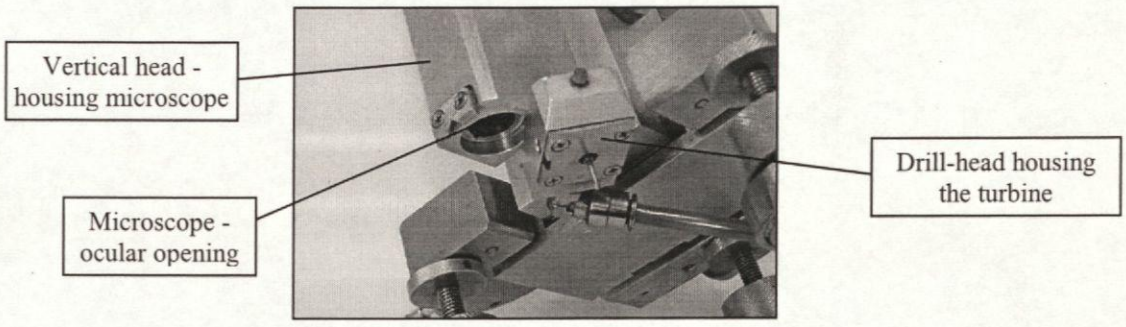

Figure 1.4. - Underside view of the vertical head showing the drill-head in the 45° open position

adjustment of the three stainless steel ball-jointed feet which are connected to the body by threaded bars. The feet also contain magnets to help maintain drilling position. After drilling is completed the drill-head is again rotated 45° out of position and the OCD is used to measure the hole diameter and eccentricity by two dial gauges on axes 90° to one another.

The air turbine is driven by compressed air at 4.5 bar supplied by a standard 3hp compressor.

1.1.2 The Electronic Control Device

The electronic control device (ECD), shown in Figure 1.2, controls the entire drilling process. It is vital to the process since it interfaces the computer/software to control the air supply, by solenoid valve, to the turbine and electrical supply to the stepper motor.

1.1.3 Computer and Software – Control and Data Acquisition Program

The desktop computer incorporating the system software is a Pentium I, 300 MHz, operating with Windows 95.

The PC-PLM-16 I/O card is used to interface the software and the ECD. SINT Technology of Italy developed the software in collaboration with HBM of Germany. The software is used to control the entire drilling process via the ECD and also controls the data acquisition via the MGC amplifier. It further processes the strain data results acquired from the amplifier during the drilling operation. The software also incorporates an evaluation program, which automatically converts the strain data to stress reading. A choice of data manipulation methods is given, namely: Standard ASTM E837.94(a) method[F3], Integral method[F4], Power Series method[F4] and the Kochelmann method[F5].

1.1.4 Amplifier

The strain amplifier unit also measures the relieved strain after drilling by converting the change in resistance of the strain rosettes. The unit used in the system is a model MGC digital amplifier manufactured by HBM of Germany. The amplifier unit is controlled by the RESTAN software as to which strain readings are to be made.

The three-gauge strain rosette is wired to the amplifier using a four-lead quarter bridge circuit with each grid having its own channel on the amplifier to facilitate simultaneous sampling. An amplifier is not unique to a residual stress measurement system, but acts as a slave unit within the system.

1.2 RESTAN Technical Data

1.2.1 Drilling Device

▪ Height	180	mm
▪ Width	175	mm
▪ Length	205	mm
▪ Weight	4.6	kg
▪ Turbine speed	300 000	rpm
▪ Max. diameter of endmill	2.2	mm
▪ Turbine feed pressure	4 – 5	bar
▪ Fast vertical motion	60	mm
▪ Fine vertical motion	7	mm
▪ Horizontal motion X and Y axes	6	mm
▪ Turbine rotation	45	degrees
▪ Height adjustment of feet	60	mm

1.2.2 Electronic Control Device

▪ Height	140	mm
▪ Width	245	mm
▪ Length	220	mm
▪ Weight	5.5	kg
▪ Electric power supply	125/220	V~ 50/60 Hz
▪ Max. compressed air feed	5	bar
▪ Fuse	1.5	Amp

1.2.3 PC – PLM – 16 I/O Card

▪ 16 analog inputs, single-ended 12-bit field ± 5 Volts	
▪ digital outputs	8
▪ digital inputs	8
▪ 16-bit counters	2

1.2.4 MGC Amplifier

▪ Height	255	mm
▪ Width	171	mm
▪ Length	367	mm
▪ Weight	6	kg
▪ Electric power supply	115/230	V~
▪ Fuse	500	mA

2 Residual Stress Measurement Procedures

2.1 Introduction

The measurement of residual stress is a high cost operation; mainly because of the cost of equipment involved but also because most methods required specially trained operators. The above considerations resulted in the Hole-Drilling Strain Gauge Method of residual stress measurement being chosen for use in this research. Another reason for the choice of method is that it is an accepted technique, which if applied according to the correct procedures and standards gives good accuracy when compared to other methods.

2.2 Surface Preparation and Strain Gauge Application

The surface preparation and installation of strain gauge is a critical area in the measurement of residual stress, since large errors in the final stress calculation can occur as a result of poor preparation procedures. It is also critical to maintain set and constant procedures so as to avoid variations in results because of varying testing parameters. Throughout this research the accepted procedures for surface preparation and strain gauge installation, as stipulated by the strain gauge manufacturer; Micro-Measurements Group, will be strictly adhered too[F6, F7].

2.3 Strain Gauge Selection

The initial step in preparing for any strain analyses is the selection of the appropriate gauge for the analysis and is of great consequence to the stress analyses. The choice of gauge for residual stress measurement by the hole-drilling method is slightly easier than for other stress analyses situations since there are specialised gauges available and fewer gauges to choose from. The primary consideration when selecting a gauge is the size and shape of the component to be analysed as well as the position and accessibility for gauge installation and drilling purposes.

Three types of standard gauges were selected for analyses during the research, all manufactured by Micro-Measurements Group, namely: EA-XX-031RE-120, EA-XX-062RE-120 and CEA-XX-062UM-120. These gauges are constructed of self-temperature-compensated foil mounted on a flexible polyamide-backing carrier and each gauge includes a centering target for use with the optical centering device.

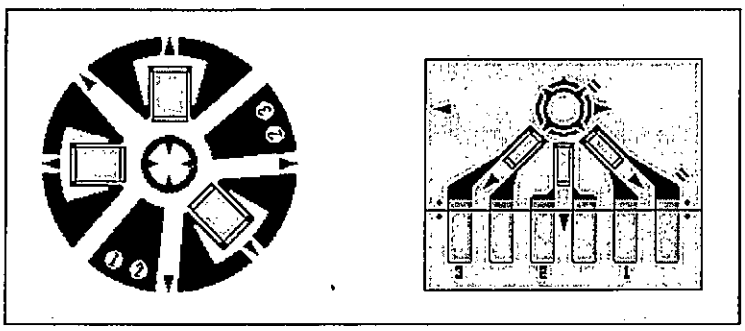

Figure 1.5. - Configuration of 031RE and 062RE (left) and the 062UM gauges

The dimensions of the gauges needs to be known in order to apply the data reduction formulae. These are given, in millimeters, for each gauge in Table 1.1.

Gauge Type	EA-XX-031RE-120	EA-XX-062RE-120	CEA-XX-062UM-120
Gauge Length	0.79 Each element	1.57 Each element	1.57 Each element
Grid Centre-line Diameter	2.56	5.13	5.13
Hole Diameter (Min.)	0.8	1.5	1.5
Hole Diameter (Max.)	1.0	2.0	2.0
Backing Length	7.4	10.7	9.6
Backing Width	7.4	10.7	12.2

Table 1.1 Dimensions in millimeters of residual stress rosette gauges

2.4 Residual Stress Analyses Procedure

2.4.1 Setting test parameters

After the strain gauge rosettes have been applied and connected to the amplifier, according to the procedures indicated by the manufacturers, the test parameters must now be entered into the system software before testing can commence.

From the main menu program panel, of the 'Residual Test Measurement System', 'Test Setup' is selected and the following test parameters must be supplied:

- The number and distribution of drilling steps required. The number of steps will depend on the hole depth required and also the detail of mapping with depth required. The distribution can either be 'linear'(evenly distributed) or 'polynomial'(increased step density in proximity to the surface). A polynomial 20 step test being preferred for our investigations.
- Diameter of endmill. A 1.6 mm diameter endmill will be used for the 062RE and 062UM gauges and a 0.8 mm diameter endmill for the 031RE gauge.
- The type of strain rosette utilized. The diameter and gauge factor must also be correctly displayed, if this is incorrect the 'customize' option is used to enter the correct values.

- The material characteristics, e.g. material type, heat treatment if any, Poisson's ratio and Young's modulus. Notes on the component, etc, can also be entered here.
- The instrument settings. Here the MGC HBM amplifier details are entered and the connections to the strain gauges are verified.
- General data such as date, operator, place of test, test description and the file path must be entered.

After all the above has been entered into the 'Test Setup' menu the configuration must be saved to the chosen file path and the 'Test Setup' exited.

2.4.2 Positioning the drilling-head

The positioning of the endmill is an important step in the testing procedure since large errors can occur in the calculated stress values as a result of any eccentricity. For acceptable accuracy the alignment of the endmill must be to within 0.025 mm of the centre of the strain rosette[F8]. It is also important to note is that for each hole a new endmill must be inserted into the drill-head mandrel to avoid errors induced by the use of a blunt cutting tool[F1].

Before aligning is undertaken the vertical head must be adjusted so that the axis of drilling is perpendicular to the surface. This is achieved by adjusting the steel ball-jointed feet by means of their threaded connecting bars, ensuring the locking nuts are tightened afterwards. The component under analyses should now ideally be bonded, using the adhesive X60, to the worktable to avoid any shifting during centering. The endmill can then be positioned in the centre of the strain gauge rosette (central target) by making use of the OCD and adjusting the horizontal positioning knobs to bring about alignment. Once the alignment is completed the feet of the drilling unit are bonded to the surface of the steel worktable.

After the X60 has set the centre should be checked and the horizontal dial gauges can then be set to zero. This is done to ensure that the measurement of the final hole diameter and position, eccentricity, is done from the correct reference position.

2.4.3 Zero-setting of strain gauges

The strain rosette readings must now be set to zero. This is done by accessing the 'Instruments Setting' panel from the 'Test Setup' panel and choosing the MGC amplifier option. The strain rosettes are then simultaneously set to zero by using the 'Tare Balance' command.

2.4.4 Determining zero measurement position

Before the drilling of the hole can commence it is necessary to position the endmill at the zero point. This is defined as the point where contact occurs between the tool and the metal surface. A system has been devised for signaling the precise moment at which the endmill actually touches the metal surface. This is achieved by measuring the electrical resistance between the metal surface and the endmill, made possible by the fact that the three supporting feet are electrically insulated.

The measurement of the electrical resistance is accomplished as follows:

- Making use of the two appropriate cables from the ECD. The black cable is connected to the drilling unit and the red cable to the component under test.
- The 'Positioning Control' is accessed from the 'Main Menu' panel and the 'Position Endmill on Surface' option is chosen. The turbine will start and automatic positioning will then take place.

- When the endmill comes into contact with the surface the feed and turbine will stop. A message will then appear to confirm that the current position is assumed as zero.

Actual drilling of the hole can now commence.

2.4.5 Drilling of the hole

From the 'Main Menu' panel the 'Test Manager' option is now chosen. A control panel will appear, from which motion and data acquisition will be controlled. Measurement can either be undertaken in a step-by-step sequence with strain data acquisition being requested after each drilling step or a completely automatic sequence where the software controls strain data acquisition. The preferred option being the automatic control, since the strain data is read at exactly the same period of elapsed time from the completion of each drilling step. The strain data is read after an elapsed time period of not less than 8 seconds. This allows for the settling of the strain readings displayed by the amplifier, since during drilling the readings fluctuate higher than the actual relieved strain values as a result of the drilling action.

The speed of the feed rate for drilling must be specified here. This is determined by preliminary drilling tests and is a compromise between the need to shorten testing time and the need to avoid blocking or irregular operation of the turbine, which would negatively affect the correct drilling of the hole. It was determined from the preliminary testing that a feed rate of 0.2 millimetres per minute would be employed for the analyses of the dual phase sheet metal.

The 'Start Test' option can now be chosen and drilling will commence. Upon completion of each drilling increment the turbine will stop after a delay of 8 seconds and the software will record the strain data. This will continue until the required number of steps is completed.

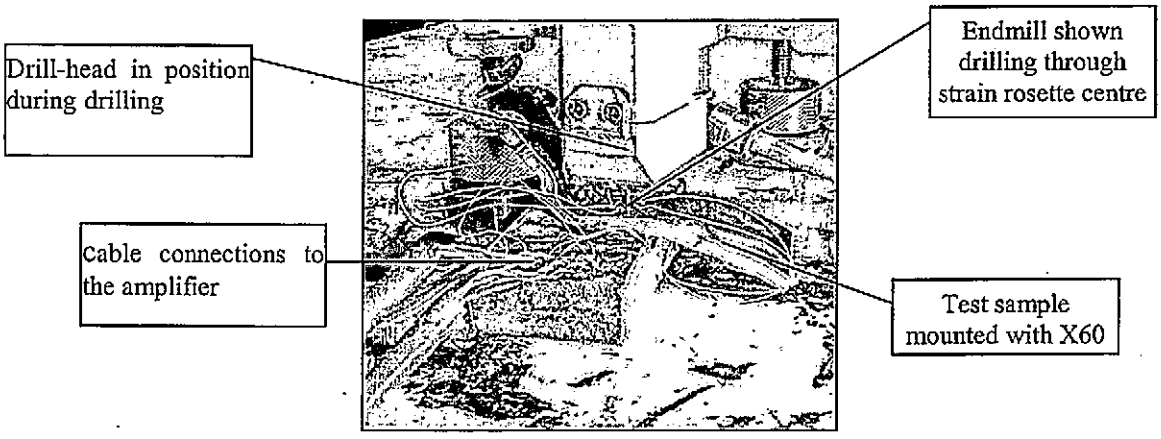

Plate 3.4 View of the mounted sample during the drilling operating

2.4.6 Measuring diameter and eccentricity of hole

After completion of drilling the hole diameter must be measured by means of the OCD. This information is entered into the 'Hole Data' option in the 'Test Manager' panel. The eccentricity of the hole will automatically be determined by the software from the diameter values measured. The procedure is carried out as follows:

- Lift the vertical head and lock in place.
- Rotate the drill-head out of alignment.
- Unlock the vertical head and focus the OCD by means of the fast vertical motion knob.
- If necessary clean the hole so that a clear view of the circumference of the hole is obtained.
- Making use of the horizontal motion knobs, X-axes and Y-axes, measure the values X1, X2, Y1, and Y_2, as shown in Figure 3.10.
- Enter the values into the 'Hole Data' option to complete the measurement procedure.

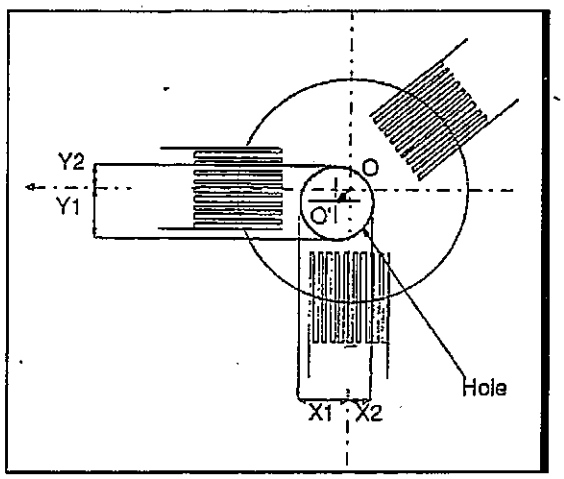

Figure 1.6. - Schematic of drilled hole showing measurement of hole eccentricity

2.4.7 Calculating the residual stress

Once the above procedure has been completed the 'Residual Stress Measurement System' program must be exited and the 'Residual Stress Evaluation' program run. This program will perform the analysis of the previously stored data from the testing procedure.

The 'Load Data' option must now be taken and the previously stored file name called up. The method for calculating the residual stresses must now also be specified, e.g. ASTM E837.94(a)[F3], Integral[F4], Power Series[F4] and Kochelmann method[F5]. The residual stress values will then be displayed instantaneously along with their corresponding graphs. The procedure is then complete and must be followed again for the next hole.

3 Hardness Testing

3.1 Introduction

Hardness, as the term is commonly used in metallurgy, is a measure of the resistance of a material to indentation by an indenter of fixed geometry, under a static load and a hardness

test of this type is known as an 'indentation hardness test'. From this hardness test a hardness number is calculated, which is expressed by a number that is either proportional to the depth of the indentation for a specified load and indenter, or proportional to a mean load over the area of the indentation. It must be noted that the term 'hardness number' has no quantitative meaning, but is merely a number in terms of a particular test in which the size and shape of the indenter, the indenting load, and other conditions of the test are specified. The hardness values obtained are however useful as an indicator of materials properties, such as ultimate tensile strength[F9]..

There are three standardised methods of indentation hardness testing, each having its own indenter shape and size, load application and range, and hardness number calculation method. The three tests methods being the Brinell, Rockwell and Vickers hardness tests[F10]. Each test, as already stated, has its own hardness number, which is calculated as follows[F9]:

- Brinell hardness number (HB) – A number related to the size of the permanent impression made by a ball indenter of specified size, usually 10 mm in diameter, presses into the surface of the material under a specified load. In reporting Brinell hardness the test load, ball diameter and load duration must be stated.
- Rockwell hardness number (HR) – A number derived from the net increase in depth of the impression as the load on an indenter is increased from a fixed minimum load to a high load and then returned to the minimum load. Indenters include steel balls of several specified diameters and a diamond cone. Rockwell numbers are quoted with a scale symbol representing the indenter, load and dial figure colour.
- Vickers hardness number (HV) – A number obtained by dividing the load in kilograms applied to a square-based pyramidal diamond indenter by the surface area of the

impression in square millimetres. The test load must be stated when reporting Vickers hardness.

The reason for these different tests is simply because no one combination of test load and indenter size can be used for the testing of specimens of all sizes and degrees of hardness.

3.2 Microhardness

Microhardness testing is an indentation method for measuring the hardness of a material on a microscopic scale. The indentations can be made using a square-based pyramid indenter (Vickers hardness scale) or an elongated, rhombohedral-shaped indenter (Knoop hardness scale). The advantages of using the microhardness test is that hardness impressions can be precisely located with the microscope to perform tests on microscopic features, small or thin samples can be tested and the change in hardness through a thin cross-section, hardness profile, of the sample can be determined.

Microhardness testing, using the square-based pyramid diamond indenter, was chosen as the hardness testing method to be employed for this project because of the advantages stated above, primarily the fact that detailed hardness profiles can be acquired by this method. All microhardness testing was undertaken according to the ASTM standard: Standard test method for microhardness of materials, E 384 – 84.

3.2.1 Microhardness Testing Principles[F10]

As previously stated microhardness testing can make use of the Vickers or Knoop hardness scales, although for purposed of this project only the Vickers hardness scale was used and therefore the Knoop scale will not be discussed here. The Vickers hardness test uses a

precision diamond indenter with face angles, α, of 136°, shown by figure 3.11. The indenter is impressed into the material under loads in the range of 15 to 1000 grams. The diagonal

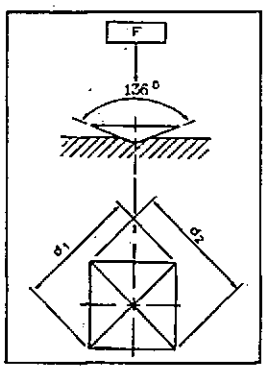

Figure 1.13 Form of pyramidal diamond indenter for microhardness tester

lengths, d_1 and d_2, of the impression are measured microscopically and their mean value used to obtain the surface area of the impression. The surface area, A_s, and the test load, P, are then used to calculate a hardness value[F10].

The formula 1.1, below is used to compute the Vickers hardness number:

$$\mathrm{HV} = \frac{P}{A_s} = \frac{2P\sin\left(\frac{\alpha}{2}\right)}{d^2} = \frac{1.8544P}{d^2} \quad \text{.....(3.1)}$$

Note that the surface area is given in square millimetres and the load in kilograms of force, kgf. Although the above formula is given it is not necessary to calculate the Vickers hardness number for each indentation. Tables computed by formula 1.1 for each test load are available and provide a convenient means of obtaining the hardness number from the measured diagonals.

3.2.2 Sample preparation and mounting

The preparation and mounting of samples for microhardness testing was undertaken according to the ASTM standard[F11]: Standard Methods of preparation of metallographic specimens, E 3 – 80.

APPENDIX - F

References

F1. Lu, J., Handbook of Measurement of Residual Stresses, Society for Experimental Mechanics Inc, 1996.

F2. Flaman, M.T., Brief Investigation of Induced Drilling Stresses in the Centre Hole Drilling Method of Residual Stress Measurement, Experimental Mechanics, January 1982, pp. 26 – 30.

F3. ASTM E 837 – 94a, Standard Test Method for Determining Residual Stresses by the Hole Drilling Strain Gauge Method, Annual Book of ASTM Standards, Vol. 03.01, October 1994.

F4. Schajer, G.S., Measurement of Non-Uniform Residual Stresses Using the Hole Drilling Method. Part 2 – Practical Application of the Integral Method, ASME, Vol. 110, October 1988, pp. 344 – 349.

F5. Schwarz, T. and Kockelmann, H. – *"The hole drilling method – the best technique for the experimental determination of residual stresses in many fields of application"*, Translated article from MTB, 29, (2), 1993, pp. 33 – 38.

F6. Hoffmann, K., An Introduction to Measurements using Strain Gages, HBM, Germany, 1989.

F7. Strain gauge installation procedures: http://www.measurementsgroup.com/guide/library/library.htm

F8. Measurements Group Tech Note, Measurement of Residual Stresses by the Hole-Drilling Strain Gage Method, TN – 503 – 3, 1988.

F9. Small, L., Hardness – Theory and Practice, Service Diamond Tool Co., Cushing – Malloy Inc., Michigan, 1960.

F10. SABS, South African Standard, Code of Practice for: Methods for hardness testing of metallic materials, SABS 055-1977, 1977.

F11. ASTM, Annual Book of ASTM Standards, Standard Test Method for Microhardness of Materials, E 384 – 84, 1988.

APPENDIX - G

APPENDIX - G

Results of Residual Stress and Hardness Analyses

1. Residual Stress Results

1.1 Results of the Residual Stress Analysis of the Initial Blank Plate [DPP]

Because of the uncoiling process of the sheet it can be expected that the induced residual stress may well vary between the upper and lower surfaces of the plate. As previously stated all measurements will be confined to the outside surface of the sheet material for each stage. Fortunately as a result of the uncoiling process the flat plate has a slight curvature, this curvature is also present in the blank and allows for the identification of each surface, i.e. convex relates to the outer surface. The blank is inserted with the convex side upwards, therefore only the convex side of the blank was analysed.

The initial blank plate was analysed by means of an 8-grid rosette in position R3, with grids 1 and 5 being orientated parallel to the rolling direction. The results of the analysis, in Table 1, showed that the grid combination 2,7,4 picked up the highest maximum principal stress of 37.8 MPa with a corresponding minimum principal stress of 17 MPa. The maximum principal stresses for all of the grid combinations were within a relatively small range of 2.6 MPa or 6.9% of the highest maximum. In later stages it will be seen that this range could increase to as much as 68% because of the complex stress field induced by the forming operation.

Grid Combination	Maximum Stress MPa	Minimum Stress MPa	Principal angle to max. stress
1,6,3	36	15	-2.6°
2,7,4	37.8	17	5.2°
3,8,5	35.9	15	-2.6°
4,1,6	35.2	13.5	0.6°
5,2,7	36.6	16	6.7°
6,3,8	36.6	16	-1.9°
7,4,1	36.4	17	4.1°
8,5,2	37.6	21	3.2°

Table 1. - Results of the residual stress analysis per grid combination for hole DPP-R3. [The principal angle is referenced from grid number 1, clockwise being positive.]

Also found was the fact that the direction of the maximum principal stress lay approximately in the rolling direction of the plate. The full relief depth, being the depth after which further drilling results in no further increase in relieved stress, was attained at approximately 1.81 mm. Now, since the stress results were similar for all grid combinations and the plate had undergone no further deformation from its manufactured state except for the uncoiling operation, it is assumed that the results of hole DPP-R3 would be representative of the entire blank.

1.2 Results of the Residual Stress Analysis of the First Stage Pressing [DP1]

1.2.1 First stage pressing - residual stress results for position 1 holes

These residual stress measurements were taken using standard EA-06-031RE-120 rosettes. The smaller rosettes were selected for analyses of position 1 for two reasons. Firstly, they allow for analysis closer to the cup radius in the subsequent production stages and secondly the required spacing of 5 times the rosette gauge diameter, given by the ASTM 837 94a standard, is maintained between positions 1 and 2. It was therefore decided that these rosettes would be used for residual stress analyses in position 1 for all the four pressed stages.

The problem arises as to which direction the reference grid should be orientated was solved by first measuring the residual stresses, using the customised 8-grid rosettes, in positions 2 and 3 in all three directions. From these analyses it was found that the highest average of the maximum principal residual stress considering the three directions for positions 2 and 3 was obtained by the grid combination 3,8,5. It was felt that this combination would also reveal the maximum stress for position 1 since all analyses would be taken on the convex side of the bulge, formed during the 1st stage pressing. The 3,8,5 orientation was therefore selected for the application of the standard three-grid rosettes for positions 1. The results of the residual stress analyses for position 1 hole locations is shown in Table 2.

Position of the Hole	031RE Rosette Orientation	Maximum Principal Residual Stress [MPa]	Minimum Principal Residual Stress [MPa]	Principal Angle to max. stress	Full Relief Depth [mm]
DP1-R1	3,8,5	106.3	49.5	15.2°	1.3
DP1-S1	3,8,5	90.2	66.2	-15°	1.14
DP1-T1	3,8,5	74.1	30.6	-2°	1.3
Average	-	90.2	48.8	-0.6°	-

Table 2. - Results of the residual stress analysis for position 1holes of the 1st stage pressing. [Principal angle referenced from the 8-grid number 1 position, clockwise positive.]

1.2.2 First stage pressing - residual stress results for position 2 holes

These residual stress measurements were taken using the customised 8-grid rosette. From these analyses the highest average of the maximum principal stress for the three directions was revealed by the grid combination 3,8,5. Table 3 shows the results of the residual stress analyses for position 2 hole locations.

Position of the Hole	Maximum Stress Grid Combination	Maximum Principal Residual Stress [MPa]	Minimum Principal Residual Stress [MPa]	Principal Angle to max. stress	Full Relief Depth [mm]
DP1-R2	3,8,5	159.1	95.3	7.6°	1.81
DP1-S2	5,2,7	181.4	79.2	-4.9°	1.63
DP1-T2	5,2,7	158.4	60.7	-10.3°	1.81
Average	-	166.3	78.4	-2.5°	-

Table 3. - Results of the residual stress analysis for position 2 holes of the 1st stage pressing. [Principal angle referenced from the 8-grid number 1 position, clockwise positive.]

1.2.3 First stage pressing - residual stress results for position 3 holes

These residual stress measurements were taken using the customised 8-grid rosette. From these analyses the highest average of the maximum principal stress for the three directions was indicated by the grid combination 3,8,5. Table 4 below shows the results of the residual stress analyses in position 3 hole locations.

Position of the Hole	Maximum Stress Grid Combination	Maximum Principal Residual Stress [MPa]	Minimum Principal Residual Stress [MPa]	Principal Angle to max. stress	Full Relief Depth [mm]
DP1-R3	5,2,7	173.3	63.2	1.16°	1.81
DP1-S3	3,8,5	130.3	88.9	3.3°	1.63
DP1-T3	3,8,5	166.1	80.3	-3°	1.63
Average	-	156.6	77.5	0.49°	-

Table 4. - Results of the residual stress analysis for the position 3 holes of the 1st stage pressing. [Principal angle referenced from the 8-grid number 1 position, clockwise positive.]

1.2.4 Discussion of residual stress results for the first stage pressing

Analyses of the 1st stage stamping operation revealed two important facts: Firstly, the principal angle was similar for all of the positions analysed. This was to be expected as all of the hole positions were on the same diametral plane where the component has undergone the same forming operation and amount of plastic deformation. If an imaginary line is drawn through the strain rosette grids 1 and 5, in other words dissecting the component in half through its centre, this line can be considered to be at 0°. The maximum principal residual stress revealed at all of the analyses locations of the 1st stage pressing were within ±15° of this 0° direction. Therefore the maximum principal residual stress can be assumed to always act in a direction approximately through the centre of the component for all similar positions. It was secondly determined that for residual stress analyses of this component standard three-grid rosettes should be applied in an orientation coinciding with the 8-grid 3,8,5 or 5,2,7 grid combinations. The lower average of the three directions maximum principal residual stress for positions 3 than positions 2 can be accepted as the plate is more curved at positions 2 than positions 3, therefore more bending and stretching or deformation of the plate had taken place in positions 2. Positions 1 on the other hand occurred on the flatter central section of the bulge where even less forming than either positions 2 or 3 had taken place, hence the lower average maximum stress.

It can be noted that the full stress relief depth was considerably shallower for the position 1 holes, within a depth of 1.3 mm, as opposed to positions 2 and 3 where the average depth was 1.81 mm. This shallower full stress relief depth for position 1 holes can be attributed to the fact that a greater degree of plastic deformation of the plate has occurred at this position.

1.3 Results of the Residual Stress Analysis of the Second Stage Pressing [DP2]

1.3.1 Second stage pressing - residual stress results for position 1 holes

Residual stress analyses of the 2nd stage position 1 holes was undertaken using standard EA-06-031RE-120 rosettes, applied in an orientation corresponding to the 3,8,5 grid combination. The selection of these gauges and their orientation was discussed in Chapter 5. Table 5 shows the results of the residual stress analyses in position 1 hole locations for the second stage, DP2.

Position of the Hole	031RE Rosette Orientation	Maximum Principal Residual Stress [MPa]	Minimum Principal Residual Stress [MPa]	Principal Angle to max. stress	Full Relief Depth [mm]
DP2-R1	3,8,5	234.1	22.1	88°	0.74
DP2-S1	3,8,5	173.3	-31.8	103.9°	1.3
DP2-T1	3,8,5	164.1	65.9	85.1°	1
Average	-	190.5	18.7	92.3°	-

Table 5. - Results of the residual stress analysis for position 1 holes of the 2nd stage pressing. [Principal angle referenced from the 8-grid number 1 position, clockwise positive.]

1.3.2 Second stage pressing - residual stress results for position 2 holes

These residual stress measurements were taken using the customised 8-grid rosette. From these analyses the highest average of the three directions maximum principal stress was found by the grid combination 4,1,6. Table 6 shows the results of the residual stress analyses in position 2 hole locations for the second stage, DP2.

Position of the Hole	Maximum Stress Grid Combination	Maximum Principal Residual Stress [MPa]	Minimum Principal Residual Stress [MPa]	Principal Angle to max. stress	Full Relief Depth [mm]
DP2-R2	3,8,5	186	-5.9	88°	1.81
DP2-S2	7,4,1	113.2	-6.3	106°	1.63
DP2-T2	4,1,6	239	21.3	86.5°	1.81
Average	-	179.4	3	93.5°	-

Table 6. - Results of the residual stress analysis for position 2 holes of the 2nd stage pressing. [Principal angle referenced from the 8-grid number 1 position, clockwise positive.]

1.3.3 Second stage pressing - residual stress results for position 3 holes

These residual stress measurements were taken using the customised 8-grid rosette. From these analyses the highest average of the three directions maximum principal stress was found by the grid combination 5,2,7. The results of the residual stress analyses in position 3 hole locations of the 2nd stage are shown in Table 7 below.

Position of the Hole	Maximum Stress Grid Combination	Maximum Principal Residual Stress [MPa]	Minimum Principal Residual Stress [MPa]	Principal Angle to max. stress	Full Relief Depth [mm]
DP2-R3	3,8,5	-296.9	-54.4	98°	1.63
DP2-S3	5,2,7	-265.7	-35.8	84.1°	1.81
DP2-T3	3,8,5	-264.9	57.8	90.6°	1.81
Average	-	-275.8	-32.4	90.9°	-

Table 7. - Results of the residual stress analysis for position 3 holes of the 2nd stage pressing. [Principal angle referenced from the 8-grid number 1 position, clockwise positive.]

1.3.4 Discussion of residual stress results for the second stage pressing

The results of the residual stress analyses of this stage displayed good repeatability, although there was however a some doubt as to the accuracy of the maximum residual stress result for the DP2-S2 position. At this position the maximum residual stress is shown as being substantially smaller than that for either of the other two directions. The graph of the

relieved stress versus hole depth also showed irregular maximum residual stress magnitudes between a depth of 0.27 and 0.74 mm. This lower as well as irregular maximum stress result could be as a result of the material not being homogeneous in nature. It is the view of the author that this result should have shown a higher maximum stress magnitude, perhaps in the region of 140 MPa or higher (this value was estimated from the 42% range in maximum residual stresses as found between DP3-R2, DP3-S2 and DP3-T2.). This however could not be verified, as only one sample was available for analyses.

It can be seen that the maximum principal residual stress results obtained for the position 3 locations are contradictory to those expected. A stamping operation makes use of tensile forces to bring about deformation, thereby usually inducing tensile residual stress into the component. Position 3 is on the outer apex of the hat radius, the predicted tensile surface, but the residual stresses are compressive in nature and not tensile as expected. This could not be due to error as all three analyses revealed compressive maximum residual stresses. These results however serve to illustrate that even though tensile forces were imparted on the component to bring about forming it cannot be automatically assumed that the induced residual stresses would be tensile in nature.

All principal angle results revealed that the minimum principal stress was acting through the centre of the disc. There has therefore been a shift of 90°, at all positions, in the principal stress axes from that existing in the 1st stage pressing.

1.4 Results of the Residual Stress Analysis of the Third Stage Pressing [DP3]

1.4.1 Third stage pressing - residual stress results for position 1 holes

Residual stress analyses of the 3rd stage position 1 holes was undertaken using standard EA-06-031RE-120 rosettes, applied in an orientation corresponding to the 3,8,5 grid positions.

Position of the Hole	031RE Rosette Orientation	Maximum Principal Residual Stress [MPa]	Minimum Principal Residual Stress [MPa]	Principal Angle to max. stress	Full Relief Depth [mm]
DP3-R1	3,8,5	265.8	93.8	97.4°	1
DP3-S1	3,8,5	155.1	90.3	90.6°	0.87
DP3-T1	3,8,5	178	66.8	83.4°	0.87
Average	-	199.6	83.6	90.5°	-

Table 8. - Results of the residual stress analysis for position 1 holes of the 3rd stage pressing. [Principal angle referenced from the 8-grid number 1 position, clockwise positive.]

Table 8 shows the results of the residual stress analyses in position 1 of the 3rd stage pressing. From the 2nd to 3rd stage pressings it was found that position 1 underwent a relatively small change in maximum residual stress, this was to be expected as no change in form occurred in this region of the centre disc.

1.4.2 Third stage pressing - residual stress results for position 2 holes

These residual stress measurements were taken using the customised 8-grid rosette. From these analyses the highest average of the three directions maximum principal stress was found by the grid combination 3,8,5.

Position of the Hole	Maximum Stress Grid Combination	Maximum Principal Residual Stress [MPa]	Minimum Principal Residual Stress [MPa]	Principal Angle to max. stress	Full Relief Depth [mm]
DP3-R2	1,6,3	113.6	75.3	102.9°	1.63
DP3-S2	4,1,6	152.5	51.6	87.3°	1.81
DP3-T2	1,6,3	109.3	54.7	89°	1.81
Average	-	125.1	60.5	93.1°	-

Table 9. - Results of the residual stress analysis for position 2 holes of the 3rd stage pressing. [Principal angle referenced from the 8-grid number 1 position, clockwise positive.]

Table 9 shows the results of the residual stress analyses in position 2 of the 3rd stage pressing. From the 2nd to 3rd stage pressings it was found that even though no change in

form occurred in the position 2 region of the centre disc, the maximum residual stress did however change. The maximum residual stress in the rolling and transverse directions decreased by 72.4 MPa and 129.7 MPa respectively. The 45° direction on the other hand was shown to have experienced an increase of 39.3 MPa, but as already stated the author is of the opinion that the maximum residual stress result for DP2-S2 was too low. Therefore it can be assumed that the forming of the flanges in the 3rd stage has resulted in a stress relief at position 2.

1.4.3 Third stage pressing - residual stress results for position 3 holes

These residual stress measurements were taken using the customised 8-grid rosette. From these analyses the highest average of the three directions maximum principal stress was found by the grid combination 8,5,2.

Position of the Hole	Maximum Stress Grid Combination	Maximum Principal Residual Stress [MPa]	Minimum Principal Residual Stress [MPa]	Principal Angle to max. stress	Full Relief Depth [mm]
DP3-R3	4,1,6	406.4	40.3	93.4°	1.63
DP3-S3	8,5,2	363.5	13	88.7°	1.81
DP3-T3	8,5,2	468.7	-14.2	89.3°	1.63
Average	-	412.9	13	90.5°	-

Table 10. - Results of the residual stress analysis for position 3 hole of the 3rd stage pressing. [Principal angle referenced from the 8-grid number 1 position, clockwise positive.]

1.4.4 Discussion of residual stress results for the third stage pressing

The results of the residual stress analyses of this stage displayed good repeatability. From the 2nd to 3rd stages the only change in form occurred where the inner and outer flanges present in the previous stage were curled over, with no change in form occurred at the residual stress analyses positions. The residual stress magnitudes were however altered. From the 2nd to 3rd stage pressings it was found that even though no change in form occurred

in the position 2 region of the centre disc, the maximum residual stress did however change. The maximum residual stress in the position 2 hole locations of the rolling and transverse directions decreased by 72.4 MPa and 129.7 MPa respectively. The 45° direction on the other hand was shown to have experienced an increase of 39.3 MPa, but as already stated the author is of the opinion that the maximum residual stress result for DP2-S2 was too low. Therefore it can be assumed that the forming of the flanges in the 3rd stage has resulted in a stress relief at position 2.

Immediately noticeable is the fact that there has been a major change in the maximum residual stresses in each direction of the position 3 hole locations. Whereas in the 2nd stage pressing where the maximum residual stress was compressive this has changed to a tensile maximum residual stress of an even higher magnitude. The total change in stress being 703.3 MPa, 629.3 MPa and 733.6 MPa for the rolling, 45° and transverse directions respectively. Since there was no change in shape or plate thickness in the region of the position 3 analyses, it can only be concluded that the forming of the adjacent outer flange was the cause of the change in maximum residual stress.

The changes in the maximum residual stress between stages 2 to 3 demonstrate that even though no change in form occurred at the measurement positions, the changes in form that occurred elsewhere did have an effect on the residual stress state of the entire component, i.e. the forming of the inner and outer flanges. This is because of the dish shape of the component, which allows less springback to take place. This energy is locked in thereby inducing a 'springback load', which alters the residual stresses throughout the component. This was proved where residual stress measurements were taken on fatigue samples machined from the centre discs and a decrease in the maximum residual stress was revealed because of the release of the 'shape or springback load'. All principal angle results revealed

that the minimum principal stress was acting through the centre of the disc. There has therefore been no change in the principal angles from that as found in the 2nd stage pressing.

1.5 Results of the Residual Stress Analysis of the Fourth Stage Pressing [DP4]

1.5.1 Fourth stage pressing - residual stress results for position 1 holes

Residual stress analyses of the 4th stage position 1 holes was undertaken using standard EA-.06-031RE-120 rosettes, applied in an orientation corresponding to the 3,8,5 grid positions. The selection of these gauges and their orientation was discussed in Chapter 5 Section 5.2.1.1. Table 11 shows the results of the residual stress analyses in position 1 of the 4th stage pressing.

Position of the Hole	031RE Rosette Orientation	Maximum Principal Residual Stress [MPa]	Minimum Principal Residual Stress [MPa]	Principal Angle to max. stress	Full Relief Depth [mm]
DP4-R1	3,8,5	307.4	62.4	93.7°	0.87
DP4-S1	3,8,5	305.8	94.5	84.4°	0.74
DP4-T1	3,8,5	300	75	90°	1
Average	-	304.4	77.3	89.4°	-

Table 11. - Results of the residual stress analysis for position 1 holes of the 4th stage pressing. [Principal angle referenced from the 8-grid number 1 position, clockwise positive.]

Since no deformations has taken place during the 4th stage the change in residual stress magnitudes could have only been brought about by the stress field attempting to seek equilibrium as a result of the material removal during the punching of the vent holes.

1.5.2 Fourth stage pressing - residual stress results for position 2 holes

These residual stress measurements were taken using the customised 8-grid rosette. From these analyses the highest average of the three directions maximum principal stress was found by the grid combination 3,8,5.

Position of the Hole	Maximum Stress Grid Combination	Maximum Principal Residual Stress [MPa]	Minimum Principal Residual Stress [MPa]	Principal Angle to max. stress	Full Relief Depth [mm]
DP4-R2	1,6,3	188.6	150.2	88.2°	2
DP4-S2	5,2,7	144.3	73.5	87.2°	1.81
DP4-T2	2,7,4	156.4	54.2	82.8°	1.81
Average	-	163.1	92.6	86.1°	-

Table 12. - Results of the residual stress analysis for the position 2 holes of the 4th stage pressing. [Principal angle referenced from the 8-grid number 1 position, clockwise positive.]

Table 12 shows the results of the residual stress analyses in position 2 of the 4th stage pressing. Since no deformations has taken place during the 4th stage the change in residual stress magnitudes could have only been brought about by the stress field attempting to seek equilibrium as a result of the material removal during the punching of the vent holes.

1.5.3 Fourth stage pressing - residual stress results for position 3 holes

Residual stress analyses of the 4th stage position 3 holes was undertaken using standard EA-06-062RE-120 rosettes, applied in an orientation corresponding to the 8,5,2 grid positions. The grid combination 8,5,2 was chosen because in the previous stage it revealed the highest average maximum residual stress result from the three directions. Table 13 shows the results of the residual stress analyses in position 3 of the 4th stage pressing.

Position of the Hole	062RE Rosette Orientation	Maximum Principal Residual Stress [MPa]	Minimum Principal Residual Stress [MPa]	Principal Angle to max. stress	Full Relief Depth [mm]
DP4-R3	8,5,2	210.5	24	87.6°	1.63
DP4-S3	8,5,2	275.5	-9.1	96.2°	1.63
DP4-T3	8,5,2	266.4	-2.5	87.8°	1.46
Average	-	250.8	4.1	90.5°	-

Table 13. - Results of the residual stress analysis for position 3 holes of the 4th stage pressing. [Principal angle referenced from the 8-grid number 1 position, clockwise positive.]

1.5.4 Discussion of residual stress results for the fourth stage pressing

The 4th stage is not a stamping process as such since only the punching of the vent holes on the outer periphery of the hat radius is affected. As shown by the results this removal of material does however influence the residual stress field of the entire component. This further illustrates the fact that because of the dished shape of the centre disc, a certain amount of the residual stress present is as a result of the shape of the component not allowing springback to occur fully. It was found that at the cup and mid positions (positions 1 and 2) the maximum residual stress increased, but at the hat apex (position 3) there was a decrease in the maximum residual stress. It was the opinion of the author that by removal of the material for the vent holes the load placed on the central region of the component by the shape of the outer flange had altered, thereby causing the residual stress field , within this central region, to alter as a new equilibrium is achieved. All principal angle results revealed that the minimum principal stress was acting through the centre of the disc. There has therefore been no change in the principal angles from that as found in the 3rd stage pressing.

1.6 Results of the Residual Stress Analysis of the Assembled Wheel [DPW]

It was felt that the residual stress at position 2 could be estimated if necessary from the position 1 and 3 results, therefore position 2 would not be analysed for the final two stages. This allowed for the use of the 8-grid gauge at positions 1 in the final two stages. The use of this gauge would then verify whether the choice of the 3,8,5 grid combination used previously for positions 1 was in fact correct or not.

1.6.1 Assembled wheel - residual stress results for position 1 holes

These residual stress measurements were taken using the customised 8-grid rosette. From these analyses the highest average of the three directions maximum principal stress was found by the grid combination 3,8,5.

Position of the Hole	Maximum Stress Grid Combination	Maximum Principal Residual Stress [MPa]	Minimum Principal Residual Stress [MPa]	Principal Angle to max. stress	Full Relief Depth [mm]
DPW-R1	1,6,3	346.8	128.8	77°	2
DPW-S1	4,1,6	381.7	77.6	96°	2
DPW-T1	3,8,5	298.3	140.2	91.7°	1.81
Average	-	342.3	115.5	88.2°	-

Table 14. - Results of the residual stress analysis for holes in position 1 of assembled wheel. [Principal angle referenced from the 8-grid number 1 position, clockwise positive.]

1.6.2 Assembled wheel - residual stress results for position 3 holes

Residual stress analyses of the assembled wheel at position 3 holes was undertaken using standard EA-06-062RE-120 rosettes, applied in an orientation corresponding to the 8,5,2 grid positions. Table 15 shows the results of the residual stress analyses in position 3 of the assembled wheel.

Position of the Hole	062RE Rosette Orientation	Maximum Principal Residual Stress [MPa]	Minimum Principal Residual Stress [MPa]	Principal Angle to max. stress	Full Relief Depth [mm]
DPW-R3	8,5,2	279.1	86.3	111.5°	1.81
DPW-S3	8,5,2	290.2	1.53	107°	1.3
DPW-T3	8,5,2	273.7	-87.7	96.9°	1.81
Average	-	281	0	105.1°	-

Table 15. - Results of the residual stress analysis for holes in position 3 of assembled wheel. [Principal angle referenced from the 8-grid number 1 position, clockwise positive.]

1.6.3 Discussion of residual stress results for the assembled wheel

The centre disc is inserted into the rim with a press-fit and welded in place. From the results above it was found that this assembly process resulted in an increase in the maximum residual stress. The principal angles revealed indicate that the minimum residual stress can be assumed to act approximately through the centre of the component (within 15°). This is

approximately the same as found in the previous stage. The choice of the 3,8,5 grid combination, selected for the application of the standard three-grid rosettes used in the previous stages for residual stress analyses at positions 1, was shown to have been correct.

1.7 Results of the Residual Stress Analysis of the Assembled and Painted Wheel [DPC]

1.7.1 Completed wheel - residual stress results for position 1 holes

These residual stress measurements were taken using the customised 8-grid rosette. From these analyses the highest average of the three directions maximum principal stress was found by the grid combination 4,1,6 (closely followed by the 3,8,5 combination). Table 16 shows the results of the residual stress analyses in position 1 of the assembled and painted wheel.

Position of the Hole	Maximum Stress Grid Combination	Maximum Principal Residual Stress [MPa]	Minimum Principal Residual Stress [MPa]	Principal Angle to max. stress	Full Relief Depth [mm]
DPC-R1	2,7,4	415.6	142.3	108.3°	1.46
DPC-S1	4,1,6	384.1	158.1	98°	1.81
DPC-T1	4,1,6	217.2	156.5	88.2°	1.63
Average	-	339	152.3	98.2°	-

Table 16. - Results of the residual stress analysis for holes in position 1 of completed wheel. [Principal angle referenced from the 8-grid number 1 position, clockwise positive.]

1.7.2 Completed wheel - residual stress results for position 3 holes

Residual stress analyses of the assembled wheel at position 3 holes was undertaken using standard EA-06-062RE-120 rosettes, applied in an orientation corresponding to the 8,5,2 grid positions. Table 17 shows the results of the residual stress analyses in position 3 of the assembled wheel.

Position of the Hole	062RE Rosette Orientation	Maximum Principal Residual Stress [MPa]	Minimum Principal Residual Stress [MPa]	Principal Angle to max. stress	Full Relief Depth [mm]
DPC-R3	8,5,2	227.1	28.4	86°	1.81
DPC-S3	8,5,2	254.3	-65	101°	1.63
DPC-T3	8,5,2	205.9	-41.7	96.2°	1.14
Average	-	229.1	-26.1	94.4°	-

Table 17. - Results of the residual stress analysis for holes in position 3 of completed wheel. [Principal angle referenced from the 8-grid number 1 position, clockwise positive.]

1.7.3 Discussion of residual stress results for the completed wheel

During this final stage in the manufacture of the wheel no forming operation has occurred. The assembled wheel has however undergone a heat treatment operation, which as we know has an influence on the residual stresses within the component. This was borne out by the results of the residual stress analyses carried out on the completed wheel, where a change in residual stress magnitudes was observed. The wheel is baked at a temperature of around 190°C, which results in the further transformation of martensite from austenite[G1]. This transformation causes a slight volume expansion, which results in certain residual stresses being induced. This makes the prior prediction of the residual stress change difficult. It was however shown that at position 3 the maximum residual stresses decreased, while at position 1 they increased. It must be stated that it was felt that the maximum residual stress result obtained for position DPC-T1 was too low in magnitude. A magnitude of 320 MPa or higher was felt to be the more expected result. The lower result could be the result of the effect of the non-homogeneous material.

The principal angles revealed show that from the 2nd stage up to the completed wheel the minimum residual stress acts through the centre of the wheel or centre disc.

1.8 Change in Residual stresses

The residual stress magnitudes and changes from stage to stage for each analysis position can be more clearly depicted by means of graphs. These graphs show for each location the relieved principal residual stresses at each production stage.

1.8.1 Principal residual stresses for position 1 hole locations

When viewing the above graphs of the principal residual stress versus production stages it can be seen that the results in each direction for positions 1 follow a similar trend to one another. However it was the opinion of the author that DPC-T1 should not have experienced a decrease in maximum residual stress, but rather should be equal to or greater that the previous stage DPW-T1.

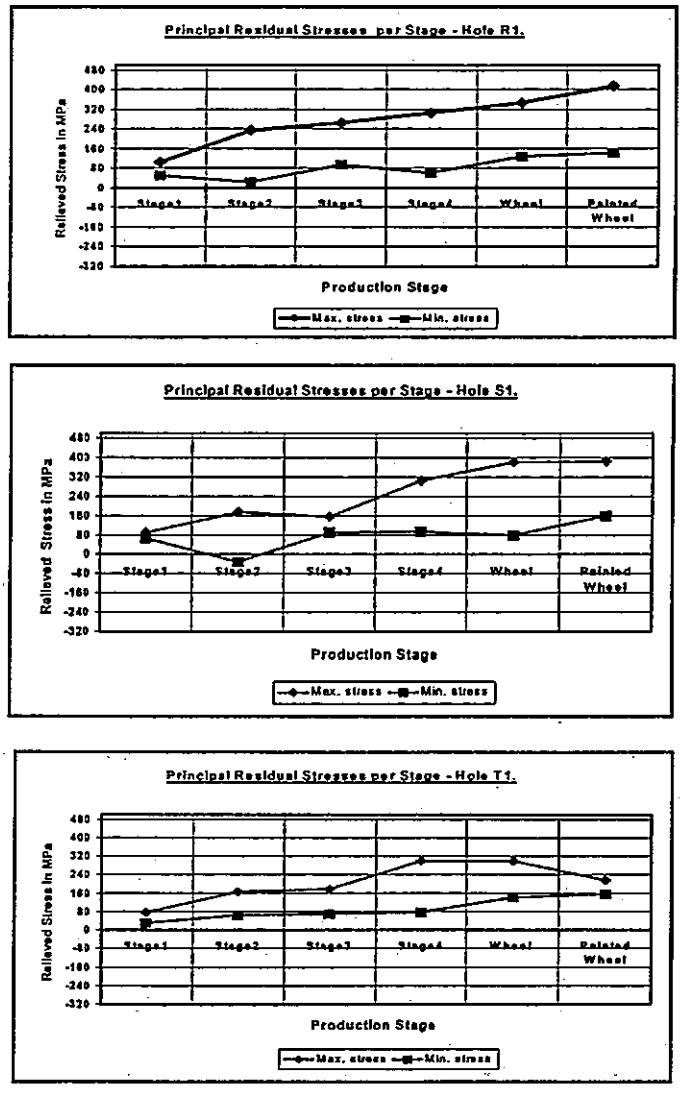

Figure 1. - Principal residual stresses at each production stage for position 1 holes.

APPENDIX - G

1.8.2 Principal residual stresses for position 2 hole locations

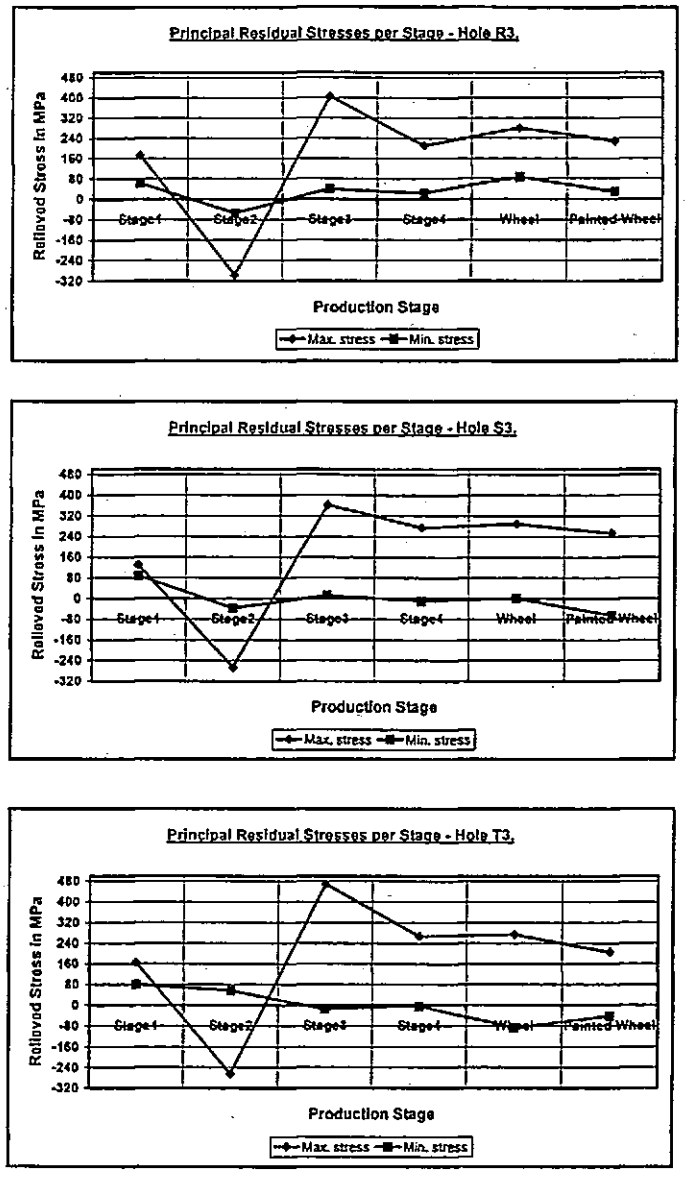

Figure 2. - Principal residual stresses at each production stage for position 2 holes.

At position 2 the maximum residual stress in position DP2-S2 decreased from DP1-S2 whereas DP2-R2 and DP2-T2 increased from the previous stage. It has however been stated that it was felt that the DP2-S2 maximum residual stress result was too low. An envisaged higher result would have resembled the rolling and transverse directions more closely.

1.8.3 Principal residual stresses for position 3 hole locations

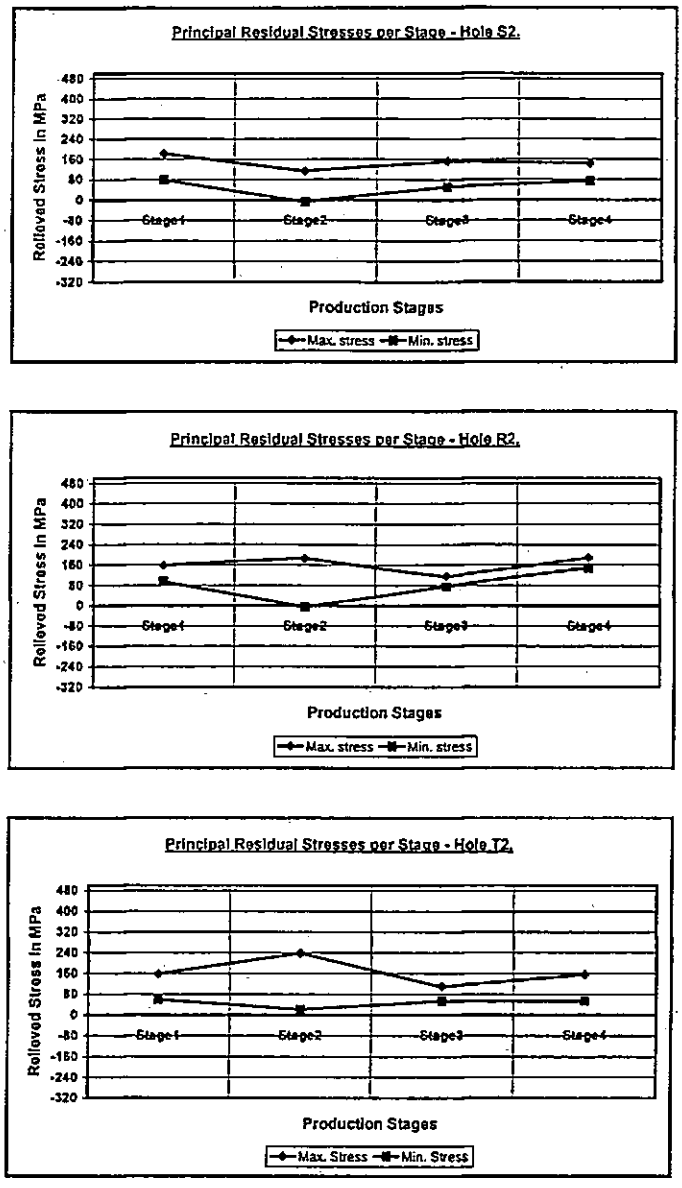

Figure 3. - Principal residual stresses at each production stage for position 3 holes.

The above graphs of the principal residual stress versus production stages show that the results in each direction for positions 3 follow a similar trend to one another.

2. Hardness Results

Surface hardness measurements were taken in order to determine an estimated yield strength of the material at each residual stress location. As stated by the ASTM 837-94a standard, residual stresses of a magnitude greater than 80% of the yield strength are not valid because

of local yielding that would take place around the drilled hole. If the residual stress result exceeds the 80% yield strength value it must be assumed that the residual stress is at that value. The hardness values will also be compared to the residual stress data already obtained to determine any relationship between the two. Microhardness profiles of certain residual stress locations will also be undertaken in order to determine any changes in hardness throughout the cross-section.

2.1 Surface Hardnesses

Surface hardnesses were taken using the Brinell scale, with a 2 millimetre diameter ball indenter and 120 kilogram load. An average surface hardness was determined from four hardness readings, which were taken at a distance of 5 millimetres around the periphery of the hole drilled during the residual stress analyses.

2.1.1 Brinell surface hardness for position 1 locations

Results of the hardness analyses for the position 1 locations throughout the various production stages is shown in Table 18 and Figure 4 below.

Location	DPP	DP1	DP2	DP3	DP4	DPW	DPC
R1	189	193	203	212	209	210	221
S1	189	194	203	216	212	211	222
T1	189	195	205	218	214	215	227
Average	189	194	204	215	212	212	223

Table 18. - Brinell surface hardnesses for position 1 locations for each production stage.

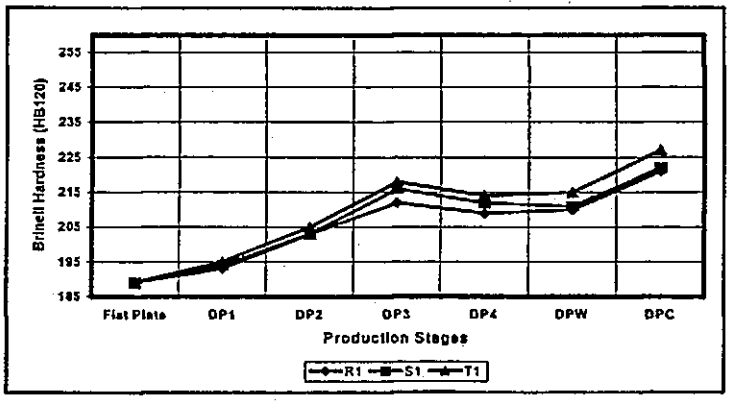

Figure 4. - Graph showing the surface hardness for position 1 locations for each production stage.

2.1.2 Brinell surface hardness for position 2 locations

Results of the hardness analyses for the position 2 locations throughout the various production stages is shown in Table 19 and Figure 5 below. Since no residual stress analyses were carried out in the position 2 locations on the DPW and DPC stages, hardness measurements were neglected at these locations for the final two stages.

Location	DPP	DP1	DP2	DP3	DP4
R2	189	196	211	222	217
S2	189	197	212	228	220
T2	189	195	214	229	219
Average	189	196	212	226	219

Table 19. - Brinell surface hardnesses for position 2 locations for each production stage.

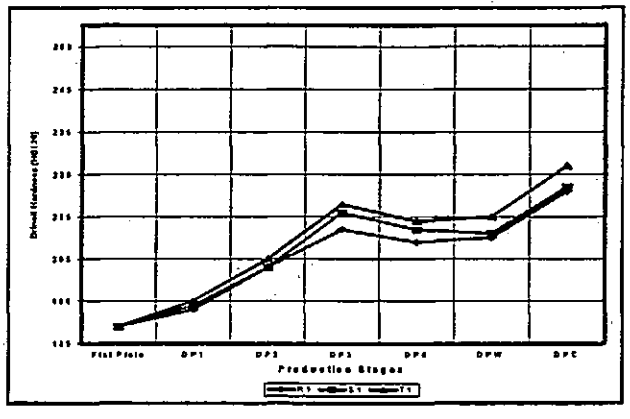

Figure 5. - Graph showing the surface hardness for position 2 locations for each production stage.

2.1.3 Brinell surface hardness at position 3 locations

Results of the hardness analyses for the position 2 locations throughout the various production stages is shown in Table 20 and Figure 6 below.

Location	DPP	DP1	DP2	DP3	DP4	DPW	DPC
R3	189	191	226	220	225	224	237
S3	189	195	229	227	239	232	239
T3	189	191	227	222	228	229	239
Average	189	192	227	223	231	228	238

Table 20. - Brinell surface hardnesses for position 3 locations for each production stage.

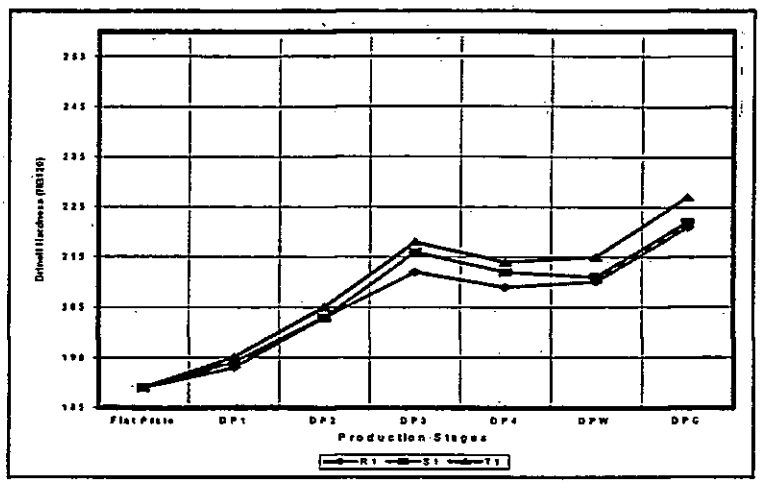

Figure 6. - Graph showing the surface hardness for position 2 locations for each production stage.

2.1.4 Discussion of hardness results

It was not possible to take hardness measurements on the centre disc stages in their manufactured form, therefore the discs had to be sectioned leaving sufficient area for hardness measurements to be taken according to the SABS 055-1977 standard. As already stated the shape of the centre disc locks in a certain amount of stress, which is relieved to some degree when the discs were sectioned for hardness analyses. The exact amount of stress relief at each position could not be determined due to a shortage of components available for analyses. The residual stress trend should however remain similar for corresponding stages to stages after sectioning, i.e. if the residual stress increased during forming from one stage to the next at a certain position a similar trend should be found in the sectioned samples from the two stages. Now according to Sines and Carlson[G2] when sheet metal plate is placed under a load still within the materials elastic range, therefore simulating a residual stress, the hardness of plate changes. They found that the hardness of rolled 0.2% carbon steel increased by 2% to a maximum when the plate is in compression, and decreases to a minimum when in tension by 11% at the elastic limit. After the elastic limit is passed the material naturally increases in hardness because of work hardening. The residual stresses should therefore have the same effect on the hardness. The residual stress variation between stages has already been determined at each position and should therefore

APPENDIX - G

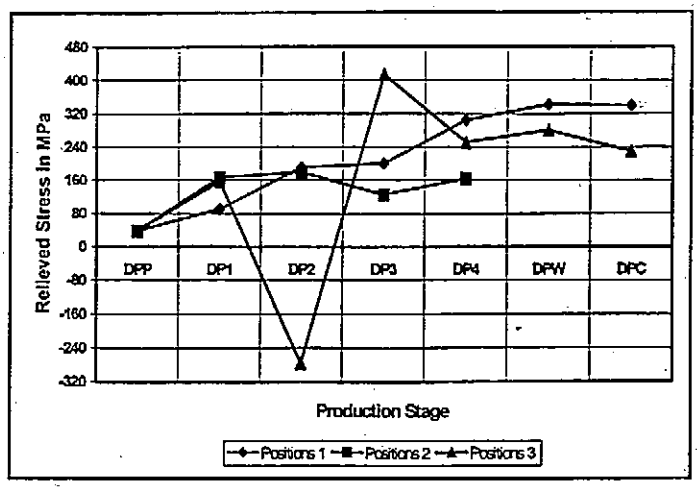

Figure 7. - Graph of the average of the three directions maximum residual stress per stage and hole position.

also be considered when evaluating the hardness changes. This effect could explain the softening that has taken place at particular positions between certain stages.

The change in hardness is because of the combined effects of the plastic deformation that has taken place and the residual stresses induced. Figure 7 shows a graph of the average of the three directions maximum residual stress per stage at each location. When comparing the graph in Figure 7 to the hardness results it was noticed that where the plastic deformation was pronounced as in stages DP1 and DP2 the residual stress showed less effect.

In stage DP3 where relatively less deformation occurred at the position 3 locations the effect of the residual stresses was more evident. At these positions the residual stress changed from a high compressive to a high tensile nature causing a softening effect of approximately 1.8 %. The same can be said of DP4 position 1 and 2 locations where the increase in tensile residual stress resulted in a softening of the steel by 1.4 % and 3.1 % respectively. The increase in hardness in the final stage DPC was brought about as a result of the bake hardenability characteristic of the dual phase steel. The paint curing of the wheel is attained by baking at a temperature of around 190°C, which results in the further transformation of

martensite from austenite[G1]. The resulting martensite is harder than the previously present austenite, therefore raising the hardness. The decrease in hardness also corresponds to the decrease in tensile residual stress revealed in stage DPC.

2.2 Approximate Yield Strength

As previously stated the hardness values of the dual phase steel at the various analyses locations are to be used to estimate the yield strength of the material at each location. This will allow for the verification of the fact that the maximum residual stress result at each location is within 80 % of yield stress magnitude as reported by Schajer[G3]. For each residual stress analysis location the hardness value of that location was used to estimate the ultimate tensile strength. This was done according to the table C-1 of the SABS 055-1977 standard, pp 42 – 43. The UTS was then divided by 1.555 to obtain an estimated yield stress magnitude.

2.2.1 Approximate Ultimate Tensile Strengths per Location and Production Stage

From the Table C-1 for the conversion of hardness to tensile strength in the SABS 055-1977 standard the ultimate tensile strengths for each location were found and are tabulated below.

Approximate Ultimate Tensile Strength (MPa)							
Location	DPP	**DP1**	**DP2**	**DP3**	**DP4**	**DPW**	**DPC**
R1	656	672	708	742	730	734	770
S1	656	676	708	755	742	738	774
T1	656	680	713	761	750	754	793
R2	656	684	738	774	758	-	-
S2	656	688	742	797	766	-	-
T2	656	680	750	800	764	-	-
R3	656	664	790	766	786	782	830
S3	656	680	801	794	834	808	834
T3	656	664	793	774	797	800	834

Table 21. - Approximate ultimate tensile strengths of residual stress analyses locations.

If we were to display these results in a graph of UTS versus production stage the graphs would follow the same trend as displayed by the hardness versus production stage graphs.

2.2.2 Approximate Yield Strengths per Location and Production Stage

The UTS values were divided by the 1.555 constant for estimating the yield strength for this particular dual phase material. It was the opinion of the author that this approximation would be accurate enough for the checking of the maximum residual stress values already calculated. The approximated yield strengths are shown in Table 22.

Approximate Yield Strength (MPa)							
Location	**DPP**	**DP1**	**DP2**	**DP3**	**DP4**	**DPW**	**DPC**
R1	422	432	455	477	470	472	495
S1	422	435	455	486	477	474	498
T1	422	437	459	489	482	484	510
R2	422	440	475	498	488	-	-
S2	422	442	477	513	493	-	-
T2	422	437	482	514	491	-	-
R3	422	427	508	493	506	503	534
S3	422	437	515	511	536	520	536
T3	422	427	510	498	513	515	536

Table 22. - Approximate yield strengths of residual stress analyses locations.

These approximated yield strength values can now be related to the maximum residual stress magnitude for each analysis location and each production stage and should be below the required 80 % of the yield stress value as stated by the standard.

2.3 Verification of Maximum Residual Stresses from Yield Strength Values

The 80 % of yield stress values for each location calculated as stated above can be plotted against its corresponding maximum residual stress magnitude for each production stage. This will then indicate whether the maximum residual stress result is within the allowable 80% yield stress limit.

The residual stress and the 80 % yield stress values for positions 1, 2 and 3 will be plotted in Figures 8, 9 and 10 on the same y-axis and is merely indicated as stress.

2.3.1 Verification of Maximum Residual Stress Magnitudes for Position 1

Figure 8 shows that for the completed wheel the maximum residual stress exceeded the 80 % yield stress limit of 396 MPa. The residual stress at DPC-R1 should therefore be taken as the 80 % yield stress value. All the remaining maximum residual stress analyses for position R1 are within the accepted 80% yield stress limit. The maximum residual stress at location DPW-S1 exceeded the 80 % yield stress limit by only 1.7 MPa, it can therefore still be accepted. All the other maximum residual stress values for position S1 are shown to be within the acceptable 80 % yield stress limit.

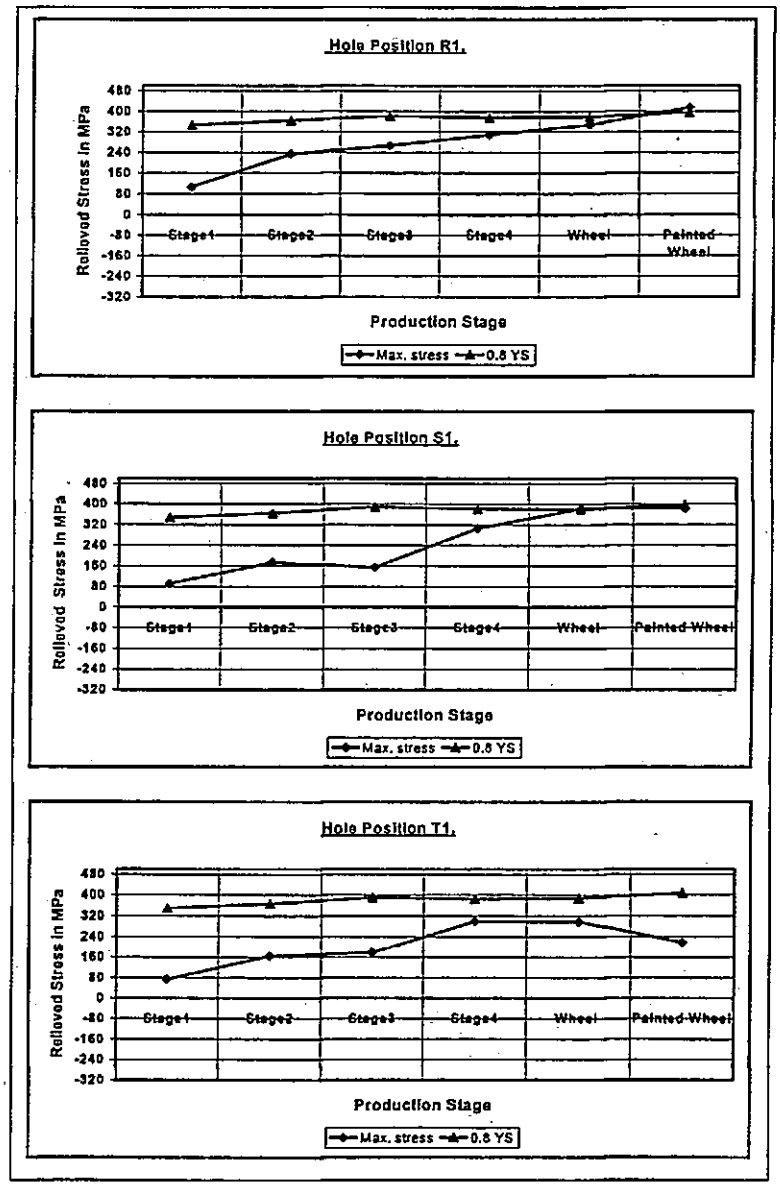

Figure 8. - Maximum residual stress and 80% yield stress magnitudes for position I holes per production stage. [0.8 YS = 80% yield stress].

All of the maximum residual stress values for position T1 are shown to be well within the acceptable 80 % yield stress limit.

2.3.2 Verification of Maximum Residual Stress Magnitudes for Position 2

As shown by Figure 9 all of the maximum residual stress analyses for positions R2, S2 and T2 are well within the acceptable 80 % yield stress limit.

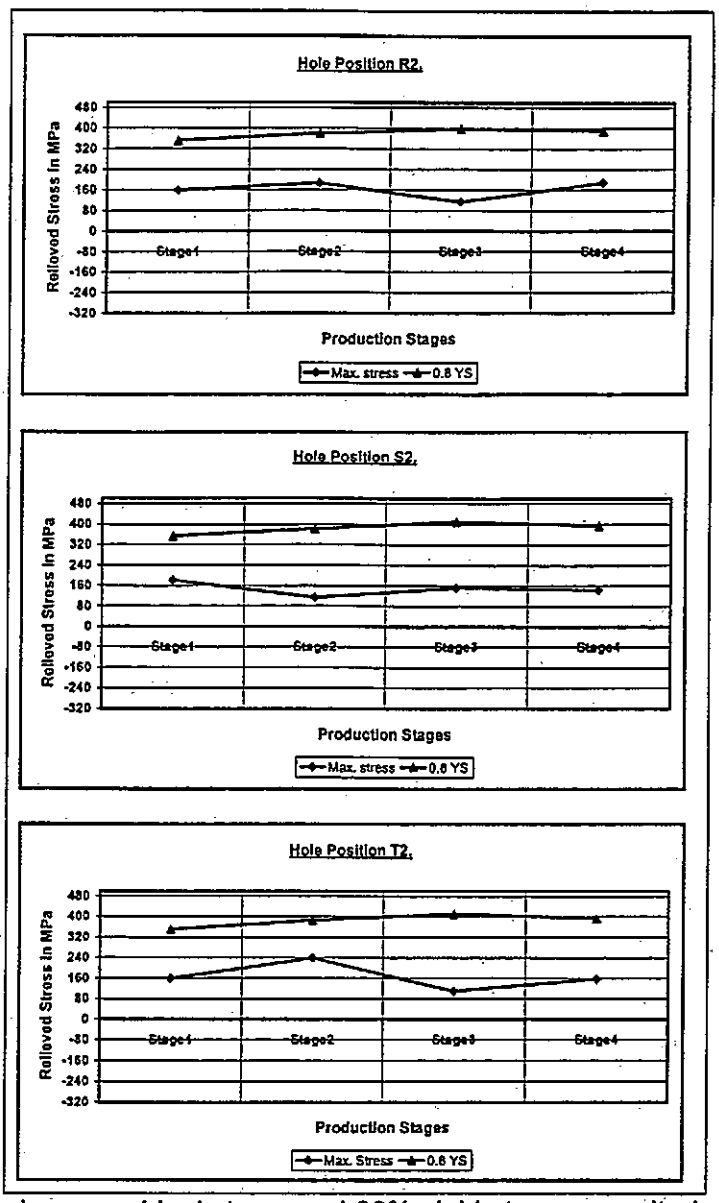

Figure 9. - Maximum residual stress and 80% yield stress magnitudes for position 2 holes per production stage. [0.8 YS = 80% yield stress].

2.3.3 Verification of Maximum Residual Stress Magnitudes for Position 3

From Figure 10, it can be seen that the maximum residual stress at position DP3-R3 exceeded the 80 % yield stress limit by approximately 12.4 MPa. The maximum residual

stress at that position should therefore be assumed to be at the 80 % yield stress magnitude of 395 MPa. All the remaining maximum residual stress analyses for position R3 are indicated to be within the acceptable 80 % yield stress limit. The maximum residual stress values for position S3 are shown to be within the acceptable 80% yield stress limit.

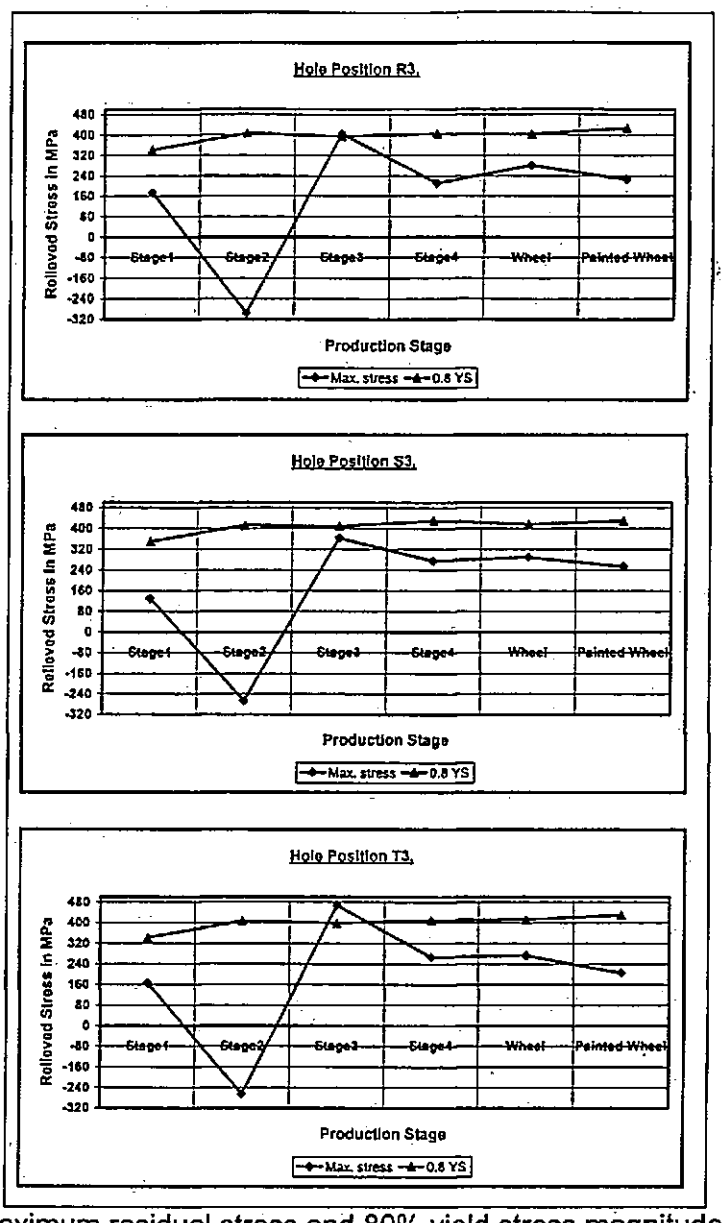

Figure 10. - Maximum residual stress and 80% yield stress magnitudes for position 3 holes per production stage. [0.8 YS = 80% yield stress].

The maximum residual stress at position DP3-T3 exceeded the 80 % yield stress limit by 70.7 MPa. The maximum residual stress at that position should therefore be assumed to be at the 80 % yield stress magnitude. All the other maximum residual stress values for position T3 are shown to be within the acceptable 80 % yield stress limit.

2.4 Analysis of Microhardness

Microhardnesses were taken of selected holes to assess changes in hardness with depth. This would indicate whether the yield strengths, which were previously estimated from the surface hardness values are in fact valid.

2.4.1 Selected Hole Locations for Microhardness Analysis

The position 3 holes from the 1st, 2nd and 3rd stage pressings were selected as the locations for assessing the hardness distributions. These positions were chosen as a result of the large differences in residual stress magnitudes regarding each stage. For each stage however, the residual stress magnitudes are similar in each direction. Table 23 below shows the residual stress magnitude for the selected hole locations.

Hole Location	Production Stage		
	DP1	DP2	DP3
R3	173.3	-296.9	394
S3	130.3	-265.7	363.5
T3	166.1	-264.9	398

Table 23. - Maximum principal residual stresses [MPa] occurring at the microhardness analysis locations.

2.4.2 Position of Microhardness Analyses

After the residual stress measurements were completed for these selected locations, the hole was sectioned and microhardness assessments were taken at a distance of 0.5 mm from the edge of the hole wall. The drilling operation would effect the hardness along the hole wall, but it was felt that the drilling effects are negligible at the distance of 0.5 mm from the edge of the hole wall. Ten microhardness readings were recorded at either side of the hole wall at incremental depths of 0.2 mm, with the surface taken as zero. The average value of the two corresponding depths was then recorded. Figure 11 shows the microhardness analyses positions.

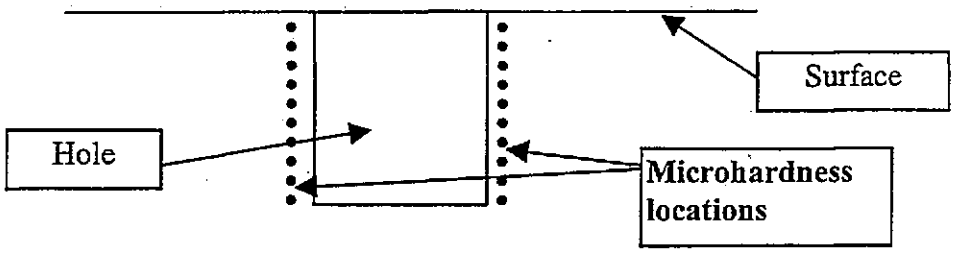

Figure 11. - Sketch of microhardness analysis locations alongside the hole wall.

2.4.3 Microhardness Distribution

As previously mentioned the microhardness values make use of the Vickers scale, however the surface hardness values were taken using the Brinell scale. Therefore for comparison purposes the microhardness values determined were converted to the Brinell scale by means of table C-1, SABS 055-1977.

2.4.3.1 Microhardness Distribution of DP1

For DP1 the hardness distributions in the locations R3, S3 and T3 all revealed similar values. The hardnesses did not vary much throughout the profile, as shown by Figure 12. Table 24 showing the average of all the microhardness values throughout the profile and the corresponding surface hardness values, indicates that the surface hardness is slightly higher in each location. The hardness values taken within 0.6 mm of the surface are however approximately equal to the hardnesses found on the surface.

Location	Surface Hardness	Average Profile Hardness
R3	191	188
S3	195	192
T3	191	188

Table 24. - Surface and average distribution Brinell hardness values for DP1.

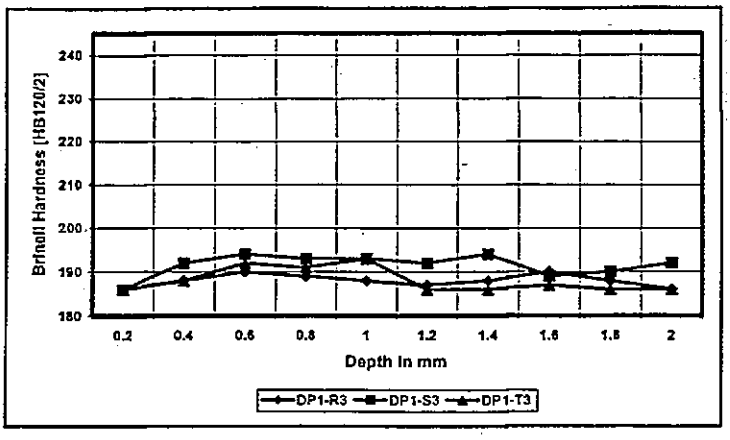

Figure 12. - Hardness distribution for position 3 hole locations from DP1.

2.4.3.2 Microhardness Distribution of DP2

For DP2 the hardness profiles in the locations R3, S3 and T3 all revealed a similar values and trends, as shown by Figure 13.

Location	Surface Hardness	Average Profile Hardness
R3	226	215
S3	229	219
T3	227	217

Table 25. - Surface and average distribution Brinell hardness values for DP2.

It can also be seen that the hardness on average decreases until the elastic core is reached at a depth of 2 mm. Table 25 shows the average of all the microhardness values throughout the profile and the corresponding surface hardness values, where it can be seen that the surface hardness is greater in each location. The hardness values taken within 0.8 mm of the surface are however approximately equal to the hardnesses found on the surface.

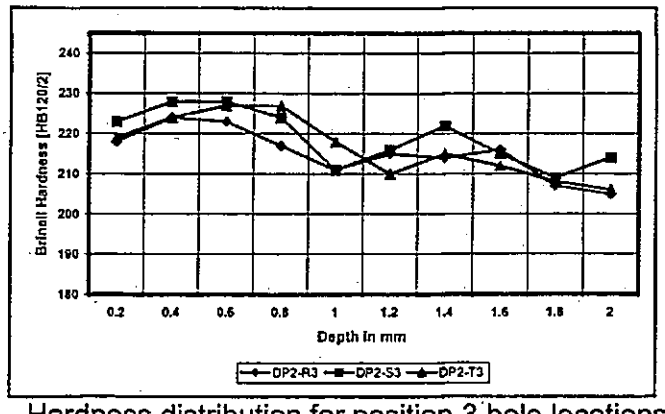

Figure 13. - Hardness distribution for position 3 hole locations from DP2.

2.4.3.3 Microhardness Distribution of DP3

For DP3 the hardness profiles in the locations R3, S3 and T3 all revealed similar values and trends, as shown by Figure 14. It can also be seen that the hardness on average decreases from a depth of 0.6 mm, with a slight increase experienced at the elastic core.

Location	Surface Hardness	Average Profile Hardness
R3	220	213
S3	227	222
T3	222	217

Table 26. - Surface and average distribution Brinell hardness values for DP3.

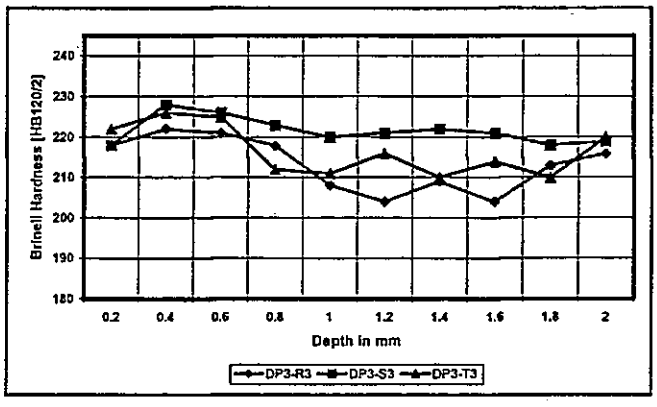

Figure 14. - Hardness distribution for position 3 hole locations from DP3.

Table 26 shows the average of all the microhardness values throughout the profile and the corresponding surface hardness values for DP3, where it can be seen that as for DP1 and DP2 the surface hardness is greater in each location. The hardness values taken within 0.6 mm of the surface are however approximately equal to the hardnesses found on the surface.

2.4.3.4 Discussion of Hardness Distributions

In all locations where hardness profiles were taken the hardness at a depth of up to 0.6 mm was shown to be similar to the surface macro hardness values, with the hardness values recorded being lower from 0.8 mm to 2 mm. This was to be expected as the forming

mechanism the component has undergone is combined bending and stretching. The outermost fibres from the neutral axis, or elastic core, will therefore undergo the most deformation, thereby resulting in a higher hardness as a result of more cold working.

It is important to note here that the maximum residual stress in fact acts at the surface. When viewing the graphs, of the relieved residual stress versus hole depth the maximum or fully relieved stress is shown at a certain depth usually from 1 mm or deeper. This relieved stress is as a result of the cumulative residual stress originally existing within that full relief depth. The residual stress however in fact acts at, or close to, the surface. Now the yield strength was estimated from the surface hardness values, which were found to be similar to a depth of 0.6 mm. It can therefore be assumed that the estimated yield strength value can be found from the surface hardness readings, even though the material will generally have a lower yield strength at depths of 0.6 mm or deeper.

The hardness profiles were expected to vary smoothly with depth decreasing in hardness to the elastic core. However the hardness did not follow a smoothly decreasing trend, but sometimes varied between successive depths. It must be remembered however that the measurement of hardness is an estimation measurement and the fact that a non-homogenous material, dual phase steel, is under investigation will result in these variations. The variations are most probably as a result of the unevenly dispersed martensite phase of the dual phase steel, which is harder than the ferrite. Therefore an analysis location could contain more martensite than ferrite thereby appearing harder, or visa versa.

References

G1. Tomoyoshi. O et.al. Production and Quality of Hot Rolled Dual Phase Steel, Nippon Kokan Technical Report, No. 43, 1985, p 25 - 32.

G2. Sines, G., and Carlson, R., Hardness Measurement for the Determination of Residual Stresses, ASTM Bulletin, February 1952, part 180, pp 35 –37.

G3. Schajer, G.S. –"*Measurement of Non-uniform Residual Stresses Using the Hole-Drilling Method. Part I – Stress Calculation Procedures*", Journal of Engineering Materials and Technology, 1, (110), 1988, pp. 335 – 343.

APPENDIX - H

PAPER REFERENCE: "3C.98"

EFFECTS OF FORMING PROCESS ON FATIGUE PERFORMANCE OF WHEEL CENTRE DISCS

P.J. M^{c} Grath [1], D.G. Hattingh [2], M.N. James [3] and A. Els-Botes [4]

[1,2 & 4] Department of Mechanical Engineering, Port Elizabeth Technikon, Private Bag X6001, Port Elizabeth, South Africa

[3] Department of Mechanical and Marine Engineering, University of Plymouth, Drake Circus, Plymouth, Devon PL4 8AA, UK

ABSTRACT

This paper considers the effects of sheet metal forming processes on the fatigue performance of automotive wheel centre discs, manufactured from dual phase steel. Characteristics of the fatigue process for such components are crack initiation in a highly strained area, and reflect the forming deformation of the sheet and a loading mode that is predominantly bending.

This work utilises waisted hour-glass specimens, machined from centre discs taken from each stage of the manufacturing process. Attention is paid to the influence of the degree of cold working on fatigue performance, with particular emphasis on the interaction between surface hardness and induced residual stresses measured on the centre discs

The results indicate a correlation between the fatigue-tested wheels and laboratory specimens for producing their respective S-N curves. It can therefore be deduced that the fatigue testing of hourglass specimens machined from the production stages will have a similar relationship if these components could be fatigue tested under industrial conditions.

REFERENCES

(1) Kalpakjian, S. – *"Manufacturing Processes for Engineering Materials"*, Second Edition, Addison-Wesley, (1991).

(2) Lange, K. – "*Handbook of Metal Forming*", Second Edition, McGraw-Hill Book Company Ltd, (1985), ISBN 0 07 036285 8.

(3) Coldren, A.P. & Eldis, G.T., - J. Metals, 32 (1980) 41.

(4) Park, S.H., Ro, K.S. & Kwon, O. – *"Microstructure and Mechanical Properties of Hot Rolled High Strength Formable Steels for Automotive Wheels"*, International Symposium on Low Carbon Steels for the 90's, The Minerals, Metals & Materials Society, (1993), pp.355 – 365.

(5) Okita, T., et. Al. – *"Production and Quality of Hot Rolled Dual Phase Steel"*, Nippon Kokan Technical Report, (43), (1985), pp. 25-32.

INTRODUCTION

Sheet materials are generally characterised by a "high ratio of surface area to thickness", and the uni-axial force applied to the sheet plate during a stamping operation is mainly tensile in nature **(1)**. This applied tensile force induces residual stresses in the component that are dependent upon the shape of the component, and vary in magnitude (and sign) with position. The fact that cold working operations enhance the tensile and fatigue crack initiation strength of a material are well understood and documented **(2)** but, in terms of fatigue performance, this may be countered by the residual stresses induced during sheet metal forming operations, which achieve high tensile values. These act to increase the mean stress in fatigue cycling which will decrease fatigue strength.

Centre discs of automotive wheels are produced from sheet metal plate through a series of four cold stamping operations and a final painting and low temperature curing cycle. Centre discs relevant to a particular light passenger vehicle wheel were obtained at each stage of the wheel manufacturing process, starting with the "as-manufactured" plate. Residual stresses were measured on the discs, at each stage, in the critical crack initiation regions found from cantilever bend tests of production wheels. Hardness and microstructure were also characterised at each stage. Hourglass fatigue specimens were machined from the discs and tested in reversed bend with the same fatigue loading cycle used for the production wheels. These specimens showed decreases in fatigue life relative to the as-manufactured plate, although the trends in life did not exactly correlate with either residual stress or hardness data. The trends in fatigue life are explained in terms of the interaction between these two influences, and surface embrittlement arising from the paint bake hardening cycle.

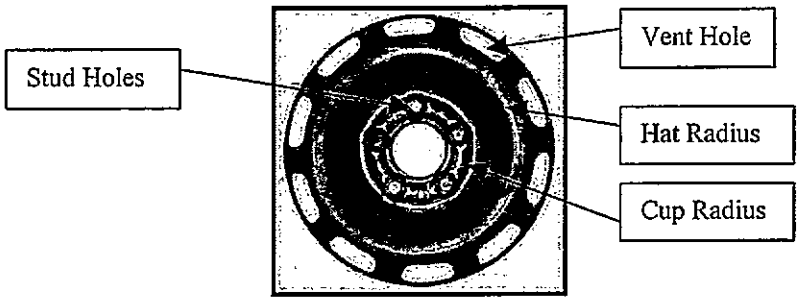

Figure 1. – Nomenclature of centre disc.

MATERIAL

In this investigation the centre discs were manufactured from Dual Phase Steel (manufacturer designation DPS600). This type of high strength low alloy (HSLA) **(3)** steel was developed during the mid-1970's and consists of ± 20% islands of martensite within a ferritic matrix and has both good drawability and formability characteristics. It is considered superior to the conventional HSLA rim steels normally used by automotive component manufacturers. The chemical composition is given in Table 1, and the mechanical properties in Table 2.

Chemical Element	C	Mn	P	S	Si	Al	Cr	Ni	Ti	Mo	Cu
&	0.05	0.50	0.01	Max	Max	0.02	Max	Max	Max	Max	Max
% Content	0.12	1.30	0.09	0.006	0.65	0.06	0.90	0.25	0.015	0.05	0.35

Table 1. – Chemical composition of DPS600.

Designation	Yield Strength (MPa)	Ultimate Tensile Strength (MPa)	% Elongation
Dual Phase Steel (DPS600)	Min. 300 Max. 470 Actual 427	Min. 550 Max. 700 Actual 662	28

Table 2. – Mechanical Properties of DPS600.

APPENDIX - H

SPECIMEN PREPARATION

Fatigue

Waisted hour-glass specimens were machined from centre discs taken from each stage of the wheel production process using a CNC milling machine (Figure 5). On completion of the machining process the specimens were assigned an identification mark, de-burred and flapper ground to remove machining marks.

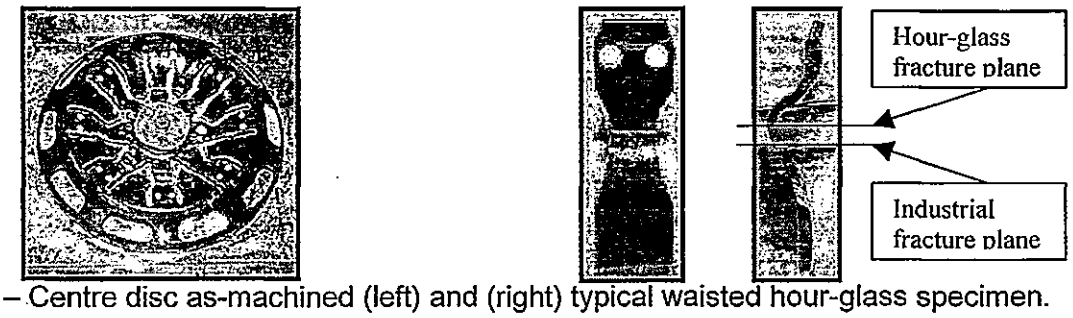

Figure 5. – Centre disc as-machined (left) and (right) typical waisted hour-glass specimen.

Because of the shape of the centre discs, specimens required jigging in the fatigue testing machine to duplicate their test conditions under cantilever bend in the dynamic wheel testing machine used commercially. This was done in an endeavour to match crack initiation and fracture planes in the specimen and the production wheels. Hence specimens were placed in a mould and a cold curing resin (Lecoset 7007) cast around them to ensure a flat seating (see Figure 6) of the specimen ends in the test grips, and the correct orientation of the specimen in the test machine. This orientation is such that the predominant fracture plane position in the centre disc, as observed under industrial fatigue testing conditions (just above the cup radius area, see Figure 1), is coincident with the axis of rotation of the fatigue testing machine. All specimens were machined to ASTM E468-82.

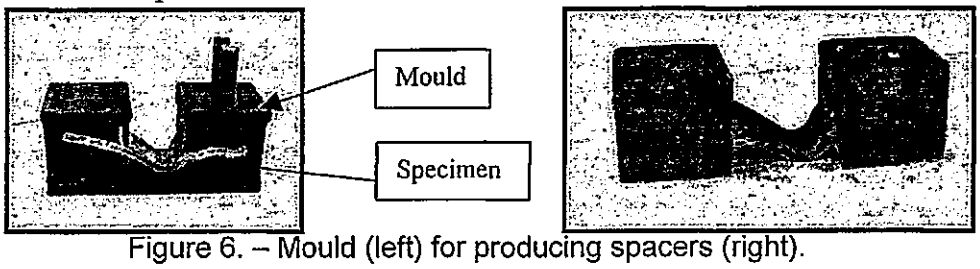

Figure 6. – Mould (left) for producing spacers (right).

Finally a strain gauge (Micro Measurements type EA-06-062-AK-120) was attached to the specimen perpendicular to the axis of rotation plane to allow for the applied load setting.

Residual Stress

Centre discs from each stage of the production process were used for assessing the residual stress magnitudes. Measurement locations considered were that above the cup radius area as mentioned above. For this investigation a customised eight-element strain rosette* was employed (see Figure 7) using three Micro Measurements type CEA-06-062-UM-120 strain rosettes for assessing the maximum arithmetical principal stresses and corresponding principal angles.

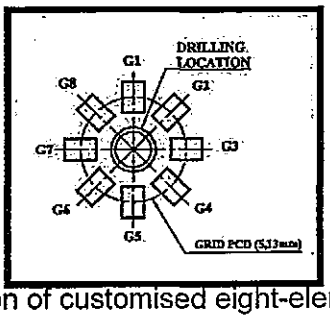

Figure 7. – Illustration of customised eight-element rosette layout.

* The concept of the customised strain rosette used for the residual stress investigations in this work is subject to a South African patent application No. 99\2855.

TESTING PROCEDURES

Fatigue

The strain amplitude was set at 1300 micro-strain (this being equivalent to 260 MPa) at the predominant industrial fracture plane (Figure 5) and a test frequency of 33 Hz. In the event this endeavour was unsuccessful, because the cross-sectional area of the specimen corresponding to the cup radius region was smaller than that corresponding to the fracture plane under industrial testing of the wheels. This region is also offset both vertically and horizontally from axis of bend (rotation) of the fatigue-testing machine. This implies that the bending stresses in this region are different to those along the predominant fracture plane in the wheel and hour-glass specimens, under similar applied load conditions.

The applied load cycle (strain ratio) gave maximum and minimum values of -1540μ strain and +1420μ strain at the fracture plane (through apex of cup radius). This assessment was fundamentally important with a view of having to fatigue test plate (*blank*) and d*raw 1* specimens. The fatigue testing procedure of the production stages commenced with the *painted* stage and finished with the plate (*blank*) specimen. It must be remembered that the cup radius region is present from *draw 2* thru *painted* specimens and it is through the apex of this region that failure occured. Both the plate (*blank*) and *draw 1* specimens (which do not have this cup radius region) were aligned such that the narrowest cross-section of the hour-glass shape corresponded with the axis of bend of the fatigue machine. Failure of these specimens would thus occur through this region. Therefore, all the production stages were fatigue tested at the same applied load cycle (strain ratio) corresponding to their respective fracture planes.

Residual Stress

In order to align the drilling location on the component to the drilling head it was necessary to extend the feet of the drilling machine, this was achieved by manufacturing a rigid framework from 20 mm solid square bar to which the feet and the machine was attached. For this investigation a 2 mm deep hole was drilled using the polynomial drilling method with 30 increments and a delay time setting of 10 seconds between each increment. Prior to commencing the drilling operation the end mill is brought into contact with the metal component, causing a short circuit between component and end mill. This position of the end mill is taken as datum and the drilling operation can commence.

Surface Hardness

Due to the peculiar shape of the components, Brinell hardness measurements were made using a 2 mm ball indenter and a 120 kgf load on the same components used for the residual stress measurements. Measurement locations were adjacent to the residual stress analysis positions.

RESULTS

For this exploratory investigation five fatigue specimens were cut from centre discs from each production stage and tested at the mean strain ratio as observed at the hour-glass fracture plane.

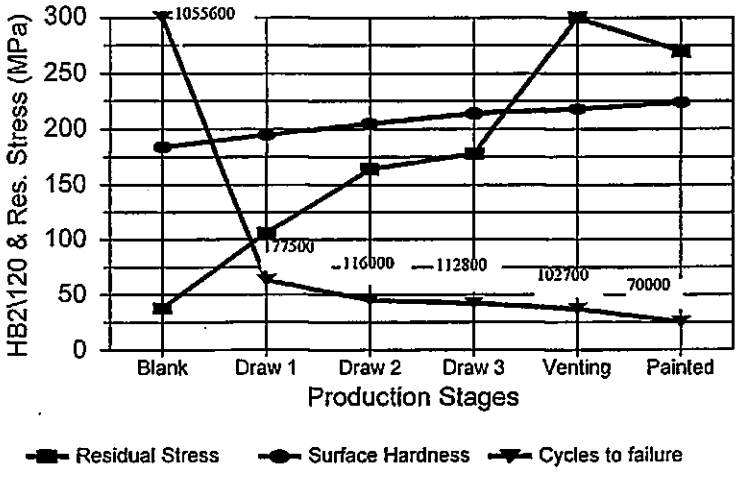

Prod. Stages	Fatigue Life (Nf)	Hardness (HB2\120)	Residual Stress (MPa)
Blank	1055600	184	38
Draw 1	177500	195	106
Draw 2	116000	205	164
Draw 3	112800	214	178
Venting	102700	218	300
Painted	70000	224	270
Wheel	72500	226	320

Figure 8. – Results of the residual stress, hardness and fatigue analysis.

The residual stress and hardness measurements were averaged from two centre discs from each stage, as the results obtained were of similar magnitude.

DISCUSSION

It is well known that cold working operations increase the ultimate tensile and yield strengths of steels. If a component is subjected to a shot peening or cold rolling operation the fatigue performance will be enhanced by the compressive residual stresses induced as a result. These compressive residual stresses are beneficial in terms of fatigue. However, if the component is subjected to cold drawing operations carried out under tensile conditions, such as is the case in sheet metal forming, the residual stresses induced will be tensile in nature and will have the opposite effect in terms of fatigue performance. The fatigue performance may also be impaired due to void formation (4) along grain boundaries see, for example, Figure 9 (x3865).

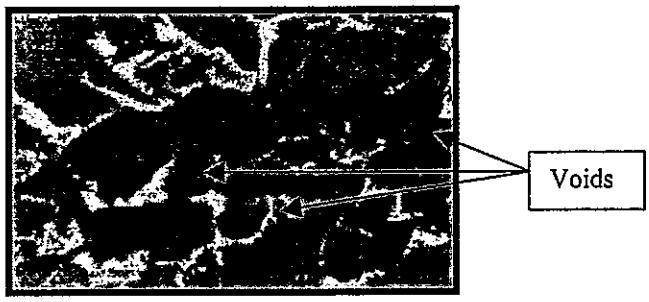

Figure 9 – Voids (near top surface) resulting from operations carried out under tensile conditions.

The trends indicated in Figure 8 for surface hardness, residual stress and fatigue performance were to be expected in terms of the cold working operations, with the exception of the residual stress and fatigue life for the *painted* stage. The substantial decrease in fatigue performance between plate (*blank*) and *draw 1* specimens is largely attributed to the tensile residual stresses and the onset of void formation within the microstructure due to the tensile natured plastic deformation. Further plastic deformation (tensile) experienced by *draw 2* components resulted in a similar increase in residual stress magnitude, and the voids being more pronounced increases the fatigue notch sensitivity resulting in a less significant decrease in fatigue life. A less pronounced decrease in fatigue life and a corresponding increase in surface hardness is observed from *draw 2* up to and including the *venting* stage. From Figure 2 it is evident that the volume of material differs between the various production stages. In terms of volume of material, the stages can be classified into the following groups:

- *Blank* and *draw 1;*
- *Draw 2* and *draw 3;*
- *Venting* stage and *paint* stage.

This is important to note since the residual stress magnitude of the *venting* stage is considerably higher than *draw 3* stage. This significant increase in magnitude can be attributed to the decrease in volume of material (punching of vent holes) leading to the re-distribution of internal energy (residual stress) to attain new equilibrium conditions.

The paint curing process is of low temperature (around 200°C) and the observed small reduction in residual stresses is to be expected. Such a reduction should be beneficial to fatigue life, as should the increase in hardness observed for this stage. However, the fatigue life actually decreases slightly after this process. It was only after microstructural analysis was carried out that this behaviour was clarified. It was found that carbonitrides had precipitated along the grain boundaries on the surface of the *painted* stage centre discs, which has a significant effect on surface hardness as reported by Okita et.al. (5). The martensite grains also show a change to a more acicular structure. The net result of these fairly subtle microstructural changes during paint baking, is that the surface is slightly 'embrittled' thereby increasing the notch sensitivity. Hence the fatigue life is reduced in this stage of the process.

The residual stress analysis was undertaken on complete production components and not on the waisted hour-glass specimens, in which the residual stress field would have been largely eradicated by the specimen manufacturing process. Fatigue data from these specimens can, however, be correlated with hardness results (which would be the similar in centre discs and specimens) and with the residual stress data from the centre discs, as indicated in Figure 10. A calibration of the residual stress information and the fatigue results can be effected by considering the difference between lives for the complete wheel and specimens cut from the *painted* and baked centre disc. This implies that if production stages could be fatigue tested under industrial conditions then the same trend as indicated in Figure 8, would apply, but that the number of cycles to failure would be in accordance with the relationship which exists at a load cycle of 260 MPa.

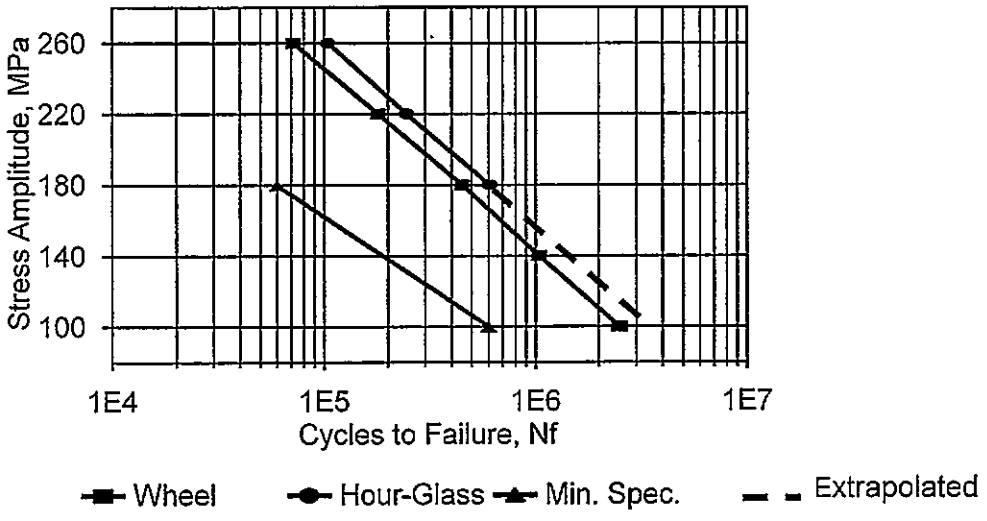

Figure 10. – Comparison of S-N curves for wheel and hour-glass specimens.

All fracture surfaces showed similar features, i.e. ratchet markings on both top and bottom surfaces, more pronounced along the top surface. It is envisaged that the crack front slows as it propagates through the elastic core region (an area around the neutral axis) where it grows laterally (secondary cracking) due to the discontinuities present in this region. These discontinuities are considered imperfections resulting from the stamping operation which cannot be removed through metallurgical or heat treatment processes. Therefore, as the crack front grows through this region (see Figure 12, x775), crack initiation commences from the bottom surface, as ratchet markings are also evident. Finally the crack fronts grow toward one another until catastrophic failure occurs which is observed by the 'fast fracture plane' evident along the lower half in Figure 11.

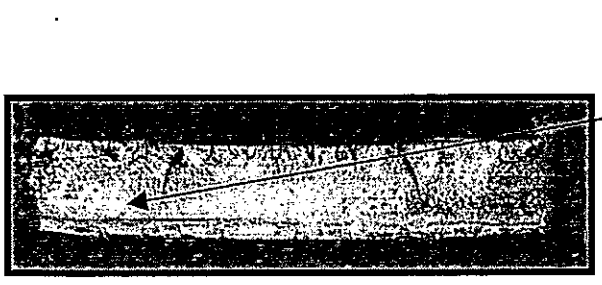

Figure 11 – Fracture Surface.

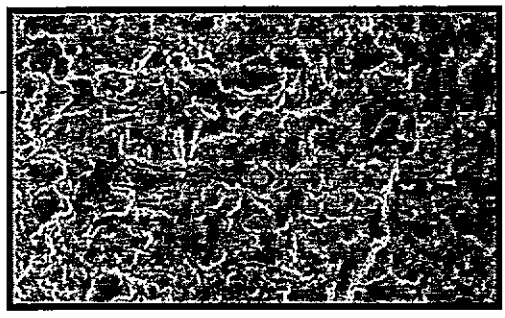

Figure 12 – Showing secondary cracking in elastic core region.

An additional interesting outcome from this work relates to the development of an eight-element strain rosette, which gives improved residual stress information when holes are drilled into a textured steel

(which causes hole ovality to occur). In such cases there is no easy way of identifying, a priori, the plane along which the maximum deformation will occur when the internal strains are relieved through the drilling of a hole. The eight-element strain rosette gives improved results because the arithmetic maximum relieved residual stresses are revealed at a particular assessment location.

CONCLUSIONS

Based on the experimental results presented in this paper, the following conclusions have been drawn:

- Fatigue testing of waisted hour-glass specimens machined from the various production stages of the centre disc is an effective tool in evaluating the fatigue strength of centre discs.
- Tensile surface residual stresses appear to play a significant role in fatigue performance, as fatigue life is more closely aligned with trends in residual stress than with trends in hardness.
- The final paint baking cycle has a larger detrimental influence on fatigue life than would be expected from residual stress or hardness data. This is due to carbonitride precipitation at the grain boundaries in this dual phase steel. Small changes in chemical composition of the steel may alleviate this phenomenon.
- The eight-element strain rosette concept offers advantages in residual stress measurement in textured metals which show significant hole ovality. It should be pursued by strain gauge manufacturers.

ACKNOWLEDGEMENTS

This investigation was performed with the support of the Manufacturing Research Unit at Port Elizabeth Technikon. The authors wish to thank Mr L Thomas of Guestro Wheels (Eastern Cape Division) for material supply, Messrs R Phillips, I Wedderburn and C DuPreez for their expert advice and assistance, and Messrs J van der Mescht, T Tonkin and Miss N Zozi for their technical support.

APPENDIX - I

APPENDIX - I

A Novel 8-Element Gauge for Residual Stress Assessment using the High Speed Centre Hole Drilling Method *

PJ McGrath[A], DG Hattingh[B] , MN James[C] and IN Wedderburn[D]

Many researchers and scientists have contributed, over the years, to the development of residual stress assessment technology since it was first reported by Mathar in 1933. Despite such work, a commonly held view is that residual stress analysis using strain gauges is a technique whose use is restricted to homogeneous and isotropic type materials. Texturing and plastic deformation are felt to lead to a significant lack of repeatability in the data. This lack of certainty has had a negative impact on beneficial uses of residual stresses in optimising fatigue and fracture performance through manipulating and controlling their magnitude.

The work reported in this paper demonstrates an improvement in repeatability of residual stress measurement via strain gauges, in the presence of plastic deformation and texturing effects. This is achieved through the identification of hole ovality as an important contributory factor to observed variability, and the development of a novel 8-element strain rosette. Plate specimens subjected to pure plastic bending were used in this investigation, and it was discovered that the periphery of the drilled hole was ovoid in shape, and that the plane of this ovality varied between nominally similar bend specimens. This led to the development of an 8-element strain rosette which allows the absolute maximum value of the relieved residual stress to be assessed (in magnitude and sign). This gives an improvement in repeatability of measurements when assessing textured sheet metal components subjected to bend forming operations. The aim of this paper is to introduce this novel strain rosette and outline the steps leading to its development and subsequent application to pressed steel wheels. It is believed that wider acceptance of this technique would lead to improvements in accuracy and repeatability of strain gauge analysis of residual stresses for complex components and load states.

NOMENCLATURE

CW, ACW	Clockwise & anti-clockwise
RS	Residual stress
HSLA	High strength low alloy
DPS	Dual phase steel
YS	Yield strength
UTS	Ultimate tensile strength
G1, G2	Strain gauge element numbering sequence
$\bar{A}$, $\bar{B}$	Blind hole drilling calibration constants
$\bar{a}$, $\bar{b}$	Dimensionless blind hole drilling calibration constants
α	Angle measured clockwise from G1 to the maximum principal stress direction
$\varepsilon_1, \varepsilon_2, \varepsilon_3$	Relieved strain values, where 1, 2, 3, refer to the element number
$\sigma_{max}, \sigma_{min}$	Maximum and minimum principal stresses

* The concept of this novel strain rosette is subject to a South African Patent Application: 2000/2042.

[A] Researcher and senior lecturer in the Department of Mechanical Engineering, PE Technikon, Private Bag X6011, Port Elizabeth, 6000, South Africa. (e-mail: mcgrath@ml.petech.ac.za).

[B] Head of Department, Mechanical Engineering, Port Elizabeth Technikon, South Africa.

[C] Professor of Mechanical Engineering, University of Plymouth, England.

[D] Researcher, Department of Mechanical Engineering, Port Elizabeth Technikon, South Africa.

INTRODUCTION AND BACKGROUND

Residual stress assessment by means of the hole drilling technique is still regarded by many analysts as being restricted to isotropic and homogeneous type materials[2], despite advances in technology achieved since the work of Mathar in 1933 [1].

The work reported in this paper developed from multiple analyses of industrial components, in which the maximum residual stresses was found to vary substantially under nominally constant evaluation conditions, e.g. maintaining the same reference plane for grid/element G1, applying the rosette to similar locations, and constant drilling method and procedure.

Upon closer inspection of such drilled holes it was clear that a slight ovality[1,3] of the hole was present and that the major axis of this ovality did not lie in a constant orientation with respect gauge G1, but varied from component to component. This indicated that structural steels commonly used in pressed components are neither isotropic nor homogeneous in their response to residual stresses when hole drilling techniques are used. Thus the hole becomes ovoid with a varying major axis orientation as a result of varying material texture and properties.

As the direction of hole ovality is not known a priori, the individual elements (3 off) of a standard strain rosette[4] are unlikely to detect the maximum relieved strain. For instance, this ovality could lie in the worst case direction, perpendicular to gauge G2 (see Figure 1). Assuming that the major axis of the oval reflects the direction of maximum relieved strain, the direction along which this occurs will remain undetected.

It became clear that applying a 3-element rosette and referencing gauge G1 to a particular plane in the component would not guarantee finding the absolute maximum value of residual stress at that particular location. Even if one does find the appropriate maximum relieved strain direction, the existence of ovality in the hole is likely to affect the strain calculation, which assumes a circular hole.

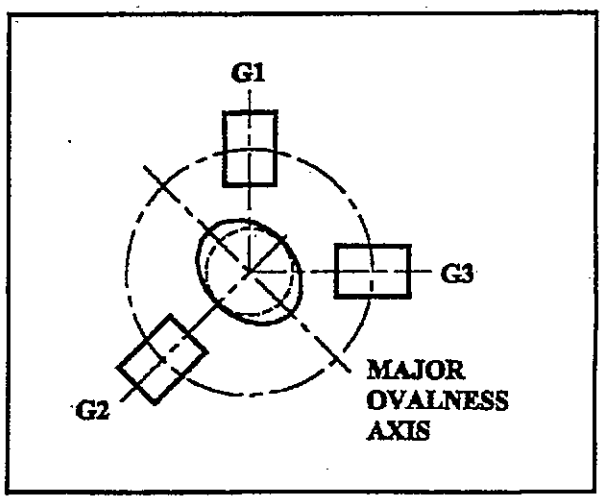

Figure 1. Schematic of a standard clockwise RS strain rosette showing hole ovality.

The above observations led to an investigation into developing a reliable method to detect this absolute maximum relieved residual stress and, in so doing, minimize repeatability problems often associated with residual stress assessment by strain gauge rosettes. The method developed uses a customised 8-element strain gauge rosette.

MATERIAL

The material used in this investigation was Dual Phase Steel Plate (DPS600). This is a HSLA steel developed in the mid-1970's whose microstructure consists of islands of martensite (about 20% by volume) in a ferritic matrix.

	C	Mn	P	S	Si	Al
Element and % Chemical Composition	0.05	0.50	0.01	Max	Max	0.02
	0.12	1.30	0.09	0.006	0.65	0.06
	Cr	Ni	Ti	Mo	Cu	
	Max	Max	Max	Max	Max	
	0.90	0.25	.015	0.05	0.35	

Table 1. Chemical composition of DPS600

Designation	Yield Strength (YS) (MPa)	Tensile Strength (UTS) (MPa)	Elongation %
(DPS600)	Min 300 Max 470	Min 550 Max 700	28
	Actual 427	Actual 664	--

Table 2. Mechanical properties of DPS600

COMPONENT

The components used for residual stress analysis during this investigation were rolled DPS plate, 4.1mm thick and automotive wheels pressed from the same plate. The residual stress assessments were undertaken on the centre disc region of the wheel between the cup and hat radii, as indicated by Figure 2.

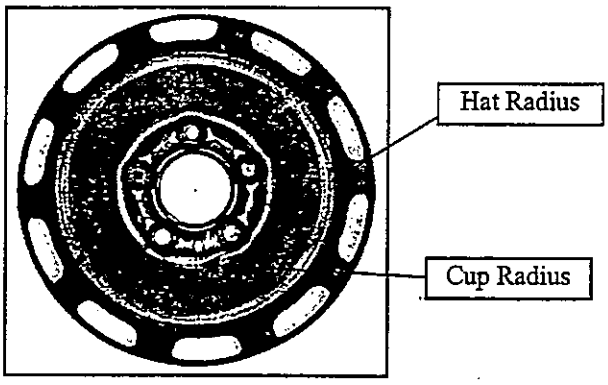

Figure 2. Wheel centre disc showing hat and cup radii.

RESIDUAL STRESS ANALYSIS

STANDARD HOLE-DRILLING METHOD

The hole-drilling method residual stress measurement used in the present work, involves the drilling of a blind hole into the surface of a component thereby locally changing the internal stress equilibrium due to material removal. The change in local strain state resulting from the hole drilling is recorded by specially designed strain gauges mounted on the surface, concentrically with the hole, in a 120° rosette arrangement. The equipment used for this work is known as the RESTAN (REsidual STress ANalysis) system and was purchased from HBM of Germany.

CUSTOMISED STRAIN GAUGE ROSETTE

For investigating the effect of hole ovality a customised 8-element strain rosette was developed using three (3) Micro-Measurements CEA-06-062-UM-120 edge-type strain rosettes. These strain rosettes were successively superimposed on one another utilising the drilling location circles for concentric alignment. Excess carrier material was removed and the three sections were joined to form the 8-element strain rosette. This technique will lead to slight misalignment errors reflecting the skill of the operator. However, concentric alignment is possible to within 0.15mm, which is much less than the hole ovality recorded in these components (typically 0.24mm). Thus it is expected that the strain values would contain marginal errors.

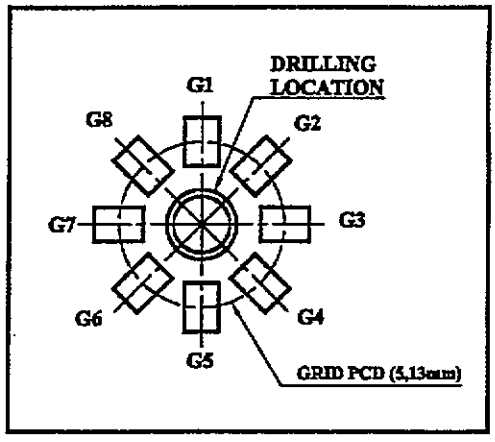

Figure 4. Layout of 8-element strain rosette.

Figure 4 illustrates the layout of the customised 8-element strain rosette. It is still possible to use the same data reduction techniques as for the standard three-element rosettes by combining the three relevant elements. The various possible CW, ACW and edge gauge combinations are indicated in Table 3.

CW	ACW	EDGE
1,6,3	3,6,1	1,2,3
2,7,4	4,7,2	2,3,4
3,8,5	5,8,3	3,4,5
4,1,6	6,1,4	4,5,6
5,2,7	7,2,5	5,6,7
6,3,8	8,3,6	6,7,8
7,4,1	1,4,7	7,8,1
8,5,2	2,5,8	8,1,2

Table 3. Gauge combinations corresponding to a three-element rosette.

RESIDUAL STRESS CALCULATION METHOD

The principal relieved residual stresses were determined according to the ASTM 837-94(a) method of calculation[4], as follows:

Principal stresses:

$$\sigma_1, \sigma_2 = \frac{\varepsilon_c + \varepsilon_a}{4\bar{A}} \pm \frac{\sqrt{(\varepsilon_c - \varepsilon_a)^2 + (\varepsilon_c + \varepsilon_a - 2\varepsilon_b)^2}}{4\bar{A}}$$

Principal angle:

$$\tan 2\alpha = \frac{\varepsilon_a + \varepsilon_c - 2\varepsilon_b}{\varepsilon_c - \varepsilon_a}$$

where: ε_a, ε_b & ε_c = measured strain values, with a, b & c, for example, corresponding to the CW combination 1, 6 & 3 as indicated in Table 3. $\bar{A}$ and $\bar{B}$ = geometrical constants as determined using ASTM 837-94(a).

RESULTS

DPS PLATE SPECIMEN

The maximum values of principal residual stresses measured in the DPS plate specimen by each gauge combination are tabulated in Table 4. Table 4 shows that the values of absolute maximum RS magnitudes recorded by the various 3-element gauge combinations in the customised rosette, differ by up to 9%. When undertaking RS measurements by the strain rosette technique this may be considered an acceptable variation.

Nonetheless, elimination of such random error in rosette measurements would be advantageous in ensuring higher levels of repeatability in rosette-based strain measurement.

CW Gauge	ACW Gauge	σ_{max}	α
1,6,3	3,6,1	36	-2.6°
2,7,4	4,7,2	38.7	5.2°
3,8,5	5,8,3	36	-2.6°
4,1,6	6,1,4	35.2	0.6°
5,2,7	7,2,5	36.6	6.7°
6,3,8	8,3,6	36.6	-1.9°
7,4,1	1,4,7	36.3	4.1°
8,5,2	2,5,8	37.6	3.2°

Table 4. Maximum residual stress magnitudes in MPa measured in DPS plate specimen.

It I also clear that the principal angles indicated by each gauge combination showed good correlation, lying in a range of 9.3°.

WHEEL CENTRE DISCS

Maximum Relieved Residual Stresses:

27 residual stress analyses were undertaken using the 8-element strain rosette on five wheel centre discs at several locations. The 8-element strain rosettes were all aligned such that a line drawn through elements G1 and G5 would pass through the centre of the wheel, in a direction co-incident with the rolling direction of the steel plate.

The highest and lowest values of maximum RS for each 8-element analysis location, together with their corresponding gauge combinations are shown in Table 5 (CW gauge combinations were employed). Also calculated and given in the table are the variation in recorded RS maxima, and the percentage variation as a function of the highest recorded maximum RS value. It can be seen that the percentage variation between maxima in these

components has a wide range, lying between 6.7% and 68%.

Gauge comb. [High / Low]	High Max. RS	Low Max. RS	RS Varia-tion	% Varia-tion
[3,8,5] [2,7,4]	166.1	155	11.1	6.7
[1,6,3] [7,4,1]	113.6	101.1	12.5	11
[3,8,5] [7,4,1]	186	161	25	13.4
[3,8,5] [8,5,2]	298.3	249	49.3	16.5
[7,4,1] [6,3,8]	113.2	94.3	18.9	16.7
[4,1,6] [8,5,2]	239	198.4	40.6	17
[1,6,3] [5,2,7]	346.8	280.8	66	19
[4,1,6] [5,2,7]	381.7	305.3	76.4	20
[4,1,6] [8,5,2]	217.2	163.9	53.3	24.5
[8,5,2] [4,1,6]	363.5	263.5	100	27.5
[5,2,7] [1,6,3]	144.3	104.3	40	27.7
[2,7,4] [1,6,3]	156.4	111.3	45.1	28.8
[2,7,4] [5,2,7]	415.6	280.4	135.2	32.5
[3,8,5] [6,3,8]	130.3	85.4	44.9	34.5
[5,2,7] [6,3,8]	181.4	118.4	63	34.7
[3,8,5] [7,4,1]	159.1	101.4	57.7	36.3
[1,6,3] [5,2,7]	109.3	68.4	40.9	37.4
[4,1,6] [8,5,2]	152.5	91.1	61.4	40.3
[5,2,7] [1,6,3]	158.4	92.4	66	41.7
[1,6,3] [5,2,7]	188.6	106.5	82.1	43.5
[5,2,7] [1,6,3]	173.3	92.7	80.6	46.5
[4,1,6] [8,5,2]	384.1	182.3	201.8	52.5
[8,5,2] [4,1,6]	468.7	202.7	266	56.8
[4,1,6] [8,5,2]	406.4	164.2	242.2	59.6
[3,8,5] [7,4,1]	-296.9	-111.7	185.2	62.4
[5,2,7] [2,7,4]	-265.7	-99.7	166	62.5
[3,8,5] [4,1,6]	-264.9	-84.8	180.1	68

Table 5. Recorded variation between highest and lowest maximum residual stress magnitudes for each 8-element analysis location [residual stresses in MPa].

The results indicate that had 8-element strain rosettes not been employed in this study, large variations in the maximum RS magnitudes would have resulted. This variation arises because recorded maxima are entirely dependent on the initially unknown hole ovality, relative to the orientation of a standard three-element strain rosette.

The ovality in the drilled hole is a result of unequal strain relaxation on opposite sides. This occurs because the textured DPS is neither isotropic nor homogeneous in its response to plastic deformation which, in itself, leads to unequal strain response around a drilled hole. The effect of this is shown in Figure 5, where the maximum relieved strains for a typical analysis are shown graphically with respect to their relative grid positions about the hole centre. These strains mirror the hole shape.

It was also observed that the highest and lowest maximum RS magnitudes were not always indicated by the same gauge combination, even when analyses were repeated in the same relative position on similar discs.

This fact further underlines the importance of the use of the 8-element strain rosette when seeking to obtain the absolute maximum RS magnitude in textured steels subjected to forming operations.

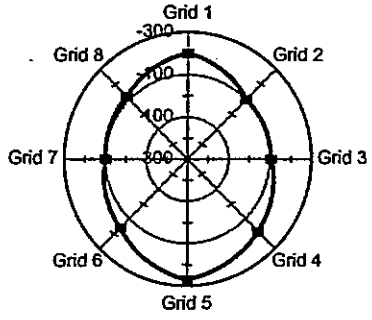

Figure 5. Example of uneven strain relief distribution on opposite sides of the hole, units in micro strain.

An exercise was undertaken to establish a typical level of error that might be expected had a standard 3-element rosette been employed instead of the 8-element strain rosette. This was done by comparing the highest relieved maximum RS value, given by the 8-element strain rosette, with the maximum RS value indicated by a (constant) 1,6,3 gauge combination in the 8-element strain rosette. The 1,6,3 gauge combination thus represents a standard CW three-element rosette, taken in a typical user orientation relative to the wheel centre

disc. Percentage errors between maxima shown by the 1,6,3 gauge combination and the 8-element rosette were then calculated.

The results of this comparison are shown in Table 6. Note that 'Gauge HRS' indicates which gauge combination revealed the highest maximum RS magnitude. All RS magnitudes are given in MPa.

Only 4 of the 27 analysis results would have yielded the same absolute maximum RS result from a 3-element gauge, as found with the 8-element rosette. The highest error in this comparison was found to be 60.7%.

Max. RS [1,6,3]	Highest Max. RS	Gauge HRS	% Difference
113.6	113.6	1,6,3	0
109.3	109.3	1,6,3	0
188.6	188.6	1,6,3	0
346.8	346.8	1,6,3	0
294.2	298.3	3,8,5	1.4
163.4	166.1	3,8,5	1.6
181.1	185	3,8,5	2.6
369.9	381.7	4,1,6	3.1
381.7	415.6	2,7,4	8.2
193.8	217.2	4,1,6	10.8
100.4	113.2	7,4,1	11.3
209.6	238	4,1,6	12.3
298.7	363.5	8,5,2	17.8
114.2	152.5	4,1,6	25.1
346.9	468.7	3,8,5	26
104.3	144.3	5,2,7	27.7
111.3	156.4	2,7,4	28.8
273.5	384.1	4,1,6	28.8
288.5	406.4	4,1,6	29
111.8	159.1	3,8,5	29.7
91	130.3	3,8,5	30.2
124.1	181.4	5,2,7	31.6
92.4	158.4	5,2,7	41.7
92.7	173.3	5,2,7	46.5
-126.3	-264.9	3,8,5	52.3
-131.6	-296.9	3,8,5	55.7
-104.4	-265.7	5,2,7	60.7

Table 6. Results of comparison showing expected error as a result of rosette orientation when using a three-element rosette.

Of concern is the fact that more than half of the analyses would have yielded differences of more that 25%. For purposes of component design and repeatability of measurement, such random variations in residual stress analysis are not acceptable.

Principal Angle:

For each analysis the angle of action of the principal residual stresses, or principal angle, was determined for all gauge combinations.

The calculated principal angles revealed by each gauge combination showed good correlation, with all values lying within a range of 10°. However, as was the case for the maximum RS magnitudes revealed through use of 8-element rosettes, the size of principal angle range obviously depended on the equality of the relieved strains on opposite sides of the hole.

Typical data for variation of principal angles shown by an 8-element rosette is given in Table 7 below:

Gauge Combination	Principal Angle α
1,6,3	4.6°
2,7,4	6.8°
3,8,5	3.3°
4,1,6	5°
5,2,7	3.5°
6,3,8	2.4°
7,4,1	6.3°
8,5,2	4°

Table 7. Typical principal angles as revealed by each gauge combination in an 8-element rosette.

DISCUSSION

When attempting to measure RS via the hole-drilling technique a question arises as to the direction along which element G1 should be aligned, and which type of rosette is required to obtain the absolute maximum RS magnitude. This concern has previously been raised by users of this

technique[6]. The information presented in this paper goes some way towards resolving some of these difficulties.

The data presented in this paper indicates that there is no way of predicting hole ovality or the uneven strain relief distribution about the hole when textured materials are analysed. It is therefore not possible to attempt to predict in what orientation a three-element rosette should be applied to reveal the absolute maximum RS magnitude. This led to the development of the novel 8-element rosette, which reduces the resultant variation in RS values to a minimum.

This gave insight into percentage differences in RS maxima revealed by the various 3-element gauge combinations contained in an 8-element rosette. This random variation reached values > 60%, indicates why strain rosette measurements of residual stress can be somewhat unreliable.

Whilst it is still feasible that use of an 8-element strain rosette could provide variable results when analysing similar components in similar locations, although likely variation is within 30%.

Use of the 8-element rosette would confer a higher confidence when applying the results of strain rosette-based RS analysis to component design and fatigue/fracture lifing. It also provides a higher level of repeatability with a lower number of hole drilling analyses.

CONCLUSION

The present work unambiguously shows that the 8-element rosette developed in this work reduces the variability inherent in strain rosette-based residual stress assessment, particularly where effects of anisotropy and lack of homogeneity in textured steels must be taken into account.

Thus the potential now exists to substantial savings in time, effort and money through use of the 8-element strain rosette in routine component testing in industry.

It is believed by the present authors, that hole ovality is important in residual stress measurement, and the concept of the 8-element gauge should be pursued by strain gauge manufacturers.

ACKNOWLEDGEMENTS

The authors wish to thank the members of the Material Research Centre of the Port Elizabeth Technikon, South Africa, for their assistance during this investigation.

Guestro Wheels (Eastern Cape), SA, for supplying the DPS600 material.

REFERENCES

1) Mathar, J., – "*Determination of Initial Stresses by Measuring Deformation Around Drilled Holes*," Trans ASME, 56 (4), 249-254, 1934.

2) Kockelmann, H., – "*The hole drilling method – the best technique for the experimental determination of residual stresses in many fields of application*", 1993.

3) Kalpakjian, S., – "*Manufacturing processes for Engineering Materials*," second edition, 1991.

4) *Standard Method for Determining Residual Stresses by the Hole-Drilling Strain Gauge Method*, - ASTM 837.94(a), - 1994.

5) Coldren, A.P. & Eldis, G.T., - "*The Dual Phase Steels*," Climax Molybdenum Company, Michigan, USA.

6) Hausler, H., Konig, G. and Kockelmann, H.,*On the Accuracy of Determining the Variation with Depth of Residual Stresses by Means of the Hole-Drilling Method*, Residual Stresses in Science and Technology, 1987, pp257-264.

7) Wedgewood, A., *Measuring Residual Stresses : The Key to Longevity*, Materials World, January 1994, pp5-7.